

https://dspace.org/

Geochemical characterisation of mine drainage from a copper mine operations at Phalaborwa (South Africa) and Kitwe (Zambia)

Mwelwa Kitondo

2022

https://hdl.handle.net/10539/34525

Mwelwa, Kitondo (2019) Geochemical characterisation of mine drainage from a copper mine operations at Phalaborwa (South Africa) and Kitwe (Zambia) University of the Witwatersrand, Johannesburg, <http://hdl.handle.net/10539/34525>

Downloaded from a DSpace repository. https://dspace.org/

GEOCHEMICAL CHARACTERISATION OF MINE DRAINAGE FROM COPPER MINE OPERATIONS AT PHALABORWA (SOUTH AFRICA) AND KITWE (ZAMBIA)



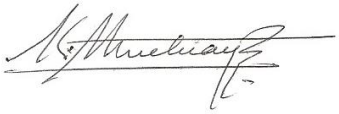
KITONDO MWELWA

A Thesis submitted to the Faculty of Science, University of the Witwatersrand, Johannesburg, in fulfilment of the requirements of the degree of Doctor of Philosophy

2019

DECLARATION

I declare that this thesis is my own unaided work. It is being submitted for the Degree of Doctor of Philosophy at the University of the Witwatersrand, Johannesburg. It has not been submitted before for any degree or examination at any other university.

Signature of candidate:  Date: 07th October, 2020

ABSTRACT

Mining and processing of copper minerals form a solid and dependable base for infrastructure, social and economic development of most countries in the Southern African region to which South Africa and Zambia belong, with Phalaborwa and Kitwe as their respective centers of copper mine operations. Copper and its auxiliary metals have benefited man in electrical, electronics, medicine and other spheres associated with modern and easy life. At the far side of societal benefits from an extended copper extractive mining, negative impacts of its operations degrade the environment of which water has always been regarded as the worst impacted target.

Phalaborwa and Kitwe study sites are characterised by Cu-sulphide minerals coexisting with carbonate minerals in host ore rocks of volcanic and sedimentary origins, respectively. Phalaborwa is supplemented by large amounts of exploitable iron minerals (Magnetite) and phosphate minerals (Apatite), a recognized residence of REEs. In Kitwe, the exploitable ore deposits are rich in Cu-Co metals.

Geochemistry was used, both as a path and a tool, to describe distinct features of a copper mine waste samples, assess potential hazards posed by contaminants resulting from their interaction with oxygen and water, evaluate metal speciation resulting from fractionation of sediments. Analytical results were further complemented by PHREEQC geochemical diagnostic simulations of surface water mixing and predictive simulations of surface water loss through evaporation. Adsorption studies were also used to investigate the recovery capacity of natural magnetite (Mgt) for rare earth elements (REEs) with essential properties for applications in electronics and medicine.

Samples, consisting of stream water and sediments, and tailings (dumps) were collected at Kitwe study area. River and dam water and sediments, and a variety of mine solid waste consisting of rocks (Rk), sand, phosphogypsum (PG), carbonatite (Cbt), copper-crust (Cu_crust), magnetite (Mgt) and and tailings ex-concentrator (TexCon) were collected at Phalaborwa study area. Physical (dry) and chemical (wet) sample preparation, of which Toxicity Characteristics Leaching Procedure

(TCLP) and Sequential Extraction (SE) form part, paved the way for qualitative and quantitative analytical determination. A combination of analytical techniques (XRD, XRF, SEM-EDS, LPS, IC, ICP-OES (ICP-MS) and CHNS Analyser) were employed to identify minerals and quantify contaminants.

For Phalaborwa, surface water was alkaline (pH 8.32 – 9.42) with Eh (432 – 555 mV, corrected values). The EC ranged between 600 and 2500 $\mu S.cm^{-1}$ in river water but was 6000 $\mu S.cm^{-1}$ in water retain dam (WRD). It was influenced, mainly, by SO_4^{2-}, Cl^-, Ca^{2+} and Mg^{2+} ions which also defined surface water classification. Major ions and trace elements concentrations were comparatively much higher in WRD than in rivers. For Kitwe, surface water was slightly alkaline (pH 7.04 – 8.42) with EC ranging between 250 to 3420 $\mu S.cm^{-1}$ and characterised by the dominance of SO_4^{2-}, Ca^{2+} and Mg^{2+} ions especially in streams linked to tailings dumps.

Tailings dumps and sediments samples, from Kitwe, were digested (*aqua regia*, $3HCl:1HNO_3$) and leached (TCLP) to assess the effects of vigorous and mild extraction conditions. For both techniques, there were more release of major and trace elements from tailings dumps than sediments. Comparisons of digestion results, (tailings </> sediments), were: Al (12434<**24774** mg kg^{-1}), Ca (58368>5594 mg kg^{-1}), K (6374>1379 mg kg^{-1}), Mg (44622>6153 mg kg^{-1}), Co (407.0>126.7 mg kg^{-1}), Cu (3368>1320 mg kg^{-1}), Fe (24753<**27600** mg kg^{-1}), Mn (3790>494.2 mg kg^{-1}) and Zn (40.8<150.0 mg kg^{-1}).

The presence of SO_4^{2-} in phosphogypsum (PG) and copper crust (Cu-crust) minerals, PO_4^{3-} in sand (Sand) and rock (Rock1) minerals, and CO_3^{2-} in carbonatite (Cbt) minerals of respective geologic samples was indicative of their association with the amorphous reactive phase whereas quartz, aluminosilicates and magnetite (Mgt) signaled the prominent presence of the crystalline inert phase. The extent of minerals dissolution and their accompanying release of inherent trace elements had a huge bearing on the composition of sample leachates. Cu was abundantly leached out from Cu-crust (45100 mg kg^{-1}), Mgt (424.9 mg kg^{-1}) and TexCon (141.8 mg kg^{-1}). Non geologic samples, in perticular elephant dung (ED), produced leachates with elevated major ions concentration than Mgt, e.g. Ca^{2+} (1.93>0.33%), Mg^{2+} (0.78>0.18%), SO_4^{2-} (964>228 mg L^{-1}), Cl^- (124>64 mg L^{-1}).

Metal species and positive saturation indices (SI > 1) of mineral precipitates, calculated from PHREEQC computation of surface water parameters, were abundant and more varied in WRD than in rivers. Furthermore, pH and Eh provided a favourable environment for the immobilization of trace metals via adsorption to, and subsequent deposition of scavengers such as iron- and Mn- oxyhydroxides. River sediments, from Phalaborwa, were crystalline (Si, Al, Fe) with silt to silty loam texture and high C/S ratio. Their leaching was reflective of these characteristics and their fractionation consistently released more bioavailable Mn and Cu. Sediments quality, assessed using bioavailable concentrations of trace elements as probable effect quotients (PEQs), was poor (mean PEQ > 0.5) and posed a risk to benthos.

Predictive evaporation simulations of Cu_crust leachates indicated, in commensuration with percentages evaporation, worrisome exponential increases in concentration (ca 32%, 120% and 1900% increase at 10%, 50% and 95% evaporation, respectively), and deposition of metal species that could precipitate the deterioration of the aquatic system.

Isotherms and kinetics models of REEs adsorption onto natural magnetite together with their thermodynamics were determined. Based on results, Langmuir isotherm model gave the best description of this adsorption process, and every indication pointed at the adsorption as obeying the pseudo-second order kinetic model. Thermodynamics adsorption studies were unanimous in determining the mechanism of REEs adsorption onto Mgt. The percentage recovery was 94.8%. The heats of adsorption, ΔH^o (av = 22, min = 17, max = 41 kJ mol^{-1}) and ΔH_x, (av = 24, min = 18, max = 40 kJ mol^{-1}), the activation energy, E_a, (av = 51, min = 16, max = 40 kJ mol^{-1}), the activation energy E_a (av = 51, min = 16, max = 102 kJ mol^{-1}), and the adsorption energy obtained from D-R isotherm E_s (12 – 15 kJ mol^{-1}) fell, generally, within the category of physisorption/ion exchange mechanism limits found in literature (ΔH^o and $\Delta H_x < 80$, $E_a < 40$ and $E_s < 16$ kJ mol^{-1}). Furthermore, REEs adsorption onto Mgt was spontaneous ($\Delta G^o < 0$) with dissipative entropy ($\Delta S^o > 0$).

This study did not seek to compare the two study areas by looking at results of one study site in parallel with results of the other study site, but to allow the evidence of similarities and differences, where possible, to come out with no demanding efforts by searching for aspects that are comparable.

DEDICATION

Vivement à toi ma Dess,

pour tout, pour quelque chose et pour rien.

ACKNOWLEDGEMENTS

To you Prof. Hlanganani Tutu, my principal supervisor, and Prof. Luke Chimuka, my co-supervisor, for generously accepting me in your Laboratory, surely showing me the tricks of the trade and patiently redressing my shortcomings,

I **truly** and **utterly** say **thank you**.

Through both of you, I salute all staff of the Environmental Analytical Chemistry Research Group (EACH) and the School of Chemistry. I extend this recognition to Dr G. Snow of the School of Animal, Plant and Environmental Science (APES) for co-opting me in his Research Group's sampling tours.

To my employer, The Copperbelt University (CBU), for according me time and support to develop academically,

I address my appreciation.

To the Environmental Department at PMC Ltd, for permission to access the mine area and the escort provided during sampling,

To the National Research Foundation (NRF) and the National Council for Science and Technology (NCST), for promoting South Africa - Zambia bilateral research cooperation

To Dr. V. Naidoo (Neurologist - Center of Advanced Medicine), for the timely intervention to alleviate signs of my ailing health,

I commend the enthusiasm for your work.

To my wife, for that Pauline Spectrum of Love,
To my sons, A and Ω, for withstanding my prolonged absence,
To my family at large, for her benevolent wishes,
To my friends, for that warm cushion,
To Dr. L. R. Lembani, for his faithful and valued companionship,
To my colleagues in EACH, for making me feel at home and young among you,

I remain indebted.

To **Him**, "**GOD ALONE**",

I sing praise for the radiance of **His** grace in my life!!!

TABLE OF CONTENTS

DECLARATION i

ABSTRACT ii

DEDICATION vi

ACKNOWLEDGEMENTS vii

TABLE OF CONTENTS viii

LIST OF FIGURES xiv

LIST OF TABLES xxi

LIST OF ABBREVIATIONS xxv

CHAPTER 1 INTRODUCTION 1

1.1 Background of the study 1

1.2 Context of the study 2

1.3 Motivation of the study 3

CHAPTER 2 LITERATURE REVIEW 4

2.1 Copper in ancient and modern times 4

2.2 Geology and mineralogy of copper ore deposits 5

2.2.1 Historical background of copper mining in South Africa 5

2.2.2 Geology of the Phalaborwa Igneous Complex (PIC) 5

2.2.3 Mineralogy of the Phalaborwa Igneous Complex 7

2.3 Geology and lithology of copper ore setting in the Copperbelt, Zambia 9

2.4 Copper mine operations 10

2.4.1 Mining and metallurgical process 10

2.4.2 Chemical process 11

2.5 Mining practices versus environmental protection 13

2.6 Rare Earth Elements (REEs) as a constituent part of carbonatite ore rock ……..14
2.7 Tailings 15
2.8 Sediment 16
2.9 Leaching studies 20
2.10 Adsorption studies 21
2.10.1 Adsorption mechanism..... 21
2.10.2 Description of Adsorption Isotherms 22
2.10.3 Adsorption Kinetics 25
2.10.4 Adsorption Thermodynamics..... 26
2.11 Sequential extraction Procedure 28
2.11.1 General principle..... 28
2.11.2 The Tessier's method of SEP..... 28
2.11.3 The BCR method of SEP 29
2.11.4 Single extraction as total and pseudo-total (*Aqua regia*) concentration..... 30
2.12 Bioavailability..... 32
2.12.1 Bioavailability concept..... 32
2.12.2 Bioavailability control processes 33
2.12.3 Sediments Quality Guidelines (SQGs)..... 34
2.13 Metal speciation..... 36
2.14 Geochemistry of mine drainage..... 37
2.14.1 Ore and gangue minerals coexistence 37
2.14.2 Weathering of rock mineral 37
2.14.3 Hydrogen ion activity (pH) 39
2.14.4 Reduction-oxidation (Redox)..... 40

2.15 Geochemical predictive speciation model 43
2.16 Speciation modelling and equilibrium solubility 44
2.17 Problem statement 45
2.18 Summary of novelty of the study 46
CHAPTER 3 AIM AND OBJECTIVES 47
3.1 Aim 47
3.2 Objectives 47
3.3 Significance of the study 48
CHAPTER 4 METHODOLOGY 49
4.1 Location and description of study site 1 - Phalaborwa, South Africa 49
4.2 Sampling points at Phalaborwa 50
4.3 Sample collection from Phalaborwa 53
4.3.1 Sand and rocks 53
4.3.2 Water and Sediments 54
4.3.3 Assorted solid samples 54
4.4 Location and description of study site 2 – Kitwe, Zambia 55
4.5 Sample collection from Kitwe 56
4.6 Chemicals and reagents 58
4.7 Apparatus and instruments used 58
4.7.1 Apparatus used 58
4.7.2 Summary of instruments used 59
4.8 Sample preparation 61
4.8.1 Sample drying and grain size normalization (separation) 61
4.8.2 Leaching procedure 62
4.8.3 Adsorption studies experiments 64

4.8.4 Important steps in Adsorption thermodynamics parameters determination 67
4.8.5 Pseudo-total metal content microwave digestion procedure..... 69
4.8.6 Microwave assisted modified Community Bureau of Reference ... 69
4.9 Quality Assurance (QA) and Quality Control (QC) 72
4.10 Data treatment..... 73
4.10.1 Stiff plots..... 73
4.10.2 PHREEQC 73
4.10.3 Partitioning of trace elements in sediments 73
4.10.4 Adsorption models 73
4.10.5 Statistical treatment..... 73
CHAPTER 5 RESULTS AND DISCUSSION 75
5.1 Characteristics of reconnaissance geologic samples from Phalaborwa..... 75
5.1.1 Mineral identification and element semi-quantification 75
5.1.2 Leachate characteristics of reconnaissance geologic samples 80
5.2 Characteristics of surface water from Phalaborwa 84
5.2.1 Physicochemical parameters 84
5.2.2 Chemical composition of surface water samples..... 85
5.3 Characteristics of assorted solid samples from Phalaborwa..... 90
5.3.1 Mineral identification and element semi-quantification 90
5.3.2 Leachate characteristics 94
5.3.3 Cu-crust leachate for predictive evaporation (dilution) simulations model ……100
5.4 REEs and U in leachates of assorted geologic solid mine waste and sediments..... 120
5.5 REEs Recovery using natural magnetite (Mgt) 121

5.5.1 The effect of adsorbent mass 121
5.5.2 The effect of adsorbate pH conditions 123
5.5.3 The effect of agitation time 125
5.5.4 The effect of adsorbate initial concentration 128
5.5.5 The effect of competing ions 130
5.5.6 Adsorption Isotherm studies 132
5.5.7 Adsorption Kinetics studies 135
5.5.8 Adsorption thermodynamics studies 141
5.6 Characteristics of surface water floor sediments from Phalaborwa . 148
5.6.1 Mineral identification and semi-quantification 148
5.6.2 Characteristics of sediment leachates 152
5.7 Sequential extraction 153
5.8 Biological significance of metal concentration in sediments 156
5.9 Geochemical speciation modelling of surface water 157
5.9.1 Soluble species distribution in surface water 158
5.9.2 Mineral precipitates 159
5.10 Characteristics of stream water from Kitwe 161
5.10.1 Physicochemical parameters 161
5.10.2 Chemical composition 162
5.11 Characteristics of tailings and stream bed sediment from Kitwe 166
5.11.1 Mineral identification and semi-quantification 166
5.11.2 Elemental analysis: carbon to sulphur ratio (C/S) 168
5.11.3 Leachates chemical of tailings and stream floor sediment 170
5.12 Hierarchical clustering multivariate of water sampling points (Kitwe) ……175

5.12.1 Clustering sampling points by spatial similarities relative to Tailings points 175
5.12.2 Clustering experimental parameters by behavioural similarities in samples 176
CHAPTER 6 CONCLUSION AND RECOMMENDATIONS 178
6.1 Conclusion 178
6.2 Recommendations 180
REFERENCES 181
APPENDIX 200

LIST OF FIGURES

Figure 2.1: Original above ground view of the surface geology of PIC. The middle pegmatoid is framed in a rectangle. Adapted from Frick (1986)..... 6

Figure 2.2: Schematic representation of the original above ground view of the central pegmatoid of the Loolekop Mountain, the vertical transgressive view of its core pipe and the current status of the open pit mine..... 7

Figure 2.3: Open pit mine at PMC. (From Google map)..... 8

Figure 2.4: Geological map of ZCB showing all major mines located on RL (McGowan et al., 2003). An insert of three mines, in Kitwe, sitting on the RL: Mindolo Shaft in the north, Central Shaft and South Orebody..... 9

Figure 2.5: A schematic concentrator flowchart for copper sulphide ore processing operations. (adapted from KCM flowsheet, Chililabombwe, Zambia). 11

Figure 2.6: Classification and textural triangle for clastic sediments components (sand, silt, and clay). (Zhao et al., 2017)..... 19

Figure 2.7: Typical shapes of surface excess isotherms in dilute solution. Surface-limited isotherm (blue curved line) and surface-unlimited isotherm (black straight line). Effect of interaction between adsorbate on the adsorbent with adsorptive in the fluid (red S-shaped line)..... 24

Figure 2.8: Model humic acid molecular structure fragment with sinusoidal lines indicating other fragment -COOH, -OH, -NH_2, -SH metal binding sites (Montoneri et al., 2008). 34

Figure 2.9: Schematic representation of reaction conditions and possible reaction progressions associated with changes in Eh –pH conditions..... 44

Figure 4.1: Copper mine area (PMC) in Phalaborwa, Limpopo province of South Africa..... 49

Figure 4.2: Two elephants seen at close range within PMC area (Photo by author, 2016). 50

Figure 4.3: a) the Selati River (upper part) behind FOSKOR at a bridge on the road to Phalaborwa Barrage. Thick rubber flaps prevent animals from going beyond the bridge. b) the Selati River (lower part) near its confluence with the Olifants River. 52

Figure 4.4: The Olifants River (upper section) at Hippo Pool resort..... 52

Figure 4.5: Water Retain Dam (WRD) within the mine area..... 53

Figure 4.6: Sand and rocks samples collected during the reconnaissance trip 53

Figure 4.7: (i) elephant dung; (ii) tailings ex-concentrator; (iii) carbonatite; (iv) copper crusts; muddy sediment (WRD shore) and dry sediment (WRD bank).... 55

Figure 4.8: The Copperbelt Province, Kitwe surrounded by other mining towns and distribution of sampling points on the western side of Kafue River stretch in Kitwe. 56

Figure 4.9: Schematic representation of MW mBCR procedure 71

Figure 5.1: Scanning electron microscopy (SEM) under backscattered electron imaging of Sand and Rock1 samples at X778 and X84 respectively. Pyrite mineral (light grey shade) and carbon containing mineral (dark grey shade)..... 80

Figure 5.2: Comparison of major anions in each sample leachate. The two vertical axes cater for the difference in magnitude between Sand and Rocks (left) and PG (right)..... 82

Figure 5.3: Comparison of major cations in each sample leachate. The two vertical axes cater for the difference in magnitude between Sand and Rocks (left) and PG (right)..... 83

Figure 5.4: pH and EC in surface water within and around the mine area 85

Figure 5.5: Dominant major anions concentration in surface water. The Selati River (SFB and SbC) contrasted with the upper and lower sections of the Olifants River (OHP, ObC, OaC, OMW (left hand side), and with WRD (right hand side) 86

Figure 5.6: Dominant major cations concentration in surface water. The Selati River (SFB and SbC) contrasted with the upper and lower sections of the Olifants River (OHP, ObC, OaC and OMW (left hand side), and with WRD (right hand side)..... 87

Figure 5.7: Stiff diagram representation of water composition at selected sampling spots on the Olifants and the Selati Rivers and the water retain dam. .. 87

Figure 5.8: Total dissolved concentration (µg L^{-1}) of trace elements in surface water. WRD elevated concentrations of trace elements dwarf concentrations in rivers (because of differences in magnitude) (RSD < 10%) 89

Figure 5.9: Time wise EC increases from paste solution to leachates of assorted samples..... 95

Figure 5.10: a) Copper crusts in the field; b) Intense blue colour of leachates obtained from Copper crusts sample..... 96

Figure 5.11: Major anions concentration in assorted solid sample leachates on different vertical axes scales in a) and b). 97

Figure 5.12: Changes in minerals SI for representative members of some mineral groups for different combinations of pH (2, 4.5 and 7), pe (4 and 7.5), and percentage evaporation (10%, 50% and 95%). 108

Figure 5.13: Changes in minerals SI for representative members of some acid-base, neutral and redox groups of minerals for different combinations of pH (7, 9.5 and 11), pe (4 and 7.5) in 50% evaporated and 50% diluted solutions..... 112

Figure 5.14: Evolution of acid/base species with respect to incremental changes of pH and pe 118

Figure 5.15: Evolution of redox species with respect to incremental changes of pH and pe 119

Figure 5.16: Concentration of REEs and U in solid waste and sediments samples from PMC. (REEs and U were not detected in Mgt and SFB leachates)..... 120

Figure 5.17: REEs recovery efficiency obtained from varying mass (50, 100, 150, 200, 300 and 500 mg) of Mgt (adsorbent), in 15 mL REEs solution at pH 2.2 (RSD < 5%)..... 122

Figure 5.18: REEs recovery capacity obtained from varying mass (50, 100, 150, 200, 300 and 500 mg) of Mgt (adsorbent), in 15 mL REEs solution at pH 2.2 (RSD < 5%)..... 122

Figure 5.19: REEs recovery efficiency obtained from varying pH of 1 mg L^{-1} REEs adsorptive carrying solutions and 150 mg Mgt (RSD < 5%)..... 124

Figure 5.20: REEs recovery capacity obtained from varying pH of 1 mg L^{-1} REEs adsorptive carrying solutions and 150 mg Mgt (RSD < 5%)..... 125

Figure 5.21: REEs recovery efficiency obtained for different agitation times of the adsorptive – adsorbent mixtures at pH 4.5, 150 mg adsorbent and 1.0 mg L^{-1} solution (RSD < 5%)..... 126

Figure 5.22: REEs recovery capacity obtained for different agitation times of adsorptive – adsorbent mixtures at pH 4.5, 150 mg adsorbent and 1.0 mg L^{-1} solution (RSD < 5%)..... 127

Figure 5.23: Diminishing REEs recovery capacity for different additional agitation times. 127

Figure 5.24: REEs recovery efficiency obtained from sequential adsorption experiment..... 128

Figure 5.25: REEs recovery efficiency obtained from sequential adsorption experiment at pH 4.5, 150 mg adsorbent and at 150 rpm (RSD < 5%) 129

Figure 5.26: REEs recovery efficiency obtained from sequential adsorption experiment at pH 4.5, 150 mg adsorbent and at 150 rpm (RSD < 5%) 129

Figure 5.27: REEs and competing ions recovery efficiency obtained from a mixed concentration of target elements solution. 131

Figure 5.28: REEs and competing ions recovery efficiency obtained from a mixed concentration of target elements solution. 131

Figure 5.29: Langmuir adsorption isotherm for interactions of Ce with Mgt.... 132

Figure 5.30: Langmuir adsorption isotherm for Ce adsorptive on Mgt adsorbent 133

Figure 5.31: Freundlich adsorption isotherm for Ce adsorptive on Mgt adsorbent 134

Figure 5.32: Pseudo-first order kinetic isotherm for Ce adsorptive on Mgt adsorbent 136

Figure 5.33: Pseudo-second order kinetic isotherm for Ce adsorptive on Mgt adsorbent 137

Figure 5.34: The Arrhenius equation plot used to find the activation energy for the adsorption of Ce onto Mgt 141

Figure 5.35: The Erying equation plot used to find the activation enthalpy and activation entropy for the adsorption of Ce onto Mgt..... 142

Figure 5.36: The Gibbs free energy equation plot used to find the standard enthalpy and the standard entropy for the adsorption of Ce onto Mgt..... 143

Figure 5.37: The Clausius-Clapeyron equation plot used to find the isosteric heat of adsorption for the adsorption of Ce onto Mgt 145

Figure 5.38: XRD graphs pattern for mineral identification in sediments (a) ObC (b) SbC and (c) WRD..... 149

Figure 5.39: Elemental composition expressed as C, H, N, S wt% (data label) and as relative percentage (vertical axis) in sediment samples..... 151

Figure 5.40: (a) Relative distribution of trace metals in various BCR (mobile) fractions of the Selati and Olifants Rivers sediment within a copper mine area. (b) Mobile fractions (left) caped with residual fractions. 154

Figure 5.41: Predominant soluble metal species which contributed over 95% of the total concentration for a given metal in surface water. 159

Figure 5.42: Surface water simulation precipitates obtained from PHREEQC output data..... 160

Figure 5.43: a) and b) Iron soluble species in surface water and c) iron precipitates in WRD 161

Figure 5.44: Trace elements content in sediment and tailings (converted from weight percentage element oxides) 168

Figure 5.45: Elemental content (wt% C, H, N and S) in sediments and tailings 170

Figure 5.46: Bar chart plot of concentration of major anions in tailings obtained by TCLP (acetic acid = aa) (pattern fill) and sulphate concentration in tailings obtained by DI water leaching (solid fill). Actual concentration for F^- and SO_4^{2-} are ten times higher than the concentrations of Cl^- and NO_3^-. 171

Figure 5.47: Side by side bar chart plot of concentration of major cations in tailings obtained through DI water leaching (DI) and TCLP (acetic acid = aa) . 172

Figure 5.48: Concentration of trace metals in tailings obtained by TCLP. 173

Figure 5.49: Concentration of trace metals in tailings obtained by TCLP. The actual concentrations of Cu and Mn can be obtained by multiplying the concentrations presented in this by ten (10x) than other trace elements investigated in this study. 173

Figure 5.50: Grouping of stream water sampling points according to their spatial similarities in chemical composition. Colours and numbers indicate different clusters at 90% similarities..... 176

Figure 5.51: Grouping of stream water analytical parameters according to their behavioural similarities in different stream water samples. Clustering at 50% and 90% similarities are indicated. 177

LIST OF TABLES

Table 2.1: The lithology of the Lower Roan group in Kitwe district..... **Error! Bookmark not defined.**

Table 2.2: Description of particle size range and quantification relative to their involvement in biogeochemical reactions. Adapted from [a]Wentworth, (1922) and [b](Foth, 1990). 18

Table 2.3: The sequence of redox reactions as a function of Eh. Adapted from Price (2009). 42

Table 4.1: Sampling sites identification codes, Global Positioning System (GPS) coordinates and description..... 51

Table 4.2: Samples identification and description 55

Table 4.3: Sampling points description and samples identification 57

Table 4.4: A mix of sulphate, nitrate and chloride salts selected for the effect of competition experiment and their measured concentrations in two different competing solutions with ~ 0.5 mg L^{-1} REEs. 64

Table 5.1: XRD mineral identification in PG, sand and rock samples..... 76

Table 5.2: Semi-quantitative (wt%) XRF overall composition analysis of major elements (as metal oxides) in PG, sand and rock samples 78

Table 5.3: Semi-quantitative (wt%) EDS overall composition analysis of trace elements in PG, sand and rock samples 79

Table 5.4: Paste pH, paste EC and leachates EC of PG, sand and rock samples . 81

Table 5.5: Leachate concentrations of selected elements in PG, sand and rock samples from Phalaborwa. 83

Table 5.6: Total dissolved concentration (µg L^{-1}) of trace elements in surface water 88

Table 5.7: Pearson correlation matrix of analytical parameters in surface water (Olifants River, Selati River and water retain dam) within and around a copper mine area in Phalaborwa. 90

Table 5.8: XRD mineral identification in assorted solid samples 91

Table 5.9: Semi-quantitative (wt%) XRF overall composition analysis of major elements (as metal oxides) in selected solid samples..... 92

Table 5.10: XRF quantitative assessment (mg kg^{-1}) of trace elements in assorted samples 93

Table 5.11: Grain size characteristics in assorted samples by laser diffraction analysis 94

Table 5.12: Paste and EC in assorted solids leachates within and around the mine area 95

Table 5.13: Concentration of major cations in assorted solid sample leachates .. 97

Table 5.14: Concentration of trace elements in assorted solid samples leachates 97

Table 5.15: Pearson correlation matrix of analytical parameters in leachates of surface water sediments and assorted mine waste samples from a copper mine in Phalaborwa. 99

Table 5.16: Specimen of input data for Cu-crust leachate initial solution for 10% evaporation and 50% dilution 100

Table 5.17: Total concentrations in mg kg^{-1}_{water} at different evaporation (dilution) levels 104

Table 5.18: Minerals SI extracted from PHREEQC speciation outputs of Cu_crust leachate solution for different combinations of pH (2, 4.5, 7, 9.5 and 11), pe (5 and 7.5) and percentage evaporation (10%, 50% qnd 95%). 106

Table 5.19: Minerals SI extracted from PHREEQC speciation outputs of Cu_crust leachate solutions for different combinations of pH (2, 4.5, 7, 9.5 and 11), pe (5 and 7.5) for comparison of 50% evaporation and 50% dilution with their initial solutions. 110

Table 5.20: Total concentration, distribution and abundance (%) of acid/base and neutral species relative to changes of pH and change in magnitude of total concentration of acid/base and neutral species with respect to pe 116

Table 5.21: Total concentration, distribution and abundance (%) of redox species relative to changes of pH and change in magnitude of total concentration of redox species with respect to pe. 117

Table 5.22: Recovery efficiency and capacity under the effect of initial concentration 130

Table 5.23: Calculated values from Langmuir adsorption isotherm equation ... 139

Table 5.24: Calculated values from Freundlich adsorption isotherm equation.. 139

Table 5.25: Calculated values from Dubinin - Radushkevich adsorption isotherm equations 139

Table 5.26: Calculated values from PSO adsorption kinetic model equation.... 140

Table 5.27: Activation energy for the adsorption of REEs onto natural magnetite calculated by fitting experimental data into the Arrhenius equation 146

Table 5.28: Activation parameters for the adsorption of REEs onto natural magnetite calculated by fitting experimental data into the Eyring equation..... 146

Table 5.29: Thermodynamic parameters for the adsorption of REEs onto natural magnetite calculated using the classical Van't Hoff equation and the Gibbs free energy equation 147

Table 5.30: Isosteric heat of adsorption for the adsorption of REEs onto natural magnetite calculated using the Clausius-Clapeyron equation..... 147

Table 5.31: Major elements expressed as weight percentage composition in sediment samples after conversion from weight percentage metal oxides assessed by XRF analysis. 150

Table 5.32: Trace elements composition (mg kg^{-1}) in sediments samples measured by XRF analysis..... 150

Table 5.33: Sediment grain sizes and texture..... 152

Table 5.34: Decreasing order of relative (%) and actual (mg kg^{-1}) bioavailable amounts of metals in extracted mobile fractions 155

Table 5.35: Bioavailable concentration of trace elements in sediments 156

Table 5.36: PHREEQC input data used for water simulation in the copper mine area 158

Table 5.37: Dissolved concentrations of major ions and selected trace elements in stream water samples from a mine area in Kitwe 164

Table 5.38: Mineral identification converted from XRD graph patterns of tailings (T32 and T45) and sediments (WS31 and WS32) into a tabulated format..... 167

LIST OF ABBREVIATIONS

ABA	Acid-Base Accounting
AMD	Acid Mine Drainage
BCR	Community Bureau of Standards
C_A	Adsorptive concentration
CACB	Central African Copperbelt
CB	Copperbelt Province
Cbt	Carbonatite
CEC	Cation Exchange Capacity
CFC	Cat fish carcass obtained at the bank of Water Retain Dam
CHNS	Carbon Hydrogen Nitrogen Sulphur
COMESA	Common Market for Eastern and Southern Africa Countries
CRM	Certified reference material
Cu-crusts	Copper crusts
Cumecs	Cubic meters per second ($m^3 s^{-1}$)
DI	Deionized water
DRC	Democratic Republic of Congo
DSTP	Deep-Sea Tailings Placement
E_a	Activation energy (kJ mol^{-1})
EC	Electrical Conductivity
Eh	Reduction Oxidation Potential
FA	Filtered Acidified
FOSKOR	The Phosphate Development Corporation
FUA	Filtered Unacidified
GDP	Gross Domestic Products
h	Plank constant (6.6261 x 10^{-34} Js)
IC	Ion Chromatography
IT	Information Technology
K_{ads}	Adsorption rate constant
K_B	Boltzman constant (1.3807 x 10^{-23} J K^{-1})
K_D	Distribution constant

K_{des}	desorption rate constant
K_L	Langmuir constant
KNP	Kruger National Park
LOD	Limit of Detection
LOQ	Limit of Quantification
LPS	Laser Particle Sizer
MEMI	Mineral Extractive Mining Company
Mgt	Magnetite
MW mBCR	Microwave
OaC	Olifants River after Confluence
ObC	Olifants River before Confluence
OHP	Olifants River at Hippo Pool
OM	Organic Matter
OMW	Olifants River at Mamba Weir
ORP	Oxidation Reduction Potential
OS mix	Olifants and Selati River waters mix
PAC	Phalaborwa Igneous Complex
pe	electron potential
PEC	Probable Effects Concentration
PEQ	Probable Effects Quotient
pH	Hydrogen Potential
PIC	Phalaborwa Igneous Complex
PMC	Palabora Mining Company Limited
PMC/KNP	Palabora Mining Company/Kruger National Park boundary
PTFE	Polytetrafluoroethylene
PXRD	Powder X-ray Diffraction
QA	Quality Assurance
QC	Quality Control
q_{max}	Maximum concentration of adsorbate on the adsorbent
R	Gas constant (8.3145 J mol^{-1} K^{-1})
r_{ads}	Adsorption rate
r_{des}	Desorption rate

RL	Lower Roan
RU	Upper Roan
SADC	Southern African Development Community
SbC	Selati River before Confluence
SEM-EDS	Scanning Electron Microscopy - Electron Dispersive X-ray Spectroscopy
SEP	Sequential Extraction Procedure
SFB	Selati River at FOSKOR Bridge
SI	Saturation Index
SQGS	Sediments Quality Guidelines
STD	Submarine Tailings Disposal
T	Absolute temperature (K)
TCLP	Toxicity Characteristic Leaching Procedure
TEC	Threshold Effects Concentration
TexCon	Tailings ex-Concentrator
UFA	Unfiltered Acidified
UFUA	Unfiltered Unacidified
USEPA	United States Environmental Protection
WHO	World Health Organization
WRD	Water Retain Dam
WRD(b)	Dry sediments at the bank of Water Retain Dam
WRD(s)	Muddy sediments at the bank of Water Retain Dam
WRD-PG	Phosphogypsum at the bank of Water Retain Dam
XRF	X-ray Fluorescence
ZCB	The Zambian Copperbelt
ΔG^*	Gibbs free energy of activation (kJ mol^{-1})
ΔG^o	Gibbs free energy change of reaction (kJ mol^{-1})
ΔH^*	Enthalpy change of activation (kJ mol^{-1})
ΔH^o	Enthalpy change of reaction (kJ mol^{-1})
ΔH_x	Isosteric enthalpy change of reaction (kJ mol^{-1})
ΔS^*	Entropy change of activation (J mol^{-1})
ΔS^o	Entropy change of reaction (J mol^{-1})

α	Intercept of linearised Langmuir equation
β	Slope of linearised Langmuir equation
θ	Fraction of occupied sites

CHAPTER 1 INTRODUCTION

This chapter constitutes the entry point to the content of this thesis. It brings to light, in a common way, the background, context and motivation of the study.

1.1 Background of the study

The products of the Mineral Extractive Mining Industries (MEMI) have globally colonized nearly every sphere of modern life: from construction industries (Fe) through electrical power generation and transmission industries (Cu) to Information Technology (IT) industries (Si, REEs), just to name but a few (Kossoff *et al.*, 2014; Vidal *et al.*, 2017; Elsaidi *et al.*, 2018). The very existence of MEMI has produced tremendous ripple effects in indirect employment creation (innovation, contractor and supplier industries) and inherent contribution to Gross Domestic Product (GDP) (Kossoff *et al.*, 2014; Carvalho, 2017; Pietrobelli, Marin and Olivari, 2018). However, social and economic benefits derived from MEMI have come at an environmental cost: the voluminous sulphidic solid waste and their content of potentially toxic contaminants (Jamieson, 2011; Dold, 2014b; Jamieson, Walker and Parsons, 2015).

Extracted rock minerals that are brought to the surface of land contain ore and gangue minerals which are set apart from each other, mechanically (Price, 2009). Ore minerals, which are of potential economic value, undergo physical and chemical treatments for the extraction of metals. These operations generate, along with targeted metal(loid)s, solid and liquid waste that contain soluble and particulate contaminants (Jamieson, Walker and Parsons, 2015). On the contrary, gangue minerals, which are of less or no economic value, are left in the open, exposed to air and water, predisposed to undergo oxidative dissolution (Dold, 2014b, 2014a). Both, processed and unprocessed mine waste, can release chemical drainage, as impoundments overflow/leakage and leachate run offs, which pose deleterious effects to the aquatic ecosystem (Kossoff *et al.*, 2014).

Mine tailings and mine drainage (acidic, near-neutral or alkaline) are particularly recognized worldwide, among mine waste, for their voluminous quantities and high

content of potentially toxic elements (Nordstrom and Alpers, 1999; Dold, 2014a; Majzlan *et al.*, 2018). Additionally, surface water and its bottom floor sediments are viewed, globally, as the main casualties of mine waste discharge (Seymore *et al.*, 1994; Sracek *et al.*, 2012; Carvalho, 2017).

The impacts of MEMI on the environments have always been around; wherever sulphide mineral-water-air interactions occurred, the release of toxic and bioavailable elements to surface water and underground water occurred as well (Hodges, 1995; Edwards *et al.*, 2000; Carvalho, 2017). Environmental impacts were, for a very long time, neglected and relegated to the second plan until recently when they have started receiving due attention (Carvalho, 2017).

Being consciously aware of the adage "water is life", and having witnessed the extent to which mining has transformed man's way of life to the better, it has been a huge dilemma for man to sacrifice either of the two (Hodges, 1995). While seemingly embracing both, man's actions have shown some inclinations towards profit making under the cover of "sustainable development" (Hodges, 1995; Carvalho, 2017; Gorman and Dzombak, 2018; Aznar-Sánchez *et al.*, 2019). Consequently, striking a balance between the pursuit for maximum profits from mineral production and the protection of the environment from mine waste will still remain a challenge.

1.2 Context of the study

Two MEMI located miles away from each other, Phalaborwa in South Africa and Kitwe in Zambia, share the exploitation of copper from sulphidic rocks and the abundance of carbonate minerals which buffer the acid generated from sulphide minerals oxidation (Mine Geological and Mineralogical Staff, 1976; Sracek *et al.*, 2010) as their common features. These two countries, located south of the equator, share the same sub regional groupings: (i) The Common Market for Eastern and Southern Africa Countries (COMESA) and (ii) the Southern African Development Community (SADC), for political, trade and security cooperation. Lately, research cooperation has come on board at bilateral level.

On one side, owing to its geographic position upstream of, and adjacent to, a conservative area, the Kruger National Park (KNP), Palabora Mining Company (PMC) has been pointed at as the principal contributor of metallic contaminants to surface water and its floor sediments, and subsequent harmful effects to the life system dependent on them (Kotze, Du Preez and Van Vuren, 1999; Avenant-Oldewage and Marx, 2000). On the other side, tailings dumps within residential community, scars of copper mining in Kitwe, are connected, through low land paths, to streams that collect and drain tailings releases to the Kafue River. They, too, have been incriminated for eco-toxicity in feeder streams and the collector river (Sracek *et al.*, 2011). Besides surface water and sediments metal pollution, findings about the negative effects of mine waste (tailings) on agricultural soils and plants have also been reported in the sub region (Ashton *et al.*, 2001; Meck, Love and Mapani, 2006; Kříbek *et al.*, 2010; Ettler *et al.*, 2014, 2019; Mileusni *et al.*, 2014; Nejeschlebová *et al.*, 2015).

1.3 Motivation of the study

Generally, so much focus is placed on benefits derived from active mine operations and only pretentious attention is given to harmful effects they cause to the environment until such a time when the mines are closed or abandoned, leaving behind a burden of mine waste legacy (Perera, 1981; Banks *et al.*, 1997; Shahid and Qiren, 2010). In the context of environmental sustainable development, man is obliged to act in the best interest of the environment, play the stewardship role and never wait until the damage is irreversible or reversible at very heavy costs (Hodges, 1995). To evaluate the pollution potential of assorted solid mine waste and the pollution state of surface water and its bottom sediments in the immediate surroundings of an active copper mine conspicuously located upstream of a national conservation area (Wepener, Van Huren and Du Preez, 1999) and a copper mine with tailings legacy found within residential communities (Perera, 1981; Sracek *et al.*, 2011) offered an appropriate perspective for this research. Additionally, predictive assessment of the implications of the ever worsening climate conditions (severe heat and drought) on biota dependent on the aquatic ecosystem, and applicable recovery (remediation) of valuable (toxic) elements using abundant, local and natural mine waste such as Mgt widened this perspective.

CHAPTER 2 LITERATURE REVIEW

This chapter seeks to encircle different literature of relevance to the subject matter, linking and converging them towards coherence. Captured topics include brief history of local copper mining, the geology and mineralogy of sulphidic and carbonate rocks, copper mine operations, mine waste and their geochemistry among many other subjects.

2.1 Copper in ancient and modern times

The passage from Stone Age to Bronze Age era signified a step forward in human civilization's long journey towards modernity (Beale, 1985a; Calas, 2017). Copper ore was mined, heated and reacted to produce copper metal in usable form, in what was called the chalcolithic Age (Hudson-Edwards, Jamieson and Lottermoser, 2011). Bronze, a copper-tin alloy, allowed the use of copper for contemporary needs. Archeological evidence of copper and bronze artifacts (as ornamental items, tools and weapons) were found in most places where mining of copper was practiced and traded, along with its subsequent environmental impacts (Beale, 1985a; Jones and Mackey, 2015).

In the course of time, the application of copper and its alloys extended to include various sectors of the economy which contributed significantly to the industrial revolution (Papyrakis, Hess and Beukering, 2006; Adamu *et al.*, 2013). The need for more copper brought about a shift in geographic distribution of copper mines outside Europe and the United States of America (U.S.) and a subsequent, unprecedented and dramatic, ascendancy in world copper production (Banks *et al.*, 1997; Papyrakis, Hess and Beukering, 2006; Lindahl, 2014).

With the exhaustion of native and high grade copper, modern civilization has experienced gradual technological improvement in mining and processing of lower copper ore grade (Lydall and Auchterlonie, 2011; Dold, 2014b). Consequently, decreasing metric tons of metal have been produced, every year, from fast and ever increasing metric tons of rock minerals, thereby exposing more gangue minerals and discharging more processed waste (Hodges, 1995; Jamieson, 2011; Dold, 2014b). In spite of this unfriendly side of mining

towards the environment and, the competition from superconducting and fiber optic materials with similar properties in electricity and telecommunication transmission, besides recycling, the demand for copper, for a variety of uses, has been ceaselessly increasing (Papyrakis, Hess and Beukering, 2006; Jones and Mackey, 2015).

2.2 Geology and mineralogy of copper ore deposits

2.2.1 Historical background of copper mining in South Africa

The O'okiepek Mountain, in Namaqualand, is known to be the cradle of copper mining in South Africa. The trade of artisanal copper works which happened nearly two centuries ago, has been traced back to the O'okiepek copper deposits (Beale, 1985a; Jones and Mackey, 2015). Through the years, a number of copper mines spread over the country.

Prospective work by Carl Mauch produced, in the third quarter of the nineteenth century (1868-1871), a geological map showing the occurrence of copper deposits in the Loolekop Mountain (Frick, 1986). Soon after this quarter, archaeological studies conducted in the same area, indicated that, actually, copper and iron artisanal activities were practised much earlier in the Loolekop Mountain by the local inhabitants (Frick, 1986). Hans Merensky, in the early twentieth century, involved himself in geological prospections which established the economic status of phosphate, copper and vermiculite in the Loolekop Mountain (Heinrjch, 1970; Beale, 1985b). These findings provoked interest in the Loolekop Mountain and attracted the original investments venture that initiated follow up studies which led to the establishment of PMC and subsequent development of its copper and other associated valuable resources (Heinrjch, 1970; Beale, 1985b; Jones and Mackey, 2015).

2.2.2 Geology of the Phalaborwa Igneous Complex (PIC)

The geology of the Loolekop Mountain was characterised by a large, multistage, intrusive complex known as the Phalaborwa Igneous Complex (PIC), with reference to its formation (origin). It is also known as the Phalaborwa Alkaline Complex (PAC), with reference to its composition. Its geological morphology has been described (Figure 2.1), based on the original view above the current ground surface, as made of the main intrusion

comprised of a thin ring of feldspathic pyroxenite rimming almost the entire large body of pyroxene within which three oval pegmatoidal intrusions were located (Frick, 1986). The middle pegmatoid surrounded the central carbonatite intrusion cushioned, in between, by a foskorite ring. A large number of smaller intrusions known as syenite plugs were scattered all around the main intrusion. Additionally, some crosscutting veins of dolerite dykes were also found in the main complex (Eriksson, 1984; Frick, 1986).

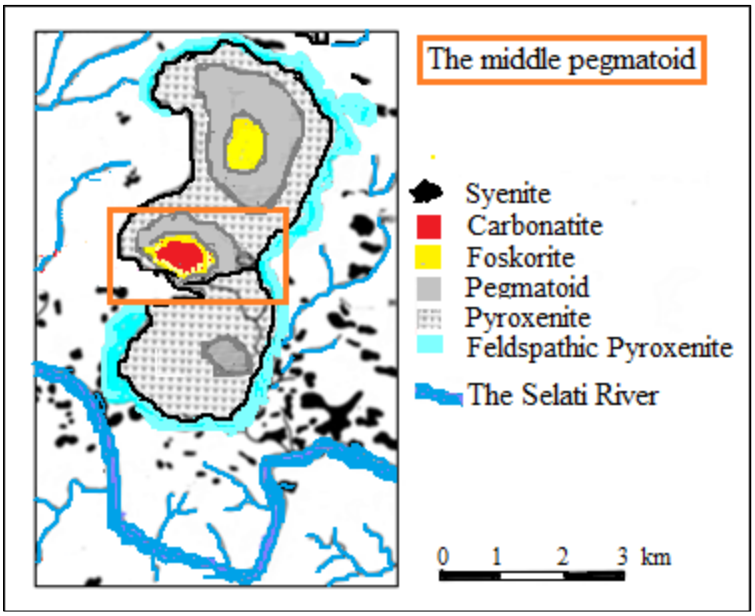


Figure 2.1: Original above ground view of the surface geology of PIC. The middle pegmatoid is framed in a rectangle. Adapted from Frick (1986)

The vertical cross sectional view through PIC showed the transgressive carbonatite core pipe standing tall into the ground, surrounded successively by the banded carbonatite, and foskorite (Fig 2.2). These intrusions were a particularity of the central pegmatoid and constituted the center of attraction for profitable copper mining. The ultramafic rock constituted of outward layers of pyroxenite, namely the pegmatic, micaceous and feldspathic pyroxenites, formed the final ring to complete the intrusion (Eriksson, 1984; Frick, 1986).

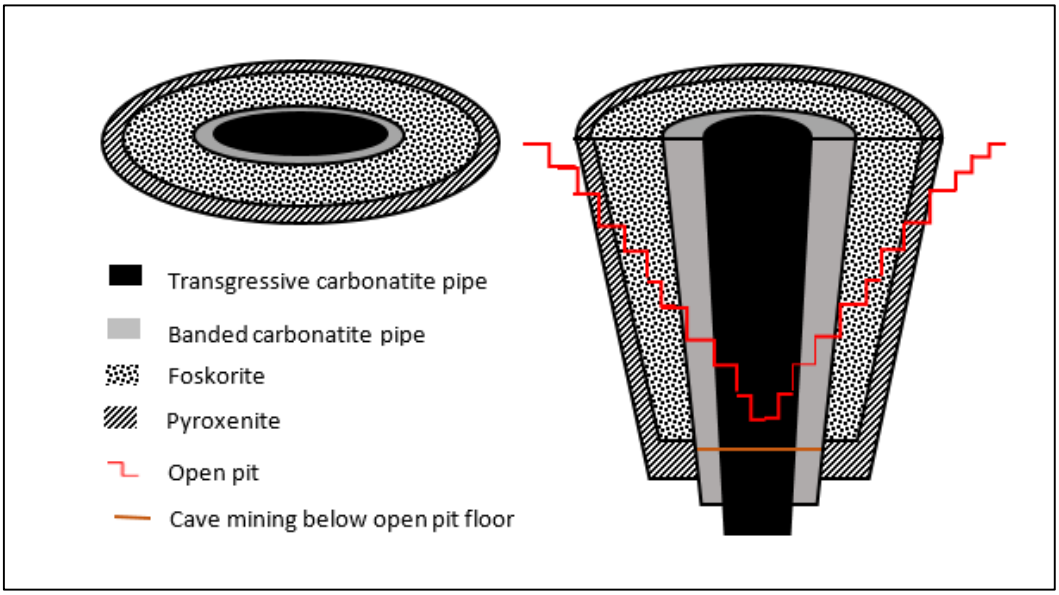


Figure 2.2: Schematic representation of the original above ground view of the central pegmatoid of the Loolekop Mountain, the vertical transgressive view of its core pipe and the current status of the open pit mine.

PIC is aged 2060±2 Ma, slightly above two billion years (2 Ga) (Heinrjch, 1970; Eriksson, 1984; Frick, 1986). Its carbonatite is a rock of volcanic origin made up of over 50% calcite, i.e. a carbonatite, with smaller amounts of titaniferrous magnetite (iron mineral), apatite (Phosphor mineral) and copper bearing minerals (Heinrjch, 1970; Eriksson, 1984; Frick, 1986). The effective exploitation, by open cast mining, of copper (about 1%) as its principal mineral, complemented by vermiculite, uranium, zirconium and some valuable minerals as byproducts, singles out the PAC from similar complexes in the whole world (Mine Geological and Mineralogical Staff, 1976; Frick, 1986; Howie, Cairncross and Dixon, 1996).

2.2.3 Mineralogy of the Phalaborwa Igneous Complex

The mineral description of any given geological setting opens up to prediction of its geochemical behaviour, and provides a basis for comparison of data from other similar sites (Price, 2009). Chalcopyrite ($CuFeS_2$), with minor cubanite ($CuFe_2S_3$) is most abundant in the transgressive carbonatite centermost pipe and in the veins. Bornite (Cu_5FeS_4), sometimes associated with chalcocite (CuS_2), is predominant in the annular

banded carbonatite and foskorite. Pyrite (FeS_2) and pyrrotite (($Fe_{(1-x)}S$), with x varying from 0.125 (Fe_7S_8) to 0.0 (FeS), troilite) are present as trace in the carbonatite section (Heinrjch, 1970). This mineralisation extended deep down and continued beyond the foreseen and conceived final open-pit floor. The economic content of copper in these sections of PIC have been exploited to its bottom floor as shown in Figure 2.3 below (Beale, 1985b).

Block cave mining method is now used to extract copper in the extended portion of the carbonatite pipe. Vermiculite $(Mg,Fe^{+2},Fe^{+3})_3[(Al,Si)_4O_{10}](OH)_2 \cdot 4H_2O)$ is being mined in the south pyroxenite area as an important accessory mineral. Ore treatment permits the recovery of metals such as uranium and zirconium. Gold, silver, platinum, nickel and palladium are recovered in small amounts, as by-products, from other minerals such as uranothoriunite (UO_2) and baddeleyite (ZrO_2). Magnetite (iron mineral, $FeFe_2(O)_4$) and apatite (phosphor mineral, $Ca_5(PO_4)_3(F, Cl, OH)$) are found in economic amounts in the foskorite section.



Figure 2.3: Open pit mine at PMC. (From Google map)

2.3 Geology and lithology of copper ore setting in the Copperbelt, Zambia

The Central African Copperbelt (CACB) is an estimated 900 kilometres long Neroproterozoic Lufilian Arc that stretches from the north-western part of the Katanga Province in the Democratic Republic of Congo (DRC) all the way into the south-eastern part of the Copperbelt Province (CB) in Zambia (McGowan *et al.*, 2003). It is known to have accumulated a substantial amount of, and a significantly high grade, copper-cobalt deposits in its sediment-hosted stratigraphy. In the external fold-thrust belt of the Lufilian Arc, the Lower Roan Group (RL) sedimentary sequence of the Katangan Supergroup is the dominant ore-bearing sequence in the Zambian share of CACB (Cailteux *et al.*, 1994; McGowan *et al.*, 2003; McGowan, Roberts and Boyce, 2005). The copper-cobalt ore deposits, in the Zambian Copperbelt (ZCB), are economically exploited, in all Copperbelt mining districts, from RL (Fig 2.4).

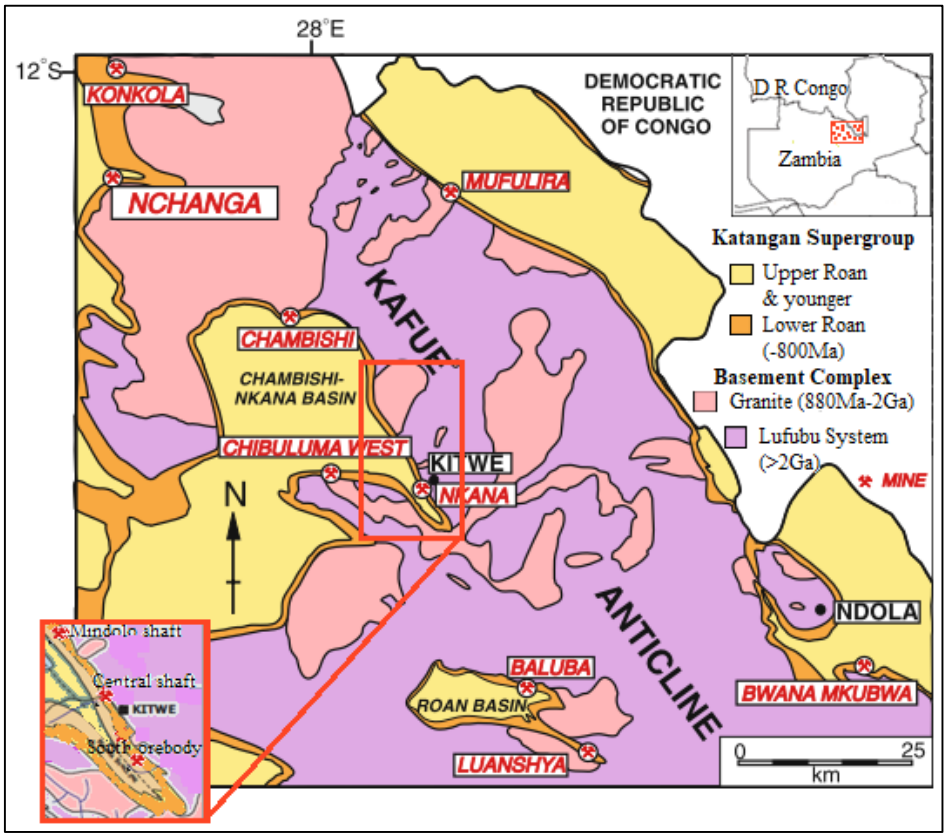


Figure 2.4: Geological map of ZCB showing all major mines located on RL (McGowan et al., 2003). An insert of three mines, in Kitwe, sitting on the RL: Mindolo Shaft in the north, Central Shaft and South Orebody.

Theories of the genesis and processes which led to copper-cobalt ore formation in ZCB have been reinterpreted in various studies (Cailteux *et al.*, 1994; McGowan *et al.*, 2003; Torremans *et al.*, 2013). Nevertheless, research findings converged in that the copper-cobalt ore deposits are of sedimentary origin. The geology of ZCB is described in terms of age divided into major groupings. The Neroproterozoic rock of the Katangan Supergroup hosts the copper-cobalt mineralisation of ZCB. Its stratified ore reveals that the bulk of copper-cobalt minerals are embedded, at lower concentrations in the Upper Roan Group (RU) and, at elevated concentrations in RL within the Katangan Supergroup (Table 2.1).

2.4 Copper mine operations

2.4.1 Mining and metallurgical process

Beal (1985a) gave an elaborate account of production processes in a copper mine from the mining and metallurgical view point. Excavated rocks are separated into ore and gangue minerals. Ore minerals are ground, milled to fine sand-silt size with large surface area. They are, then, taken to the concentrator where copper sulphide minerals are released and recovered as floatation concentrates. At this point, tailings are discharged as processed waste containing gangue minerals and residual sulphides (Figure 2.5). The ratio of tailings to concentrate is usually very disproportionate (>200:1 tones) and gives an indication of the voluminous tailings burden accumulation (Jamieson, 2011; Kossoff *et al.*, 2014). Concentrates are dried before they are fed into the concentrator and progress through matte production, blister production, anode refining and anode casting. Slag, another solid waste material, is discharged at blister stage and, sulphuric acid could be produced at the same stage if facilities allow. Smelter anode is refined further to produce high grade cathodes with subsequent recovery of nickel sulphate and anode slimes rich in precious metals (Ag, Au, Pt, Pd) as by products. Finally, cathodes are cast into rods which are consumed, in various industries, as pure copper (99.9%) and as cast or wrought alloys. Lindsay *et al.* (2015) indicated that sulphide mineral concentrates were still obtained, through milling and froth floatation, concomitantly with tailings deposition. An

overview of improved copper smelting technologies in some mining companies of the Southern Africa sub-region are given in Jones and Mackey (2015).

2.4.2 Chemical process

Langa *et al.* (2014) evaluated the efficiency of sodium isobutyl xanthate (SIBX) as a collector in the earlier steps of froth flotation. SIBX turns ore mineral particles hydrophobic. Subsequent aeration of the slurry and water results in the formation of bubbles which rise to the surface and attract ore particles to them (Ramirez-llodra *et al.*, 2015). It was established that SIBX did not recover all chalcopyrite into concentrate and that concentrate grade decreased along successive recovery cells. Kalichini (2017), in his turn, determined that the use of sodium hydrogen sulphide (NaHS) as a froth stabilizer in the later steps of froth flotation allowed the recovery of chalcopyrite which was not recovered in the earlier steps of froth flotation (Figure 2.5). This shows that combining SIBX in the earlier steps and NaHS in the later steps of froth flotation improves, tremendously, the recovery of chalcopyrite into the concentrate leaving very little to discharge with tailings.

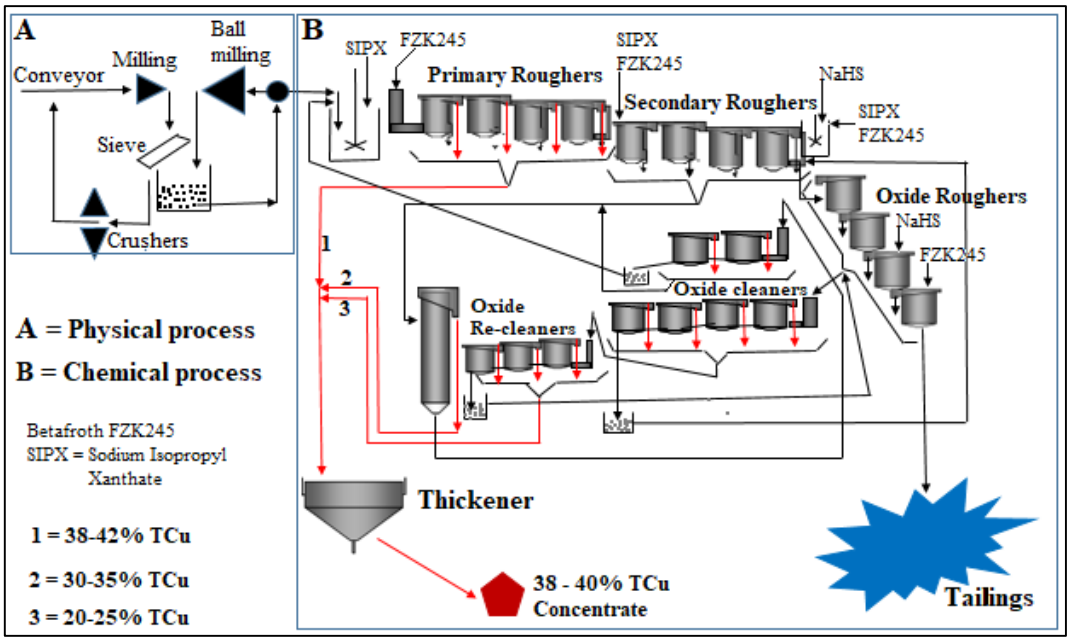


Figure 2.5: A schematic concentrator flowchart for copper sulphide ore processing operations. (adapted from KCM flowsheet, Chililabombwe, Zambia).

Table 2.1: The lithology of the Lower Roan Group in Kitwe district.

Group	Subgroup	Formation	Member		Lithology	
Nguba		Kipushi				
		Kakontwe				
		Mwale				
Roan	Mwashia					
	Upper Roan	Bancroft		RU1		
		Kanwangungu		RU2		
	Lower Roan	Kitwe	Kibalongo	RL3	shales with grit (Antelope Clastics)	
			Chingola	RL4	dolomite, argillite beds at top	
			Pelito arkosic	RL5	arkoses, sandy to dolomitic argillites	
			Ore shale	RL6	arenites, argillaceous dolomites, argillites, dolomites, evaporites; Cu-Co	
		Mindola		RL7	conglomerates, coarse arkoses and argillaceous siltstones	
					quartzites	
					pebble and cobble conglomerate	

Evaporitic depositional environments

Currently, as indicated by Ndoro and Witika (2017), adjustment in chemical conditions of hydrometallurgy could improve the recovery efficiency of copper ore minerals (sulphide, oxide or mixed sulphide/oxide ores).

2.5 Mining practices versus environmental protection

Naturally, copper mining from acid producing ores (chalcopyrite and pyrite), all over the world, have an inherent potential to generate contaminants which could pose a serious pollution threat to the environment as it could negatively impact underground and nearby surface waters (Piatak, Hammarstrom and Ii, 2006; Sracek *et al.*, 2012; Atibu *et al.*, 2013; Abraham and Susan, 2017). The extent of the impact is chiefly dependent on the host rock of a given mine deposit and the waste generated from it. Vermont, USA, provide an illustration of three abandoned mines sharing the same Copperbelt of which Pike Hill deposits was rich in carbonate minerals and, Elizabeth and Ely deposits contained less neutralizing minerals (Piatak, Hammarstrom and Ii, 2006). Their tailings behaviour manifested in nearby surface water as neutral and acidic respectively. The Otjihase Copper Mine deposits near Windhoek, Namibia, which generated acid mine drainage (Hudson, Fox and Plumlee, 1999) and Chambishi Copper Mine which generated near-neutral (or alkaline) mine drainage (Sracek *et al.*, 2012) are some of such contrasting examples of the influence of the parent material on environmental pollution.

Currently, improvement in the mechanization of mining equipment and the advances in mineral processing methods, both aiming at maximizing profits, have led to an increase in the daily quantity of mined waste rocks and in the discharge rate of processed waste, respectively (W&EMBC, 2006; Jamieson, 2011). Consequently, mine drainage volume and leachable amounts of trace metals could increase in proportion with the afore mentioned drastic increase in mine wastes (Jamieson, 2011). Should economic growth be achieved at the expense of environmental destruction?

Water is vital to the sustenance of all forms of life on earth and its fitness for use depends on its various bio-physicochemical characteristics (Banks *et al.*, 1997; Nordstrom and Alpers, 1999). Acid mine drainage changes water characteristics, e.g., by reducing its pH,

increasing its sulphate and dangerous trace metals concentration making it injurious to aquatic and animal life, man included (Soltani *et al.*, 2014). For as long as solid mine waste remain exposed to air and water, pollution from mine drainage may last for decades or even centuries, may be difficult to reverse or irreversible, may be localized or extend to distant places (Sarkar *et al.*, 2014). Anti-pollution proponents, sustainable development agencies, and government departments promote in various ways, using different strategies, environmental protection and encourage mining companies to embrace it and develop practices that prevent or mitigate pollution (Boocock, 2002; Hoadley, Limpitlaw and Weaver, 2002). This is, in an effort to reconcile mining development with environmental protection and mainstream them into sustainable development framework (Lindahl, 2014; Calas, 2017).

2.6 Rare Earth Elements (REEs) as a constituent part of carbonatite ore rock

Carbonatites are igneous rocks known for their accumulation of economically minable elements (in high amounts) such as Cu and P and complexly extractable elements (in small amounts) such as REEs (Xu *et al.*, 2010). This explains, partly, why there are large productions of Cu and P in Phalaborwa, for instance, but REEs are rare and relegated behind. Modal amounts of carbonate minerals and high enrichment of apatite minerals are the main factors controlling the distribution and residence of REEs in carbonatite ore rocks (Hornig-kjarsgaard, 1998). Currently, deposits of REEs are topical because of their use in green and emerging technologies (e.g. wind turbines, catalytic converters) and sensitive applications (Xu *et al.*, 2010; Owens *et al.*, 2019); the more reason why REEs deposits are sought for on Earth, and their search may possibly be extended to places such as the Moon and Mars (Owens *et al.*, 2019).

Carbonatite ore contains a lower percentage of apatite minerals, hosts of REEs. Froth floatation allows the enrichment of apatite in the concentrate which is then leached with H_2SO_4 to produce H_3PO_4 (leachate) and PG (leaching residues) (Yang, Tapani Makkonen and Pakkanen, 2019). At the end of this process, more REEs are collected in beneficiation tailings and PG and less REEs are found in H_3PO_4. Yang, Tapani Makkonen and Pakkanen (2019) discussed the prospective recovery of REEs from the beneficiation of

tailings and PG. Soltani *et al.* (2014) leached apatite concentrate in order to produce H_3PO_4 and REEs as carbonate precipitates through a selective recovery process.

2.7 Tailings

Excavated overburden and gangue minerals are disregarded and dumped/stockpiled as waste because they do not contain or contain target minerals at negligible economic value (Dold, 2014b). However, gangue minerals may, depending on the mineralogy of the parent rock, contain a considerable amount of acid generating sulphide minerals and associated trace elements which can be released as run off (Dold, 2014b). On the contrary, there is much interest in ore minerals which are processed for the beneficiation of extractive mine resources *viz*, base metals, precious metals and so forth. The fine particle slurry, separated from mineral concentrate as waste, forms the bulk of the initial ore minerals (e.g. 99% for Cu, 99.9% for Au) (Kossoff *et al.*, 2014). Hence, it carries with it sulphide minerals and its inherent trace elements. This waste, known as tailings, brings with it two major problems: (i) the demand for storage space and (ii) the permanent threat for environmental impacts (Dold, 2010; Ramirez-llodra *et al.*, 2015; Pedersen *et al.*, 2019). The advent of lower grade ore minerals, coupled with high demand and high price tags for target minerals, have exacerbated these problems (Dold, 2014b; Ramirez-llodra *et al.*, 2015).

In the past, tailings were released and kept under water (rivers and natural dams), seemingly away from oxidizing conditions to which sulphide minerals are reactive (Hudson-Edwards, Jamieson and Lottermoser, 2011; Dold, 2014b). It was discovered afterwards that this practice impaired, in a dramatic way, the aquatic fauna and flora and, human life with lower pH and, elevated toxic elements and sulphate concentration (Ramirez-llodra *et al.*, 2015). Later, engineering constructed (conventional) dams were introduced to seclude tailings. To correlate the volume of tailings produced currently to safe disposal of tailings, more of these impoundments are needed even though they take up more land. However, reported regular occurrences of tailings dams overflow/leakage and partial/total failure indicate that these facilities are not fool proof (Shahid and Qiren, 2010; Kossoff *et al.*, 2014; Ramirez-llodra *et al.*, 2015). Social issues (e.g. tailing dams

in residential areas, scarcity of fertile land) and environmental issues (water pollution, conflict with conservative area) associated with tailings deposition on land are yet to vanish (Perera, 1981; Hodges, 1995; Songolo, Moono and Mwenya, 2016). Attention has turned on to Submarine Tailings Disposal (STD) and Deep-Sea Tailings Placement (DSTP) in some countries such as Norway, Canada and Greenland. STD consists of the disposal of tailings through an underwater pipeline in shallow waters (at < 100 m) which subsequently deposit on sea floor in deeper areas below the euphotic zone whereas DSTP consists of tailings disposal in deep waters (>100 m) through a submerged pipe below the euphotic zone which subsequently deposit on deep sea floor (~1000 m) (Dold, 2014b; Ramirez-llodra *et al.*, 2015). This new project has lured some mining companies and offers a glimpse of hope in as far as inorganic and inert geological materials are concerned (Dold, 2014b; Ramirez-llodra *et al.*, 2015).

Currently, ore rocks are obtained from much deeper down the ground and most of them are sulphidic in nature but, do not exclude oxidation minerals (silicates, carbonates, oxides) (Dold, 2014b; Jamieson, Walker and Parsons, 2015). Mine tailings share the same mineralogical composition as its parent rock and are, commonly, constituted of primary minerals that remain after beneficiation namely, quartz, feldspars, calcite, dolomite and sulphides. They also contain particulate secondary minerals produced from chemical reactions (e.g. goethite, gypsum). Tailings particle size range includes sand and silt. Unlike unprocessed waste, tailings have potential to largely influence chemical reactions due to particles large surface area and interstitial space (Jamieson, Walker and Parsons, 2015; Ramirez-llodra *et al.*, 2015).

2.8 Sediment

The term sediment is used in reference to a collection of particles that settle on the floor of a body of water (NYSDEC, 2014; Zhang et al., 2014). In running water (stream and river), sediment is never static; it moves either as particles in water (suspended load) or as particles in contact with river/stream floor (bed load). The faster the water flow and the finer the particles, the further downstream the load is moved. Owing to this motion and sediment association with contaminants, the effects on benthos are not spatially

localized (Besser, Brumbaugh and Ingersoll, 2015; Hasenmueller *et al.*, 2017; Pedersen *et al.*, 2019).

The nature or origin of particles allow the segregation of sediment into three classes: (i) particulates, (ii) precipitates and (iii) organic sediments (Zhang *et al.*, 2014; Simpson, Batley and Maher, 2016; Reichelt-Brushett, Clark and Birch, 2017). The first class is mainly comprised of particles from rock weathering (e.g. clay, silt and sand); the second class is made of precipitates from natural chemical reactions (e.g. ochres, salt rock and gypsum), the third class is composed of carbon materials from living organisms (e.g. plant and animal discharges and decomposed matter). Inorganic particles or clastic sediments form the most abundant (> 3/4) of the three classes and are, in practice, the most used and, generally, the ones referred to when the term sediment is used in its generic sense. Sieving allows the separation of the analytically useful clastic sediment from the natural sediment mixture obtained from the environment (Xu and Li, 2015). A nest of sieves *viz*, a set of sieves that fit on top of one another, is used to obtain further separation from clastic sediment (sand-silt-clay) which are categorised and named based on their different size range (Wentworth, 1922; Foth, 1990; Xu and Li, 2015). Sediment separation is useful in descriptive nomenclature of geological rocks (Cailteux *et al.*, 1994) as well as in geochemical characterisation of rock related mineral particles (soil, tailings and sediment) (Karaca, Cameselle and Reddy, 2016). Table 2.2 and Figure 2.6 give the nomenclature of relative percentage of different grain size ranges obtainable from mixtures of sand-silt-clay (texture). A similar textural triangle with more soil texture classes, as suggested by the U S Department of Agriculture, in found in Bleam (2017).

Table 2.2: Description of particle size range and quantification relative to their involvement in biogeochemical reactions. Adapted from [a]Wentworth, (1922) and [b](Foth, 1990).

[a]Particle size range	[a]Descriptive name	[a]General category		[b]No of particles (g^{-1})	[b]Surface area ($cm^2\ g^{-1}$)
> 256 mm	Boulder		Rubble		
64 - 256 mm	Cobble gravel	Gravel			
4 - 64 mm	Pebble gravel				
2 - 4 mm	Granite gravel				
1 - 2 mm	Very coarse sand	Sand		90	11
0.5 - 1 mm	Coarse sand			720	23
0.25 - 0.5 mm	medium sand			5,700	45
0.125 - 0.25 mm	Fine sand			46,000	91
0.0625 - 0.125 mm	Very fine sand			722,000	227
0.04 - 0.0625 mm	Silt	Mud		5,776,000	454
0.004 mm	Clay			90,260,853,000	8,000,000

Sediment particles with smaller diameter possess a greater number of electric charges on their surface which gets larger as the particle size gets smaller. These properties give to silt and clay an enhanced ability to pull together, form a larger surface area and provide more sites with better adsorption capacity (NYSDEC, 2014; Reichelt-Brushett, Clark and Birch, 2017). However, these properties are attributed more to their chemical composition rather than to their size. For instance, clays reactivity is due to aluminosilicates minerals organized, structurally, in multi-layer platy sheets. Additionally, clay surface is mostly coated with oxides of Al, Fe and Mn, and organic substances which provides sites for metal accumulation. Particles of similar size but, made of quartz, feldspar or calcite are chemically less reactive or inert (Reichelt-Brushett, Clark and Birch, 2017). Clay charge is independent of pH and remains ever negative (Price, 2009).

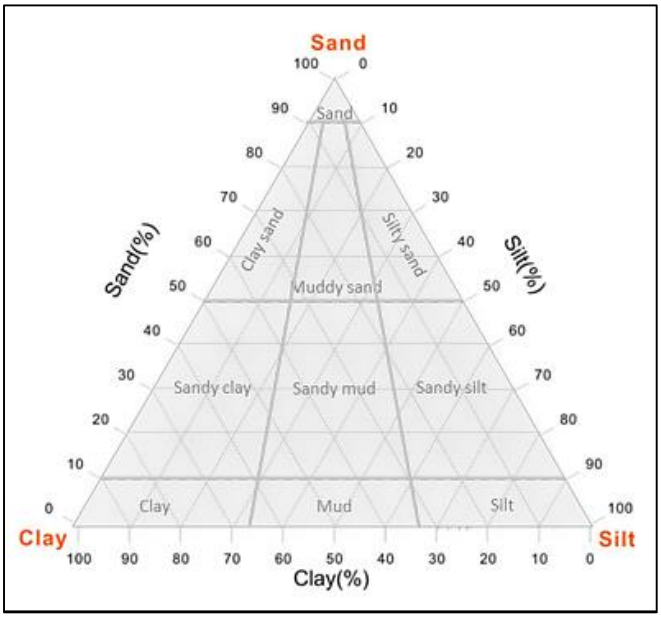


Figure 2.6: Classification and textural triangle for clastic sediments components (sand, silt, and clay). (Zhao *et al.*, 2017)

In the sediment-water system, the "to and fro" movement of contaminants from sediments into water and vice-versa is controlled by pH dependent reactions such as adsorption and desorption, precipitation and dissolution (Jamieson, Walker and Parsons, 2015). Sediments play the role of a contaminant collector or a contaminant sink by binding and accumulating chemical contaminants onto the surface of fine particles until such a time when conditions are favourable for their release into water (Adamu et al., 2013; Saleem et al., 2015). This process of contaminants accumulation can go on for as long as it may take but, the potential for their remobilization remains, though, a looming threat. Undoubtedly, the assumption that contaminants are permanently stored in sediments could be unfounded (Kossoff *et al.*, 2014). Because metallic contaminants are toxic, persistent and non-biodegradable, their release into water, with respect to aquatic fauna and flora, could cause instant harm (e.g. death) or leave behind a trail of delayed biological impairment conditions (e.g. reduced reproduction) (de Villiers and Mkwelo, 2009; Gitari *et al.*, 2018).

2.9 Leaching studies

Interactions between geological material (e.g. tailings) and water (e.g. rain water) is a natural and universal process during which soluble constituents are released from geological material into water (Bouchez *et al.*, 2011; Kossoff *et al.*, 2014). Consequently, the natural condition of water is altered by the increase in the amounts of soluble and particulate constituents, and the subsequent change of pH. Nordstrom and Alpers (2014) noted that this phenomenon was known, several thousands of years back in time, as natural lixiviation (leaching). The chemical composition (potentially toxic and bioavailable elements) of geological waste material run off or seepage constitute a major concern for the environment (Kwok *et al.*, 2014). Determining whether contaminated geological waste have the potential to impact negatively nearby surface or underground water is achieved through leaching. This is a non-aggressive laboratory extraction procedure, simulating environmental conditions, used to assesses metal mobility in geological material (Kwok *et al.*, 2014; Karaca, Cameselle and Reddy, 2016).

A good number of leaching tests are known to have been used for assessing trace metal mobility in sediment (Cappuyn and Swennen, (2008); Karaca *et al.*, 2016). They find their differences in leaching fluid composition, size of particles utilized, mass of solid, liquid to solid ratio, and shaking time, even though, most of them converge in as far as characterisation of material is concerned (Cappuyn and Swennen, 2008). Among this mix of tests, the pH dependence leaching test is considered a central characterisation test to which the majority of other tests could identify with (Guo *et al.*, 2013).

Cappuyns and Swennen (2008) described and applied some common laboratory leaching practices. Laboratory leaching tests fall into two types: (i) Batch (single extraction) tests and (ii) dynamic (multiple extraction) tests. The former is achieved by mixing a solid sample with a known amount of leaching fluid, shaking the mixture and collecting the leachate, after some time, to end the process. The solid to liquid ratio should not allow for saturation. The latter involves mixing of a solid sample with a known amount of leaching fluid in two distinguishable ways: either with periodic collection of leachates and renewal of leaching fluid (e.g., cascade leaching) or with continuous collection of leachates and renewal of leaching fluid (e.g., column leaching), for an extended period of

time in both ways. A large variety of batch and dynamic leaching have been identified (Xu and Li, 2015).

The toxicity Characteristic Leaching Procedure (TCLP) is a batch leaching test that uses size-reduced solid material and glacial acetic acid or its buffer at liquid to solid ratio of 20, a fixed pH dictated by the alkalinity of soil and a slow motion shaking (30 rpm) for 18 hours ±2 (Karaca, Cameselle and Reddy, 2016). TCLP is a rigorous test intended for prediction of labile and toxic elements that could potentially be generated by waste material of a given geological setting. TCLP analytical results are compared with regulatory limits such as the United States Environmental Protection Agency (US-EPA), Preliminary Recommendation Goals (PRG) and/or standards set by concerned countries (Piatak, Hammarstrom and Ii, 2006).

2.10 Adsorption studies

When a solution containing metallic ions (adsorptive) is mixed with (or running through) a molecular solid (adsorbent) in a batch (or column) set up, and agitated to increase the chances of contact between the adsorptive and the adsorbent, adsorption of the adsorptive on to the adsorbent surface takes place (Kajjumba *et al.*, 2018). This adsorption results in the decrease of the adsorptive concentration in the aqueous phase and the concomitant increase of the amount of adsorbate on the solid phase; this process can continue until equilibrium between the adsorptive and adsorbate in the two phases is reached (Rouquerol, Rouquerol and Sing, 1999; Kajjumba *et al.*, 2018; Ugwu and Igbokwe, 2018). The equilibrium relationship attained thereafter and the processes that led to it can be described by linear graphical displays of typical shapes, known as adsorption isotherms (Lyubchik *et al.*, 2011). For instance, a curvilinear graph representing the Langmuir adsorption model is subdivided into a three-parts slope: steep at the beginning (fast and more adsorption), gentle in the middle (slow and less adsorption) and flat at the end (no adsorption). This is presented in Figure 2.7 by blue dots and a blue dotted line.

2.10.1 Adsorption mechanism

When functional groups at the surface of a molecular solid ionise, through protonation and deprotonation (Equations 2.1 and 2.2), surface charge ensues from it. This creates a

potential difference between the adsorptive and the adsorbent. Adsorption is achieved either through (a) substitution of protons to form inner sphere complexes (Equation 2.3); (b) attraction of ions to form outer sphere complexes (Equation 2.4); (c) replacement of surface hydroxyl groups by monodentate or bidentate ligands (Equation 2.5) or (d) attachment of ligands to already adsorbed metals (Equation 2.6) or vice versa (Ugwu and Igbokwe, 2018). Technology and spectroscopic studies (e.g. Fourier Transform Infrared (FTIR) spectroscopy, Powder X-ray Diffraction (XRD), X-ray Photoelectron Spectroscopy (XPS), Electron Paramagnetic Resonance (EPR), Extend X-ray absorption fine structure spectroscopy (EXAFS), etc.) have made understanding of sorption mechanism a lot easier (Ugwu and Igbokwe, 2018).

$$>S\text{-}OH + H^{+} \rightarrow >S\text{-}OH_2^{+} \qquad \text{Equation 2.1}$$

$$>S\text{-}OH \rightarrow >S\text{-}O^{-} + H^{+} \qquad \text{Equation 2.2}$$

$$>S\text{-}OH + M^{Z+} \rightarrow >S\text{-}O\text{-}M^{Z-1} + H^{+} \qquad \text{Equation 2.3}$$

$$>S\text{-}O^{-} + M(H_2O)_6^{2+} \rightarrow >S\text{-}O\ldots(H_2O)M_6^{2+} \qquad \text{Equation 2.4}$$

$$>S\text{-}OH + L^{-} \rightarrow >S\text{-}L + H_2O \qquad \text{Equation 2.5}$$

$$>S\text{-}O\text{-}M^{Z-1} + L^{-} \rightarrow >S\text{-}O\text{-}M\text{-}L^{Z-2} \qquad \text{Equation 2.6}$$

2.10.2 Description of Adsorption Isotherms

Adsorption isotherm is an equilibrium relationship between the amount of substance in the adsorbed state (adsorbate) and the amount of substance in the fluid (adsorptive) at constant temperature. It is interpreted using mathematical expressions (Empirical model) or using calculations of equilibrium constants via the molecular approach (Chemical model).

2.10.2.1 Langmuir Isotherm Model

The Langmuir Isotherm Model is a curvilinear (site-limited) adsorption isotherm derived by Langmuir, in 1916, to explain his adsorption theory on the basis of a kinetic model as follows (Rouquerol, Rouquerol and Sing, 1999; Bleam, 2017b):

(i) Adsorbate (A) desorbs from the surface of adsorbent at a rate that is proportional to the fraction of occupied site (θ). The proportionality constant (K), represented

by the desorption rate constant (K_{des}), is then used to write the desorption rate $(r_{des})_A$ equation (Equation 2.7).

$(r_{des})_A \propto \theta$ $(r_{des})_A = (K_{des})_A.\theta$ Equation 2.7

(ii) Adsorptive (*A*) adsorbs to the surface of adsorbent at a rate that is proportional to the fraction of unoccupied sites (1- θ) and the adsorptive concentration (C_A). The proportionality constant (K), represented by the adsorption rate constant (K_{ads}), is then used to write the rate $(r_{ads})_A$ equation (Equation 2.8).

$(r_{ads})_A \propto (1 - \theta).\, C_A$ $(r_{ads})_A = (K_{ads})_A\,.\,(1 - \theta).\, C_A$ Equation 2.8

(iii) At equilibrium, the rate of adsorption and desorption are equal (Equation 2.9), and its adsorption rate become K_{eq}° (Equation 2.10)

$(K_{ads})_A.(1 - \theta).\, C_A = (K_{des})_A.\theta$ Equation 2.9

$$K_{eq}^{\circ} = \frac{(K_{ads})_A}{(K_{des})_A}$$ Equation 2.10

(iv) Using K_{eq}° to solve Equation 2.9 gives the Langmuir adsorption isotherm expression (Equation 2.11)

$$\theta = \frac{K_{eq}^{\circ}.C_A}{1+(K_{eq}^{\circ}.C_A)}$$ Equation 2.11

(v) Plotting θ as a function of adsorptive concentration (C_A) yields the Langmuir adsorption isotherm (Figure 2.7). Here, the fraction of occupied sites (θ) represents the ratio of the amount of adsorbate at any time 't' (q_A) to the *maximum* amount of adsorbate at saturation ($q_{A(\max)}$) (Equation 2.12).

$$\theta = \frac{K_{eq}^{\circ}.C_A}{1+(K_{eq}^{\circ}.C_A)} = \frac{q_A}{q_{A(max)}}$$ Equation 2.12

Owing to the fact that the original assumptions on which the empirical site-limited adsorption isotherms were based are not fully satisfied, a similar isotherm befitting the experimental adsorption isotherm is now used instead. In this isotherm, K_L(a quantification of the adsorbent affinity for adsorptive *A*) is used in lieu of K_{eq}° (Equation 2.13).

$$\theta = \frac{K_L.C_A}{1+(K_L.C_A)} = \frac{q_A}{q_{A(max)}}$$ Equation 2.13

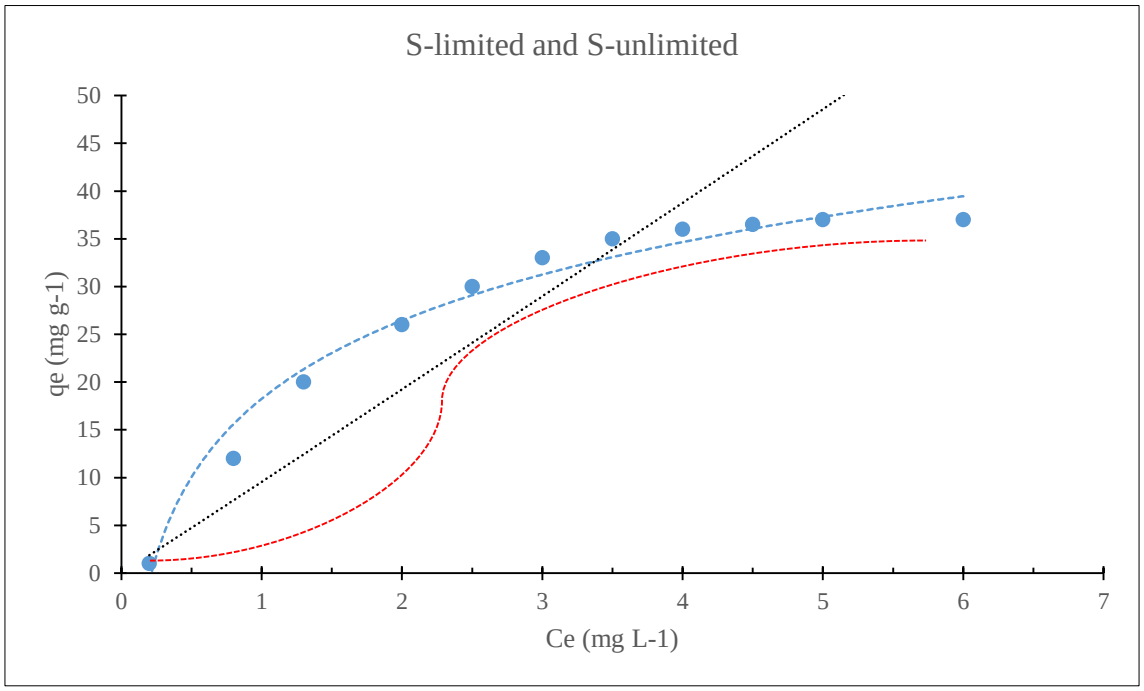


Figure 2.7: Typical shapes of surface excess isotherms in dilute solution. Surface-limited isotherm (blue curved line) and surface-unlimited isotherm (black straight line). Effect of interaction between adsorbate on the adsorbent with adsorptive in the fluid (red S-shaped line).

The above equation transforms into a linearised expression of adsorption isotherm (Equation 2.14). A linear regression of the plot will generate the intercept (α) and the slope (β) from which $q_{A(\max)}$ and K_L can be calculated as shown below (Equation 2.15).

$$\frac{C_A}{q_A} = \left(\frac{1}{q_{A(max).K_L}}\right) + \left(\frac{1}{q_{A(max)}}\right).\boldsymbol{C_A}$$ Equation 2.14

$$q_{A(max)} = \frac{1}{\beta} \quad \text{and} \quad K_L = \frac{\beta}{\alpha}$$ Equation 2.15

2.10.2.2 Freundlich Isotherm Model

This isotherm model is also a two-parameter isotherm. Unlike the Langmuir adsorption isotherm which considers maximum adsorption and a monolayer, the Freundlich

adsorption isotherm has no apparent maximum adsorption because it considers infinity sites (straight, black dotted line in Figure 2.7) and multilayers. It corresponds to Equation 2.16.

$$q_e = k_F . C_e^{1/n} = \frac{\Delta C_i . V}{m} \quad \text{Equation 2.16}$$

$$lnq_e = lnk_F + \frac{1}{n} lnC_e \quad \text{Equation 2.17}$$

k_F is the Freundlich isotherm constant ((mg g^{-1})/(mg L^{-1})$^{1/n}$) and *n* is the adsorption intensity. Both parameters can be obtained from a plotted Freundlich linearised equation (Equation 2.17).

2.10.2.3 Dubinin-Radushkevich (D-R) Isotherm Model

The D-R isotherm model involves the Polanyi constant, ε (Equation 2.18), which itself is connected to concentration of the adsorptive *A* at equilibrium (C_e) (Equation 2.19). The mean free energy of adsorption (E_s) is given by Equation 2.20.

$$lnq_e = lnX_m - K_{ad} . \varepsilon^2 \quad \text{Equation 2.18}$$

$$\varepsilon = RTln(1 + \frac{1}{C_e}) \quad \text{Equation 2.19}$$

$$E_s = \frac{1}{\sqrt{2K_{ad}}} \quad \text{Equation 2.20}$$

2.10.3 Adsorption Kinetics

Adsorption Kinetics is a line (straight or curved) that describes the rate of release of the adsorptive from the aqueous phase on to the surface of the adsorbent, under batch or flow-through experimental set up and specified experimental conditions such as adsorbent mass, adsorptive pH, agitation time, flow rate, adsorptive initial concentration and the likes (Kajjumba *et al.*, 2018). Adsorption mechanism and rate determination are investigated using experimental data and Kinetics equations calculations.

2.10.3.1 Pseudo First Order model (PFO)

The adsorption of adsorptive on to the surface of adsorbent is given below in the form of a curvilinear and linear expressions (Equations 2.21 and 2.22) of the PFO reaction

mechanism. The rate constant k_1 is always inversely proportional the initial concentration of adsorptive.

$$\frac{dq_t}{dt} = k_1(q_e - q_t) \quad \text{Equation 2.21}$$

$$ln(q_e - q_t) = ln\, q_e - k_1.t \quad \text{Equation 2.22}$$

Plotting $\ln(q_e - q_t)$ vs t gives a better fit of the PFO kinetic model.

2.10.3.2 Pseudo Second Order model (PSO)

Two assumptions are noted about this model: (i) the rate of adsorption for the adsorptive is proportional to the available space on the adsorbent; (ii) the reaction is dependent on the amount of adsorbate on the surface of adsorbent, i.e. $\ln(q_e - q_t)$ is proportional to the active sites on the surface of the adsorbent. Equation 2.23 is the curvilinear expression of PSO.

$$\frac{dq_t}{d_t} = k_2(q_e - q_t)^2 \quad \text{Equation 2.23}$$

$$\frac{t}{q_t} = \frac{1}{(k_2.q_e^2)} + \frac{1}{q_e}.t \quad \text{Equation 2.24}$$

PSO can be determined from the plot of $\frac{t}{q_t}$ as a function of t (Equation 2.24). The slope and intercept of the line equation can then be used to calculate q_e and k_2 respectively.

2.10.4 Adsorption Thermodynamics

The theoretical framework of thermodynamics of adsorption includes parameters that explain the effects of heat, brought by changes of temperature, on the adsorption process. Three realms of adsorption energies are considered here: the activation energy, the activation parameters and the thermodynamic parameters of partial and complete adsorption processes (Lyubchik *et al.*, 2011; Saha and Chowdhury, 2011; Inglezakis and Zorpas, 2012).

2.10.4.1 Activation energy

The activation energy deals with the energy barrier to be overcome before effective interactions between adsorptive in solution and reactive sites on the adsorbent could occur. It is a sine qua non requirement for all processes to cross this energy obstacle (Saha

and Chowdhury, 2011). Its magnitude provides information about the type of adsorption process under consideration (physical, ion exchange or chemical sorption) by comparing E_a with demarcation limits set in literature (Inglezakis and Zorpas, 2012).

2.10.4.2 Heats of activation

A set of activation parameters, comprised of the standard entropy change (ΔS^*, J mol^{-1}), standard enthalpy change (ΔS^*, kJ mol^{-1}) and the standard Gibbs free energy change (ΔG^*, kJ mol^{-1}) of activation, provide information about whether the process follows the path leading to an activated complex or not (Saha and Chowdhury, 2011). The sign of these activation parameters provide some insights about the adsorption process progression. The sign and magnitude of heat of activation parameters provide some indications about the adsorption reaction energy requirement and mechanism (Saha and Chowdhury, 2011).

2.10.4.3 Heats of adsoption

Another set of parameters made of the standard entropy change (ΔS^o, J mol^{-1}), the standard enthalpy change (ΔH^o, kJ mol^{-1}) and the standard Gibbs free energy change (ΔG^o, kJ mol^{-1}) of adsorption provide conclusive information, from heats of complete reactions, i.e. for complete surfaces coverage, about the spontaneity of adsorption processes (Lyubchik *et al.*, 2011). The standard free energy of adsorption is linked to the equilibrium constant (K_{eq}) through the Van't Hoff equation, $\Delta G^o = RT \ln K_{eq}$. However, the distribution constant (K_D) is used instead, as a palliative option, in order to calculate ΔG^o. K_D is the ratio of the equilibrium constant for the distribution of the concentration of the adsorbate on the adsorbent over the concentration of the adsorptive in the fluid. It is used to determine the reaction affinity of the binding sites on the adsorbent towards adsorptive in a reaction mixture. Greater values of K_D express higher binding affinity of adsorbent towards adsorptive (Elsaidi *et al.*, 2018). The distribution constant (K_D) varies with the initial concentration and the liquid to solid ratio (Saha and Chowdhury, 2011).

A separate parameter, the standard heat of partial adsorption (ΔH_x, kJ mol^{-1}), relating to the state of the system before and after a differential amount of adsorptive (x) is taken up by the adsorbent, can also be obtained. When calculated for several coverage levels, the total of ΔH_x sum up to the heat of complete surface coverage, ΔH^o. It gives some

indication about the adsorption mechanism as physical, ion exchange or chemical sorption (Saha and Chowdhury, 2011). Its variation is used in estimating the performance of the adsorbent and its surface heterogeneity. Just like for other thermodynamic parameters, a comparison with limits set in literature is required for assessing their meaning. Inglezakis and Zorpas (2012) defines it as the heat from which the heat of vaporisation (for gas phase adsorption) or the heat of immersion (for liquid phase adsorption) is subtracted to get the adsorption energy.

2.11 Sequential extraction Procedure

2.11.1 General principle

The Sequential Extraction Procedure (SEP) is a laboratory technique that removes elements from a solid matrix in successive packages (Castillo *et al.*, 2011; Nemati *et al.*, 2011). The order of packages removal is dictated, on one hand, by the type and strength of chemical interactions particular elements share with their matrix and, on the other hand, by the specificity of extracting fluids for a targeted package as well as by the appropriateness of reaction conditions (Ure *et al.*, 1993; Rauret *et al.*, 1999; Michalke, 2003). The most labile elements are removed earlier whereas the least labile elements are taken out later (Passos *et al.*, 2011). Elements contained in each of the removed packages can then be quantified.

Changes of pH, temperature, redox and microbial activity in environmental conditions provide chemical means of breaking different types of bonds tying elements to different phases of their solid matrix. The intensity of these changes, generally brought about by anthropogenic sources, triggers progressive metal leach outs affecting inner phases of solid matrices. Dissolution, desorption, ion exchange are chemical processes responsible for the release of elements into solution (Jamieson, Walker and Parsons, 2015).

2.11.2 The Tessier's method of SEP

The SEP pioneered by and named after Tessier (Tessier, Campbell and Bisson, 1979; Rosado, Usero and Morillo, 2016) is made of five steps extraction sequence founded upon elements' decreasing ease of release from their matrix as and when affected by possible

changes in the natural environment. The exchangeable, acid soluble, bonded to oxides, bonded to organic matter and residual steps could be briefly described, in terms of extractant-matrix interactions, as follows:

Step 1. The extracting fluid is involved in exchange and complexation reactions through its cations and anions respectively. The order of exchange capacity is Ca^{2+} > Mg^{2+} > NH_4^+ whereas that of complexation power is CH_3COO^- > Cl^- > NO_3^- depending on the extraction fluid used. Labile elements (weakly attached to a matrix) are extracted as mobile (endowed with some freedom of movement in solution) and bioavailable (susceptible to uptake by living organisms) cations in solution.

Step 2. The extracting fluid works at slightly lower pH to liberate, through dissolution, metals which are essentially associated with carbonate (CO_3^{2-}).

Step 3. This step is referred to as the trap (sink) for many metals. The extracting fluid is a reducing agent which attack oxy- and hydroxy-metal compounds. Released metals could be retained in solution by complexation.

Step 4. The extracting fluid creates an oxidizing condition which favours the degradation of organic matter (OM) and the release of sulphide compounds. The retention of metals as complexes prevents their re-adsorption back on to the matrix.

Step 5. A multi acid extracting fluid is used to break the crystalline fabric of the sample in order to free metals.

The Tessier's SEP has seen a number of variations in terms of methodology (protocol and number of steps) and reaction conditions (reactants, pH, concentration, time and temperature) with the aim of addressing some of the limitations observed during different steps (Rauret *et al.*, 1999; Nemati *et al.*, 2011). The insufficient-selectivity of reactants and the re-adsorption and/or precipitation of some metals could be mentioned among the limitations.

2.11.3 The BCR method of SEP

The Community Bureau of Reference (BCR) method of sequential extraction, presently known as the European Community Standards Measurement and Testing Program, is one among diverse and non-uniform multiple protocols of sequential extraction procedures of

chemical speciation. It has the recognition of having harmonized sequential extraction schemes (e.g. extracting fluids) for sediment analysis and has been accepted by a large group of researchers (Okoro and Fatoki, 2012; Benson, Anake and Olanrewaju, 2013; Wali, Colinet and Ksibi, 2015).

BCR is a three step sequential extraction which avoids the complexity of procedures and allows the inter comparison of results (Ure *et al.*, 1993; Rauret *et al.*, 1999). It combines in the first step the extraction of elements which are weakly adsorbed to matrix (exchangeable) and those which are bound to carbonate (acid soluble). In the second step, the increase of the extracting fluid concentration coupled with pH reduction have improved its selectivity towards targeted reducible metal oxides which are principally known to be iron and manganese oxides. Here, the attack on these oxides is made effective (Rauret *et al.*, 1999; Okoro and Fatoki, 2012). In the third and last step, metals retained by strong affinity to OM and sulphide are dealt with as amorphous (anthropogenic) metals, clearly distinguishing them from crystalline (lithogenic) metals which are integrated in the sample's residual solid remaining at the end of the third step. The residue is additionally digested to obtain concentrations which complement the amounts obtained from the previous steps to give the total or pseudo-total concentration of the solid sample (Rauret *et al.*, 1999; Wali, Colinet and Ksibi, 2015).

2.11.4 Single extraction as total and pseudo-total (*Aqua regia*) concentration

Total and pseudo-total concentration provide information about the total amount of metals released, in a single extraction, from a solid sample into its digest solution. Despite indicating a hot spot concentration at a particular site, total and pseudo-total concentration remain silent about the mobility and bioavailability of elements released and present in solution at that particular site (Taraškevičius *et al.*, 2012). Toxicity of metals in solution is related to the chemical forms in which they are found, how much freedom of movement they enjoy (mobility), how easily they can find their way into the biota (bioavailability) where they ultimately affect the metabolic system as the end result (John and Leventhal, 1995). The toxicity of a given sample, mine waste for instance, does not find a convincing explanation in the quantification of metals as total or pseudo-total content in solution because there is poor and inconsistent correlation between total or pseudo-total metal

content and the potential risk of that sample in the biophysical environment where it can cause damage (Yuan *et al.*, 2004; Wojtkowska, 2011; Adamu *et al.*, 2013).

Even though total and pseudo-total metal content of trace metals in environmental solid samples could sometimes but wrongly mean the same thing, they are fundamentally different. Total metal content means completeness of extraction facilitated by the use of a concoction (combination) of strong acids which attack and dissolve the core of the solid material. Taraškevičius et al.(2013) referred to it as "real total". It has its application and full meaning in the field of geological exploration and mapping. On the contrary, pseudo-total metal content means extraction to near completeness. It mobilizes metals that are adsorbed, precipitated and complexed (*Aqua regia*-extractable) leaving behind those that form part of the crystalline structure of particulate matter. The term or extraction process *aqua regia* refers to the solution produced from the reaction between hydrochloric acid (3/4) and nitric acid (1/4) (Equation 2.1). It is an effective extractant for most base metal sulphates, sulphides, oxides and carbonates but leaves some elements in the core of the solid sample which remains undestroyed. In spite of this, elements that are commonly considered for environmental study (Cd, Co, Cu, Fe, Mn, Ni, Pb and Zn) are excluded from those that are underestimated due to incomplete digestion (Price, 2009).

$$3HCl + HNO_3 \rightarrow 2\,H_2O + NOCl + Cl_2 \qquad \text{Equation 2.25}$$

Aqua regia is widely used in environmental analyses where mobility and bioavailability of harmful elements are of essence. Over the years and for many, the clear demarcation line between the two metal contents (total and pseudo total) has turned to be a blurred demarcation zone in the sense that the denomination "total content" is indiscriminately and interchangeably used in one and the other field of study (Taraškevičius *et al.*, 2012). Despite this created confusion, it is clear that the two terms relate to two different processes, have different meanings and should not be mixed up as they cannot be used one for the other. To avoid the mix up, the procedure leading to these two metal contents should always accompany their respective results. *Aqua regia* has little value in studies meant to identify metal sources, because total metal concentrations are more closely linked to sediment mineralogy and diagenetic conditions than to surficial variations

connected with bioavailability and toxicity effects of metals (Piatak, Hammarstrom and Ii, 2006; Zhang *et al.*, 2014).

2.12 Bioavailability

2.12.1 Bioavailability concept

Although metals do not undergo degradation, they are not necessarily bioavailable (EMERITE Consortium, 2003). It is now a fact, recognized by most scientists (Simpson, Batley and Maher, 2016; Vidmar *et al.*, 2017; Gitari *et al.*, 2018), that predicting the deleterious environmental risks associated with sediment total metal concentration is somehow wrong. This is because (i) solutions with very similar metal concentration may contain very different metal bioavailable fractions, (ii) only some of metals making total concentration can be mobile enough to enter into contact with living organisms (bio-accessibility) and, of this portion of metals, (iii) only a fraction can be assimilated by target receptors in living organisms (bioavailability) where they can thereafter cause beneficent or toxic responses (Besser, Brumbaugh and Ingersoll, 2015; Simpson, Batley and Maher, 2016; Mehta *et al.*, 2019). The solution immediate to sediments, the interstitial (pore) water, is the principal medium for benthos exposure to metallic contaminants (Simpson, Batley and Maher, 2016).

In sediments, metals are arranged in different compartments defined by their metal-to-sediment bond type and strength and, as such, they are not equally affected by the bond breaking influence of solutions they are in direct contact with (Cipullo *et al.*, 2018). Whichever the case, when metals from any sediment compartment find themselves in solution, they either remain as free cations or get subjected to reactions that will either keep them in solution as soluble complexes (organic and/or inorganic) or remove them from solution through adsorption and precipitation (Simpson, Batley and Maher, 2016). Bioavailability is concerned with the formation and transformation of compounds which remain in solution and are susceptible to absorption by living organisms (Landner and Reuther, 2005; Cipullo *et al.*, 2018; Tardif *et al.*, 2019). It is greatly affected by the affinity, or the lack of it, of organic and inorganic ligands as well as fine clastic particles towards free metal cations.

2.12.2 Bioavailability control processes

The attenuation of trace metal cations bioavailability is achieved through different reaction mechanisms that remove them from solution or reduce their chances of being absorbed by living organisms (Apostoli et al., 2006; Nordstrom and Alpers, 1999). Adsorption and desorption as well as dissolution and precipitation processes are regarded as dominant reaction mechanisms controlling the availability of metallic contaminants in sediment-water system (Apostoli *et al.*, 2006).

The removal of metal cations from solution is facilitated by processes such as (i) adsorption (binding and exchange) to surfaces with high Cation Exchange Capacity (CEC), sand and silt (0 – 7 meq 100 g^{-1}) < clay (10 – 150 meq 100 g^{-1}) < OM (> 200 meq 100 g^{-1}), brought about by a large number of permanent negative charges for which trace metals cations and major cations compete for (Apostoli *et al.*, 2006), (ii) co-precipitation with secondary minerals such as aluminium-, iron- and manganese hydroxides (Nordstrom and Alpers, 1999) and (iii) precipitation of metal sulphides in anoxic environment (Nordstrom and Alpers, 1999).

Soluble organic compounds (e.g. humic and fulvic acids) are complex organic molecules possessing carboxylic, phenolic, amino, sulphur groups within their molecular structures (Figure 2.8) and to which a variety of metal cations can bind (Simpson, Batley and Maher, 2016). The resulting complexes still remain in solution but lack ease of mobility and, consequently make metal cations less bioavailable (Alvarez-Puebla, Valenzuela-Calahorro and Garrido, 2004). Their high negative charge coupled with large surface area give rise to a capacity of adsorption as important as the one provided by clay particles (Reichelt-Brushett, Clark and Birch, 2017)**.** As such, organic compounds play a major role in the retention/remobilization processes of contaminants in aquatic media. Simpson, Batley and Maher, (2016) mentioned that the presence of synthetic organic ligands, such as EDTA, can add to the attenuation of metal ions in surface water.

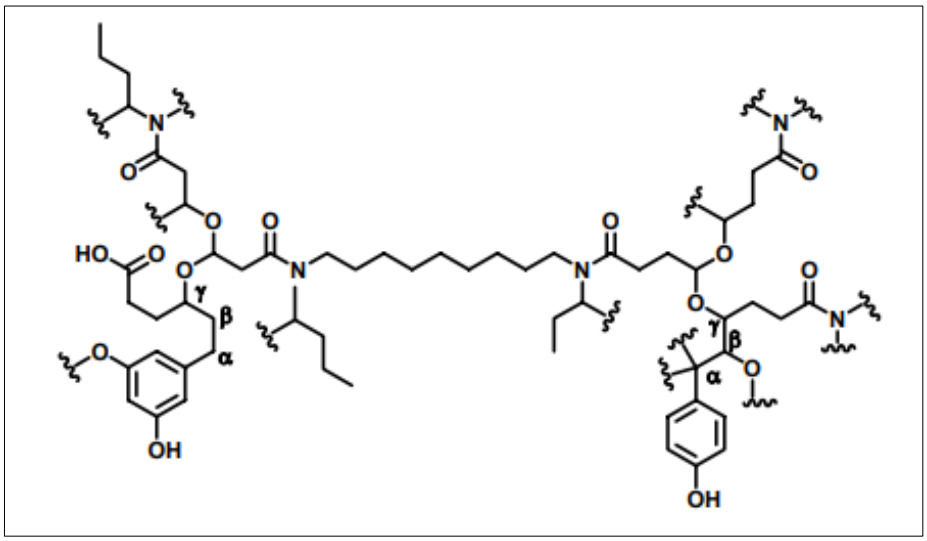


Figure 2.8: Model humic acid molecular structure fragment with sinusoidal lines indicating other fragment -COOH, -OH, -NH_2, -SH metal binding sites (Montoneri *et al.*, 2008).

Inorganic complexes can also be formed from metal cations binding with inorganic anions (e.g. CO_3^{2-}, Cl^-, OH^-, NO_3^-, SO_4^{2-}). Products obtained from this 'complexation' (e.g. $CuOH^+$, $CuCO_3$) have relative ease of movement and, are more susceptible to absorption by living organisms than organic complexes. Nevertheless, free cation (e.g. Cu^{2+}, Ni^{2+}) is the most bioavailable form in aqueous solution (Miwa, Murakami and Mizuike, 1989; Michalke, 2003; Landner and Reuther, 2005; Simpson, Batley and Maher, 2016).

2.12.3 Sediments Quality Guidelines (SQGs)

Surface water bottom sediment is the habitat for benthic invertebrates (Besser, Brumbaugh and Ingersoll, 2015). Its geochemical characteristics are a reflection of the mineralogy of its underlying rock geology and the anthropogenic activities taking place in surrounding areas. Mining industries, for instance, impact sediments with metal contaminants which affect the health of benthos, an important group of aquatic organisms that are commonly used in the assessment of the quality of aquatic ecosystems. Burton, (2002), elaborately presented various aspects of numerous SQGs including the evolvement and application of their two primary methodologies: the empirical and the theoretical approaches. The first approach focuses on relationships

between the frequency of observed effects and the variability of sediment contaminants whereas the second relies on bioavailability differences obtained through the Equilibrium Partitioning (EqP) based on the difference between molar concentrations of Simultaneously Extracted Metals (SEM) and Acid Volatile Sulphide (AVS) (Besser, Brumbaugh and Ingersoll, 2015).

The response of benthic invertebrates to metal-contaminated sediment toxicity is most commonly assessed using SQGs, a screening tool based on quantitative metal concentration threshold values above or below which adverse effects on benthos may or may not be frequently expected. Among these SQGs, the Probable Effects Concentrations (PEC) and the Threshold Effects Concentrations (TEC), with PEC > SQG and TEC < SQG, are "consensus based" guidelines meant to harmonize variations among investigators (Burton Jr., 2002). These predictive SQGs derived their strength from sediments field chemistry coupled with a large collection of actual field and laboratory existing and continually expanding data. Their weakness resides in the fact that adverse effects on benthos are attributed (i) to metal total concentrations, not to metal bioavailable concentrations and (ii) to the co-occurrence of metal contaminants rather than their individual occurrence.

Any element with total concentration exceeding its PEC standards may be a contributor to sediments potential hazards. However, the biological significance of contaminant mixtures in sediment is obtained by dividing metal total concentrations of each element by its "consensus based" PEC standard. Resulting quotient values are then summed, normalized to the numbers of PECs for each sediment sample and then compared with the threshold mean PEC standard of 0.5 above which sediment samples were expected to affect benthos adversely.

Piatak, Hammarstrom and Ii (2006) observed that the threat to benthic invertebrates evaluated in this way may give an overestimation of sediments potential hazards because it takes into account concentration from the dissolution of crystalline minerals which are of no use for bioavailability characterisation of sediments. Additionally, even though total recoverable metal concentrations did not contain residual crystalline metals and could provide a conservative estimate of bioavailable metals, they were

found to have weaker relationships with the toxicity to some benthos than metals in labile fraction obtained by sequential extraction (Besser, Brumbaugh and Ingersoll, 2015).

2.13 Metal speciation

The aim of Sequential Extraction Procedure (SEP) methodologies is to assess the speciation of metals. As concerns metallic contaminants in environmental chemistry, "speciation" is defined in two different contexts: (i) the *process* of identifying and quantifying species present in soil and sediments; (ii) the *description* of the concentration of species present in solution, i.e., the distribution of an element amongst aqueous chemical species (Ure *et al.*, 1993; Kot and Namiesnèik, 2000; Apostoli *et al.*, 2006; Adamu *et al.*, 2013; Benson, Anake and Olanrewaju, 2013). In both contexts, the concept of "species" could be triply understood: (i) functionally, (ii) operationally and (iii) as specific compounds or as an element in a given oxidation state. According to IUPAC (International Union of Pure and Applied Chemistry) official definition, speciation analysis is the process leading to the identification and determination of the different chemical and physical forms of an element existing in a sample (Kot and Namiesnèik, 2000).

Operationally, species relate to different SEPs followed to free metals from matrices (e.g. types and concentrations of extraction fluids, particle size…). Mossop and Davidson (2003) stated that they lead to the obtainment of results that are difficult to compare. With reference to a defined protocol, "extractable trace metals" is thought to be appropriate a term even though it could be used synonymously with "species" (Ure *et al.*, 1993).

Functionally, species relate to the role mobile cations assume as available nutrients or toxicants to living organisms. It avails additional analytical results information required for the assessment of environmental pollution and toxicological risks associated with metallic forms found in a given sample as well as the determination of their lithogenic or anthropogenic origin (Lin, 1997; Michalke, 2003; Okoro and Fatoki, 2012; Benson, Anake and Olanrewaju, 2013; Jena *et al.*, 2013).

From existing literature, it is clear that the term chemical species is a wide net which captures a variety of elements or compounds distinguishable only by their isotopic compositions, conformational structures, oxidation states and nature of complexes (Ure *et al.*, 1993; Roberts, Nactegaal and Sparks, 2005; Okoro and Fatoki, 2012; Benson, Anake and Olanrewaju, 2013). Such minute details could be critical in making species respond differently to certain interactions or absorption mechanisms in similar environments (Benson, Anake and Olanrewaju, 2013).

2.14 Geochemistry of mine drainage

2.14.1 Ore and gangue minerals coexistence

Sulphidic geological material exists as an assemblage of different types of minerals coexisting within the same rock. Sulphide minerals, a distinct family of ore minerals, contain in their make-up (fabric) valuable components that are sought after if present at economically minable content (Dold, 2010; Jamieson, Walker and Parsons, 2015). Mining of these ore minerals, which have liking associations with trace elements, is known to be the primary source of potentially toxic elements (Price, 2009; Dold, 2014b). Carbonates, aluminosilicates and silicates, among others, form another specific family of gangue minerals. Viewed from an environmental standpoint, this is an equally important group of minerals in the sense that they dissolve, principally, to contain sulphide minerals generated acidity and create conditions that are conducive for the attenuation of metallic contaminants (Dold, 2010).

2.14.2 Weathering of rock mineral

Weathering is a natural process by which the quality of water, before and after running over the surface of, and/or through, geological material, is different in terms of its content in particles and chemical substances (John and Leventhal, 1995). The types and amounts of these new additions into water are controlled by interactions between water, oxygen and geological materials (John and Leventhal, 1995). In the absence of human activities, the chemical content of the resulting water, referred to as background content, is solely dictated by the lithogenic setting of geological materials (parent material). On the contrary, anthropogenic activities introduce more chemical substances in excess of the

natural content of water which, eventually, comes to be termed as contaminated water. In both situations, Price (2009) referred to the resulting water as drainage chemistry which, on the basis of its pH, could be categorised into acidic (pH<6), near neutral (pH 7±1) or alkaline (pH>8) drainages.

2.14.2.1 Water involvement in weathering reactions

Water is, directly or indirectly, an important factor in weathering processes of geologic materials. It acts alone, either as water molecules (e.g. hydration, dissolution) or as water in the form of its constituent ions (i.e. hydrolysis) as exemplified by Equation 2.2, Equation 2.3, Equation 2.4 and Equation 2.5. It also acts as an auxiliary compound by providing a medium for other substances and organisms to operate in (e.g. oxidative dissolution of sulphidic minerals, microbial reduction of Fe(III), ion exchange) or get transported by (e.g. bed and suspended loads) (Banks *et al.*, 1997; Price, 2009).

$CaSO_4 + H_2O \rightleftharpoons CaSO_4.2H_2O$ (hydration/dehydration) Equation 2.26

$CaCO_3 + H_2O \rightarrow Ca^{2+} + HCO_3^- + OH^-$ (dissolution) Equation 2.27

$Fe^{3+} + 3\ H_2O \rightarrow Fe(OH)_3 + 3\ H^+$ (hydrolysis) Equation 2.28

$KAlSi_3O_8 + H_2O \rightarrow HAlSi_3O_8 + K^+ + OH^-$ (hydrolysis) Equation 2.29

2.14.2.2 Rock mineral in weathering reactions

The chemistry of water-oxygen-geological material interactions has been used many a times to elucidate processes that lead to the generation of sulphate and acidity, and the release of trace metals in water (Banks *et al.*, 1997; Nordstrom and Alpers, 1999; Dold, 2010, 2014a). Like for any other chemical reaction, prior knowledge pertaining to chemical characteristics of reactants (e.g. soil mineralogy) and reaction conditions (e.g. pH, Eh), are key to predicting the type of water likely to be produced. For example, Cu, Fe and S originally held together in sulphidic mineral chalcopyrite ($CuFeS_2$) undergo oxidative dissolution (Equations 2.6 and Equation 2.7) which transforms them into more soluble and mobile Cu^{2+}, Fe^{2+} and SO_4^{2-} ions. Trace metals which are contained in sulphide ore minerals, but not accounted for in their ideal chemical formulae, are also freed as dissolved metal ions into solution. Most of these ions may possibly undergo

further transformations depending on reaction conditions (Abbassi, Khan and Hawboldt, 2009).

$$CuFeS_2 + 4\ O_2 \rightleftharpoons Cu^{2+} + Fe^{2+} + 2\ SO_4^{2-} \qquad \text{Equation 2.30}$$

$$CuFeS_2 + 16\ Fe^{3+} + 8H_2O \rightarrow Cu^{2+} + 17\ Fe^{2+} + 2\ SO_4^{2-} + 16\ H^+ \qquad \text{Equation 2.31}$$

2.14.3 Hydrogen ion activity (pH)

The meeting together of the atmosphere, hydrosphere and lithosphere in the form of oxygen, water and sulphide minerals (e.g. FeS_2, $Fe_{(1-x)}S$, $CuFeS_2$) is at the origin of acidity, sulphate and trace metals in chemical drainage (Banks *et al.*, 1997; Nordstrom and Alpers, 1999; Abbassi, Khan and Hawboldt, 2009). Whether this acidity is permitted to freely increase or prevented from extending its influence is chiefly dependent on the amount of minerals driving two sets of antagonistic reactions between acid producing minerals (pyrites) and acid neutralizing minerals (carbonates, hydroxides and silicates) coexisting in sulphidic rocks (Dold, 2010). The prevailing acidity or alkalinity, short-lived or long lasting, is the expression of the dominant reactant at a particular point in time.

Changes in pH play a crucial role in water-oxygen-geological material interactions. The increase of acidity in the reaction environment governs the release of more metals into water whereas their sequestration by solid compounds or particles is influenced by the decrease of acidity. Dissolution, precipitation (co-precipitation), adsorption and desorption processes are all linked, to a larger extent, to variations of acidity in the water-geological material environments (Nordstrom and Alpers, 1999). While precipitation (co-precipitation) and adsorption work towards the attenuation of the amount of toxic metals in solution, dissolution and desorption do just the opposite work.

The acidity produced by pyrite minerals dissolution provokes the release of alkalinity, at a faster rate, from highly soluble carbonate minerals (Dold, 2014a). The acidity of the mine drainage is buffered at near neutral pH until the reservoir of carbonate minerals is possibly consumed. At this point, the aluminosilicate group of minerals (mafic silicates, feldspars and clays) would take over in buffering the mine drainage, though at a slower

rate, allowing the pH to slowly decrease with time until it settles at pH<3.5 (Banks *et al.*, 1997). Elevated concentration of aluminum in mine drainage of slightly acidic pH could be assigned to silicate dissolution (Equation 2.8). Between near neutral and slightly lower pH, ochres precipitation happens with some trace metals co-precipitation. Trace metals deposition (adsorption and ion exchange) to surfaces of clastic particles and organic matter also take place.

$$Al_2Si_2O_5(OH) + 6\ H^+ \rightarrow 2\ Al^{3+} + 2\ H_4SiO_4 + H_2O \qquad \text{Equation 2.32}$$

Price (1999) observed that the highest unit mass ion exchange capacity is provided by clay > OM > ochres which, together, greatly attenuate trace metals content in mine drainage. The bioavailable portion of trace metals remains in solution as free cations or soluble complexes with complete or limited freedom of movement respectively (John and Leventhal, 1995). At pH<3.5 ochres dissolution releases ferric iron and trace metals. In that very acidic environment, ferric iron oxidizes sulphide minerals, at a faster rate, releasing more acidity and sulphates. Banks *et al.* (1997) noted that relative rates of antagonistic dissolution of sulphide minerals on one side (Equation 2.9 and Equation 2.10) and carbonate and silicate minerals dissolution on the other side (Equation 2.11 and Equation 2.12) could decisively confirm or reject predictions obtained from acid-base accounting results. Similar remarks were echoed by Price (2009).

$$FeS_2 + 3.5\ O_2 + H_2O \rightleftharpoons Fe^{2+} + 2\ SO_4^{2-} + 2\ H^+ \qquad \text{Equation 2.33}$$

$$4\ CuFeS_2 + 17\ O_2 + 10\ H_2O \rightleftharpoons 4\ Fe(OH)_3 + 8\ SO_4^{2-} + 4\ Cu^{2+} + 8\ H^+ \qquad \text{Equation 2.34}$$

$$CaCO_3 + 2\ H^+ \rightleftharpoons H_2CO_3 + Ca^{2+} \qquad \text{Equation 2.35}$$

$$CaAl_2Si_2O_8 + 2\ H^+ + 2\ H_2O \rightleftharpoons Ca^{2+} + AlSi_2O_5(OH)_4 \qquad \text{Equation 2.36}$$

2.14.4 Reduction-oxidation (Redox)

2.14.4.1. Sulphide minerals

The solubility of some minerals are triggered by the exchange of electrons between reacting species. Pyrite minerals, for instance, undergo a stepwise oxidative dissolution which produces, as a function of their oxidation-reduction potential (Eh), sulphate ions at first and ferric ions after (equations 2.13 and Equation 2.14). The latter ions will follow a

reaction path (equations 2.15 and Equation 2.16) that will transform them, at a slower rate, into hydroxide precipitates (at near neutral to slightly acidic pH) which will in turn be disintegrated, at a faster rate, into ferric ions (at lower pH) which will eventually cause more oxidative dissolution of sulphide minerals (Banks *et al.*, 1997; Nordstrom and Alpers, 1999). Undoubtedly, sulphide minerals oxidation constitutes the initial reaction leading to a series of reactions that contribute to mine drainage formation as shown in the equations below (Banks *et al.*, 1997; Abbassi, Khan and Hawboldt, 2009; Dold, 2014b).

$FeS_2 + 3.5\ O_2 + H_2O \rightarrow Fe^{2+} + 2\ \mathbf{SO_4^{2-}} + 2\ H^+$ (at near neutral pH) Equation 2.37

$4\ Fe^{2+} + O_2 + 4\ H^+ \rightarrow 4\ \mathbf{Fe^{3+}} + 2\ H_2O$ (at near neutral pH) Equation 2.38

$\mathbf{Fe^{3+}} + 3\ H_2O \rightleftharpoons \mathbf{Fe(OH)_3} + 3\ H^+$ (at near neutral and acidic pH) Equation 2.39

$FeS_2 + 14\ \mathbf{Fe^{3+}} + 8\ H_2O \rightarrow 15\ Fe^{2+} + 2\ SO_4^{2-} + 16\ H^+$ (at acidic pH) Equation 2.40

2.14.4.2. Organic matter

Organic matter are complex polymeric compounds among which, primarily, humic substances (humic, fulvic and fulvin fractions) structurally made of many aromatic rings studded with phenolic hydroxides and carboxylic acids, and secondarily, carbohydrates, proteins and their building parts and units (peptides and amino acids) are the most referred to in relation to soil and sediment (Alvarez-Puebla, Valenzuela-Calahorro and Garrido, 2004; Kirchman, 2010). Dead organic matter (detritus) and living organisms accumulate on the surface of inorganic particles and offer sites, i.e. functional groups such as hydroxyl, carboxyl, amine and thiol, to which a number of molecular and ionic substances can attach (Simpson, Batley and Maher, 2016). Organic matter, at high content, is a good adsorbent and a major immobilizer of most trace metals (Rae and Allen, 1993; Ibragimow, Walna and Siepak, 2013). Under appropriate redox conditions (low Eh), they reduce in size through a degradative oxidation process and thereby releasing trace metals.

Following the redox reactions order in Table 2.3, oxygen is the preferred electron acceptor for microbial aerobic respiration (Szögi *et al.*, 2004). In anaerobic conditions, the electron acceptors sequence is $NO_3^- > MnO_2 > Fe_2O_3 > SO_4^{2-}$. On the contrary, oxidation follows the reverse order, i.e. $S^{2-} > Fe^{2+} > Mn^{2+}$. Szögi *et al.* (2004) noted that there was no strict rule to the fact that a preceding oxidation or reduction reaction should go to completion

before the next one in sequence could start; there was possible overlapping between successive redox reactions. This is valid for Fe_2O_3 reduction and OM decomposition which release co-precipitated and adsorbed metals into solution. Interestingly, there is a connection between soluble Fe(III) and the decomposition of OM (Lovley, 1987). It has been established that Fe(III) reduction requires the intervention of microbial organisms and that soluble Fe(III) is an important pathway to OM decomposition (Lovley, 1987; Szögi *et al.*, 2004). Its availability, determined by its amorphous or crystalline origin, controls the extent of OM mineralisation.

Table 2.3: The sequence of redox reactions as a function of Eh. Adapted from Price (2009).

Eh	Reduction →		← Oxidation	Eh
+15	O_2	⇌	H_2O	+20
	NO_3^-	⇌	N_2	
	Mn(IV)	⇌	Mn(II)	
	NO_3^-	⇌	NH_4^+	
Redox potential →	Fe(III)	⇌	Fe(II)	Redox potential →
	CO_2	⇌	OM	
	SO_4^{2-}	⇌	S^{2-}	
	CO_2	⇌	CH_4	
	N_2	⇌	NH_4^+	
-10	H_2O	⇌	H_2	-5

With reference to humid tropical forest soil, Hall and Silver (2013) suggested a different mechanism responsible for the decomposition of OM. Ferrous iron obtained from anaerobic reduction of ferric iron undergoes aerobic oxidation to stimulate a three one electron steps mechanism that produces, ultimately, a reactive species (hydroxyl radical) capable of driving organic matter degradation (Equation 2.17 to Equation 2.19).

$$Fe^{(II)} + O_2 + H^+ \rightarrow Fe^{(III)} + \mathbf{HO_2^{\bullet}} \quad \text{(peroxide radical)} \qquad \text{Equation 2.41}$$

$$Fe^{(II)} + H^+ + HO_2^{\bullet} \rightarrow Fe^{(III)} + \mathbf{H_2O_2} \quad \text{(peroxide)} \qquad \text{Equation 2.42}$$

$$Fe^{(II)} + H_2O_2 \rightarrow \mathbf{OH^{\bullet}} + Fe^{(III)} + HO^- \quad \text{(hydroxyl radical)} \qquad \text{Equation 2.43}$$

The third step reaction has actually been used independently to degrade organic matter in waste water treatment (Hall and Silver, 2013). This indicates that ferrous iron oxidation by hydrogen peroxide could achieve organic matter degradation in the absence of enzymatic catalysis. A similar mechanism was used by James and Brose (2012) to explain the reduction of O_2 to H_2O in a four one electron reduction steps aerobic respiration mechanism.

2.15 Geochemical predictive speciation model

In a redox system, electrons move from one species (donor) to another (receiver). In an acid-base system, the movement of protons from one species (donor) to another (receiver) is achieved in a similar way. These two systems are independent, concordant and non-exclusive. Relating redox conditions, *viz.* reducing or oxidizing (expressed as the activity of electrons = Eh), with acid-base conditions, *viz.* acidic or alkaline (expressed as the activity of hydrogen ions = pH) helps predict the stability and dominancy of a chemical species under specific geochemical conditions (Nordstrom and Alpers, 1999). Four possible redox equilibrium combinations can be obtained: oxidizing acidic, oxidizing alkaline, reducing acidic and reducing alkaline (Figure 2.9).

Eh-pH diagrams also known as Pourbaix diagrams, schematized in Figure 2.7, find their usefulness in geochemistry; they show stability fields appropriate to different species of a specific element as dictated independently by acid-base and redox relationships or by a combination of both (Nordstrom and Alpers, 1999; Abbassi, Khan and Hawboldt, 2009; Nyirenda *et al.*, 2015). Changes in acidity along the pH axis (indicated by a vertical line) allows to track changes in the stability or dominancy of different species of an element. For an example, soluble species are stable at low pH with weakly binding metals remaining in solution whereas insoluble species are favoured at higher pH with metals adhering to them (Ibragimow, Walna and Siepak, 2013). Additionally, changes of Eh towards lower and/or negative values (indicated by a horizontal line) favour the prevalence of reductive conditions leading, for instance, to the dissolution of hydrous metal oxides and the reduction of sulphate to sulphide. Changes of Eh in the opposite direction promote the establishment of oxidative conditions in which, for instance, the

decomposition of organic material do happen (Ibragimow, Walna and Siepak, 2013). The stability fields limit of species that are dependent on both acid-base and redox conditions (water included) are indicated by slanted lines. Nordstrom and Alpers (1999) state that of the two changes, pH is the independent or master variable *viz*, the cause whereas pe is the dependent or subordinate variable i.e. the effect.

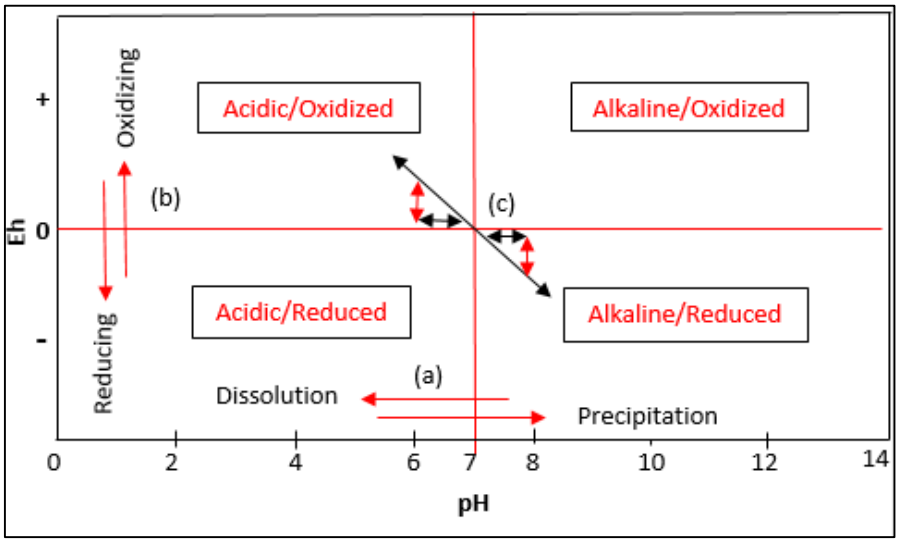


Figure 2.9: Schematic representation of reaction conditions and possible reaction progressions associated with changes in Eh –pH conditions

2.16 Speciation modelling and equilibrium solubility

The Concise Oxford English Dictionary (20th edition, 2011) defines the word model as a simplified description of a system or process to assist calculation and prediction. A model can, hence, be interpreted as a simplification of a complex reality; a quick, effective and predictive answer to incomplete understanding of interlinked phenomena. Geochemical modelling allows the prediction of possible minerals (and their dissolution) responsible for major reactions in chemical drainage through computer programs such as PHREEQC (Parkhurst and Appelo, 1999, 2013), Geochemists Workbench among others, by inputting actual data from chemical drainage field measurements and laboratory analysis (Nordstrom and Alpers, 1999; Abbassi, Khan and Hawboldt, 2009; Muchez and Corbella, 2012; Nyirenda *et al.*, 2015; Naderi Peikam and Jalali, 2016). The output provides information about the speciation of dissolved minerals and the equilibrium solubility or

saturation index (SI) between dissolved and undissolved minerals in a typical chemical drainage. The solubility equilibrium constant at standard conditions of temperature and pressure (298 K, 1 atm), Ksp, and the Ion Activity Product (IAP) *viz*, equilibrium constant at prevailing conditions of temperature and pressure, relate through the logarithm of the ratio IAP/Ks (Equation 2.20 to Equation 2.23) to give an indication of the level of saturation for minerals of interest. Three levels of saturation are found: undersaturation (SI < 1), satutation (SI = 1) and over saturation (SI > 1).

$A_aB_{b\,(s)} \rightleftharpoons aA^{b+}_{(aq)} + bB^{a-}_{(aq)}$ K_s Equation 2.44

$A_aB_{b\,(s)} \rightleftharpoons aA^{b+}_{(aq)} + bB^{a-}_{(aq)}$ IAP Equation 2.45

$K_s = \frac{[A^{b+}{}_{(aq)}]^a * [B^{a-}{}_{(aq)}]^b}{[A_aB_{b\,(s)}]}$ and $IAP = \frac{[A^{b+}{}_{(aq)}]^a * [B^{a-}{}_{(aq)}]^b}{[A_aB_{b\,(s)}]}$ Equation 2.46

$SI = \log\frac{IAP}{K_s}$ Equation 2.47

Geochemical modelling is used as a diagnostic and predictive model to determine actual and potential sources of threats to the aquatic ecosystem (Naderi Peikam and Jalali, 2016). The oversaturation and under saturation of a chemical species of interest could be used to assess their mobility, bioavailability and toxicity impacts on aquatic living organisms (Pourret *et al.*, 2015).

2.17 Problem statement

Globally, metal mining industry is, by its nature, deemed incompatible with (unfriendly to) the environment (Ramirez-llodra *et al.*, 2015; Carvalho, 2017). Its impacts on water systems, particularly at low pH, constitute a major concern of metal mining operations (Calas, 2017). Despite denouncing and vilifying the mining industry, various studies have striven to understand different causal and sustaining aspects of water/sediment mining pollution in order to create awareness and contribute possible solutions (Nicholson, Gillham and Reardon, 1989; Atkinson, Jolley and Simpson, 2007; Kollias *et al.*, 2014; Zhang *et al.*, 2014; Lindsay *et al.*, 2015).

Chemical mine drainage from sulphide minerals lowers pH, increases sulphate and dissolved/particulate trace elements concentration, in receiving surface water (Jamieson, Walker and Parsons, 2015). Trace elements are potentially hazardous to organisms dwelling in water column and floor sediment (Besser, Brumbaugh and Ingersoll, 2015). However, circumneutral pH chemical mine drainage brings conditions that influence the removal of toxic metals from the water column, via precipitation and adsorption processes, which subsequently accumulate in floor sediments (Nordstrom and Alpers, 1999; Jamieson, Walker and Parsons, 2015; Majzlan *et al.*, 2018).

From solid waste to surface water and floor sediments, toxic trace elements are mobilized (e.g. leaching) into mine drainage, transported to surface water, immobilized by sediment (e.g. adsorption) and remobilized into water (e.g. dissolution) (Jamieson, Walker and Parsons, 2015; Karaca, Cameselle and Reddy, 2016). The movement and transformation of toxic elements influence the pollution status of environmental matrices (e.g. sediment, water, tailings). Studies linking various geochemical characteristics between mine waste, vicinal surface water and bottom sediments in a copper mine area under consideration are scanty (Sracek *et al.*, 2011, 2012; Addo-Bediako *et al.*, 2014).

2.18 Summary of novelty of the study

Besides other geochemical characterization techniques, modeling was used to compute:

i. actual surface water data for diagnostic simulations of mixed waters in an area where accessibility to all key sampling points was difficult.
ii. copper crust leachate data for predictive simulations of evaporated surface water in a locality where foreseeable worsening climatic conditions are slowly becoming a reality.

The separation of REEs from ore is one of the seven fields of research that are predicted to change the world for the better. Any contribution to this endeavour, no matter how small, is welcome because no one knows how, where and when the breakthrough will come about. The recovery of REEs using local, natural and abundant magnetite was a contribution towards this exciting area of research.

CHAPTER 3 AIM AND OBJECTIVES

This chapter frames the study by stating its aim; it adjusts expectations by giving the aim's supporting objectives. The significance of the study follows then.

3.1 Aim

The aim of this research project was:

To geochemically characterise surface water, bottom sediments and assorted solid waste in copper mining areas at Phalaborwa (South Africa) and Kitwe (Zambia).

3.2 Objectives

The aim was underpinned by the following objectives:

i. To determine physicochemical properties, chemical contents of surface water [(P, K)] and establish the water classification of surface water[(P)]

ii. To determine mineral identification and elemental composition of sediments [(P, K)] and assorted mine waste[(P)]

iii. To determine leachable metal concentrations in sediments[(K)] and assorted solid waste[(P)] using Toxicity Characteristic Leaching Procedure (TCLP).

iv. To assess the partitioning of trace elements in sediments[(P)] using microwave assisted modified Bureau of Community Reference (MW mBCR)

v. To compute speciation simulations for (a) diagnostic mixing of surface water[(P)] and (b) predictive evaporation/dilution of copper crust[(P)] leachate.

vi. To assess the conditions for high recovery capacity of natural magnetite[(P)] for REEs

Note: superscripts P and K stand for Phalaborwa and Kitwe, and specify the source of samples used in achieving a particular objective.

3.3 Significance of the study

Combining geochemical characterisation of surface water, leaching of assorted mine waste and metal portioning of sediments with geochemical modeling calculations of leachates and surface water in a copper mine area the study will help better understand the potential impacts of trace elements pollution and the phenomenon of evaporation related to it on the aquatic environment and life dependent on it in the localities concerned *viz*, Phalaborwa and Kitwe, and beyond.

CHAPTER 4 METHODOLOGY

Sample collection (field outings) and, sample preparation and analysis (indoor laboratory work) are described. Leaching and digestion were used to release chemical components into solution for analysis using different analytical techniques for different purposes. Results were used for assessment of trace elements in leachates and their speciation in sediments, for surface water mixing diagnostic simulations and surface water evaporation predictive simulations, for assessment of REEs recovery using natural magnetite. Statistical methods were used for classification of variables and observations.

4.1 Location and description of study site 1 - Phalaborwa, South Africa

Phalaborwa is located in the north eastern part of the Limpopo Province (Figure 4.1). It is in the locality of Phalaborwa Igneous Complex (PIC) which is mined mainly for its copper and phosphate by the Palabora Mining Company Limited (PMC Ltd) and the Phosphate Development Corporation (FOSKOR) respectively (Heinrjch, 1970; Beale, 1985b).

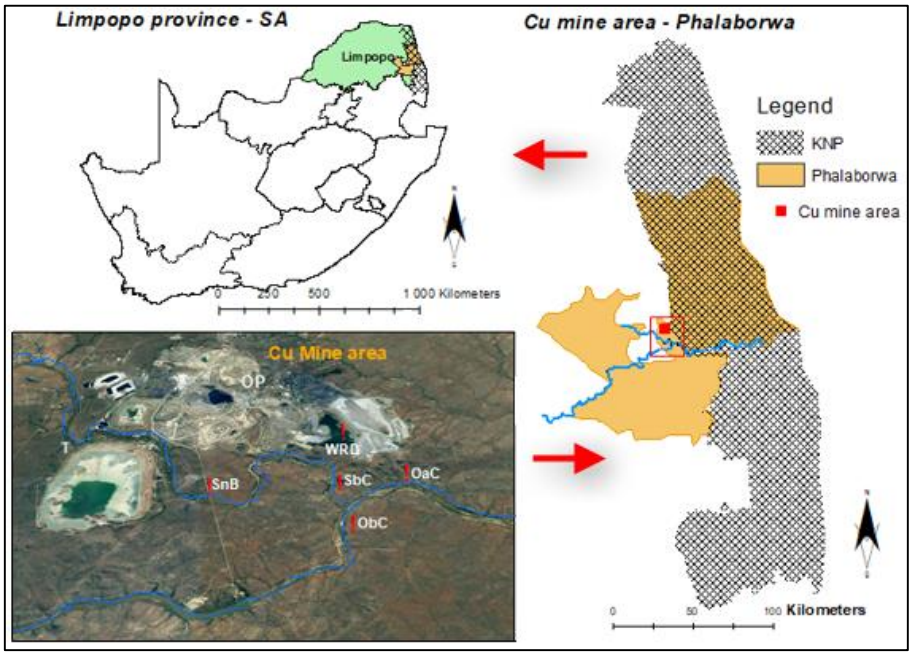


Figure 4.1: Copper mine area (PMC) in Phalaborwa, Limpopo province of South Africa

PMC is sandwiched on its eastern boundary by the Kruger National Park (KNP) and on its western boundary by FOSKOR. It is drained by the Selati River and the Olifants River, both, members of the Olifants catchment (Fig 4.1) (Ashton *et al.*, 2001). The Olifants River is the main water flow of this catchment. Most water from the higher, middle and lower parts of this catchment collects into the Olifants river (Frick, 1986; Ashton *et al.*, 2001). The Selati River meanders the southern boundary of the twin mines before pouring its water into the Olifants River near the PMC/KNP boundary. A stretch of the Olifants River, in the lower part of the Olifants catchment, flows past near the southern boundary of PMC and continues through KNP where it receives water from the Letaba River, in the Gorge, just before crossing into Mozambique. Wild animals such as elephants, monkeys and others form part of the usual scenery in PMC yard (Fig 4.2). Crocodiles and hippopotamuses form another scenery in the Olifants River around the PMC/KNP boundary.



Figure 4.2: Two elephants seen at close range within PMC area (Photo by author, 2016).

4.2 Sampling points at Phalaborwa

Selection of sampling points was guided, from the theoretical perspective, by the classification of samples as sources or receivers of pollution. Convenience sampling, dictated by safety and accessibility of sampling sites, influenced the practical perspective of sampling sites selection. Well before sampling, permission and escort provision were

granted as all sampling sites were located within or required passing through private properties (PMC, FOSKOR, KNP and Hippo pool resort (HP)).

A total of seven sampling sites were identified (Table 4.1). Two sites along the Selati River: (i) upstream close to a bridge behind FOSKOR mine backyard, on the road leading to the Olifants barrage and (ii) downstream before the confluence with the Olifants River near PMC southeastern boundary (Figure 4.3). Two other sites along the upper section of the Olifants River: (i) upstream at Hippo Pool resort (HP) (Figure 4.4) and (ii) downstream before its confluence with the Selati River. Two more sites along the lower section of the Olifants River: (i) between the confluence and the PMC/KNP boundary, and (ii) at Mamba Weir (MW) a few meters within the KNP. The Water Retain Dam (WRD) within PMC made the seventh and isolated sampling site (Figure 4.5). The latter together with the former sites constituted the sources of water and sediments samples.

Table 4.1: Sampling sites identification codes, Global Positioning System (GPS) coordinates and description

Identification codes	Latitude	Longitude	Description
OHP	24˚11'49.5"S	30˚48'34.6"E	Olifants at Hippo Pool resort
ObC	24˚2'46.4"S	31˚10'34.6"E	Olifants before confluence
SFB	24˚2'16.6"S	31˚7'34.6"E	Selati at 'FOSKOR Bridge'
SbC	24˚2'18.6"S	31˚10'34.6"E	Selati before confluence
OaC	24˚2'24.0"E	31˚12'34.6"E	Olifants before PMC/KNP
OMW	24˚2'31.4"	31˚12'34.6"E	Olifants at Mamba Weir
WRD	24˚0'49.2"S	31˚9'34.6"S	Water retain dam



Figure 4.3: a) the Selati River (upper part) behind FOSKOR at a bridge on the road to Phalaborwa Barrage. Thick rubber flaps prevent animals from going beyond the bridge. b) the Selati River (lower part) near its confluence with the Olifants River.



Figure 4.4: The Olifants River (upper section) at Hippo Pool resort



Figure 4.5: Water Retain Dam (WRD) within the mine area

4.3 Sample collection from Phalaborwa

4.3.1 Sand and rocks

A random collection of a few samples was carried out during the reconnaissance trip of the mine area in Phalaborwa. A granular material consisting of finely divided rock particles (sand) and stones composed of an aggregate of minerals (rocks) were collected (Figure 4.6).



Figure 4.6: Sand and rocks samples collected during the reconnaissance trip

4.3.2 Water and Sediments

Well before sampling, polyethylene bottles (500 mL) were thoroughly washed with a detergent, rinsed profusely with tap water, soaked overnight in 10% nitric acid bath, rinsed successively with distilled water and deionized water (DI) and, finally, air dried. Zipper plastics were also prepared for sediments collection. Each pair of water and sediment samples were collected at the same place; water was collected before sediment.

Sampling bottles were rinsed twice with sample water and then held underneath water until they were filled up and then caped immediately. On site measurements of pH, electrical conductivity (EC), oxidation reduction potential (Eh) and temperature were taken from a separate bottle of freshly collected water sample. Water samples were then split into two subsamples: the first portion of unfiltered water was acidified (UFA) to pH of slightly less than 2 with 1 mol L^{-1} HNO_3 to minimize adsorption and, the second portion of unfiltered water remained un-acidified (UFUA). Sediments were subsequently collected into polyethylene zipper bags. All samples were kept under ice. At the camp house, splits of UFUA portions were later filtered with 0.45 µm pore size syringe filter to obtain filtered un-acidified (FUA) water. All samples were transferred to the refrigerator. They were later transported under ice in a cooler box until their delivery to the laboratory in Johannesburg.

4.3.3 Assorted solid samples

Three rocks from a conveyor belt and sand were collected during the reconnaissance trip. Later on, a variety of samples were collected from the PMC yard (Table 4.2) some of which are shown in Figure 4.7.

Table 4.2: Samples identification and description

Sample ID	Sample Description
Cbt	Carbonatite
Cu-crusts	Copper crusts
Mgt	Magnetite
TexCon	Tailings ex-Concentrator
WRD MS	Muddy sediments on the shore of WRD
WRD DS	Dry sediments at the bank of WRD
WRD-PG	Phosphogypsum at the bank of WRD
CF carcass	Cat fish carcass at the bank of WRD



Figure 4.7: (i) elephant dung; (ii) tailings ex-concentrator; (iii) carbonatite; (iv) copper crusts; muddy sediment (WRD shore) and dry sediment (WRD bank)

4.4 Location and description of study site 2 – Kitwe, Zambia

The Kafue River is a conspicuous feature in map description of Kitwe district as a sampling area. Inhabited municipal land as well as exploited mine land are both, one after the other, situated on the western side of the Kafue River. Hence, streams to which selected sampling points are attributed run eastwards the Kafue River through residential communities. Two abandoned tailings dumps are located within mine residential area

near town business centre; the other one is situated behind mine land on a separate site at the boundaries of Kitwe with Kalulushi. Sample type, identification code, and description details of sampling sites are tabulated (Tab 4.3) and visual reconnaissance is also given in the form of a map (Fig 4.8)

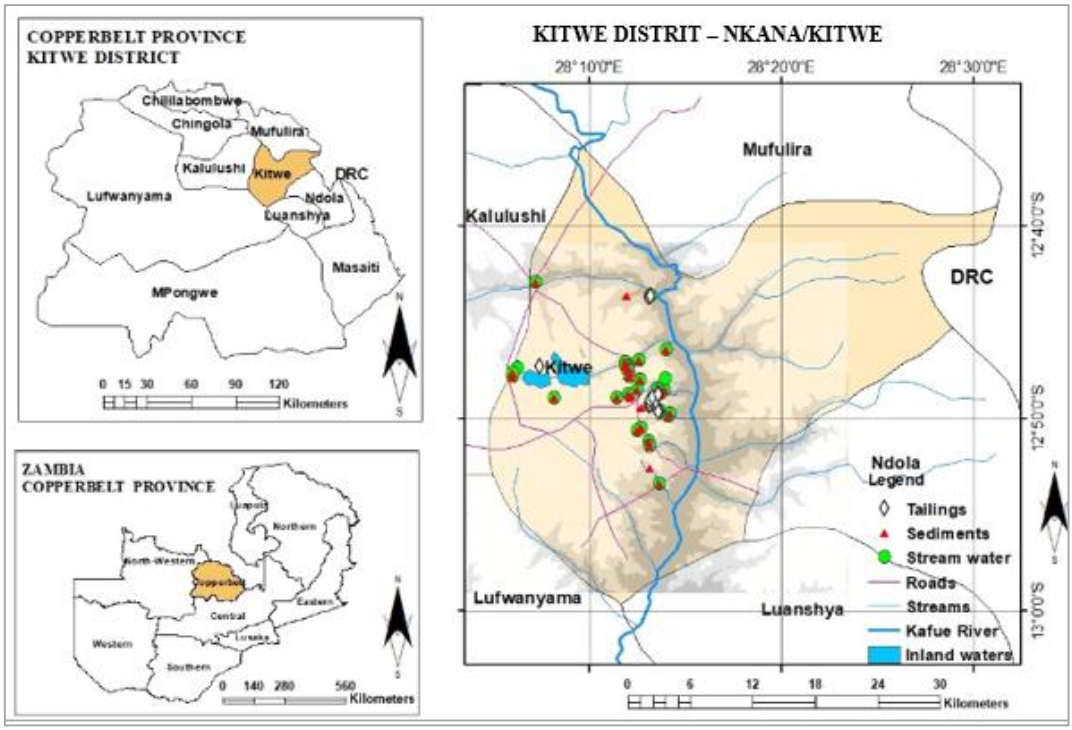


Figure 4.8: The Copperbelt Province, Kitwe surrounded by other mining towns and distribution of sampling points on the western side of Kafue River stretch in Kitwe.

4.5 Sample collection from Kitwe

Samples consisted of tailings collected from three abandoned tailings dumps (TD15A, TD25 and TD26/27). Sediments and water were obtained from streams which were classified as having (i) obvious, (ii) probable and (iii) no connection with selected tailings dumps (soil samples were sparse). Solid samples were air dried, crushed, sieved and kept in polyethylene zipper bags awaiting various qualitative and quantitative analyses. Physicochemical parameters of water samples were taken before pre-treatment. Their pH was reduced, for preservation where necessary, to slightly below 2 with nitric acid and

kept refrigerated at 4°C. All samples were then sent to The University of the Witwatersrand, South Africa, for analyses.

Table 4.3: Sampling points description and samples identification

	Sample identification code	**Sample type**	**Sampling site description**
1	W/S1, W/S2 ●	water and sediments	Kantanta st and Chiwala Av south and north of TD25
2	T1, **T2,** T3, T4, T5, T45, T46 Δ	Tailings	TD25 Between Nkana East and Park land
3	W/S3, W/S4, W/S5 ●	water and sediments	TD25 Between Nkana East and Park land
4	W/S6, W/S7, W/S8, W/S17 ●	water and sediments	Along Kitwe stream
5	W/S11, W/S13, W/S14, W/S15 ●	water and sediments	Near / Around TD 15A
6	T12 Δ	Tailings	TD15A behind mine land in Kitwe west
7	W/S16 ●	water and sediments	Bridge at T-junction Chingola/Mufulira Rd
8	W/S18, W/S19, W/S20, W/S34 ●	water and sediments	Along Wusakile stream
9	W/S21, W/S25 ●	water and sediments	Bridge and wet land at Copper Hill Mall
10	W/S22, W/S23 ●	water and sediments	Kamitondo and Ipusukilo
11	S26, S27, S28 ◊	sediments	Industrial Area
12	W/S37, W/S38 ●	water and sediments	Industrial Area
13	T32, T48 Δ	Tailings	TD26/27 Nkana East
14	W/S30, W/S31, W/S33 ●	water and sediments	TD26/27 Nkana East and Natwange
15	W/S35 ●	water and sediments	Bridge at Lwanshimba stream along Luangwa Rd to ZNS
16	W/S29, W/S44 ●	water and sediments	Wet land at Kitwe Central Hospital and behind Ganerton
17	W9 *	water	Riverside
18	S36 ◊	sediments	behind Chamboli
19	S41, S43, S47 ◊	sediments	Behind Ganerton and near business centre

Letters stand for: W = water, S = sediments, T = tailings. Numbers denote sampling points.

4.6 Chemicals and reagents

Analytical grade chemicals, Nitric acid (55% HNO_3), Hydrochloric acid (32% HCl), Hydrogen peroxide (30% H_2O_2), sodium hydroxide (NaOH), hydroxylamine hydrochloride ($NH_4OH.HCl$), were purchased from Merck Chemicals (PTY) Ltd, Johannesburg, South Africa. Acetic acid (98.9% CH_3COOH), Sodium fluoride (NaF), sodium chloride (NaCl), Sodium nitrate ($NaNO_3$), Potassium dihydrogen phosphate (KH_2PO_4) and (Na_2SO_4) salts were purchased from (Associated Chemicals Enterprises, Johannesburg, SA). Deionized water (DI), 18 MΩ cm^{-1}, obtained from a Milli-Q system (Millipore Corp., Bedford, MA, USA) was used to prepare and dilute solutions.

4.7 Apparatus and instruments used

4.7.1 Apparatus used

Hanna Instruments field multi-meter HI 98130 (Woonsocket RI, USA) was used for measurements (and adjustments) of pH, electrical conductivity (EC) and temperature. Field multi-meter, Celsius Scientific PCT-407 (South Africa), was used for pH, ORP, EC, TDS, Salinity and Temperature. Other instruments used included the following: Analytical balance (OHAUS, Adventurer, Switzerland), Sartorius microbalance (A.T. Göttingen, Germany) connected to Elemental Analyzer, centrifugation instrument (Hettich, ROTOFIX 32 A), reciprocal platform shaker (Labcon, Apollo Scientific), sieve shaker (Retsch, South Africa), microwave digestion system Multiwave GO (Anton Paar, South Africa), WiseCube Incubator (WIS-30) with adjustable shaking speed and environmental temperature, Ion Chromatography 761 IC Compact (Metrohm, Switzerland), Inductively Coupled Plasma-Optical Emission Spectroscopy (ICP-OES, Spectro Genesis, Germany), Inductively Coupled Plasma-Mass Spectroscopy (ICP-MS, Agilent 7700 Series, USA). Accessories included micropipettes (100 and 1000 µL) (Gilson, France), syringe filters (Science, SA), and hot plates (Heidolph MR 3001K).

4.7.2 Summary of instruments used

4.7.2.1 X-ray diffraction spectroscopy (XRD)

Bruker D2 Phaser powder diffractometer Co $k_{\alpha 1}$ radiation (at 30 mA and 40 kV) was used to collect ex-situ variable temperature X-ray diffraction measurements. Phase analysis was done with the help of Bruker-AXS Evaluation Package (EVA) version 4.2.1.10. and the X'Pert High Score software, version 1.0d (Panalytica, the Netherlands) was utilised to interpret the resulting XRD patterns.

4.7.2.2 X-ray fluorescence spectroscopy (XRF)

The instrument Axios Max (Analytica, the Netherlands) was helpful in the determination of elements in powder sediments and tailings. The fused disk method with La-tetraborate flux on a program called Super-Q was used to analyse major elements. Traces elements were analysed using the pressed pellet method on a Pro-Trace program. The instrument was run at 50 mA and 50 kV.

4.7.2.3 Scanning emission spectroscopy / energy dispersive spectroscopy

The Calzeiss Sigma Field Emission Scanning Emission Spectroscopy equipped with Oxford X'act Energy Dispersive Spectroscopy detector (UK) was used for SEM-EDS analysis. Homogeneous sample powder was sprinkled on a carbon sticker tape the excess of which was blown off with compressed air. The sample was coated with Au/Pd (80:20) and thereafter placed in the vacuum chamber of the SEM-EDS

4.7.2.4 Total carbon hydrogen nitrogen sulphur analyser (CHNS)

The Elementar vario EL cube (Elementar-Straβe, Germany) was used to determine total carbon, hydrogen, nitrogen and sulphur, by combustion of samples in high temperature. A succession of duplicates of Run in (to burn the system clean) and blank, and a quadruplet of sulphanilamide (standard) followed by a set of sample duplicates are run with the same method. The combustion runs effectively at pressure ranging between 1200 and 1250 mbar and temperature of 1150 K and 850 K for the combustion tube and the reduction tube respectively.

4.7.2.5 Laser Particle Sizer (LPS)

Grain size distribution of tailings and sediment samples were determined using the Mastersizer 3000 Laser Diffractometer instrument (Malvern Pananalytical, United Kingdom) capable of analysing particle sizes between 0.02 and 20,000 µm. The method is based on the correlation between the angles of light scattered from particles in a laser beam and the size distribution of these particles. Fractionation results are statistical averages of three replicate measurements.

4.7.2.6 Microwave digestion

Multiwave GO (Anton Paar, Johannesburg, South Africa) is a microwave digestion system suited for environmental samples and other materials. It is equipped with a 12 slot XF-100 rotor for 12 XF-100 digestion vessels. Various official methods are preloaded, such as US-EPA method 3050B, US-EPA method 3051 and US-EPA method 3052 and, a provision for loading new methods exists. Multiwave GO has features that allow for heat distribution across all pressure vessels in an efficient and uniform manner. It is mounted with infra-red (IR) sensors for localized overheating monitoring.

4.7.2.7 Ion Chromatography

The Ion Chromatography 761 Compact IC (Metrohm Company, Switzerland) operated with IC Net 2.3 software was employed for the determination of anions content in leachates and stream water. Its principal components are the separation column Metrosep A supp5 (150/4.0 mm) and the Metrohm Suppressor Module (MSM) for chemical suppression. The eluent (2.0 mM Na_2CO_3 and 1.0 mM $NaHCO_3$), regenerating (50 mM H_2SO_4) and rinsing (DI) solutions were used. A mixed calibration standard (1, 5, 10 and 20 mg L^{-1}) of F^{1-}, Cl^{1-}, NO_3^{1-}, $H_2PO_4^{1-}$ and SO_4^{2-} were prepared from solid salts. Standards/samples were collected in the injection loop (20 µL) and transported by the eluent to the separation column at the flow rate of 0.7 mL min^{-1}. Carbonate anions from the eluent were neutralized by chemical suppression.

4.7.2.8 Inductively Coupled Plasma-Optical Emission Spectroscopy

The Inductively Coupled Plasma-Optical Emission Spectroscopy instrument (Spectro Genesis, Germany), operated by the Smart Analyser Vision software 6.01.0943, was used to determine metal concentration in digests, leachates and surface water samples. Multi-elemental standards 1000 µg L^{-1} (De Bruyn Spectroscopic Solutions, SA) were diluted to prepare 0.1, 0.5, 1.0 and 2.0 mg mL^{-1} instrument calibration solutions. HNO_3 (5%) was used as diluent for standards and as rinsing solution for the instrument.

4.7.2.9 Inductively Coupled Plasma-Mass Spectroscopy

The Inductively Coupled Plasma-Mass Spectroscopy instrument (Agilent 7700 Series, USA), equipped with MassHunter software, was used to determine (i) REEs + U concentration in Mgt leachate, prior to Mgt use as adsorbent in REEs recovery experiments and (ii) trace elements concentration in Cu_crust leachates, for use in evaporation/dilution simulations. Multi-elemental standards 1000 µg L^{-1} (De Bruyn Spectroscopic Solutions, SA) were used to prepare 50, 100, 200, 500, 1000 and 2000 µg L^{-1} instrument calibration solutions. HNO_3 (2.5%) was used as diluent for standards and as rinsing solution for the instrument.

4.8 Sample preparation

Nondestructive (physical) and destructive (chemical) sample preparations were executed to obtain solids and solutions in appropriate conditions for various qualitative, semi-quantitative and quantitative analyses.

4.8.1 Sample drying and grain size normalization (separation)

Thawing consisted of simply allowing samples to defrost at room temperature. It was followed by air drying which was done by spreading samples on a clean polyethylene sheet with a large surface. Samples were covered with paper towel in order to protect them from dust particles. The time lapse for samples to dry was close to a week.

Mechanical pulverization of some samples (e.g. rocks) was done using crushing and milling instruments at Geoscience Department. Normalization of samples into grains of

specific size intervals were obtained using a sieve shaker instrument and a set of sieves. Small portions of grain size < 50 µm were destined for powder X-ray diffraction (PXRD), X-ray fluorescence (XRF), Scanning Electron Microscopy–Electron Dispersive X-ray Spectroscopy (SEM-EDS) and Total carbon, hydrogen, nitrogen and Sulphur (CHNS) analyzer. Mixed and homogenized grain size < 125 µm were used in leaching and digestion.

4.8.2 Leaching procedure

The Toxicity Characteristic Leaching Procedure (TCLP) simulates natural leaching phenomena. It employs acid leaching fluids that entice the release of elements from the environmental sample's mobile phase into leachate (Marguí *et al.*, 2004).

2.8.2.1 Extraction fluids preparation

Extraction fluid 1 was prepared by adding 5.7 mL of 99.8% CH_3COOH, 64.3 ml of 1 mol L^{-1} NaOH into a 1000 mL volumetric flask and, filling it up to the mark with DI. The pH of extraction fluid 1 was adjusted to 4.92 ± 0.05. Extraction fluid 2 was prepared by adding 5.7 mL of 99.8% CH_3COOH into a 1000 mL volumetric flask and filling it up to the mark with DI. The pH of fluid 2 was adjusted to 2.88 ± 0.05. Extraction fluids pH were adjusted with 1 mol L^{-1} NaOH and 1 mol L^{-1} HNO_3, accordingly.

4.8.2.2 TCLP protocol

Following the 1 to 20 TCLP rule (TCLP-Method 1311 (USEPA, 1992), 2g of solid samples were weighed, in triplicate, directly into 50 mL polytetrafluoroethylene (PTFE) centrifuge tubes. To one of each triplicate samples, 40 mL of DI was added and mixtures were agitated on a "to and fro" horizontal shaker at 150 rpm for 5 min. Then, paste pH of shaken solutions was measured to determine which extraction fluid was appropriate for which solid samples. Extraction fluid 1 was required for solid samples which generated solutions of pH values less than 5 (pH < 5) whereas extraction fluid 2 was required for solid samples which generated solutions of pH values greater than 5 (pH > 5) (Karaca, Cameselle and Reddy, 2016).

To the remaining duplicates of each sample, already weighed in centrifuge tubes, 40ml of the appropriate extraction fluid was added to each 2g of sample. The solid-extraction fluid mixture was shaken at a speed of 50 rpm (the lowest speed the shaker could be adjusted to) at room temperature for 18 hours. At the end of this time, leachate solutions were obtained. Their pH and conductivity were measured as mandatory physicochemical parameters. Leachate solutions were passed through 0.45 µm pore size filters and then split into two portions. The first two portions of each leachate, destined for Inductively Coupled Plasma - Optical Emission Spectrometry (ICP - OES) analysis, had their pH adjusted to slightly below 2. The second two portions of each leachate, meant for Ion Chromatography (IC) analysis, remained unacidified. All samples were kept at 4^{o}C in the refrigerator.

4.8.2.3 Cu_crust leaching for evaporation simulations

Crusts, in the context of geochemistry, are hardened layers of soil containing a mixture of salts in large amounts besides salts of the dominant base metal after which they are named (e.g. Cu_crusts, Fe_crusts). By leaching Cu_crusts, solutions with characteristics as close as possible to the natural and field environment were obtained (Pourret *et al.*, 2015). Evaporation and dilution predictions of surface water were approached from the geochemical modelling simulations angle using Cu_crust leachates.

Cu_crust (1.0 g) was weighed in triplicates. DI (100 mL) was then added to Cu-crust in 250 mL beakers. The mixtures were stirred mechanically, for 5 h at room temperature, to allow Cu-crust leaching to take place. Syringe filtering, through 0.22 µm filters, was used to separate Cu_crust leachates from Cu_crust residues. Filtrates were splits into three (3) portions destined for trace analysis on ICP-MS, major elements analysis on ICP-OES and major anions on IC. Calibration standards were prepared accordingly for each set of analysis. Results were fed into PHREEQC computation for evaporation (dilution) simulations.

4.8.3 Adsorption studies experiments

4.8.3.1 Preparation of adsorptive (REEs) carrying fluid and adsorbent (Mgt)

i. REEs standards solution (1000 mg L^{-1} in HNO_3) from Sigma Aldrich, South Africa, was used to prepare 100 mg L^{-1} stock solution in 50 mL graduated centrifuge tubes. This solution was used for further dilutions to appropriate concentrations as required.

ii. Selected solid salts (Figure 4.4) were used to prepare single element stock solutions (50 mL, 100 mg L^{-1}) of competing ions. These solutions were then used to obtain multi element solutions as per adsorption experiment dictate.

Table 4.4: A mix of sulphate, nitrate and chloride salts selected for the effect of competition experiment and their measured concentrations in two different competing solutions with ~ 0.5 mg L^{-1} REEs.

Salt	Salt Molar mass	Metal molar mass	Purity (%)	Fix low conc (mg L^{-1})	Mix high conc (mg L^{-1})
$CaCl_2$	110.99	40.08	0.95	0.31	1.78
$MgSO_4$	120.39	24.31	0.99	0.37	2.10
$CuCl_2$	134.452	63.55	0.99	0.51	1.81
$ZnSO_4.4H_2O$	179.45	65.41	0.99	0.50	1.24
$MnSO_4.4H_2O$	223.07	54.94	1	0.63	1.48
$NiSO_4$	262.86	58.69	0.99	0.64	1.41
$CoSO_4.7H2O$	281.12	58.93	0.98	0.65	1.52
$Pb(NO_3)_2$	331.2	207.2	0.99	0.84	1.27

iii. Natural magnetite, obtained from PMC Limited, was sieved to < 125 µm diameter particle size fractions and then used as it is (without any prior treatment and functionalization) in REEs recovery experiments.

4.8.3.2 Batch recovery experiments

Batch experiments for the recovery of REEs were carried out to determine the effects of varying adsorbent mass, adsorptive carrying solution initial concentration, adsorption pH

condition and agitation time on the adsorbent recovery efficiency (%) and capacity (mg L^{-1}).

i. Effect of adsorbent mass

Varying mass of adsorbent (Mgt) (50, 100, 150, 200, 300 and 500 mg) were weighed in triplicates, mixed with adsorptive carrying fluid (REEs solution) (150 mL, 1 mg L^{-1}), agitated for 5 hrs on a horizontal shaker (Labcon, South Africa) at a speed of 150 rpm. Syringe filtering through 0.22 µm filters was employed to separate adsorptive fluid supernatants from adsorbent residues. Analysis using ICP-OES (Spectro Genesis, Germany) followed thereafter.

ii. The effect of pH

A fixed (optimum) mass of adsorbent was weighed (mg) in triplicates, mixed with adsorptive carrying fluid (15 mL, 1 mg L^{-1}) of varying pH (2.5, 4.5, 6, 7, and 9.5), and agitated for 5 hrs on a horizontal shaker (Labcon, South Africa) at a speed of 150 rpm. Syringe filtering, through 0.22 µm filters, was employed to separate adsorptive carrying fluid supernatants from adsorbent residues. Analysis using ICP-OES (Spectro Genesis, Germany) followed thereafter. Care was taken that the original REEs solution (before pH adjustments with NaOH (0.1) and HNO3 (0.1) using syringe needles) and all excess adsorptive carrying fluid of different pH were kept and analysed together with filtered adsorptive carrying fluid supernatants.

iii. Effect of agitation time

A fixed (optimum) mass of adsorbent was weighed (mg) in triplicates, mixed with adsorptive carrying fluid (15 mL, 1 mg L^{-1} and optimum pH), and agitated for different agitation times (30, 60, 90, 135, 180 and 240 min) on a horizontal shaker (Labcon, South Africa) at a speed of 150 rpm. Syringe filtering, through 0.22 µm filters, was employed to separate adsorptive carrying fluid supernatants from adsorbent residues. Analysis using ICP-OES (Spectro Genesis, Germany) followed thereafter.

iv. Effect of initial concentration

A fixed (optimum) mass of adsorbent was weighed (mg) in triplicates, mixed with adsorptive carrying fluid (15 mL, optimum pH) of varying initial concentrations (0.1, 0.5, 1.0, 1.5, 2.0 and 2.5 mg L^{-1}), and agitated for optimum time (min) on a horizontal shaker (Labcon, South Africa) at a speed of 150 rpm. Syringe filtering, through 0.22 µm filters, was employed to separate adsorptive carrying fluid supernatants from adsorbent residues. Analysis using ICP-OES (Spectro Genesis, Germany) followed thereafter. Care was taken to keep the REEs solution of optimum pH, but of different initial concentrations for analysis together with filtered adsorptive carrying fluid supernatants.

v. Effect of temperature

Two sets of 150 mg of adsorbent were weighed (mg) in triplicates, mixed with adsorptive carrying fluid (15 mL, pH 4.5, 1.0 mg L^{-1}). One set was agitated at $25^{O}C$ for 30, 60, 90, 135, 180 and 240 minutes on a horizontal shaker (Labcon, South Africa) at a speed of 150 rpm. The other set was agitated in a WiseCube Incubator (WIS-30) with shaking speed and environmental temperature adjusted to 150 rpm and $35^{o}C$ respectively. Syringe filtering, through 0.22 µm filters, was employed to separate adsorptive carrying fluid supernatants from adsorbent residues. Analysis using ICP-OES (Spectro Genesis, Germany) followed thereafter. Care was taken to keep the REEs solution used for analysis together with filtered adsorptive carrying fluid supernatants.

vi. Effect of competing ions

A fixed (optimum) mass of adsorbent was weighed (mg) in triplicates, mixed with adsorptive carrying fluid (15 mL, optimum pH) containing REEs initial concentration (0.5 mg L^{-1}) and competing ions initial concentration (~0.5 mg L^{-1}), and agitated for optimum time (min) on a horizontal shaker (Labcon, South Africa) at a speed of 150 rpm. Syringe filtering, through 0.22 µm filters, was employed to separate adsorptive carrying fluid supernatants from adsorbent residues. A second set of adsorbent mixed with adsorbate (15 mL, optimum pH) containing REEs initial concentration (0.5 mg L^{-1}) and competing ions initial

concentrations ranging between 1.0 - 2.5 mg L^{-1} was concomitantly run through the same process. Analysis using ICP-OES (Spectro Genesis, Germany) followed thereafter. Care was taken to keep both unused competing ions adsorptive carrying fluid for analysis together with their corresponding filtered adsorptive carrying fluid supernatants.

4.8.4 Important steps in Adsorption thermodynamics parameters determination

Adsorption thermodynamic parameters were determined following important steps involving a series of calculations and plotting for each group of parameters.

4.8.4.1 Activation energy

The Arrhenius equation (Equation 4.1) was used to show the dependence of adsorption rate constants on temperature and deduce the minimum energy needed for adsorption process to proceed (activation energy, E_a). Rate constants (k) obtained from Experimental measurements at different temperatures (T) were fitted in the linearised expression of the Arrhenius equation (Equation 4.2) in order to plot ln k versus 1/T. The value of Ea (kJ mol^{-1}) was calculated from the slope of the line equation. R is the gas constant (8.3145 J mol^{-1} K^{-1}), T is the absolute temperature (K), k is the rate constant (min^{-1}) and A is the frequency factor (constant).

$$k = \mathrm{A}\, \mathrm{e}^{\frac{-\mathrm{E_a}}{\mathrm{RT}}} \qquad \text{Equation 4.1}$$

$$ln\, k = ln\, A - \left(\frac{E_a}{R}\right) \frac{1}{T} \qquad \text{Equation 4.2}$$

4.8.4.2 Activation parameters during the adsorption process

With the help of the adsorption rate constants obtained from isotherm studies at different temperatures, the Eyring equation (Equation 4.3) was employed to determine the activation enthalpy (ΔH^*, kJ mol^{-1}) and the activation entropy (ΔS^*, J mol-1) from the slope and intercept of the line equation obtained by plotting (ln k)/T versus 1/T. These two activation parameters were used to calculate the free energy of activation ($\Delta G*$, kJ mol^{-1}) from Equation 4.4 below. The Boltzman constant (k_B, 1.3807 x 10-23 J K^{-1}) and the Plank constant (h, 6.6261 x 10-34 Js)

$$ln\,k = (ln\frac{k_B}{h} + \frac{\Delta S^*}{R}) - (\frac{\Delta H^*}{R})\frac{1}{T}$$ Equation 4.3

$$\Delta G^* = \Delta H^* - T\Delta S^*$$ Equation 4.4

4.8.4.3 Activation parameters of complete adsorption process

The adsorption distribution constant (K_D) was first determined using qe and Ce obtained from isotherm studies (Equation 4.5). This apparent equilibrium constant, the ratio of the equilibrium liquid phase concentration (Ce) with its corresponding constant solid phase concentration (qe), was then used in lieu of the equilibrium constant, as is always the case for sorption systems, to determine the standard free energy using the Van't Hoff equation (Equation 4.6). The standard entropy (ΔS^o) and standard enthalpy (ΔH^o) values were calculated from the slope and intercept of the line equation obtained by plotting either ln K_D versus 1/T using the linearised Van't Hoff equation (Equation 4.7) or ΔG^o versus T using Gibbs free energy expression in Equation 4.8 below.

$$K_D = \frac{q_e}{C_e}$$ Equation 4.5

$$\Delta G^o = RT\,ln\,K_D$$ Equation 4.6

$$ln\,K_D = (\frac{-\Delta H^o}{R})\frac{1}{T} + \frac{\Delta S^o}{R}$$ Equation 4.7

$$\Delta G^o = \Delta H^o - T\Delta S^o$$ Equation 4.8

4.8.4.4 Standard heat of partial adsorption process

In order to find the standard heat of partial adsorption (differential isosteric heat of adsorption) the integrated expression of the Clausius-Clapeyron (Equation 4.9) was employed to plot ln Ce against 1/T. This was made possible by the use of the equilibrium concentration (C_e) of the adsorptive in solution at constant amount of the adsorbate on the adsorbent at different temperatures obtained from isotherm studies. The differential isosteric enthalpy (ΔH_x) was then calculated from slope of the line equation obtained from this plot.

$$ln\,C_e = -(\frac{\Delta H_x}{R})\frac{1}{T} + K$$ Equation 4.9

4.8.5 Pseudo-total metal content microwave digestion procedure

Samples of particle size < 125 µm were weighed directly into microwave pressure vessels. *Aqua regia*, 12 mL made up of three portions of HCl and one portion of HNO_3, was added to microwave pressure vessels containing 0.25 g samples. The *aqua regia*-solid sample mixtures were gently hand swirled and allowed to stand for 5 minutes. Seals were then plugged up into the reaction vessels' mouth before closing them, finger tight, with screws caps. Care was taken that spring holders lied level on caps' surface for proper venting. All pressure vessels were then loaded into the rotor's numbered holes for easy sample identification. The rotor was then covered with its lid before introducing it in the Multiwave GO for digestion. The preloaded *aqua regia* extraction method for inorganic samples was selected and applied to these samples. It involved a microwave succession of ramping, holding and cooling events of the mixtures programmed to last for 10 minutes each. The rotor was taken out of the microwave at the end of digestion and placed in the fume hood. Caps were unscrewed and seals removed from pressure vessels. Since microwave digestion left solid residues, the digests were filtered through 0.45 µm syringe filters. The supernatants were then transferred into a 50 ml centrifuge tubes and brought to volume with DI. Samples were kept in the fridge at 4^oC awaiting ICP-OES analysis.

4.8.6 Microwave assisted modified Community Bureau of Reference

Modified Community Bureau of Reference (mBCR) is an improved version of the conventional three step Community Bureau of Reference (BCR) sequential extraction method. Its protocol increased, at step 2, the concentration of hydroxylamine hydrochloride, $NH_2OH.HCl$, from 0.1 mol L^{-1} to 0.5 mol L^{-1} and lowered the pH from 2 to 1.5 (Mossop and Davidson, 2003).

The microwave assisted version of the modified Community Bureau of Reference (MW mBCR), as proposed by Castillo et al. (2011), was used to extract elements from solid samples in a stepwise manner similar to mBCR. Except for the replacement of 1.0 mol L^{-1} ammonium acetate (CH_3COONH_4) by 5.0 mol L^{-1} acetic acid and its subsequent simultaneous use with H_2O_2 in step 3, MW mBCR employs the same chemicals, number of steps and ratio of mass to volume reduced to lower values suitable for pressure microwave vessels' maximum volume.

4.8.6.1 Reagents preparation procedure

The three steps of MW mBCR require, each, its own extraction fluid (s).

Fluid A: 0.11 mol L^{-1} Acetic acid (CH_3COOH) served as extraction fluid for step 1 and was prepared, in a fume hood, by adding 25 ± 0.2 mL of acetic acid to about 500 mL of DI in a 1000 mL polypropylene volumetric flask and made up to the mark with DI. This was a stock solution (0.43 mol L^{-1}) from which 250 mL was taken and diluted to 1000 mL to make 0.11 mol L^{-1} CH_3COOH solution.

Fluid B: 0.5 mol L^{-1} Hydroxyl ammonium chloride ($NH_4OH.Cl$) also known as hydroxylamine hydrochloride ($NH_3OH.HCl$) was the extraction solution for step 2. It was prepared in a beaker by dissolving 34.75 g of $NH_4OH.Cl$ in 400 mL of DI, and then transferred into 1000 mL volumetric flask to which 25 mL of 2 mol L^{-1} HNO_3 was added before making up the volume to the mark with DI. This extracting solution was freshly prepared before use.

Fluid C and D: A set of two reagents were simultaneously used in step 3. Hydrogen peroxide (H_2O_2, 30% 2 mL) and acetic acid (CH_3COOH, 5 mol L^{-1}) adjusted to pH of about 2.0.

4.8.6.2 Extraction procedure

A schematic form of the following procedure is illustrated in Figure 4.9 below.

Step 1 (Exchangeable fraction): Solid samples, 0.25 g of < 1.25 µm grain size, were weighed directly into 50 mL microwave vessels, ready to undergo the three step MW mBCR extraction. CH_3COOH (10 mL of 0.11 mol L^{-1}) was then added to microwave vessels. The vessels were finger tight closed with screw caps making sure the spring holder inserts were neither protruding nor intruding. They were then loaded inside the rotor marrying slot numbers with sample (vessel) identification code. The rotor was covered with its lid before placing it properly on the drive ring. The Multiwave Go door was closed and the method created for step 1 was then run. When the experiment had finished, the rotor was removed from the Multiwave Go and placed in the fume hood where caps were unscrewed carefully and kept aside. Parafilm was used, instead, to firmly hold in place plugged up seals and, in doing so, allow microwave vessels to fit in the centrifugation instrument. Samples were centrifuged, four at a time, at 3000 rpm for 30

minutes. Supernatants were then decanted into 50 mL centrifuge tubes. In order to re-suspend the solid that remained at the bottom, 10 mL DI was added to microwave pressure vessels which were then closed with seals and caps before placing them on a "to and fro" horizontal shaker set to run at 150 rpm for 10 minutes. Parafilm was used, as earlier, before centrifugation. The supernatants from rinsing process were discarded carefully, and the solids that remained at the bottom of the vessels were for use in the next step.

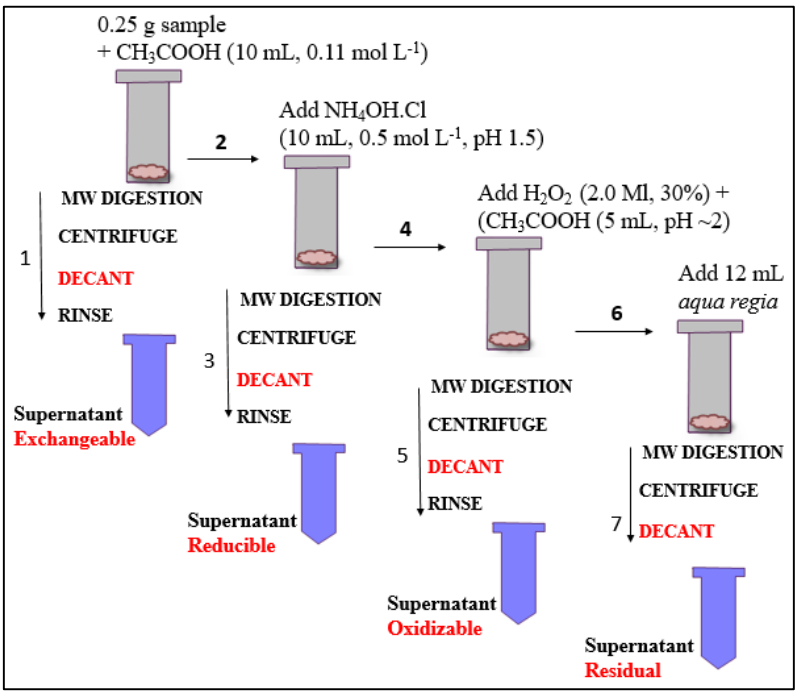


Figure 4.9: Schematic representation of MW mBCR procedure

Step 2 (Reducible fraction): $NH_4OH.Cl$ (10 mL of 0.5 mol L^{-1}, pH = 1.5) was added to the residue from step 1 in the microwave pressure vessels. Manual shaking was used to break the cake and bring back residues into solution. The step 1 procedure cycle was repeated making sure supernatants from the extracting fluid were kept for analysis, supernatants from rinsing with DI were discarded and residues were kept for use in the next step.

Step 3 (oxidizable fraction): H_2O_2 (2.0 mL, 30%) was added to the residue from step 2 followed by the addition of CH_3COOH (5 mL, pH ~ 2). Manual shaking was used to bring back residues into solution. The procedure was repeated making sure supernatants from

the extracting fluid were kept for further processing before analysis i.e. supernatants obtained in this step were heated to reduce the volume to near dryness to release unreacted reagents. Then, HNO_3 (1 mol L^{-1}) was used to dissolve the residue and make up the volume to 25 mL. Supernatants from DI rinsing were discarded. Residues in microwave vessels were washed with DI and kept as before for the next step. (Ammonium acetate in nitric acid = complexing agent)

Step 4 (Residual fraction):

Aqua regia, (3HCl:1HNO_3, 12 mL), was added to microwave pressure vessels containing the residue from step 3. The single extraction protocol, for pseudo-total metal content, was applied.

4.9 Quality Assurance (QA) and Quality Control (QC)

Quality Assurance (QA) and Quality Control (QC) appropriate to sample types (water, sediment, tailings) and analytical protocols (leaching, digestion) and techniques (ICP-OES, IC) were observed during sample collection in the field and sample preparation and analysis in the laboratory. Required field measurements were taken, with calibrated instruments, on one of each set of field replicate water samples. QA/QC plans involved also taking necessary precautions and applying them to prevent the alteration of samples through the introduction or loss of chemical analytes: a clean surroundings, the use of plastic containers, filters with correct aperture and sample preservation (acidifying with HNO_3, refrigeration at approximately 4^oC and sample holding times).

Procedures for sample preparation were followed. Analytical standards were used for calibration. Laboratory triplicate/duplicate samples, Certified Reference Material (CRM) and blank were digested together in the same batch to check the analytical performance and to normalize any alteration of concentrations. The use of procedural blank indicated negligible external influence on samples. Analytical standards together with analytical blank were used in determining the Limit of Detection and the Limit of Quantification relative to the concerned instrument. The reproducibility of triplicate/duplicate sample measurements expressed as relative standard deviation (RSD) was generally at ± 10%. CRM (BCR 701) was used in this study to evaluate the accuracy of mBCR and provide

an internal check. Results were found to be satisfactory. The precision (variability) of replicate measurements was below 5%. Results were converted into appropriate units.

4.10 Data treatment

4.10.1 Stiff plots

Concentrations of major ions in surface water were converted from mg L^{-1} to mEq L^{-1} to facilitate the visual assessment of surface water quality at different sampling spots. Stiff diagrams were used to represent water classification and allow comparisons of water in Phalaborwa.

4.10.2 PHREEQC

Surface water data was used in mixing water simulations in order to find out the type of water that results from mixing. Cu_crust leachate data was also used in predictive evaporation (dilution) simulations in order to assess changes in the chemistry of water.

4.10.3 Partitioning of trace elements in sediments

Sequential extraction data was employed to assess the distribution of trace elements in different fractions of surface water sediments. Fractionation plots were drawn.

4.10.4 Adsorption models

Adsorption studies data were used to understand the equilibrium, kinetics and thermodynamic of adsorption processes involving REEs adsorptive and Mgt adsorbent.

4.10.5 Statistical treatment

4.10.5.1 Correlation matrix

Pearson's correlation matrix was used to investigate the relationships between variables in surface water and leachates data sets. Minitab 18 was employed to compute data sets and generate matrix correlation displays in which the Pearson correlation coefficient (a value ranging from -1 to +1), indicating the type (sign) and strength (magnitude) of the relationships, and the P-values ($P < 0.05 < P$), giving the significance of the relationships for each paired variables. These two numbers allow the comparison of variables to one

another (Livingstone, 2009; Currell, 2015). The correlation coefficient expresses the percentage of variance shared by paired variables.

This treatment of results was applied to compare relationships between analytical parameters used in the analysis of samples from a copper mine site in Phalaborwa and its vicinity. Data sets included: (i) surface water sediments and assorted solid mine waste samples leachates, and (ii) surface water samples from the Olifants and Selati Rivers as well as the water retain dam.

4.10.5.2 Cluster Analysis (CA)

Cluster analysis was used for the identification of groups of similar objects within a data set. It was employed, in this study, to examine relationships between observations (cases or samples) as well as relationships between variables (parameters), for stream water data set from a copper mine area in Kitwe. In the case of observations, the method and identifier used were "Complete Linkage, Euclidean Distance" calculation, and in that of variables, "Complete Linkage, Correlation Coefficient Distance" calculation was used as the method and identifier. Clustering is agglomerative and hierarchical, i.e. it constructs groups from individual points and joins them by proceeding from points of higher similarities to those of lower similarities (Newton, 2014).

Minitab 2018 was used to produce graphical outputs of segregations, known as dendrograms, with the aim of making apparent, at a glance, related classes of observations or variables (Livingstone, 2009; Currell, 2015). For the case in point, water samples from streams with different spatial locations, and analytical parameters used for their analysis were clustered to obtain two different dendrograms with the same data set.

CHAPTER 5 RESULTS AND DISCUSSION

In this chapter, results from duly prepared and analyzed samples are presented using narrative, tables and graphs. They are, principally, constituted of geochemical characteristics of surface water and, mine waste and surface water bottom sediments and their leachates and/or digests. Results for geochemical simulations for mixed waters and evaporated Cu-crust leachates, and REEs recovery are also found here. Discussion in form of theoretical, illustrative and comparative explanations are weaved together with results.

5.1 Characteristics of reconnaissance geologic samples from Phalaborwa

In this section, qualitative, semi-quantitative and quantitative analytical results obtained from samples of geologic nature (derived from the earth), collected during the reconnaissance trip, are presented and discussed.

5.1.1 Mineral identification and element semi-quantification

5.1.1.1 X-ray diffraction

Samples collected during the reconnaissance trip, consisting of phosphogypsum (PG), sand and rocks, produced XRD graph patterns from which mineral identification shown in Table 5.1 was derived. A total of three mineral classes were identified in samples as follows: silicate and phosphate in sand and rocks, and sulphate in PG. Silicates and phosphates are primary minerals; their presence in fine-grained particles signifies that a physical weathering event happened and reflects the mineralogy of the rock from which they originate (Bleam, 2017a). Sulphates are secondary minerals transformed chemically from primary minerals (Chou, Seal and Wang, 2013).

Constituent parts of the identified minerals ideal formulae, i.e. Ca, Mg and Fe, on one side, and PO_4^{3-}, SO_4^{2-}, F^- and SiO_2, on the other side, are all common members of the Phalaborwa Igneous Complex (PIC) geology made of carbonatite, phoscorite and pyroxenite rocks (Heinrjch, 1970). These rocks are defined in terms of their mineral

contents as follows: (i) carbonatite: characterised by over 50% dominance of carbonate (CO_3^{2-}) minerals (Xu *et al.*, 2010); (ii) phoscorite: comprised of magnetite (Fe_3O_4), apatite ($Ca_5(PO_4)_3(F,Cl,OH)$) and any of the silicates diopside ($CaMgSi_2O_6$), phlogopite ($KMg_3(AlSi_3O_{10})(F,OH)_2$) and fosterite ($Mg_2SiO_4$); and (iii) pyroxenite: made of minerals rich in iron (Fe) and magnesium (Mg) like Olivine $(Mg,Fe)_2SiO_4$), pyroxenes (single chain silicates, $R_2(SiO_3)_2$) and amphiboles (double chain silicates, $R_7(OH)_2Si_8O_{22}$) with R representing various divalent cations, most commonly Ca^{2+}, Mg^{2+}, Fe^{2+}, in chains known as inosilicates (Hem, 1985).

Besides its distinct physical appearance (whitish and amorphous), PG's mineral content (gypsum) made the real difference from sand and rock samples. It is a secondary mineral generated by the reaction between apatite concentrate (obtained by beneficiation of natural phosphate ore) with sulphuric acid (Lottermoser, 2011; Soltani *et al.*, 2019), i.e. a by-product of phosphoric acid production used in the processing of phosphorous fertilizers (Equation 5.1). It can be deduced from Equation 5.1 and Table 5.1 that PG is obtained from a mineral (Fluorapatite) contained in sand and rock.

$$\underset{\text{(Apatite)}}{Ca_5F(PO_4)_3} + 5\,H_2SO_4 + 10\,H_2O \rightarrow 3\,H_3PO_4 + 5\,\underset{\text{(Gypsum)}}{CaSO_4.2H_2O} + HF \qquad \text{Equation 5.1}$$

Table 5.1: XRD mineral identification in PG, sand and rock samples

Mineral	Ideal formula	Sample				
		PG	Sand	Rock1	Rock2	Rock3
Fluorapatite	$Ca_5(PO_4)_3F$	x	id	id	id	x
Diopside ferroan	$CaMgFeSi_2O_6$	x	x	x	id	x
Diopside	$CaMgSi_2O_6$	x	x	x	x	id
Iron phosphate	$Fe_7(PO_4)_6$	x	id	x	x	x
Gypsum	$CaSO_4.2H_2O$	id	x	x	x	x

id = identified, x = unidentified

Mineral identification is not synonymous with mineral quantification and as such, "unidentified" minerals does not necessarily imply absence of minerals in samples

(Jamieson, Walker and Parsons, 2015). Therefore, XRD results required complementary support from other techniques.

5.1.1.2 X-ray fluorescence and electron dispersive spectroscopy

Elements present in different samples (Figure 5.1.), regardless of minerals that contained them, were quantified as metal oxides using XRF technique. Table 5.2 shows that Si, Al and Fe, known to be major natural members of the earth crust (Foth, 1990; Stefansson, 2007; Bleam, 2017a; Lark *et al.*, 2017), were abundant in sand and rock samples. The amounts of Ca, Mg, K and P were equally higher in sand and rock samples. In spite of Al and K total absence in all of the ideal formulae of minerals identified by XRD, they were quantified by XRF. It was also observed that some elements, present in mineral ideal formulae but unidentified in some samples, were also quantified in those samples. The case in point was P (Rock 3), Fe (Rock 1 and Rock 3) and Si (sand and Rock 1).

Silicate is the most common component of smaller grain particles obtained from rocks. Its contribution to the overall composition of these grain particles determines their hardness and degree of resistance to chemical weathering. Silicon and oxygen are arranged in polymeric silicate anions structures in which oxygen atom bridges two silicon atoms (Si-O-Si) or is terminally bonded to silicon (Si-O). The first bond determines the resistance to cleavage by water and the second bond (corresponding to the number of negative charges) determines the basicity to water (Bleam, 2017a). Silicate minerals resist chemical weathering to different degree in proportion to the Si-O-Si bond in the silicate anions. However, silicates identified in Table 5.1 belong to the inosilicate group ($Si_2O_6^{4-}$) containing two bridged oxygen atoms and four terminal oxygen atoms per unit silicate anion structure and, as such, belong to the group of easily weathered silicate minerals (e.g., olivine, pyroxene and amphibole). The type of cations in silicate minerals will determine whether the hydroxide ions yielded by leaching will remain in solution (e.g. Ca^{2+} and Mg^{2+}) or will form precipitates (e.g. $Al(OH)_3$).

XRF results for SiO_2, CaO, MgO, P_2O_5, seemed to suggest close similarities between Rock 1 and Rock 2. Furthermore, based on the statement that the level of P_2O_5 ranging between 4% and 20% was indicative of the presence of apatite ore (Yang, Tapani

Makkonen and Pakkanen, 2019), there is good agreement between PXRD and XRF results for Sand, Rock1 and Rock2 samples as shown in Table 5.1 and Table 5.2.

PG was contrastingly different from sand and rock samples in that it contained very high amounts of CaO, but very low amounts of all other determined element oxides. The explanation to this is found in Equation 5.1 which indicates that PG is obtained from Apatite concentrate and is a single mineral rather than an assemblage of several minerals found in rocks.

These XRF findings, i.e. attaching relative weight percentage to major element oxides, did not contradict XRD results; they were instead complementary to them. Loss on ignition (LOI) was higher for PG, moderate for sand and lower for rocks in commensuration with the amounts of compounds lost as vapours on high temperature heating.

Table 5.2: Semi-quantitative (wt%) XRF overall composition analysis of major elements (as metal oxides) in PG, sand and rock samples

	Samples				
Metal oxide	PG	Sand	Rock1	Rock2	Rock3
SiO_2	0.68	**36.11**	**23.75**	**30.37**	**48.8**
Al_2O_3	0.14	**6.18**	**6.13**	**2.61**	**5.63**
Fe_2O_3	nd	0.67	0.78	0.52	0.43
FeO	0.02	**5.45**	**6.29**	**4.2**	**3.47**
MnO	0.02	0.07	0.07	0.08	0.05
MgO	nd	**16.57**	**11.74**	**10.9**	**21.79**
CaO	**37.12**	**19.05**	**24.71**	**31.1**	**13.25**
Na_2O	nd	0.17	0.01	0.11	0.85
K_2O	nd	**4.42**	**5.74**	**2.42**	**5.45**
TiO	nd	0.93	1.11	0.58	0.63
P_2O_5	1.23	**8.74**	**17.41**	**15.35**	0.12
Cr_2O_3	nd	0.04	0.02	0.03	0.12
NiO	nd	0.03	0.01	0.01	0.02
LOI	**21.13**	**6.35**	2.01	1.29	2.59
Total %	**60.34**	**104.78**	**99.76**	**98.56**	**103.21**

Table 5.3 shows results of elements content in samples, as weight percentage, determined using EDS technique. In support of minerals identified in PG, sulphur (13.1%) fell into steps with calcium (20.4%) as its dominant elements. Sulphur content which could not be measured as SO_2 by XRF explains in part the higher LOI percentage obtained for PG (~ 21%). But also the oxygen, present in PG's minerals, lost on ignition as O_2 was not accounted for by XRF analysis, is another explanation for the shortfall in the total percentage (Appendix A.4). Furthermore, in agreement with XRF results, Ca, Fe, Si, Al, Mg and K were found at elevated amounts in sand and rock samples. SEM photos of samples (Figure 5.1) were also obtained at the same time with EDS determination of elements, as the two techniques were coupled.

Table 5.3: Semi-quantitative (wt%) EDS overall composition analysis of trace elements in PG, sand and rock samples

Sample	Cu	Fe	Ti	Ca	K	Cl	Si	
PG	0.2	0.01	nd	**20.4**	nd	nd	0.3	
Sand	0.1	**5.7**	0.4	**5.5**	**4.1**	nd	**14.3**	
Rock1	0.1	**7.0**	0.6	**5.3**	**5.4**	nd	**12.9**	
Rock2	nd	**4.4**	0.08	**11.9**	**1.8**	0.1	**15.1**	
	Al	Mg	Na	O	S	P	F	**Total %**
PG	nd	0.1	nd	**64.5**	**13.1**	0.3	**1.1**	**99.8**
Sand	**3.7**	**11.3**	**0.3**	**53.4**	nd	**1.3**	nd	**100**
Rock1	**3.9**	**9.8**	**0.4**	**52.7**	nd	**2.1**	nd	**100.1**
Rock2	**1.5**	**8.3**	**0.4**	**54.7**	nd	**1.7**	nd	**99.9**

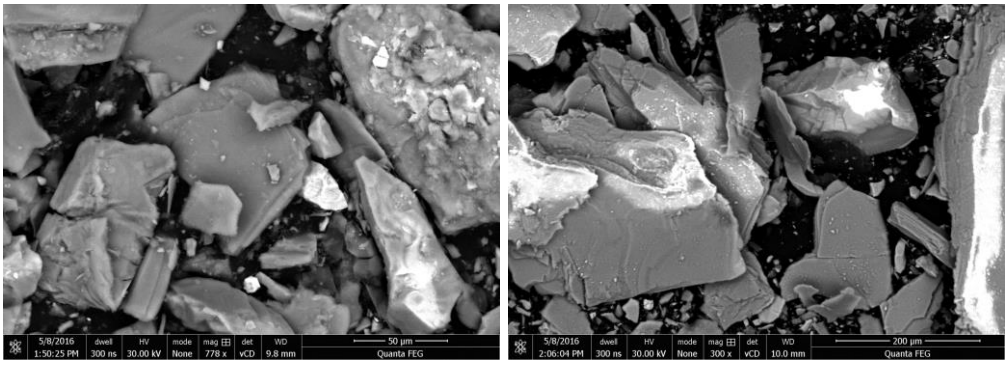


Figure 5.1: Scanning electron microscopy (SEM) under backscattered electron imaging of Sand and Rock1 samples at X778 and X84 respectively. Pyrite mineral (light grey shade) and carbon containing mineral (dark grey shade)

5.1.2 Leachate characteristics of reconnaissance geologic samples

5.1.2.1 Physicochemical parameters

Short time agitation of ground samples mixed with DI water indicated that all samples were slightly alkaline (pH 8.5 - 9.0) and had very low EC (10 - 100 µS cm^{-1}) except for PG (2200 µS cm^{-1}) which contained $CaSO_4.2H_2O$, an easily soluble compound (Price, 2009), as its sole component (Table 5.1 and Table 5.4). Majzlan *et al.* (2018) and Hageman *et al.* (2015) described $CaSO_4.2H_2O$ as a viable candidate for the modification of the ionic composition of water because of its high reactivity and solubility readiness. PG being a neutral salt derived from a strong acid (H_2SO_4) and a strong base ($Ca(OH)_2$), it does not increase nor decrease acidity on dissolution into water, i.e. Ca^{2+} and SO_4^{2-} added to water do not take away nor add any proton to it and, as such, do not bring any risk associated with the rise of pH (Price, 2009). Nevertheless, PG obtained as waste (equation 5.1) contains impurities that may affect the pH of water (Carvalho, 2017).

Table 5.4: Paste pH, paste EC and leachates EC of PG, sand and rock samples

Sample	Paste pH	Paste EC µS cm^{-1}	Leachate EC µS cm^{-1}
PG	8.7	**2200**	**3000**
Sand	8.5	100	1410
Rock 1	9.0	10	610
Rock 2	9.0	10	745
Rock 3	9.0	10	725

The basic pH obtained for sand and rock samples was as a result of the hydrolysis of silicates exemplified by equation 5.2 below. Long-time shaking of samples in TCLP leaching fluid produced a moderate leap in EC for all samples (Table 5.4), indicating the extent of their potential to release more ions under acidic conditions provided by the leaching fluid. This observation was in agreement with studies by Guo *et al.* (2013) on the effects of pH and contact time on mine waste.

$$CaMgSi_2O_6 + 6H_2O \rightarrow Ca^{2+} + Mg^{2+} + 4OH^- + 2H_4SiO_4 \qquad \text{Equation 5.2}$$

Based on Hageman *et al.* (2015) findings after a comparison study of acid–base accounting (ABA) methods, paste pH > 4.5 suggested that sand and rock samples had a likely base producing propensity. In affirming the veracity of his findings, Hageman *et al.* (2015) added that the prediction ensuing from paste pH was not only an estimation of a short term but also a long term net acid-base characteristic of metal mining waste samples. This affirmation is in support of our results.

5.1.2.2 Chemical composition of leachates

Leachate results showed that PG released more ions into leaching fluid, with particularly SO_4^{2-} approaching 25000 mg kg^{-1} and Ca^{2+} nearing 20000 mg kg^{-1}. Other considerable contributions were, in decreasing order, 6431.7 mg kg^{-1} (F^-) > 3548.0 mg kg^{-1} (PO_4^{3-}) > 2927.5 mg kg^{-1} (NO_3^-) and 273.7 mg kg^{-1} (Mg^{2+}) > 106.5 mg kg^{-1} (Al) > 26.5 mg kg^{-1} (K^+) for anions and cations respectively. Sand leached out more Cl^- (442.8 mg kg^{-1}) than all other samples (< 200 mg kg^{-1}). Its SO_4^{2-} content (590.2 mg kg^{-1}) was only second, but

comparatively much lower, to PG (24964 mg kg^{-1}). Leachates from rock 1 and rock 2 contained more PO_4^{3-} (441.1 and 389.0 mg kg^{-1}) than SO_4^{2-} (168.3 and 146.6 mg kg^{-1}) and Cl^- (165.4 and 175.7 mg kg^{-1}). This high PO_4^{3-} content in rock 1 and rock 2 leachates (Fig 5.2) agreed with the high content of P_2O_5 obtained by XRF analysis and suggested the easy solubility nature of phosphorus compounds contained in rock 1 and rock 2. The small amounts of cations in sand and rock leachates (Fig 5.3) indicated their association with less soluble compounds. The high amount of Ca^{2+} in PG leachate (Fig 5.3) testified for its association with more soluble compounds, mainly $CaSO_4$.

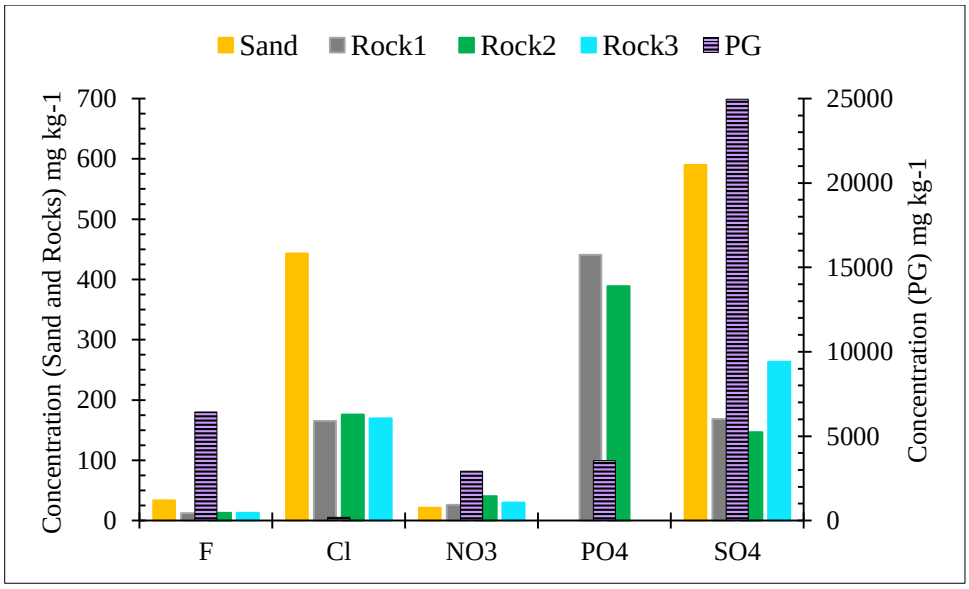


Figure 5.2: Comparison of major anions in each sample leachate. The two vertical axes cater for the difference in magnitude between Sand and Rocks (left) and PG (right).

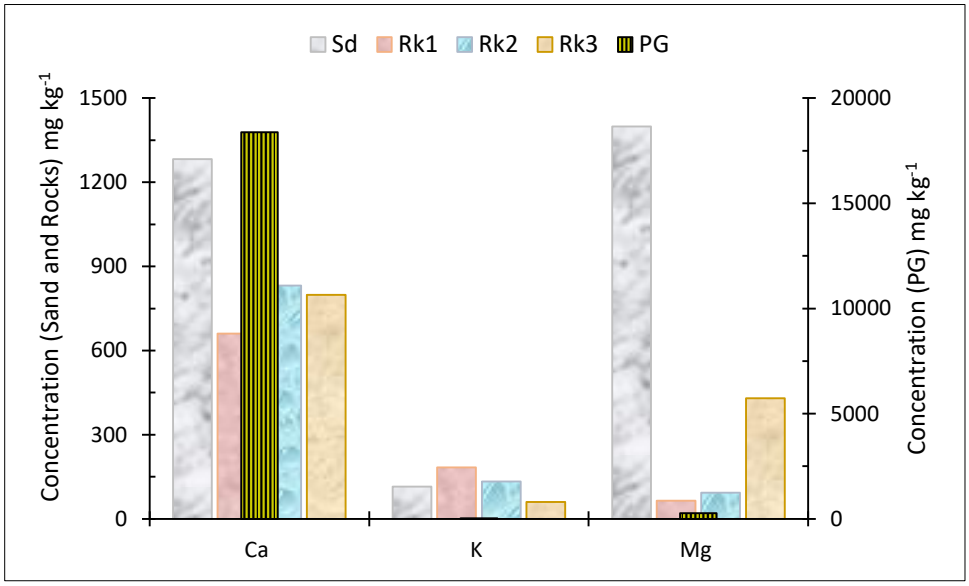


Figure 5.3: Comparison of major cations in each sample leachate. The two vertical axes cater for the difference in magnitude between Sand and Rocks (left) and PG (right).

In relation to trace elements in leachate samples, PG displayed distinct leaching characteristics from sand and rocks. The former leached out more Mn (53.33 mg kg^{-1}) > Cu (3.28 mg kg^{-1}) > Zn (1.35 mg kg^{-1}) whereas the later were characterised by the release of elevated amounts of Fe (13.1 to 49.0 mg kg^{-1}) into leaching fluids (Table 5.5). In the case of PG, it could be safely said that the degree to which trace metals were released by solid samples was as a result of its ease to dissolve. Instead, Fe concentration in leachates may have emanated from amorphous (poorly or non-crystalline) Fe minerals present in sand and rock samples.

Table 5.5: Leachate concentrations of selected elements in PG, sand and rock samples from Phalaborwa.

Sample	Co mg kg^{-1}	Cr mg kg^{-1}	Cu mg kg^{-1}	Fe mg kg^{-1}	Mn mg kg^{-1}	Ni mg kg^{-1}	Zn mg kg^{-1}
PG	0.10	0.36	**3.28**	**33.5**	**53.3**	nd	**1.35**
Sand	0.02	nd	1.82	**13.1**	9.44	0.16	0.19
Rock1	0.02	nd	1.28	**49.0**	2.27	nd	0.72
Rock2	0.02	nd	nd	**30.8**	7.14	0.12	0.20
Rock3	0.01	0.35	nd	**24.3**	3.45	0.14	nd

Gypsum is, on its own, completely soluble in water, yet not harmful to the environment. By virtue of its easy solubility, it released also F^-, PO_4^{3-} and some trace elements such as Cu and Zn into leaching fluid thereby indicating that there were considerable amounts of these impurities that occur within stockpile waste from which PG was obtained. PG showed potential to pose pollution threats to water and its ecosystem; this is as a consequence of PG acting as a collector of an acid waste mixture (Carvalho, 2017).

5.2 Characteristics of surface water from Phalaborwa

In this section, analytical results obtained from surface water samples, are presented and discussed.

5.2.1 Physicochemical parameters

Surface water samples from WRD and rivers in the vicinity of the mine area were slightly alkaline with a pH range of 8.32 to 9.42 which fell within the brackets [5.5 to 9.5] of pH suitable for aquatic life (Jamieson, Walker and Parsons, 2015). The geology of the area, comprised of dominant carbonate minerals over sulphide minerals, could mainly be responsible for this pH. Water flowing from the upper section of the Olifants and the Selati Rivers towards their confluence had EC of less than 1 mS cm^{-1} and close to 2 mS cm^{-1} respectively. They produced mixed water, in the lower section of the Olifants River, with EC still less than 1 mS cm^{-1} but greater than the EC obtained in the upper section of the Olifants River (Figure 5.4). On the contrary, water contained in WRD had EC greater than 6 mS cm^{-1} indicating higher content of soluble compounds. Corrected values of surface water Redox potential (Eh) (Piatak *et al.*, 2004) ranged between 432 and 555 mV, and hence, provided a moderate oxidizing conditions to surface water environment.

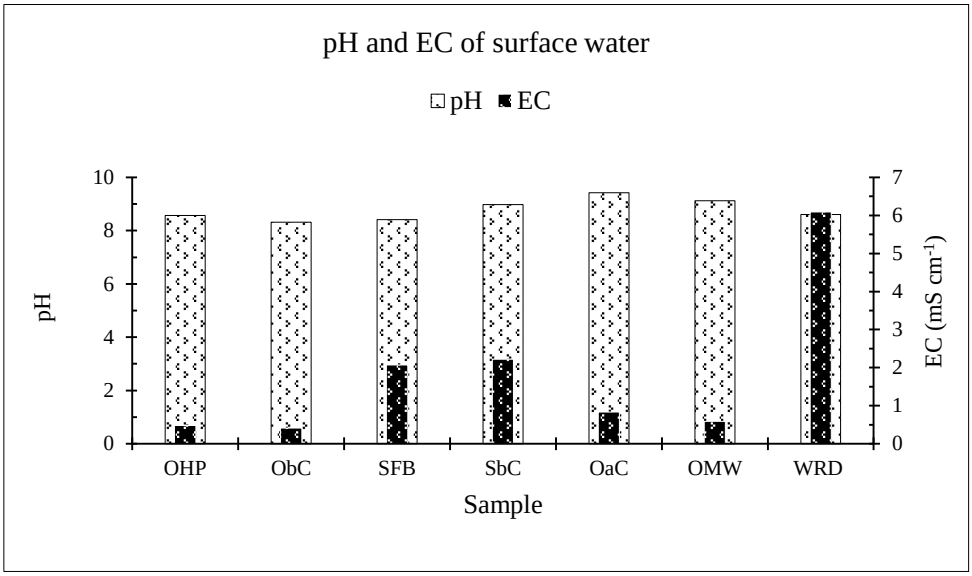


Figure 5.4: pH and EC in surface water within and around the mine area

5.2.2 Chemical composition of surface water samples

5.2.2.1 Major ions

Figure 5.5 portrays, on the left side, the progression of dominant anions concentrations from the Selati and the Olifants Rivers until after their confluence and, on the right side, a comparison of the highest concentrations of the same anions in the Selati River with their corresponding anions in WRD. Due to the mixing ratio of the two rivers (~ 20:1, Olifants:Selati), calculated from actual flow rates measured in the field at OHP (2.6 Cumecs), SFB (0.12 Cumecs) and OMW (2.75 Cumecs), anions from the upper section of the Olifants River were slightly accentuated whereas those from the Selati River were greatly atenuated; this is shown on the left hand side graph in Figure 5.5. On the right hand side graph of the same figure, WRD had an elevated content of SO_4^{2-} (~ 4500 mg L^{-1}), almost seven times higher than the Selati River. WRD had, on the contrary, only twice as much Cl^- (~ 700 mg L^{-1}) than the Selati River. The elevated concentration of major anions in WRD suggested that a significant proportion of these anions were provided by a large amount of easy soluble secondary minerals.

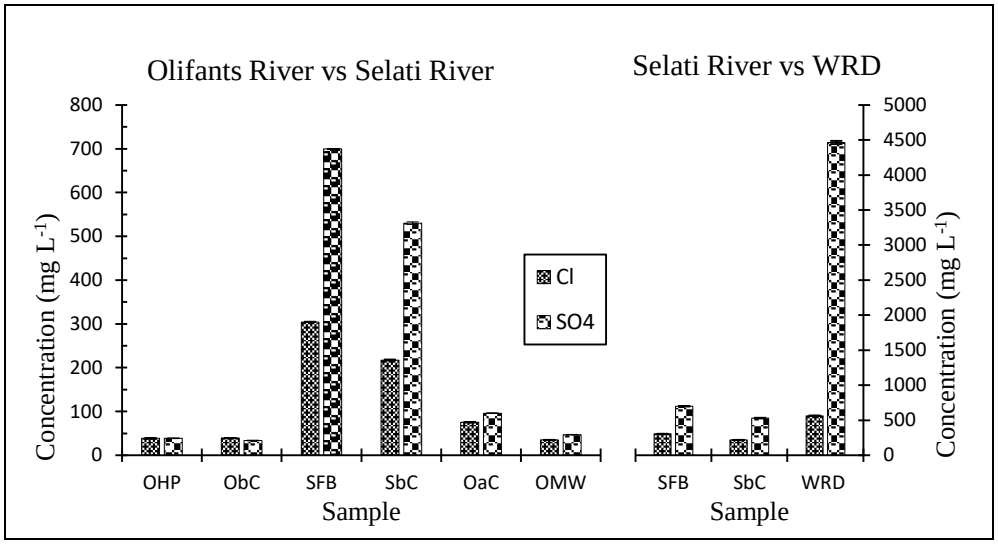


Figure 5.5: Dominant major anions concentration in surface water. The Selati River (SFB and SbC) contrasted with the upper and lower sections of the Olifants River (OHP, ObC, OaC, OMW (left hand side), and with WRD (right hand side)

The progression of dominant cations concentration presented in Figure 5.6 resembled in many aspects to changes observed for anions, i.e. Ca^{2+} and Mg^{2+}, in the stretch of the Olfants River after the confluence indicated a concomitant accentuation and atenuation of concentrations attributed to the mixing ratio of the Olifants and the Selati waters at the confluence. Additionally, Ca^{2+} and Mg^{2+} concentrations were much higher in WRD than the Selati River, implying a large amount of easy soluble secondary minerals in WRD than in the Selati River.

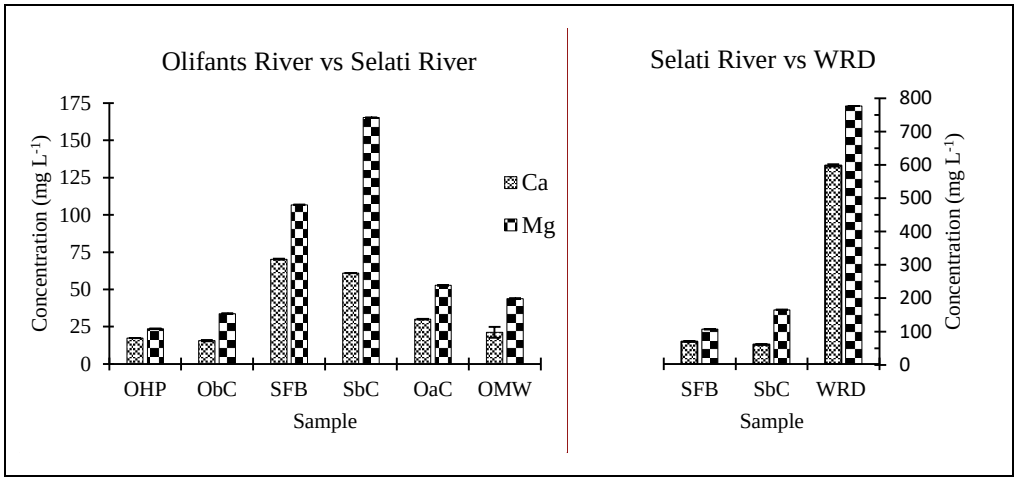


Figure 5.6: Dominant major cations concentration in surface water. The Selati River (SFB and SbC) contrasted with the upper and lower sections of the Olifants River (OHP, ObC, OaC and OMW (left hand side), and with WRD (right hand side)

5.2.2.2 Surface water classification

A visual description of surface water at selected sampling spots, based on the concentration of major cations and anions, expressed in meq L^{-1}, is given in Figure 5.7. Although stiff plots look similar in shape, the graduated horizontal axes show marked differences in concentrations. For instance, SO_4^{2-} and Mg^{2+} were dominant ions, followed by Cl^- and Ca^{2+}, in both WRD and SbC but their concentration differed markedly in magnitute. Surface water was classified, generally, as SO_4^{2-} - Mg^{2+} - Ca^{2+} - Cl^- water.

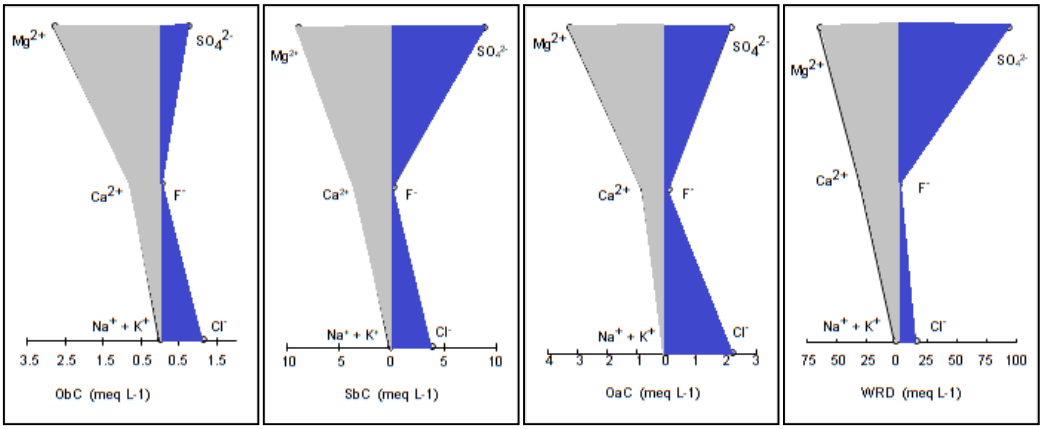


Figure 5.7: Stiff diagram representation of water composition at selected sampling spots on the Olifants and the Selati Rivers and the water retain dam.

5.2.2.3 Trace elements

Trace elements determined in surface water had consistently much higher concentration in WRD than in river water (Table 5.6). This was attributed to the fact that WRD collects and retains, to a greater extent, run off and effluent water from various sources whilst rivers allow water, with its soluble and particulate content, to follow their courses to distant places. This could explain why trace elements in Table 5.6 below and major ions in Figures 5.5, 5.6 and 5.7 above showed higher concentrations in WRD. Copper and zinc were consistently determined in all water samples. Uranium was not detected in surface water, but Au and Gd had an average concentration of about 10.0 µg L^{-1} in rivers.

Table 5.6: Total dissolved concentration (µg L^{-1}) of trace elements in surface water

Sample	Co	Cu	Mn	Ni	Pb	Zn	Au	Gd
OHP	nd	**13**	2	nd	nd	**30**	8	8
ObC	7	**22**	nd	nd	106	**192**		8
SFB	nd	**13**	73	nd	nd	**19**	11	9
SbC	5	**22**	22	nd	nd	**10**	11	10
OaC	nd	**28.5**	nd	nd	138	**382**	8	9
OMW	4	**13**	10	nd	nd	**20**	9	9
WRD	**10**	**67**	**187**	**700**	**1321**	**4770**		181

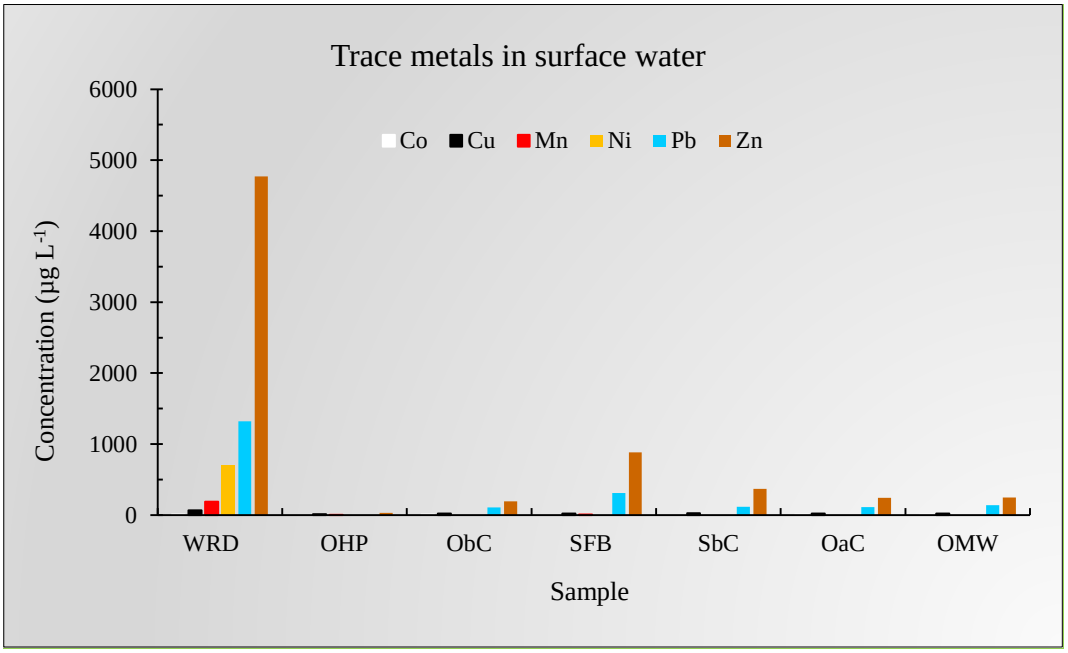


Figure 5.8: Total dissolved concentration (µg L^{-1}) of trace elements in surface water. WRD elevated concentrations of trace elements dwarf concentrations in rivers (because of differences in magnitude) (RSD < 10%)

5.2.2.4 Correlation coefficient between variables in surface water

Perfect correlations (r = 1.0, p = 0.05) were observed, in Table 5.7 below, between pairs of some variables (F^- with SO_4^{2-} and Mg^{2+}; Ca^{2+} with Gd^{3+} and Zn^{2+}; Gd^{3+} with Zn^{2+}) in surface water. Very strong correlations (r > 0.81, p = 0.05) were observed between EC and Cl^-, F^-, SO_4^{2-}, Ca^{2+}, K^+, Mg^{2+}, Cu, Mn, Zn and Gd, and among Cl^-, F^-, SO_4^{2-}, Ca^{2+}, K^+, Mg^{2+}, Cu, Mn, Zn and Gd. Weak negative or weak positive relationships were exhibited by pH, Eh, Na^+ and NO_3^- in all different variable pairs they were involved in except for the correlation of Eh with NO_3^- (r = 0.6). In spite of low variations in the values of pH and Eh to which their negative correlation with other variables could be attributed, these two variables could not be left out in running the correlation table because of their importance in the analysis of water (Currell, 2015). The weak correlation of Na^+ and the negative correlation of NO_3^- with other variables could be attributed to the fact that their extreme distribution, *viz.* their values were way too high or too low from other variables (Currell, 2015). The EC was the influential variable to which the abundance and positive

coexistence of soluble parameters in water referred to. These soluble parameters may share common sources of easy soluble minerals and base metals.

Table 5.7: Pearson correlation matrix of analytical parameters in surface water (Olifants River, Selati River and water retain dam) within and around a copper mine area in Phalaborwa.

	pH	EC	Eh	F^-	Cl^-	NO_3^-	SO_4^{2-}	Ca^{2+}	K^+	Mg^{2+}	Na^+	Cu	Mn	Zn
EC	-0.05													
Eh	-0.40	-0.33												
F^-	-0.09	**0.97**	-0.38											
Cl^-	-0.15	**0.98**	-0.19	**0.91**										
NO_3^-	-0.18	-0.28	**0.60**	-0.23	-0.31									
SO_4^{2-}	-0.12	**0.97**	-0.34	**1.00**	**0.93**	-0.23								
Ca^{2+}	-0.11	**0.93**	-0.36	**0.99**	**0.86**	-0.19	**0.99**							
K^+	0.00	**0.98**	-0.46	**0.99**	**0.90**	-0.25	**0.98**	**0.97**						
Mg^{2+}	-0.07	**0.96**	-0.42	**1.00**	**0.89**	-0.23	**0.99**	**0.99**	**0.99**					
Na^+	0.33	0.32	-0.27	0.09	0.36	-0.28	0.10	-0.02	0.23	0.09				
Cu	-0.12	**0.90**	-0.54	**0.97**	**0.82**	-0.29	**0.96**	**0.97**	**0.96**	**0.98**	0.04			
Mn	-0.44	**0.96**	-0.32	**0.95**	**0.96**	-0.42	**0.97**	**0.94**	**0.91**	**0.94**	-0.04	**0.91**		
Zn	-0.13	**0.91**	-0.39	**0.99**	**0.84**	-0.20	**0.98**	**1.00**	**0.96**	**0.99**	-0.06	**0.98**	**0.93**	
Gd	-0.12	**0.92**	-0.40	**0.99**	**0.84**	-0.21	**0.98**	**1.00**	**0.96**	**0.99**	-0.05	**0.98**	**0.93**	**1.00**

5.3 Characteristics of assorted solid samples from Phalaborwa

This section deals with Analytical results obtained from assorted solid samples (geologic and non-geologic).

5.3.1 Mineral identification and element semi-quantification

5.3.1.1 X-ray diffraction

Minerals identified in assorted geologic samples (Table 5.8) were also derived from XRD graph patterns. Among these samples, the Cu-crust comprised uniquely sulphate (SO_4^{2-}) minerals and the carbonatite was of calcite ($CaCO_3$) nature (Xu *et al.*, 2010). They were associated with mineral classes consisting of sulphates (SO_4^{2-}) and carbonates (CO_3^{2-}) and considered to have undergone considerable weathering. Mgt and TexCon contained,

solely, magnetite ($FeO.Fe_2O_3$) whereas WRD-PG contained a mixture of the tectosilicate quartz (SiO_2), magnetite ($FeO.Fe_2O_3$) and starkite ($MgSO_4.4H_2O$) minerals. The presence of SO_4^{2-} in Cu-crust and CO_3^{2-} in Cbt signaled that these two samples were chemically weathered materials. Quartz and magnetite were primary minerals indicating that Mgt and TexCon underwent physical weathering. WRD-PG contained both primary (SiO_2, Fe_3O_4) and secondary ($MgSO_4.4H_2O$) minerals.

Except for gypsum in Cu-crust, all other minerals in assorted geologic samples were different from those identified in reconnaissance geologic samples (Table 5.1) suggesting, thereby, that these two groups of samples may have different parent rocks. Minerals in both sets of geologic samples (reconnaissance and assorted) contained common elements (components) arranged in different structures with distinct properties. Physical and chemical properties of minerals are associated with the structural combination of elements rather than the mere presence of individual elements in minerals (Jamieson, Walker and Parsons, 2015).

Table 5.8: XRD mineral identification in assorted solid samples

Mineral or *elements listed	Ideal formula	Sample				
		Cbt	Cu-crust	Mgt	TexCon	WRD-PG
Chalcantite	$CuSO_4.5H_2O$	x	id	x	x	x
Hexahydrite	*$MgSO_4.6H2O$	x	id	x	x	x
Starkyte	$MgSO_4.4H_2O$	x	id	x	x	id
Silicon oxide	SiO_2	x	x	x	x	id
Iron oxide	Fe_3O_4	x	x	id	id	id
Calcium carbonate	$CaCO_3$	id	x	x	x	x
Gypsum	$CaSO_4.2H_2O$	x	id	x	x	x

Id = identified, x = unidentified

5.3.1.2 X-ray fluorescence

Carbonatite (Cbt), copper crusts (Cu_crust), magnetite (Mgt) and tailings ex-concentrator (TexCon) assessment for relative content (weight percentage) of element oxides, using XRF, produced results which were compiled in Table 5.9 below. Close to 90% of

carbonatite consisted of CaO (42.20 wt%), SiO_2 (12.26 wt%) and matter lost on ignition, (LOI, 33.99 wt%). TexCon contained FeO (27.45 wt%), CaO (25.62 wt%), SiO_2 (8.87 wt%), MgO (7.57 wt%) and LOI (17.93 wt%) summing up to over 85 wt%. Mgt had an exclusive content of Fe_3O_4 (~ 90%) responsible for its strong magnetic properties. Loss on ignition (LOI, 24.3%) and CaO (37.5%) were dominants in Cu_crust which could be attributed to sulphur and calcium, both constituent members of gypsum. The XRF assessment added some semi-quantitative information to XRD qualitative assessment.

Table 5.9: Semi-quantitative (wt%) XRF overall composition analysis of major elements (as metal oxides) in selected solid samples

Metal oxide	Cbt (wt%)	Cu_crust (wt%)	Mgt (wt%)	TexCon (wt%)
SiO_2	**12.26**	**11.45**	**4.78**	**8.87**
Al_2O_3	2.03	0.69	0.95	1.75
Fe_2O_3	0.32	**5.08**	**88.05**	3.39
FeO	2.63	-	-	**27.45**
MnO	0.04	0.08	0.25	0.17
MgO	3.41	**5.44**	**3.09**	**7.57**
CaO	**42.20**	**37.46**	**1.26**	**25.62**
Na_2O	0.18	0.00	0.00	0.18
K_2O	0.82	0.06	0.17	0.27
TiO	0.43	0.31	1.76	0.84
P_2O_5	2.28	4.11	0.23	3.44
Cr_2O_3	0.02	0.01	0.1	0.02
NiO	0.01	0.16	0.06	0.02
LOI	**33.99**	**24.33**	-0.57	**17.93**
Total	100.62	89.19	100.13	97.51

Trace elements content was assessed using XRF and gave results which are presented in Table 5.10. Copper crusts (Cu-crust) contained the highest amounts of trace elements except for Pb and U which were highest in TexCon. Copper content was high in most samples; its excessive content in Cu-crust reached about 21%. Trace elements content in

Mgt was only second to Cu_crust, but followed by TexCon. The geochemical composition of samples was Cu >> Ni > Co >Zn > Cr in Cu_crust, Cr > Ni > Zn > Cu > Co in Mgt and Cu > Ni > U > Zn in TexCon. Cbt had the least content of trace elements.

Table 5.10: XRF quantitative assessment (mg kg^{-1}) of trace elements in assorted samples

Samples	Cr mg kg^{-1}	Cu mg kg^{-1}	Ni mg kg^{-1}	Pb mg kg^{-1}	Zn mg kg^{-1}	Co mg kg^{-1}	U mg kg^{-1}
Cbt	86.4	85.8	39.8	7.5	18.5	20.8	nd
Cu-Crust	**102.7**	**209010**	**5732**	48.7	**1713**	**4654**	43.6
Mgt	**503.8**	**2574**	**367.6**	23.4	**348**	**224.3**	15.1
TexCon	78.9	**1326**	**127.2**	83.0	**103.0**	84.0	**121.3**
WRD-PG	133.0	**705.7**	72.9	16.8	82.6	72.7	12.9

5.3.1.3 Grain size distribution and texture of assorted solid samples

Fractionation of grain particles, using Malvern 3000, showed that over 60% of particles fell in the silt range (Table 5.11). This could have a bearing on samples interaction with solutions they enter in contact with because silt particles may potentially emulate the adsorption effects of clay particles by shear of the huge number of silt grain particles (Foth, 1990). Therefore, Mgt presented itself to be a better candidate for adsorption. Samples were classified with respect to texture as silt and silty loam on the basis of their particle size distribution. Fine sand, whose adsorption characteristics are closest to silt, constituted the portion of sand with the highest contribution to total sand.

Table 5.11: Grain size characteristics in assorted samples by laser diffraction analysis

Fraction in %	Cbt	Cucrust	Mgt	TexCon
Clay (<2 µm)	8.80	9.92	1.91	3.94
Silt (2 – 50 µm)	**63.59**	**80.05**	**93.21**	**64.26**
Very fine sand (50-100 µm)	19.24	9.86	4.88	28.68
Fine sand (100-250 µm)	8.13	0.17	0.00	3.12
Medium sand (250-500 µm)	0.25	0.00	0.00	0.00
Coarse sand (500-1000 µm)	0.00	0.00	0.00	0.00
Very coarse sand (1000-2000 µm)	0.00	0.00	0.00	0.00
Total sand (50-2000 µm)	27.62	10.03	4.88	31.8
Texture	**Silty loam**	**Silt**	**Silt**	**Silty loam**

5.3.2 Leachate characteristics

5.3.2.1 Physicochemical parameters

Assorted mine solid geologic waste materials produced alkaline solutions (pH > 8) after short time agitation with DI water except for Cu-crust (pH ~ 4.5). Among these solutions, WRD-PG and Cu-crust had very high EC, indicating the release of more readily soluble substances into DI water (Table 5.12). These substances could be none other than sulphate minerals which, generally, belong to the family of soluble compounds (Price, 2009). On the contrary, Cbt, TexCon and Mgt paste solutions had low EC, an indication of their reluctance to release soluble substances into DI water. However, prolonged agitation of the same solid samples in TCLP leaching fluids entrained a steep increase of EC for Cbt and TexCon samples which translated into a contribution of solutes in excess of 4500 µS cm^{-1} (Figure 5.9). This could be attributed, for Cbt, to the reactivity of carbonate in acidic environment and for TexCon, to calcium containing compounds, as suggested by XRF in Table 5.9, which remained unidentified by XRD in Table 5.8. Magnetite had the lowest

increase in EC with a gentle (smooth) slope because it belongs to a group of less soluble iron compounds due to its crystalline Fe.

Table 5.12: Paste and EC in assorted solids leachates within and around the mine area

Sample	Paste pH	Paste EC µS cm^{-1}	Leachate EC µS cm^{-1}
Cbt	9.1	50	5300
Cu-crust	**4.6**	**10080**	**11200**
Mgt	8.5	680	1700
TexCon	10.3	150	4800
WRD-PG	9.7	**12180**	**13200**
CFC	5.6	2450	5885
ED SA	7.7	2040	4600
ED ZM	6.9	1090	2400

Cat fish carcass (CFC), left behind by the retirement of swelling waters, was obtained from the bank of WRD; elephant dung (ED) from a copper mine area in South Africa (ED SA) and a conservative area in Zambia (ED ZM) were also leached. The increase in EC from paste solutions to leachates was, in decreasing order, CFC > ED SA > ED ZM corresponding to 3435, 2440 and 1310 µS cm^{-1} respectively (Figure 5.9). These non-geologic samples had greater EC than some geologic materials, in particular magnetite.

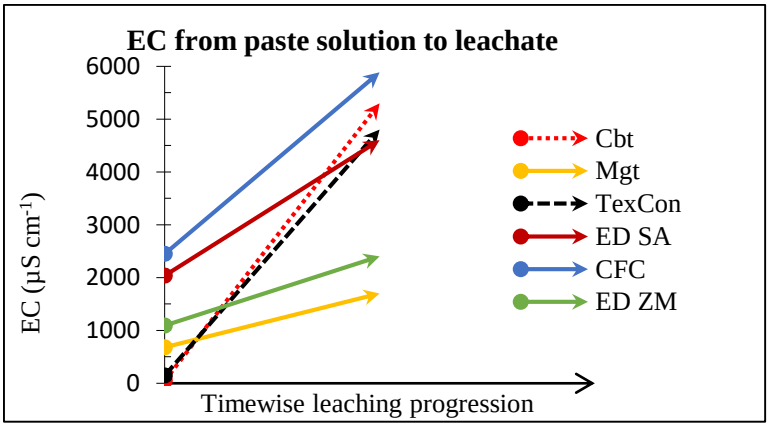


Figure 5.9: Time wise EC increases from paste solution to leachates of assorted samples

5.3.2.2 Chemical composition of leachates

The amounts of SO_4^{2-}, leached out by TCLP from Cu-crust and WRD-PG, were noticeably high (15119 and 11581 mg L^{-1}). WRD-PG leachates contained also higher amounts of Cl^- (1264.51 mg L^{-1}). Fluoride was comparatively higher than Cl^-, NO_3^- and SO_4^{2-} in all other samples except for Cl^- in WRD-PG and SO_4^{2-} in Cu-crust and WRD-PG (Figure 5.11). Dominant cations in leachates were Ca^{2+}, chiefly supplied by carbonatite (5332.50 mg L^{-1}) and to a lesser extent by TexCon (984.0 mg L^{-1}), and Mg^{2+} which emanated from Cu-crust (2463 mg L^{-1}) (Table 5.13).

Concerning trace elements (Table 5.14), Cu was commonly high in leachates of most samples and expectedly very high in Cu-crust (45100 mg kg^{-1}) which, consequently, produced a blue colour, characteristic to Cu (II) cations, straight from short time agitation (Figure 5.10). Mgt (424.9 mg kg^{-1}) and TexCon (141.8 mg kg^{-1}) contained elevated amounts of leachable Cu. ED SA leached out more Cu (84.0 mg kg^{-1}) than WRD-PG (13.7 mg kg^{-1}) and Cbt (2.82 mg kg^{-1}). This could be partly explained by the findings of Grobler (1999) about wild ruminants feeding on leaves together with copper mineral particles deposited on them which resulted in the death of some animals. Mgt, in spite of it being considered a natural source of iron because of its mineralogy, leached out more copper (424.9 mg kg^{-1}) than iron (258.3 mg kg^{-1}). CFC leachate contained, comparatively, higher levels of trace metals (Table 5.14).

a)  b) 

Figure 5.10: a) Copper crusts in the field; b) Intense blue colour of leachates obtained from Copper crusts sample

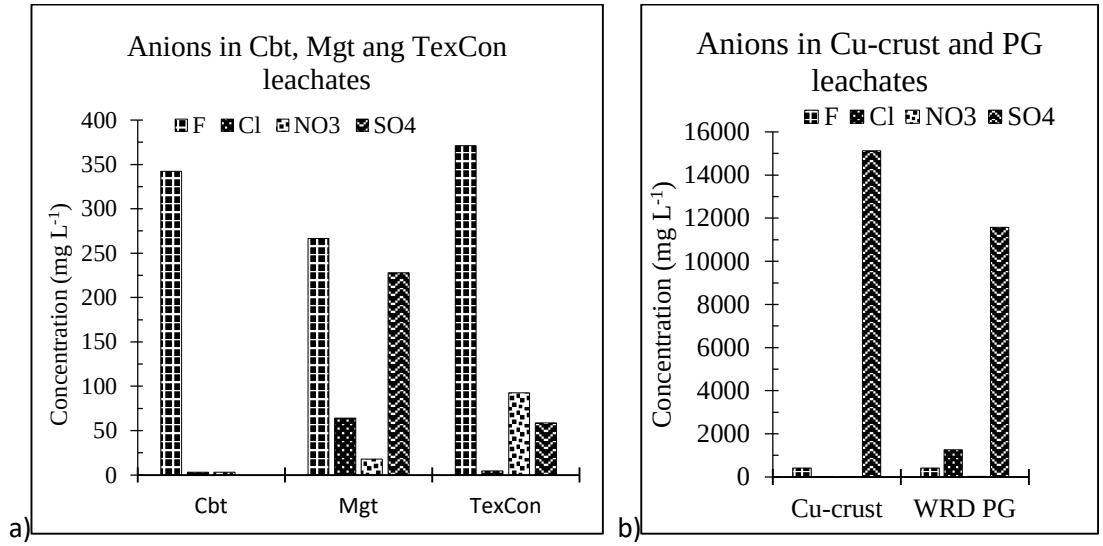


Figure 5.11: Major anions concentration in assorted solid sample leachates on different vertical axes scales in a) and b).

Table 5.13: Concentration of major cations in assorted solid sample leachates

Sample	Al mg kg^{1-}	Ca %	K mg kg^{1-}	Mg %	Na mg kg^{1-}
Cbt	5.06	10.67	5.26	0.07	nd
Cu crust	5.04	0.43	nd	**4.93**	14.62
Mgt	**27.80**	0.33	19.69	0.18	10.35
TexCon	9.54	1.97	20.24	0.11	nd
WRD-PG	1.64	>>	nd	>>	7.40
ED	nd	1.93	nd	0.78	nd

Table 5.14: Concentration of trace elements in assorted solid samples leachates

Sample	Cd mg kg^{-1}	Cu mg kg^{-1}	Fe mg kg^{-1}	Mn mg kg^{-1}	Ni mg kg^{-1}	Pb mg kg^{-1}	Zn mg kg^{-1}
Cbt	nd	2.8	15.4	8.0	0.39	nd	3.1
Cu crust	0.2	**45100**	nd	26.9	10.4	nd	7.6
Mgt	0.05	**424.9**	**258.3**	32.84	2.8	nd	15.2
TexCon	0.04	**141.8**	55.0	72.2	1.7	nd	6.7
WRD-PG	nd	13.7	6.0	0.8	nd	nd	nd
CFC	0.3	5.4	nd	0.2	10.6	1.3	16.5
ED SA	nd	8.4	nd	nd	nd	nd	1.1

5.3.2.3 Correlation matrix for leachates variables

The association between leachate variables (Table 5.15) had only one perfect correlation (Cu with Mg). A number of very strong correlations ($0.81 \leq r \leq 0.99$, $p = 0.05$) with 32 to 49% contribution from each variable were identified for (EC with Mg^{2+}, Co and Cu), (Cl^- with Zn, Al and Fe), (Al with Fe), (Ce with La and Pr), (NO_3^- with Ce, La and Pr), (Mn with Au), (Ni with Au) and (La with Pr). Strong positive relationships ($0.64 \leq r < 0.81$), $p = 0.05$) were also observed among some variable pairs (pH with K^+), (EC with F^-), (clay with U), (silt with Cl^- and Zn), (sand with Gd^{3+}), (F^- with Mg^{2+}), (NO_3^- with Gd^{3+}), (Al with Zn), (Ca with U), (K^+ with Ce, La and Pr), (Mg^{2+} with Co), (Co with Cu), (Fe with Zn), (Ni with Mn) and (Cu with Fe).

A display of very strong negative correlations ($-0.81 \leq r \leq -0.99$, $p = 0.05$) was also seen for (pH with EC, Mg, Cu); (sand with silt), (clay with Fe), (Al with F^-). Strong negative correlations ($-0.64 \leq r < -0.81$), $p = 0.05$) were exhibited by some pairs of parameters (pH with Co), (clay with Cl^-, Al, K^+ and Pr), (sand with Cl^-, Co and Zn), (F- with Fe), (U with Al, Fe and Pr), (Ca^{2+} with Co and Zn), (K+ with Mg^{2+} and Cu) and (Gd with Co and Zn). Weak positive and negative correlations dominated the correlation table.

Positive correlations between EC and soluble species expresses the mobility of these species in sediments (Xu and Li, 2015). A Very strong negative correlation between EC and pH means that as pH increases, species mobility decreases because of their removal (deposition/co-precipitation) from solution by oxides of Al/Fe/Mn or clay/silt. The correlation table displays also some antagonistic correlations between grain particles and/or compounds with scavenging properties (e.g. clay with sand; clay with Fe) signalling some differences in their degree of affinity for soluble species. The types and amounts of soluble species in water depend on a combination of factors (competition for deposition/solubility, pH conditions, types and quantity of sediments, distribution in parent sediments) which make the interpretation of correlations very challenging.

Table 5.15: Pearson correlation matrix of analytical parameters in leachates of surface water sediments and assorted mine waste samples from a copper mine in Phalaborwa.

	pH	**EC**	**Clay**	**Silt**	**Sand**	**F**	**Cl**	**NO3**	**Al**	**Ca**	**K**	**Mg**	**Co**	**Cu**	**Fe**	**Mn**	**Ni**	**Zn**	**Au**	**Ce**	**Gd**	**La**	**Pr**
EC	***-0.82***																						
Clay	-0.34	**0.55**																					
Silt	-0.26	0.37	-0.33																				
Sand	0.36	-0.52	0.11	***-0.97***																			
F	-0.41	**0.67**	0.44	0.01	-0.12																		
Cl	-0.03	-0.12	***-0.67***	**0.80**	***-0.68***	-0.55																	
$NO3^-$	0.35	-0.32	-0.60	-0.18	0.33	0.23	-0.11																
Al	0.20	-0.39	***-0.69***	0.44	-0.29	***-0.83***	**0.87**	-0.03															
Ca	0.28	-0.38	0.20	-0.31	0.28	0.09	-0.35	-0.16	-0.47														
K	**0.76**	-0.56	***-0.67***	0.24	-0.09	-0.46	0.46	0.46	**0.62**	-0.31													
Mg	***-0.95***	**0.88**	0.35	0.21	-0.30	**0.64**	-0.13	-0.12	-0.38	-0.30	***-0.72***												
Co	***-0.72***	**0.93**	0.39	**0.55**	***-0.67***	0.43	0.15	-0.36	-0.07	-0.60	-0.29	**0.73**											
Cu	***-0.95***	**0.87**	0.34	0.21	-0.30	**0.65**	-0.14	-0.11	-0.39	-0.28	-0.72	**1.00**	**0.72**										
Fe	0.14	-0.43	***-0.84***	0.48	-0.30	-0.74	**0.91**	0.11	**0.94**	-0.31	**0.54**	-0.30	-0.18	-0.30									
Mn	0.34	0.11	0.45	-0.07	-0.04	-0.10	-0.18	-0.31	0.02	-0.32	0.33	-0.33	0.28	-0.34	-0.30								
Ni	0.19	0.35	0.37	0.44	-0.56	0.25	0.04	-0.31	-0.12	-0.09	0.27	-0.14	0.47	-0.14	-0.30	**0.74**							
Zn	0.03	0.11	-0.41	**0.77**	***-0.72***	-0.43	**0.84**	-0.16	**0.79**	-0.65	**0.59**	-0.13	0.44	-0.14	**0.66**	0.34	0.43						
Au	0.45	0.08	0.42	-0.01	-0.09	0.05	-0.22	-0.19	-0.11	-0.15	0.39	-0.38	0.21	-0.39	-0.38	**0.95**	**0.85**	0.27					
Ce	**0.55**	-0.36	-0.55	-0.09	0.23	0.21	-0.09	**0.94**	-0.02	-0.13	**0.65**	-0.32	-0.34	-0.31	0.06	-0.05	-0.01	-0.03	0.11				
Gd	**0.51**	-0.66	-0.33	-0.54	**0.65**	0.08	-0.38	**0.64**	-0.30	**0.62**	0.11	-0.39	**-0.85**	-0.37	-0.09	-0.48	-0.48	-0.67	-0.33	**0.57**			
La	**0.55**	-0.36	-0.62	-0.01	0.16	0.14	0.02	**0.93**	0.09	-0.20	**0.71**	-0.33	-0.31	-0.33	0.16	-0.04	0.01	0.08	0.11	**0.99**	**0.51**		
Pr	**0.51**	-0.47	***-0.80***	0.03	0.17	-0.06	0.20	**0.93**	0.30	-0.26	**0.74**	-0.35	-0.39	-0.34	0.40	-0.20	-0.20	0.16	-0.10	**0.93**	**0.51**	**0.96**	
U	-0.11	0.30	**0.73**	-0.01	-0.17	0.40	-0.40	-0.60	-0.64	**0.68**	-0.53	0.09	0.12	0.10	-0.65	0.17	0.48	-0.37	0.29	-0.48	-0.06	-0.54	-0.72

5.3.3 Cu-crust leachate for predictive evaporation (dilution) simulations model

5.3.3.1 Cu_crust leachate input data

Analytical results obtained for Cu_crust leachate (1g of Cu_crust in 1000 mL DI) were computed with PHREEQC interactive 3.4.0-12926 version software, for evaporation (dilution) simulations, using Minteq. v4. dat database. The input data of the initial solution, presented in Table 5.16 below, was kept constant except for changes in the combinations of pH, pe and percentage evaporation (dilution) values.

Table 5.16: Specimen of input data for Cu-crust leachate initial solution for 10% evaporation and 50% dilution

```
SOLUTION 1  #10% evaporation
temp      25
pH        4.5
pe        4
redox     pe
units     mg/l
density   1
Al        1.834
Ca        6523.86
Cl        41.86
Co        17.16
Cr        0.01
Cu        646
F         3.78
Fe        0.304
K         127.96
Mg        13740.42
Mn        7.65
N(5)      0.12
Na        151.55
Ni        29.41
Pb        0.126
S(6)      3685.72
Zn        9.82
-water    1 # k

REACTION 1
H2O   -0.9

SAVE solution 2

END
```

```
SOLUTION 1  #50% dilution
temp      25
pH        7.0
pe        7.5
redox     pe
units     mg/l
density   1
Al        1.834
Ca        6523.86
Cl        41.86
Co        17.16
Cr        0.01
Cu        646
F         3.78
Fe        0.304
K         127.96
Mg        13740.42
Mn        7.65
N(5)      0.12
Na        151.55
Ni        29.41
Pb        0.126
S(6)      3685.72
Zn        9.82
-water    1 # kg

REACTION 1
H2O    0.5

SAVE solution 2

END
```

5.3.3.2 Mineral solubility equilibrium systems

Minerals saturation indices extracted from Cu-crust leachate simulations outputs and the effects of different combinations of pH, pe and percentage evaporation on minerals solubility equilibria are presented in Table 5.18 further below. These three factors (pH. pe and % evaporation) were connected, in decreasing order of importance in solution chemistry, using a tree diagram arrangement from pH to pe, and from pe down to percentages evaporation. It was noted that, in general, incremental changes of pH brought about substantial changes in SI for all tabulated minerals, except for gypsum of which Ca^{2+} and SO_4^{2-} concentrations did not exceed as much the solubility limit. The solutions were undersaturated (SI < 0) with respect to these minerals at pH 2, tending towards saturation (SI = 0) and oversaturation (SI > 0) as increases to pH 4.5, 7, 9.5 and 11 were effected. Aluminium minerals (Al-minerals) displayed an amphoteric behaviour, with SI tending back towards under-saturation, at alkaline pH. A similar behaviour, i.e. a high solubility in both acidic and alkaline environments, was observed for K-Jarosite, a Fe-hydroxide mineral with molecular formula containing K and SO_4^{2-} like Alunite ($KAl_3(SO_4)_2(OH)_6$). K-Jarosite was more soluble in acidic reductive conditions (redox behaviour), but its solubility was influenced, in alkaline medium, by pH only. On the contrary, the solubility of Alunite was only dependent, at all pH, on acid-base interactions. Thus, for non-redox group of minerals (e.g. $Al(OH)_3$, $Zn(OH)_2$, $Pb(OH)_2$ and $CaSO_4.2H_2O$), SI were unresponsive to incremental changes of pe. Similar observations were made for this group of metals initial leachate solutions at various combinations of pH and pe. Increases in percentage evaporation did not entrain any significant changes in minerals SI. Examples of dissolution and precipitation reactions, using $Pb(OH)_2$, for minerals controlled by acid-base conditions only, are given below (Equations 5.3 and 5.4).

$$Pb(OH)_2 + 2H^+ \rightarrow Pb^{2+} + 2H_2O \qquad \text{Equation 5.3}$$

$$Pb^{2+} + 2OH^- \rightarrow Pb(OH)_2 \qquad \text{Equation 5.4}$$

Redox minerals responded to changes of pe, from 4 to 7.5, with increasing tendencies in SI. For Mn-minerals, increases in SI were observed at all pH, whereas for Fe minerals, likewise increases in SI were observed in acidic and neutral environments only while SI

remained unresponsive in alkaline medium. K-Jarosite took exception, as alluded to earlier, by being undersaturated in alkaline solutions (Dold, 2014b). Hee, Kim and Chon (2018), obtained similar indications about Fe- and Mn-minerals from geochemical modelling of six different Korean mine water. This behaviour of redox minerals was attributed, for Mn-minerals, to the high concentration of its reduced form (Mn^{2+}), at all pH, which drove the redox equilibrium further in favour of its oxidised forms, every time the pe was increased. The attainment of redox equilibria for Fe-minerals, within the confines of the acidic medium (pH 2 and 4.5), was similarly caused by high concentration of ferrous ions coupled with increases in pe. For both Mn- and Fe- minerals, the pattern in changes of minerals SI, from reduced to oxidised conditions (Table 5.18), and changes in concentrations of soluble species from reduced to oxidised conditions (Table 5.21), coincided in illustrating these minerals' responses to increases of pe. In fact, it is documented that the formation of hydroxide complexes and hydroxide precipitates affects the activities of reduced and oxidised forms of redox couples through the Nernst equation as shown in Equation 5.5 (Hem, 1962; Dold, 2014b). This means that the predominance of a redox state and its concentration is greatly influenced by pH (Hageman *et al.*, 2015). Equations 5.6 and 5.7 below illustrate the fact that the tendency of Fe^{2+} to be increasingly oxidised to Fe^{3+} is accompanied by hydrolysis and at least partial precipitation of iron hydroxides (ochres) (Banks *et al.*, 1997), and they also evidence the link between pH and pe.

$$Eh = E^o + 0.0592 \log \frac{[\text{Oxidised form}]}{[\text{Reduced form}]} \qquad \text{Equation 5.5}$$

Eh = redox potential

E^o = Standard redox potential

$$4Fe^{2+} + O_2 + 4H^+ \rightarrow 4Fe^{3+} + 2H_2O \quad \text{(Oxidation)} \qquad \text{Equation 5.6}$$

$$Fe^{3+} + 3H_2O \rightarrow FeOOH + H_2O + 3H^+ \rightarrow Fe(OH)_3 + 3H^+ \quad \text{(Hydrolysis)} \qquad \text{Equation 5.7}$$

For the case in point, acidic environment promoted the dissolution of most minerals, thereby decreasing their SI to under-saturation. On the contrary, alkaline environment facilitated the precipitation of most minerals, as hydroxides, thereby increasing their SI

to oversaturation. Graphical changes of selected minerals SI with respect to incremental changes of pH, pe and percentage evaporation are shown in Figure 5.12. It is evident that pH was the master variable (Nordstrom and Alpers, 1999) as it affected, indiscriminately, acid-base and redox minerals solubility equilibria. Increases in pH offered to both, Mn- and Fe- minerals, favourable (or unfavourable) media for redox reactions. Differences in behaviours between Mn- and Fe- minerals, as pointed out by Nordstrom and Alpers (1999), could also be explained by the fact that, unlike pH, pe does not correlate to the chemistry of a solution but to a specific redox couple, and as such it commands changes that are specific to a particular redox couple.

On all occasions, evaporation increases the concentration of acids, sulphates, chlorides and metals in solution and, as a result, saturation equilibrium tends towards the formation of precipitates (SI > 0) (Nordstrom and Alpers, 1999; Dold, 2014b). In AMD waters, for instance, evaporation leads to the formation of efflorescent SO_4^{2-} salts as a result of S^{2-} oxidation (Price, 2009; Dold, 2014b). For the case in point, the instance of pH 2 and pe 4 solutions evaporated to 10%, 50%, 95% and diluted to 50% illustrate the effects of evaporation and dilution on the concentrations of acid, sulphate and metal ions in solution (Table 5.17). Successive higher evaporation caused 33%, 120% and 1900% increases in concentration; dilution entrained 34% decrease in concentration. Concentrations were, indeed, amplified in solutions near dryness.

Table 5.17: Total concentrations in mg kg^{-1}_{water} at different evaporation (dilution) levels

	Initial solution	10% Evap	50% Evap	95% Evap	50% Dil
Al	1.88	2.49	4.135	37.61	1.24
Ca	6693	8875	14709	133941	4422
Cu	662.8	878.4	1457	13268	437.6
Fe	0.31	0.41	0.69	6.21	0.21
Mn	7.85	10.41	17.25	157.0	5.18
Pb	0.13	0.17	0.28	2.59	0.09
Zn	10.1	13.35	22.14	201.6	6.66
U	0.13	0.17	0.25	2.53	0.083
Cr	0.010	0.014	0.023	0.21	0.007
Co	17.60	23.37	38.68	352.3	11.63
SO_4^{2-}	3778	5010	8304	75629	2496
H^+	11.39	15.16	25.00	226.4	7.47
		% increase ~32	% increase ~120	% increase ~1900	% decrease ~34

5.3.3.3 Comparison of mineral SI in 50% evaporated and 50% diluted solutions

Speciation output extracts for 50% dilution simulations of the same Cu-crust leachate data, under the same conditions of pH and pe are presented, side by side with 50% evaporation results, in Table 5.18. Comparison of SI values revealed that minerals in diluted solutions had similar values to those in evaporated solutions. In both solutions, SI values either changed by similar margins (in the same direction) or did not depart as much (in opposite directions) from the SI of their initial solution. It became clear, from Figure 5.13, that in the absence of pH and pe, percentage evaporation or dilution had no meaningful effect on minerals SI.

5.3.3.4 Consequences of evaporation and dilution of Cu_crust leachate

Rainfall and drought periods affect chemical equilibrium systems in water. Therefore, the amounts and types of soluble ions that dissolved in dilution simulations and minerals that precipitated in evaporation simulations were as a result of shifts in direction of the equilibrium processes. The consequences of evaporation could be that in lower pH conditions, elevated amounts of free trace metal ions (e.g. Cu^{2+}, Mn^{2+}, Zn^{2+}, Cd^{2+}), which

are very mobile and feature among the best predictors of toxicity, may lead to bioaccumulation and trigger the impairment, and even death of aquatic biota. Elevated amounts of metals in gills, liver, muscles and skins of fish were reported in the Selati and Olifants Rivers (Seymore *et al.*, 1994; Kotze, Du Preez and Van Vuren, 1999; Avenant-Oldewage and Marx, 2000). Terrestrial animals, who quench their thirst from highly evaporated rivers, may be at risk of leaking poisonous salts formed during evaporation. In different scenario, Grobler (1999) attributed copper poisoning of wild ruminants in KNP to mineral depositions (dust and particles) on leaves and grasses which are eaten as unwashed (in dry seasons) and as washed (in rainy seasons).

The amounts of Fe-mineral that precipitated in mild acidic to neutral conditions, in particular Hematite and Goethite, could play a crucial role in removing toxic elements from the water system through co-precipitation.

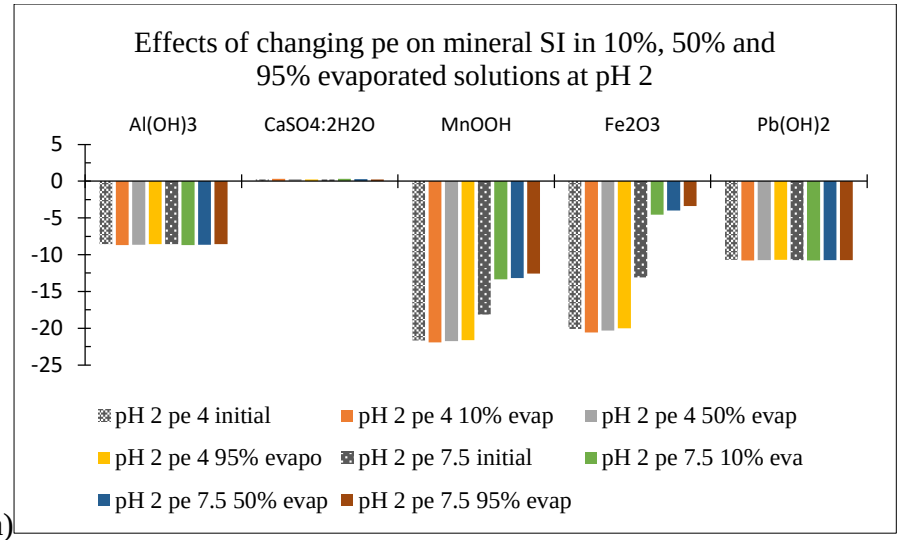
Table 5.18: Minerals SI extracted from PHREEQC speciation outputs of Cu_crust leachate solution for different combinations of pH (2, 4.5, 7, 9.5 and 11), pe (5 and 7.5) and percentage evaporation (10%, 50% qnd 95%).

pH	pe	Solution	Alunite KAl3(SO4)2(OH)6	Gibbsite Al(OH)3	Gypsum CaSO4:2H2O	Hausmannite Mn3O4	Manganite MnOOH	Pyrolusite MnO2	Ferrihydrite Fe(OH)3	Goethite FeOOH	Hematite Fe2O3	K-Jarosite KFe3(SO4)2(OH)6	Magnetite Fe3O4	Pb(OH)2	UO2(OH)2(beta)	Zn(OH)2
2	4	initial	-14.6	-8.56	0.23	-55.96	-21.66	-31.7	-13.95	-11.25	-20.09	-32.68	-28.62	-10.71	-11.03	-12.3
		10% evaporation	-14.84	-8.71	0.31	-56.85	-21.91	-31.84	-14.21	-11.51	-20.6	-33.25	-29.51	-10.76	-12.03	-12.33
		50% evaporation	-14.72	-8.64	0.27	-56.39	-21.77	-31.74	-14.07	-11.37	-20.32	-32.93	-29.05	-10.73	-11.51	-12.32
		95% evaporation	-14.58	-8.55	0.23	-55.89	-21.62	-31.63	-13.92	-11.51	-20.01	-32.57	-28.55	-10.7	-10.96	-12.3
	7.5	initial	-14.6	-8.56	0.23	-48.97	-18.16	-24.7	-10.45	-7.75	-13.09	-22.18	-21.68	-10.72	-8.55	-12.3
		10% evaporation	-14.84	-8.71	0.31	-39.75	-13.36	-14.12	-6.19	-3.49	-4.57	-9.19	-14.02	-10.78	-8.63	-12.34
		50% evaporation	-14.73	-8.64	0.27	-39.17	-13.16	-14.51	-5.91	-3.2	-4	-8.43	-13.19	-10.75	-8.59	-12.32
		95% evaporation	-14.6	-8.56	0.23	-38.55	-12.55	-14.27	-5.61	-2.9	-3.4	-7.65	-12.31	-10.72	-8.55	-12.3
4.5	4	initial	0.13	-1.16	0.24	-35.94	-14.15	-21.69	-6.45	-3.74	-5.07	-17.63	-8.6	-5.71	-3.63	-7.31
		10% evaporation	-0.71	-1.61	0.32	-37.7	-14.73	-22.27	-7.03	-4.32	-6.24	-18.87	-10.36	-5.98	-3.9	-7.75
		50% evaporation	-0.16	-1.32	0.28	-36.64	-14.37	-21.87	-6.67	-3.96	-5.51	-18.09	-9.3	-5.8	-3.73	-7.39
		95% evaporation	0.41	-1.02	0.24	-35.52	-13.98	-21.45	-6.28	-3.57	-4.72	-17.27	-8.18	-5.62	-3.54	-7.21
	7.5	initial	0.13	-1.16	0.24	-28.95	-10.65	-14.69	-2.95	-0.24	1.92	-7.14	-1.61	-5.72	-3.61	-7.31
		10% evaporation	-0.99	-1.75	0.32	-25.72	-8.7	-10.1	-1.64	1.07	4.54	-2.55	-0.94	-6.09	-3.98	-7.65
		50% evaporation	-0.44	-1.13	0.28	-24.71	-8.36	-9.75	-1.22	-1.49	5.38	-1.6	0.94	-5.91	-3.8	-7.48
		95% evaporation	0.13	-1.16	0.24	-23.64	-7.99	-9.34	-0.77	1.93	6.27	-0.62	2.25	-5.72	-3.61	-7.31

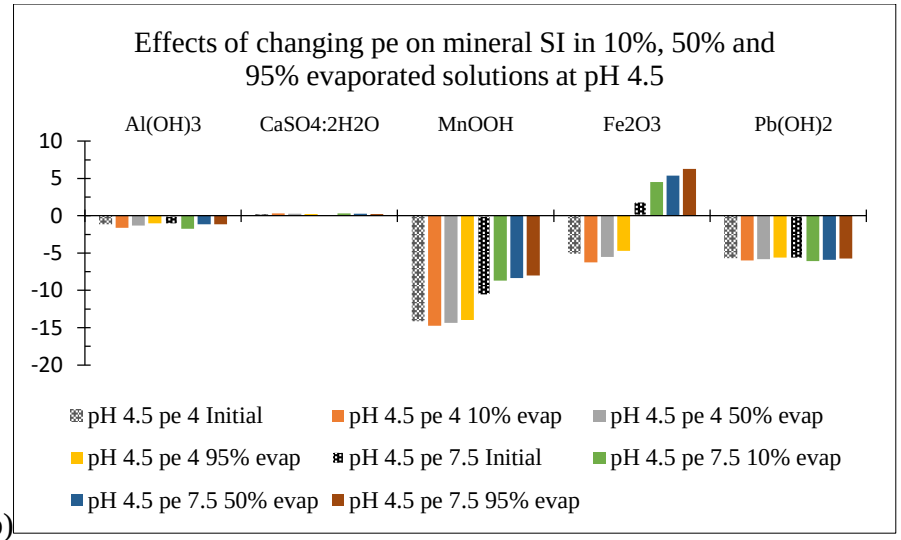
Table 5.18 (Continued): Minerals SI extracted from PHREEQC speciation outputs of Cu_crust leachate solution for different combinations of pH (2, 4.5, 7, 9.5 and 11), pe (5 and 7.5) and percentage evaporation (10%, 50% and 95%).

pH	pe	Solution	Alunite KAl3(SO4)2(OH)6	Gibbsite Al(OH)3	Gypsum CaSO4:2H2O	Hausmannite Mn3O4	Manganite MnOOH	Pyrolusite MnO2	Ferrihydrite Fe(OH)3	Goethite FeOOH	Hematite Fe2O3	K-Jarosite KFe3(SO4)2(OH)6	Magnetite Fe3O4	Pb(OH)2	UO2(OH)2(beta)	Zn(OH)2
7	4	initial	5.09	2.99	0.24	-15.92	-6.64	-11.68	1.06	3.76	9.93	-2.61	11.4	-0.94	-0.61	-2.32
		10% evaporation	6.36	3.24	0.32	-13.7	-5.23	-8.27	2.28	4.99	12.38	1.6	13.07	-1.29	-0.77	-2.57
		50% evaporation	5.79	3.13	0.29	-12.94	-4.99	-8.08	2.47	5.17	12.75	1.91	13.68	-1.1	-0.69	-2.42
		95% evaporation	5.09	2.99	0.24	-12.11	-4.73	-7.86	2.64	5,35	13.1	2.15	14.25	-0.94	-0.61	-2.32
	7.5	initial	5.09	2.99	0.24	-8.92	-3.14	-4.68	1.06	3.76	9.93	2.94	11.4	-0.94	-0.61	-2.32
		10% evaporation	6.38	3.24	0.32	-9.07	-2.97	-3.64	2.59	5.3	13	2.53	11.69	-1.29	-0.77	
		50% evaporation	5.79	3.13	0.29	-8.2	-2.63	-3.34	2.8	5.5	13.41	2.91	12.29	-1.12	-0.69	-2.46
		95% evaporation	5.1	2.99	0.24	-7.3	-2.33	-3.05	2.91	5.62	13.64	2.96	12.65	-0.94	-0.61	-2.32
9.5	4	initial	-9.79	0.53	0.25	4.1	0.87	-1.67	3.36	6.07	14.55	-3.17	15.83	1.96	0.29	1.36
		10% evaporation	-9.03	0.71	0.33	5.32	1.96	0.89	3.53	6.23	14.84	-2.48	14.85	1.77	0.26	1.38
		50% evaporation	-9.4	0.62	0.29	6.54	2.18	1.14	3.45	6.15	14.71	-2.81	14.58	1.88	0.28	1.38
		95% evaporation	-9.78	0.53	0.25	7.15	2.39	1.38	3.37	6.07	14.55	-3.16	14.3	1.96	0.29	1.36
	7.5	initial	-9.79	0.53	0.25	11.1	4.37	**5.33**	3.36	6.07	14.55	-3.17	15.83	1.96	0.29	1.36
		10% evaporation	-9.03	0.71	0.33	10.49	4.25	5.46	3.56	6.23	14.87	-2.48	12.56	1.77	0.26	1.38
		50% evaporation	-9.4	0.62	0.29	11.11	4.46	5.71	3.45	6.15	14.71	-2.81	12.29	1.88	0.28	1.38
		95% evaporation	-9.78	0.53	0.25	11.72	4.68	5.95	3.37	6.07	14.55	-3.16	12.04	1.96	0.29	1.36
11	4	initial	-18.5	-0.97	0.31	**16.54**	5.51	4.47	1.96	4.66	11.73	-11.63	10.1	1.03	0.81	0.02
		10% evaporation	-17.78	-0.8	0.39	18.71	6.76	7.28	2.12	4.83	12.07	-10.91	9.05	1.1	0.78	0.11
		50% evaporation	-18.13	-0.88	0.35	19.22	6.93	7.48	2.04	4.75	11.91	-11.25	8.78	1.07	0.8	0.07
		95% evaporation	-18.5	-0.97	0.31	19.75	7.72	7.68	1.96	4.66	11.73	-11.62	8.5	1.03	0.81	0.03
	7.5	initial	-18.5	-0.97	0.31	23.53	**9.01**	**11.47**	1.96	4.66	11.73	-11.63	**6.6**	1.03	0.81	0.02
		10% evaporation	-17.78	-0.8	0.39	22.85	8.83	11.43	2.12	4.83	12.07	-10.91	6.97	1.1	0.81	0.11
		50% evaporation	-18.13	-0.88	0.35	23.18	8.92	11.45	2.04	4.75	11.91	-11.25	6.79	1.07	0.8	0.07
		95% evaporation	-18.5	-0.97	0.31		9.01	11.47	1.96	4.66	11.73	-11.62	6.6	1.03	0.81	0.03

a)



b)



c)

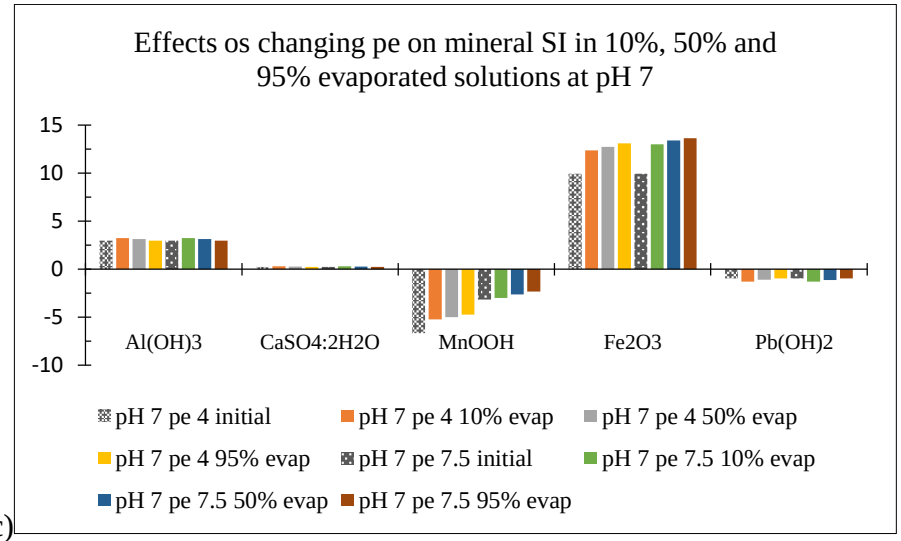
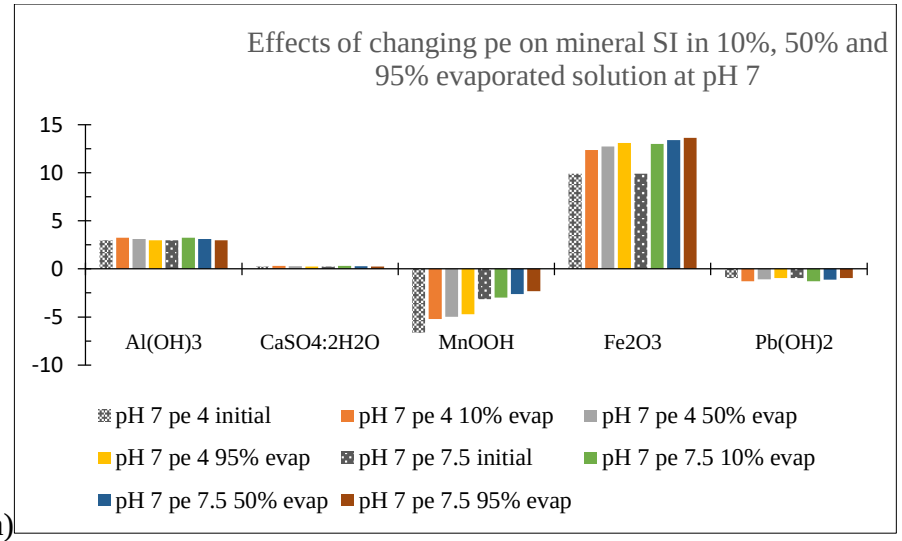
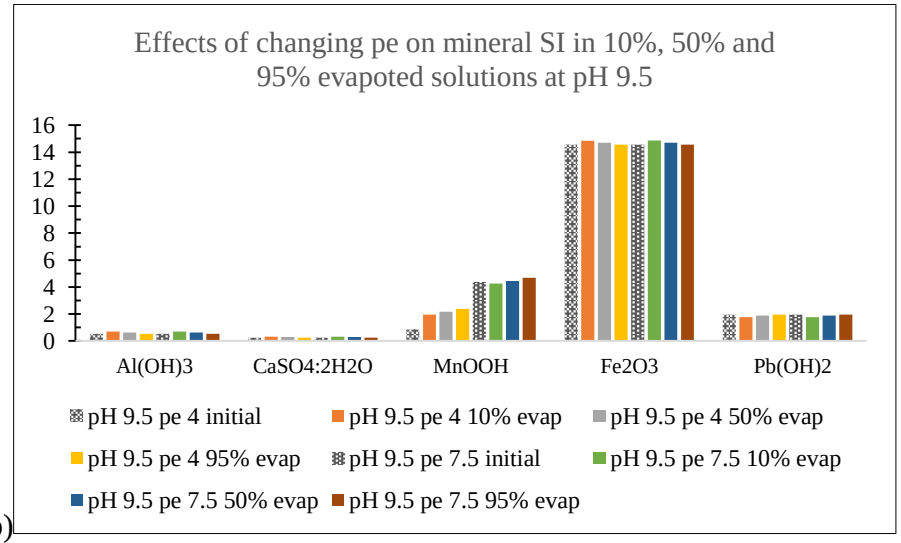


Figure 5.12: Changes in minerals SI for representative members of some mineral groups for different combinations of pH (2, 4.5 and 7), pe (4 and 7.5), and percentage evaporation (10%, 50% and 95%).

a)



b)



c)

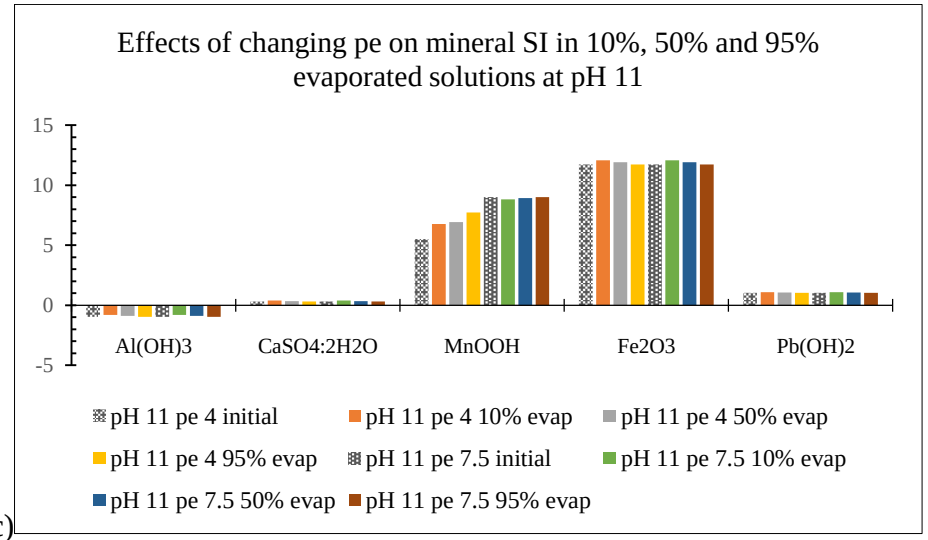


Figure 5.12 (Continued): Changes in minerals SI for representative members of some groups of minerals for different combinations of pH (2, 4.5 and 7), pe (4 and 7.5), and percentage evaporation (10%, 50% and 95%).

Table 5.19: Minerals SI extracted from PHREEQC speciation outputs of Cu_crust leachate solutions for different combinations of pH (2, 4.5, 7, 9.5 and 11), pe (5 and 7.5) for comparison of 50% evaporation and 50% dilution with their initial solutions.

pH	pe	Solution	Alunite KAl3(SO4)2(OH)6	Gibbsite Al(OH)3	Gypsum CaSO4:2H2O	Hausmannite Mn3O4	Manganite MnOOH	Pyrolusite MnO2	Ferrihydrite Fe(OH)3	Goethite FeOOH	Hematite Fe2O3	K-Jarosite KFe3(SO4)2(OH)6	Magnetite Fe3O4	Pb(OH)2	UO2(OH)2(beta)	Zn(OH)2
2	4	initial	-14.6	-8.56	0.23	-55.96	-21.66	-31.7	-13.95	-11.25	-20.09	-32.68	-28.62	-10.71	-11.03	-12.3
		50% evaporation	-14.72	-8.64	0.27	-56.39	-21.77	-31.74	-14.07	-11.37	-20.32	-32.93	-29.05	-10.73	-11.51	-12.32
		50% dilution	-14.57	-8.54	0.23	-55.83	-21.6	-31.61	-13.9	-11.19	-19.98	-32.54	-28.49	-10.7	-10.5	12.59
	7.5	initial	-14.6	-8.56	0.23	-48.97	-18.16	-24.7	-10.45	-7.75	-13.09	-22.18	-21.68	-10.72	-8.55	-12.3
		50% evaporation	-14.73	-8.64	0.27	-39.17	-13.16	-14.51	-5.91	-3.2	-4	-8.43	-13.19	-10.75	-8.59	-12.32
		50% dilution	-14.58	-8.55	0.23	-38.49	-12.92	-14.25	-5.58	-2.87	-3.34	-7.57	-12.22	-10.71	-8.55	-12.3
4.5	4	initial	0.13	-1.16	0.24	-35.94	-14.15	-21.69	-6.45	-3.74	-5.07	-17.63	-8.6	-5.71	-3.63	-7.31
		50% evaporation	-0.16	-1.32	0.28	-36.64	-14.37	-21.87	-6.67	-3.96	-5.51	-18.09	-9.3	-5.8	-3.73	-7.39
		50% dilution	0.47	-0.99	0.23	-35.4	-13.94	-21.4	-6.24	-3.53	-4.66	-17.19	-8.06	-5.6	-3.52	-7.2
	7.5	initial	0.13	-1.16	0.24	-28.95	-10.65	-14.69	-2.95	-0.24	1.92	-7.14	-1.61	-5.72	-3.61	-7.31
		50% evaporation	-0.44	-1.13	0.28	-24.71	-8.36	-9.75	-1.22	-1.49	5.38	-1.6	0.94	-5.91	-3.8	-7.48
		50% dilution	0.18	-1.13	0.23	-23.53	-7.96	-9.34	-0.73	1.98	6.36	-0.52	2.28	-5.71	-3.59	-7.29
7	4	initial	5.09	2.99	0.24	-15.92	-6.64	-11.68	1.06	3.76	9.93	-2.61	11.4	-0.94	-0.61	-2.32
		50% evaporation	5.79	3.13	0.29	-12.94	-4.99	-8.08	2.47	5.17	12.75	1.91	13.68	-1.1	-0.69	-2.42
		50% dilution	5.02	2.97	0.24	-12.02	-4.71	-7.84	2.66	5.36	13.13	2.17	14.3	-0.92	-0.61	-2.31
	7.5	initial	5.09	2.99	0.24	-8.92	-3.14	-4.68	1.06	3.76	9.93	2.94	11.4	-0.94	-0.61	-2.32
		50% evaporation	5.79	3.13	0.29	-8.2	-2.63	-3.34	2.8	5.5	13.41	2.91	12.29	-1.12	-0.69	-2.46
		50% dilution	5.02	2.98	0.24	-7.21	-2.3	-3.03	2.92	5.63	13.66	2.96	12.68	-0.92	-0.61	-2.31

Table 5.19 (Continued): Minerals SI extracted from PHREEQC speciation outputs of Cu_crust leachate solutions for different combinations of pH (2, 4.5, 7, 9.5 and 11), pe (5 and 7.5) for comparison of 50% percentage evaporation and 50% dilution with their initial solutions.

pH	pe	Solution	Alunite KAl3(SO4)2(OH)6	Gibbsite Al(OH)3	Gypsum CaSO4:2H2O	Hausmannite Mn3O4	Manganite MnOOH	Pyrolusite MnO2	Ferrihydrite Fe(OH)3	Goethite FeOOH	Hematite Fe2O3	K-Jarosite KFe3(SO4)2(OH)6	Magnetite Fe3O4	Pb(OH)2	UO2(OH)2(beta)	Zn(OH)2
		initial	-9.79	0.53	0.25	4.1	0.87	-1.67	3.36	6.07	14.55	-3.17	15.83	1.96	0.29	1.36
	4	50% evaporation	-9.4	0.62	0.29	6.54	2.18	1.14	3.45	6.15	14.71	-2.81	14.58	1.88	0.28	1.38
		50% dilution	-9.82	0.52	0.24	7.21	2.41	1.4	3.36	6.06	14.53	-3.2	14.27	1.97	0.29	1.36
9.5		initial	-9.79	0.53	0.25	11.1	4.37	**5.33**	3.36	6.07	14.55	-3.17	15.83	1.96	0.29	1.36
	7.5	50% evaporation	-9.4	0.62	0.29	11.11	4.46	5.71	3.45	6.15	14.71	-2.81	12.29	1.88	0.28	1.38
		50% dilution	-9.82	0.52	0.24	11.78	4.7	5.97	3.36	6.06	14.53	-3.2	11.99	1.97	0.29	1.36
		initial	-18.5	-0.97	0.31	**16.54**	5.51	4.47	1.96	4.66	11.73	-11.63	10.1	1.03	0.81	0.02
	4	50% evaporation	-18.13	-0.88	0.35	19.22	6.93	7.48	2.04	4.75	11.91	-11.25	8.78	1.07	0.8	0.07
		50% dilution	-18.53	-0.98	0.3	19.8	7.13	7.7	1.95	4.65	11.71	-11.66	8.47	1.03	0.81	0.02
11		initial	-18.5	-0.97	0.31	23.53	**9.01**	**11.47**	1.96	4.66	11.73	-11.63	**6.6**	1.03	0.81	0.02
	7.5	50% evaporation	-18.13	-0.88	0.35	23.18	8.92	11.45	2.04	4.75	11.91	-11.25	6.79	1.07	0.8	0.07
		50% dilution	-18.53	-0.98	0.3	23.56	9.02	11.47	1.95	4.65	11.71	-11.66	6.58	1.03	0.81	0.02

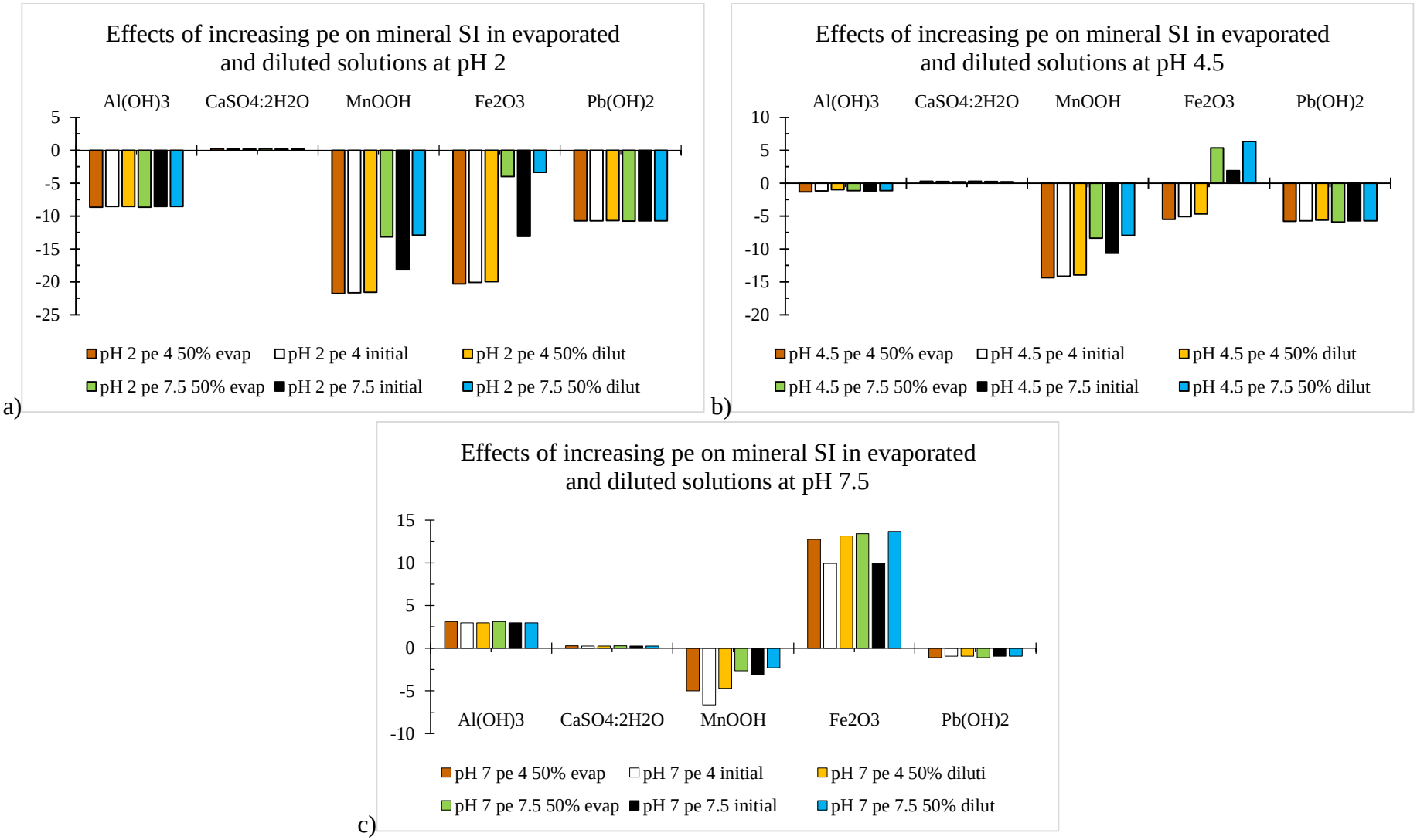
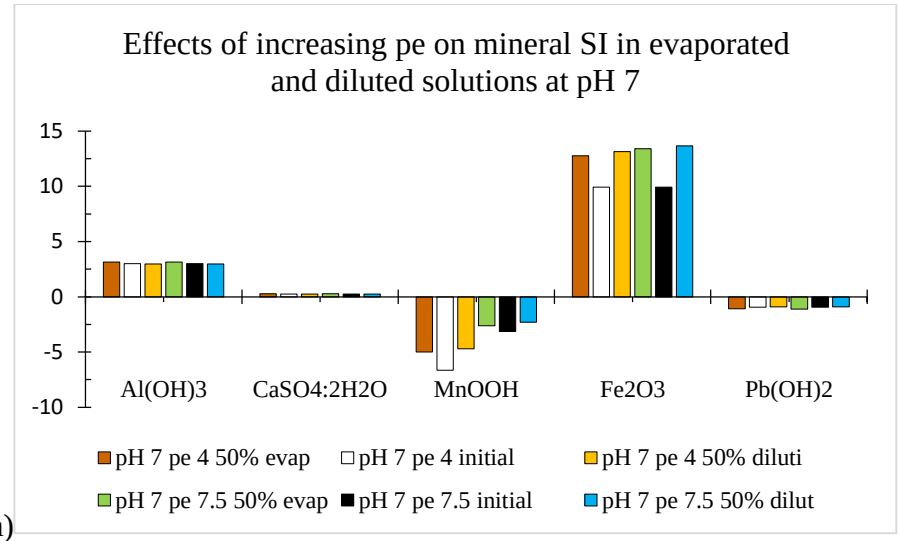
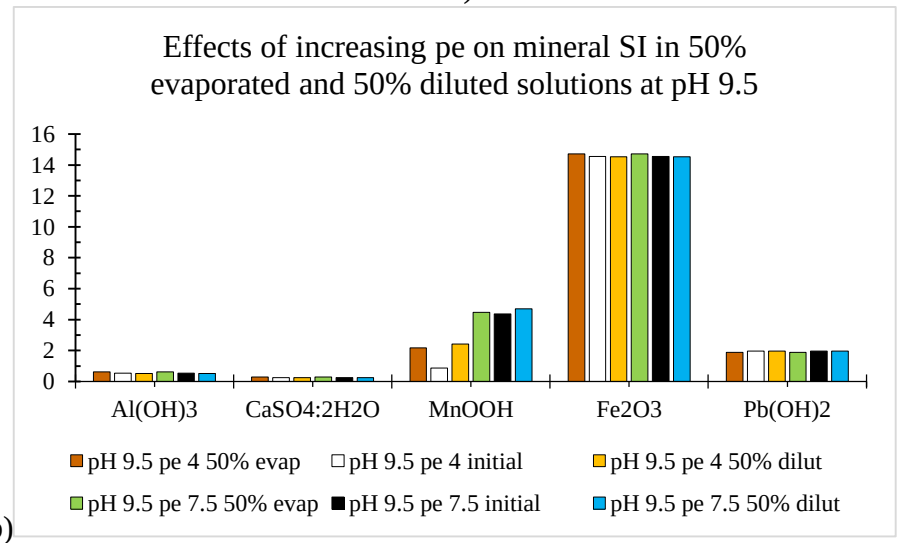


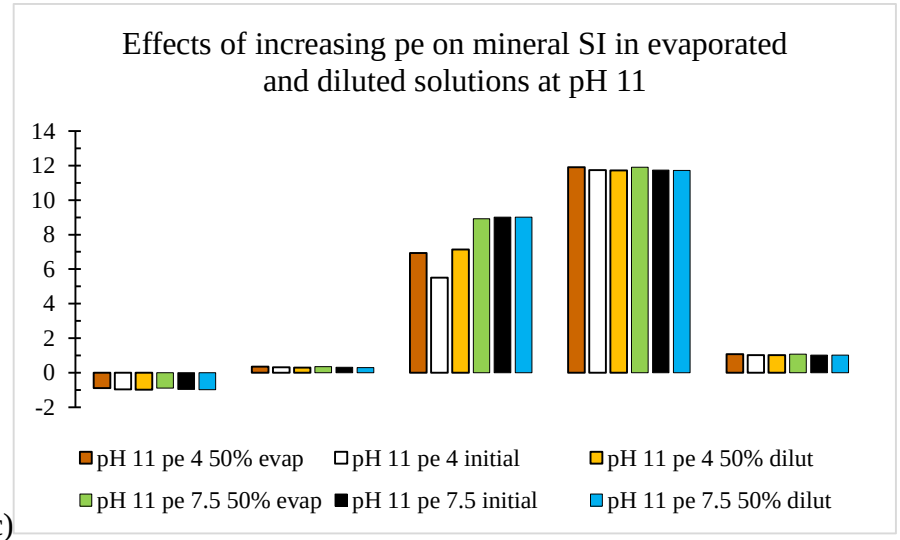
Figure 5.13: Changes in minerals SI for representative members of some acid-base, neutral and redox groups of minerals for different combinations of pH (7, 9.5 and 11), pe (4 and 7.5) in 50% evaporated and 50% diluted solutions.



a)



b)



c)

Figure 5.13 (Continued): Changes in minerals SI for representative members of some acid-base, neutral and redox groups of minerals for different combinations of pH (7, 9.5 and 11), pe (4 and 7.5) in 50% evaporated and 50% diluted solutions.

5.3.3.5 Distribution of dissolved species

The distribution of species in Cu-crust leachate simulations outputs, for different pH and pe combinations, are presented in Table 5.19 for selected acid-base and neutral species, and in Table 5.20 for selected redox species. Generally, changes of pH brought with them changes in the distribution and percentage abundance of acid-base and redox species. However, the distribution of acid-base and redox species was not affected by increases in percentage evaporation. The evolution of acid-base species was, solely, commanded by the pH environment of the solution, i.e. it remained insensitive to changes of pe (Table 5.19). Free cations were highly abundant in acidic environment where F^- and SO_4^{2-} were found to be common ligands. Hydroxide complexes were highly abundant in alkaline environment. There was no evolution of neutral species. The concentration of acid-base and neutral species remained constant with incremental changes of pH.

Incremental changes of pH and pe entrained few or no changes in the distribution and percentage abundance of redox species containing lower oxidation state metals (Table 5.20). The evolution of species containing higher oxidation state metals was observed. For these species, changes of pH had a greater influence on their speciation. Large redox equilibrium shifts in favour of oxidation were noted in acidic medium for Cu(I)/Cu(II), Fe(II)/Fe(III) and U(IV)/U(VI) redox couples, and in alkaline medium for Cr(III)/Cr(VI) and Mn(II)/Mn(VI) redox couples. These shifts in redox equilibrium were signalled by a large increase in the concentration of oxidised species caused by a large decrease in the concentration of reduced species and signified that particular pH environments, in which they occurred, were conducive for intense redox activities of specific redox couples.

These results indicate that chemical processes (precipitation, dissolution, adsorption, desorption…) were commanded, in order of priority, by variations of pH (master variable), followed by variations of pe (subordinate variable) in the reaction environment. They also show that at different combinations of pH and pe, chemical interactions yielded species (soluble or insoluble) capable of affecting the pollution status of water body.

5.3.3.6 Evolution of species relative to incremental changes of pH

Acidic cations have affinity for OH^-, hence they hydrolyse to form dissolved complexes (Price, 2009). Ferric and aluminium ions follow a similar, stepwise reaction path leading to the formation of higher hydroxides (ferrate and aluminate) as pH increases (Equations 5.8 and 5.9).

Other acidic cations (e.g. Cu^{2+} and Pb^{2+}) formed, as well, higher soluble hydroxides complexes in commensuration with their ionic charge.

$$Al^{3+} \rightarrow AlOH^{2+} \rightarrow Al(OH)_2^{+} \rightarrow Al(OH)_3 \rightarrow Al(OH)_4^{-} \quad \text{Equation 5.8}$$

$$Fe^{3+} \rightarrow FeOH^{2+} \rightarrow Fe(OH)_2^{+} \rightarrow Fe(OH)_3 \rightarrow Fe(OH)_4^{-} \quad \text{Equation 5.9}$$

Knowledge of the types and amounts of species present in impacted water body at a given pH can allow for appropriate remedial actions to be taken on the basis of pH shifts in the direction leading to less hazardous chemical species. Depending on pH conditions of water, species like $Fe(OH)_3$ can act as a sink or source of trace elements and, hence, promote the improvement or deterioration of the quality of water (Carbone *et al.*, 2013; Zhang *et al.*, 2014; Saleem, Iqbal and Shah, 2015; Hee, Kim and Chon, 2018).

5.3.3.7 Evolution of total concentrations of species relative to incremental changes of pH and pe

The concentration of acid-base and neutral species remained constant at all pH and pe combinations (Table 5.19). Acidic environment offered a favourable environment for intense redox species interactions. At some pH and pe combinations, appreciable changes in the concentrations of redox species were observed (Table 5.20). For instance, at pH 2 and pH 4, changing pe from 4 to 7.5 decreased the concentration of Cu(I) from $[10^{-3}]$ mol kg^{-1} to $[10^{-12}]$ mol kg^{-1} which translated into a concomitant increase in the concentration of Cu(II) from $[10^{-3}]$ mol kg^{-1} to $[10^{-2}]$ mol kg^{-1}. A similar observation was also noted for Fe(II)/Fe(III), under the same conditions of pH and pe. Although the concentrations of Fe(II), $[10^{-6}]$ mol kg^{-1}, seemed constant, the unnoticed changes were large enough to increase the concentration of Fe(III) from $[10^{-16}]$ mol kg^{-1} to $[10^{-6}]$ mol kg^{-1} and $[10^{-13}]$ mol kg^{-1} to $[10^{-6}]$ mol kg^{-1} at pH 2 and pH 4 respectively. (Cu(I)/Cu(II) and Fe(II)/Fe(III)) redox reactions were still active at higher pH, but the order of magnitude of changes in concentrations were too low and probably indicative of systems that had attained their equilibrium states. Modal representations of the evolution of abundant species at different pH and pe combinations are given in Figure 5.14 for acid-base species and in Figure 5.15 for redox species.

Table 5.20: Total concentration, distribution and abundance (%) of acid/base and neutral species relative to changes of pH and change in magnitude of total concentration of acid/base and neutral species with respect to pe

% evaporation	Species/Concentration	pH 2, pe (4 →7.5)	pH 4.5, pe (4 →7.5)	pH 7, pe (4 →7.5)	pH 9.5, (4 →7.5)	pH 9.5, (4 →7.5)
10%, 50% and 95%	Al^{3+}	AlF^{2+} (79%) AlF_2^+ (13%)	AlF^{2+} (76%) AlF_2^+ (16%)	$Al(OH)_4^-$ (92%) $Al(OH)_3$ (4**]**%)	$Al(OH)_4^-$ (99.9%)	$Al(OH)_4^-$ (100%)
	Concentration (mol kg^{-1})	**[10^{-5}]**	**[10^{-5}]**	**[10^{-5}]**	**[10^{-5}]**	**[10^{-5}**
10%, 50% and 95%	Pb^{2+}	Pb^{2+} (77%) PbSO4 (10%) $Pb(SO4)_2^{2-}$ (8%)	Pb^{2+} (76%) PbSO4 (10%)	Pb^{2+} (46%) $Pb(OH)^+$ (27%) PbSO4 (6%)	$Pb(OH)^+$ (63%) $Pb(OH)_2$ (17%)	$Pb(OH)_4^{2-}$ (91%) $Pb(OH)_3^-$ (7%) Pb^{2+} (18%)
	Concentration (mol kg^{-1})	**[10^{-7}]**	**[10^{-7}]**	**[10^{-7}]**	**[10^{-7}]**	**[10^{-7}]**
10%, 50% and 95%	Zn^{2+}	Zn^{2+} (88%) $Zn(SO4)_2^{2-}$ (6%) ZnSO4 (5%)	Zn^{2+} (86%) $Zn(SO4)_2^{2-}$ (6%) ZnSO4 (5%)	Zn^{2+} (86%) $Zn(SO4)_2^{2-}$ (6%) ZnSO4 (1%)	$Zn(OH)_2$ (37%) $Zn(OH)^+$ (31%) $Zn(OH)_3^-$ (24%)	$Zn(OH)_4^{2-}$ (65%) $Zn(OH)_3^-$ (32%) $Zn(OH)_2$ (2%)
	Concentration (mol kg^{-1})	**[10^{-4}]**	**[10^{-4}]**	**[10^{-4}]**	**[10^{-4}]**	**[10^{-4}]**
10%, 50% and 95%	Ni^{2+}	Ni^{2+} (94%) $NiSO_4$ (5%)	Ni^{2+} (94%) $NiSO_4$ (5%)	Ni^{2+} (94%) $NiSO_4$ (5%)	Ni^{2+} (38%) $NiOH^+$ (35%) $Ni(OH)_2$ (22%)	$Ni(OH)_3^-$ (78%) $Ni(OH)_2$ (21%)
	Concentration (mol kg^{-1})	**[10^{-4}]**	**[10^{-4}]**	**[10^{-4}]**	**[10^{-4}]**	**[10^{-4}]**
10%, 50% and 95%	Ca^{2+}	Ca^{2+} (94.9%) $CaSO_4$ (5.5%)	Ca^{2+} (93.9%) $CaSO_4$ (6.0%)	Ca^{2+} (93.7%) $CaSO_4$ (6.1%)	Ca^{2+} (93.7%) $CaSO_4$ (6.2%)	Ca^{2+} (91.0%) $CaSO_4$ (7.1%)
	Concentration (mol kg^{-1})	**[10^{-1}]**	**[10^{-1}]**	**[10^{-1}]**	**[10^{-1}]**	**[10^{-1}]**

Table 5.21: Total concentration, distribution and abundance (%) of redox species relative to changes of pH and change in magnitude of total concentration of redox species with respect to pe.

% evaporation		pH 2 pe (4 →7.5)	pH 4.5 pe (4 →7.5)	pH 7 pe (4 →7.5)	pH 9.5 pe(4 →7.5)	pH 11 pe(4 →7.5)
10%, 50% and 95%	Copper(I)	Cu^{+} (79%)	Cu^{+} (77%)	Cu^{+} (69%)	Cu^{+} (69%)	Cu^{+} (68%)
		$CuCl_2$ (13%)	$CuCl_2$ (16%)	$CuCl_2$ (22%)	$CuCl_2$(22%)	$CuCl_2$ (23%)
		$CuCl_2^{-}$ (5%)	$CuCl_2^{-}$ (4%)	$CuCl_2^{-}$ (9%)	$CuCl_2^{-}$ (9%)	$CuCl_2^{-}$(8%)
	Concentration (mol kg^{-1})	**$[10^{-3}] \rightarrow [10^{-12}]$**	**$[10^{-3}] \rightarrow [10^{-9}]$**	**$[10^{-7}] \rightarrow [10^{-9}]$**	**$[10^{-9}] \rightarrow [10^{-11}]$**	**$[10^{-12}] \rightarrow [10^{-13}]$**
	Copper(II)	Cu^{2+} (94%)	Cu^{2+} (90%)	$Cu_2(OH)_2^{2+}$ (49%)	$Cu_2(OH)_2^{2+}$ (49%)	$Cu(OH)_3^{-}$ (64%)
		$Cu(SO)_4$ (6%)	$Cu(SO)_4$ (6%)	Cu^{2+} (2%)	$Cu(OH)_2$ (2%)	$Cu(OH)_4^{2-}$ (26%)
			$Cu_2(OH)_2^{2+}$ (2%)	$Cu(OH)^{+}$ (1%)	$Cu(OH)^{+}$ (1%)	$Cu(OH)_2$ (8%)
	Concentration (mol kg^{-1})	**$[10^{-3}] \rightarrow [10^{-2}]$**	**$[10^{-3}] \rightarrow [10^{-2}]$**	**$[10^{-2}]$**	**$[10^{-2}]$**	**$[10^{-2}]$**
10%, 50% and 95%	Iron(II)	Fe^{2+} (99%)	F^{e2+} (99%)	Fe2+ (99%)	Fe^{2+} (99%)	$Fe(OH)_3^{-}$ (98%)
	Concentration (mol kg^{-1})	**$[10^{-6}]$**	**$[10^{-6}]$**	**$[10^{-6}] \rightarrow [10^{-8}]$**	**$[10^{-12}] \rightarrow 10^{-15}]$**	**$[10^{-17}] \rightarrow 10^{-19}]$**
	Iron(III)	FeF^{2+} (42%, 15%)	$Fe(OH)_2^{+}$ (97%, 9%)	$Fe(OH)_2^{+}$ (93%)	$Fe(OH)_4^{-}$ (81%)	$Fe(OH)_4^{-}$ (99%)
		$Fe(SO_4)^{+}$ (30%, 10%)	$Fe(OH)^{2+}$ (3%, 0%)	$Fe(OH)_3$ (6%)	$Fe(OH)_3$ (18%)	
		$Fe(OH)^{2+}$ (15%, 5%)	$Fe_3(OH)_4^{5+}$ (0%, 18%)			
		$Fe_2(OH)_2^{4+}$ (0%, 48%)	$Fe_2(OH)_2^{4+}$ (0%, 18%)			
	Concentration (mol kg^{-1})	**$[10^{-16}] \rightarrow 10^{-6}]$**	**$[10^{-13}] \rightarrow [10^{-6}]$**	**$[10^{-6}]$**	**$[10^{-6}]$**	**$[10^{-6}]$**
10%, 50% and 95%	Mn(II)	Mn^{2+} (100%)	Mn^{2+} (100%)	Mn^{2+} (100%)	Mn^{2+} (99%)	Mn^{2+} (98%)
	Concentration (mol kg^{-1})	**$[10^{-4}] \rightarrow [10^{-4}]$**	**$[10^{-4}] \rightarrow [10^{-4}]$**	**$[10^{-4}] \rightarrow [10^{-4}]$**	**$[10^{-4}] \rightarrow [10^{-4}]$**	**$[10^{-4}] \rightarrow [10^{-4}]$**
	Mn(III)	Mn^{3+} (100%)	Mn^{3+} (100%)	Mn^{3+} (100%)	Mn^{3+} (100%)	Mn^{3+} (100%)
	Concentration (mol kg^{-1})	**$[10^{-28}] \rightarrow [10^{-19}]$**	**$[10^{-28}] \rightarrow [10^{-21}]$**	**$[10^{-26}] \rightarrow [10^{-23}]$**	**$[10^{-26}] \rightarrow [10^{-24}]$**	**$[10^{-26}] \rightarrow [10^{-24}]$**
	Mn(VI)			MnO_4^{2-} (100%)	MnO_4^{2-} (100%)	MnO_4^{2-} (100%)
	Concentration (mol kg^{-1})			**$[10^{-35}]$**	**$[10^{-26}] \rightarrow 10^{-17}]$**	**$[10^{-14}] \rightarrow [10^{-6}]$**
	Mn(VII)			MnO_4^{-} (100%)	MnO_4^{-} (100%)	MnO4- (99%)
	Concentration (mol kg^{-1})			**$[10^{-37}]$**	**$[10^{-31}] \rightarrow [10^{-19}]$**	**$[10^{-18}] \rightarrow [10^{-9}]$**

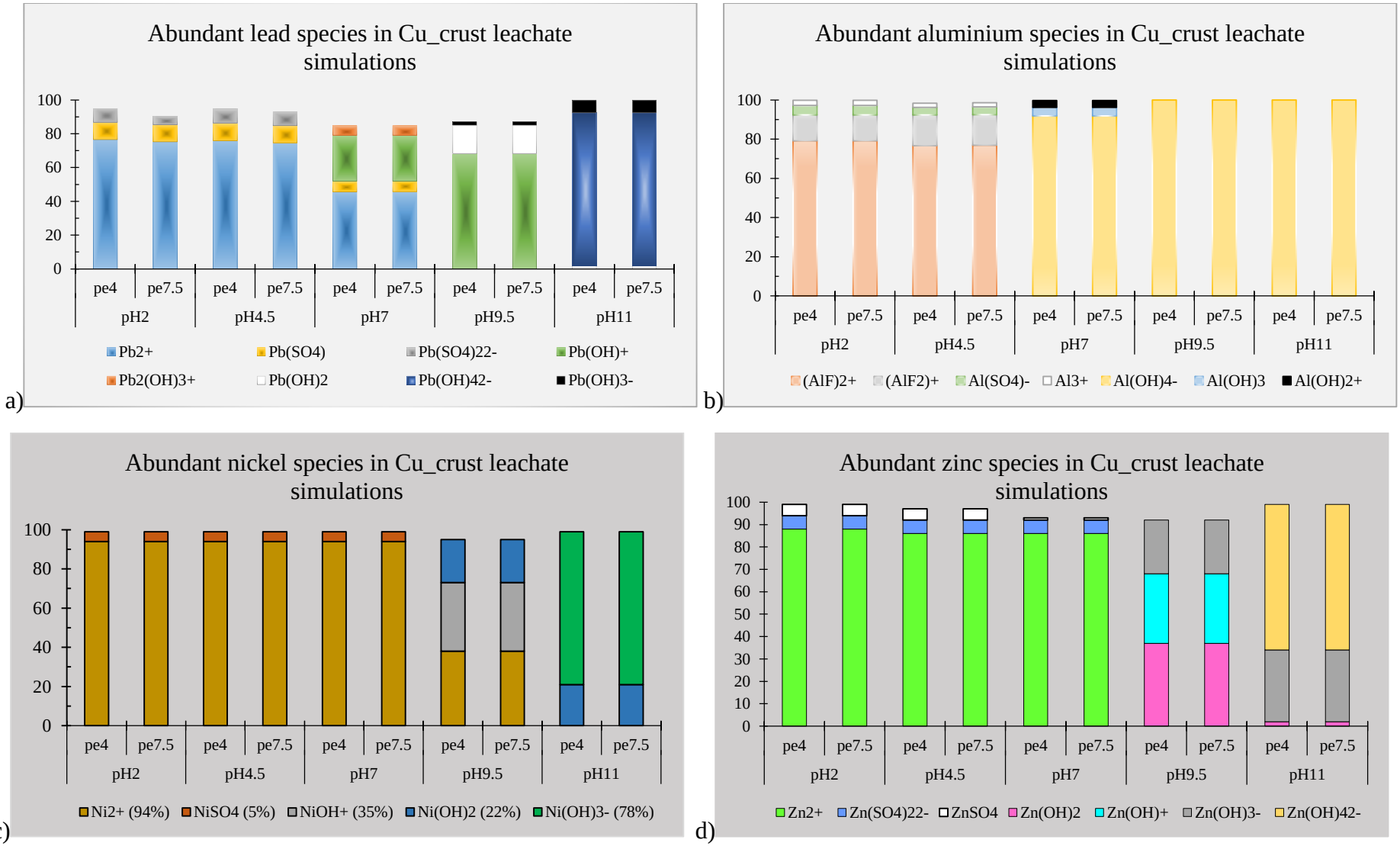


Figure 5.14: Evolution of acid/base species with respect to incremental changes of pH and pe

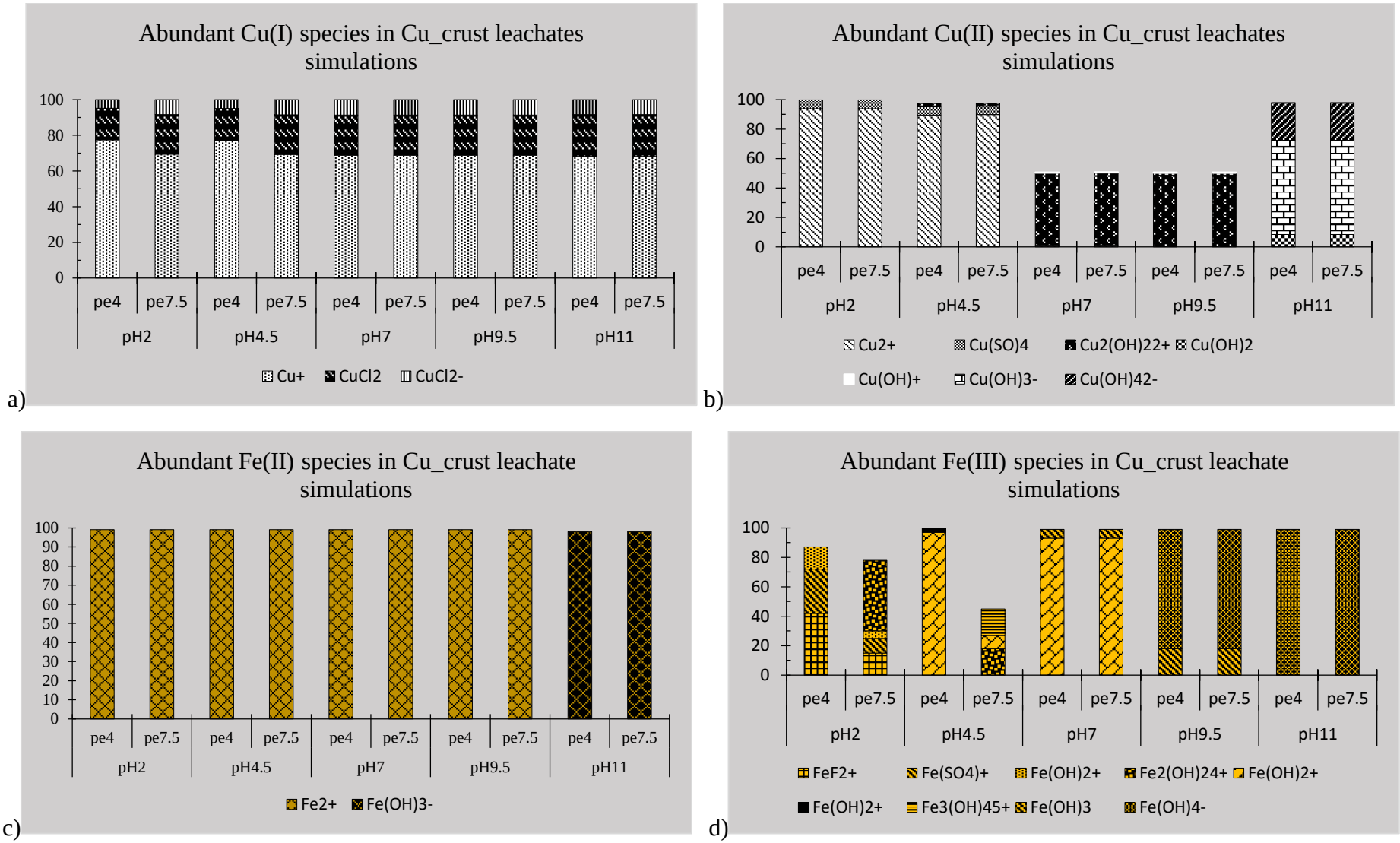


Figure 5.15: Evolution of redox species with respect to incremental changes of pH and pe

5.4 REEs and U in leachates of assorted geologic solid mine waste and sediments

Results for REEs and U leached out from assorted geologic solid mine waste and sediments, obtained using ICP-MS, are presented in Figure 5.16 below. The main focus of the experiment was to determine the content of REEs in Mgt which was to be used as adsorbent in the recovery of REEs. Leachates results did not indicate the presence of REEs in Mgt at detectable levels. It was likewise for REEs in SFB sediments leachates. These results were much in favour of the use of Mgt as adsorbent for REEs batch recovery experiments. However, WRD(s), WRD(b), WRD_PG, TexCon and Cu_crust leachates contained REEs at detectable levels. Generally, geologic solid mine waste contained more REES and U than WRD sediments. Cu_crust released more Y and U in leachates. TexCon and WRD_PG leached out more Ce, Nd and La. WRD leachates contained relatively elevated amounts of Ce, Nd and La.

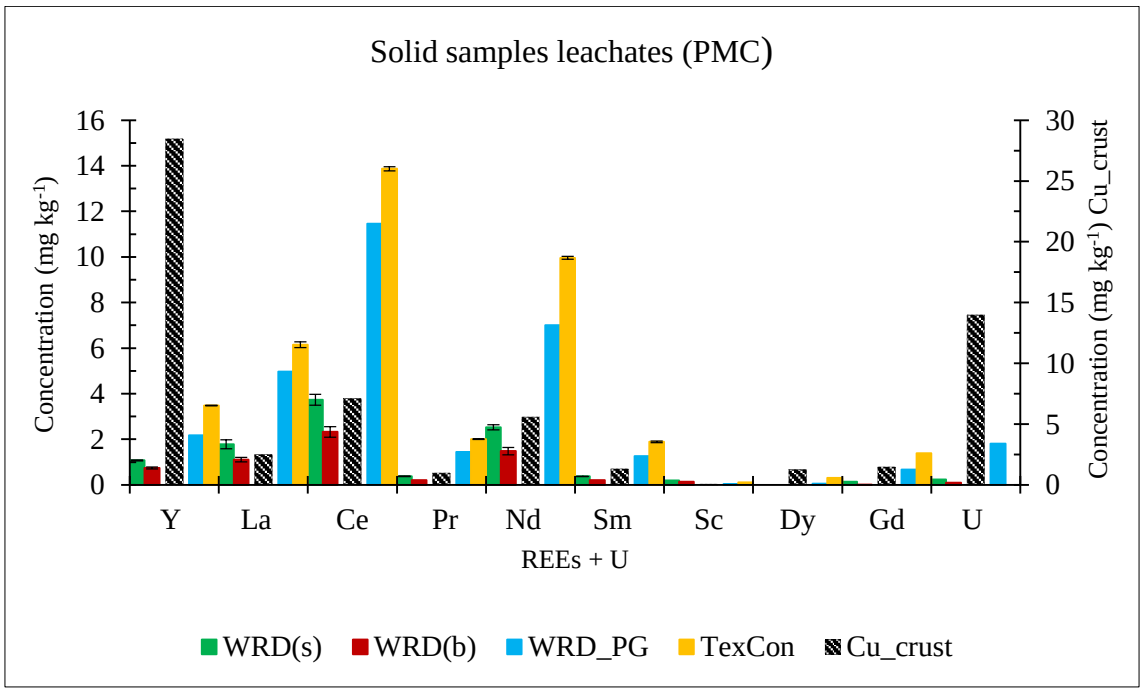


Figure 5.16: Concentration of REEs and U in solid waste and sediments samples from PMC. (REEs and U were not detected in Mgt and SFB leachates)

5.5 REEs Recovery using natural magnetite (Mgt)

A series of mass-based adsorption experiments involving REEs (adsorptive) and Mgt (adsorbent) were carried out and the following subsections are based on the results obtained. The standard deviation of adsorption parameters was under 5% for most measurements.

5.5.1 The effect of adsorbent mass

The recovery efficiency and capacity obtained from the agitation (150 rpm, 5 hrs) of REEs adsorptive carrying solution (1 ppm, 15 mL) with varying mass of natural magnetite (Mgt) adsorbent (50, 100, 150, 200, 300 and 500 mg) in 50 mL centrifuge tubes are presented in Figures 5.17 and 5.18 below. It was clear, at a glance, that all REEs behaved in a similar way. The difference between the initial concentration of REEs had similar curvatures with different degrees of curving signalling a similar behaviour. Their concentrations at the end of the shaking period increased with increasing adsorbent mass because higher masses of Mgt made available larger adsorption surface areas for a constant amount of adsorptive. This decreased the amounts of REEs in solution to undetectable levels where the adsorption process reached a plateau. The recovery efficiency (Figure 5.17) ranged from 92.5 to 98.8% with an average of 88.8% which coincided with 200 mg of adsorbent. The recovery capacity (Figure 5.18) was highest, for most REEs, for 150 mg of adsorbent. It ranged from 84.3 to 109.3 µg g^{-1} (average 99.0 µg g^{-1}) except for Lu, Yb and Tm which had higher recovery capacity of 120.4, 117.9 and 108.4 µg g^{-1} respectively, for 100 mg of Mgt. The adsorbent mass of 150 mg was considered optimum for use in the next step. Recovery efficiency is related to achieving the state of more adsorbate collected on the adsorbent with less adsorptive remaining in solution, in less time (with minimum effort, expense). Recovery capacity is related to the maximum amount of adsorptive fully occupying the available space on the adsorbent.

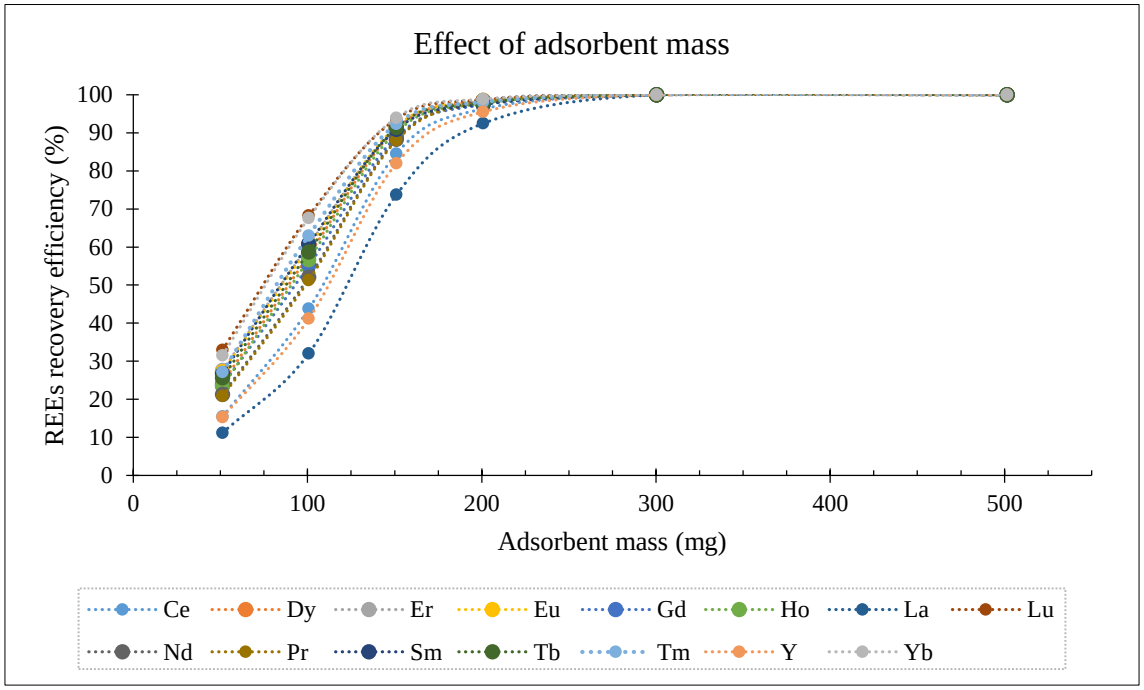


Figure 5.17: REEs recovery efficiency obtained from varying mass (50, 100, 150, 200, 300 and 500 mg) of Mgt (adsorbent), in 15 mL REEs solution at pH 2.2 (RSD < 5%)

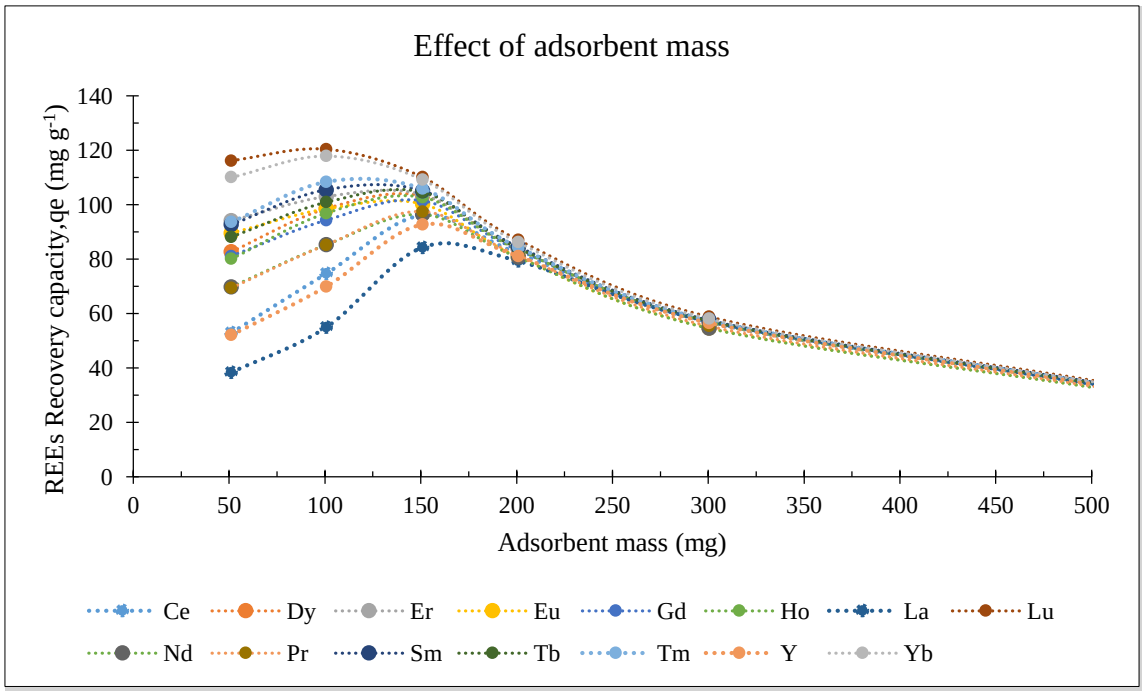


Figure 5.18: REEs recovery capacity obtained from varying mass (50, 100, 150, 200, 300 and 500 mg) of Mgt (adsorbent), in 15 mL REEs solution at pH 2.2 (RSD < 5%)

5.5.2 The effect of adsorbate pH conditions

The recovery efficiency and capacity obtained from the agitation (150 rpm, 5 hrs) of REEs adsorptive carrying solution (1 ppm, 15 mL), under different pH conditions (2.5, 4.5, 6, 7, 8 and 9.5), with natural magnetite (Mgt) adsorbent mass of 150 mg in 50 mL centrifuge tubes are presented in Figures 5.19 and 5.20 below. Here too, REEs curves gave, immediately, an indication of a similar behaviour. Percentage adsorption was higher in strong acidic conditions (pH 2.5 – 4.5), became negligible in mild acidic conditions (pH 6.0 – 7.0), reached a plateau at about pH 7, and continued likewise in alkaline medium. At pH < 7, the recovery efficiency (Figure 5.19) ranged from 92.1 (La) to 99.9% (Yb), was highest at pH 6 for most REEs (average 97.6%) and reached a plateau at pH 7. The plausible explanation to this observation is that the OH^- used to adjust adsorptive carrying fluid pH to higher target values had reacted with REEs cations to form soluble REEs hydroxides (REEOHs) thereby reducing the amounts of free REEs cations available for adsorption. For instance, analytical measurements of adsorptive carrying solution prior to mixing with Mgt revealed that cerium (Ce) concentration in the initial solution (pH 2.3) was 1.087 mg L^{-1} before pH incremental adjustments. Cerium concentration changed slightly to 1.077 mg L^{-1}, 1.042 mg L^{-1}, 0.995 mg L^{-1} and 0.992 mg L^{-1} at pH 2.5, 4.5, 6 and 7, but changed moderately to 0.77 mg L^{-1}, and significantly to 0.046 mg L^{-1} at pH 8 and 9.5 respectively. It was clear that REEs free cations had reacted with OH^- and that the extent of this reaction was noticeable in mild alkaline conditions and severe thereafter, leaving a small amount of $REEs^{3+}$ in solution, thereby changing the recovery scenario. Using the theory of hard and soft acid and base theory, Elsaidi *et al.* (2018) attributed this behaviour of REEs to their hard acid properties (cations with higher oxidation state and low polarizability) which give them higher affinity for hard bases (high electronegativity and highest occupied molecular orbitals) such as OH^-. Therefore, REEs formed hydroxides complexes and precipitated out of solution.

In comparison with other $REEs^{3+}$, at pH 7 and 8, La, Ce and Y showed higher adsorption capacities conversely to their adsorption capacities at pH 2.5, 4.5 and 6, assumingly because they precipitated less in the acidic range of pH incremental adjustments, and were consequently adsorbed more than the other $REEs^{3+}$ in the alkaline range of pH

incremental adjustments. The recovery capacity was much lower at pH > 8 because the small amount of $REEs^{3+}$ left in the adsorptive carrying solution was all taken up in a quick exhaustion by the adsorbent; this amount of $REEs^{3+}$ could only occupy a very small number of adsorption sites on natural magnetite. For most $REEs^{3+}$, the recovery capacity was highest at pH 4.5 (Figure 5.20), ranging from 91.0 (La) to 102.5 µg g^{-1} (Yb) with an average of 98.9 µg g^{-1}. Therefore, pH 4.5 was the adopted candidate for the next step of reactions.

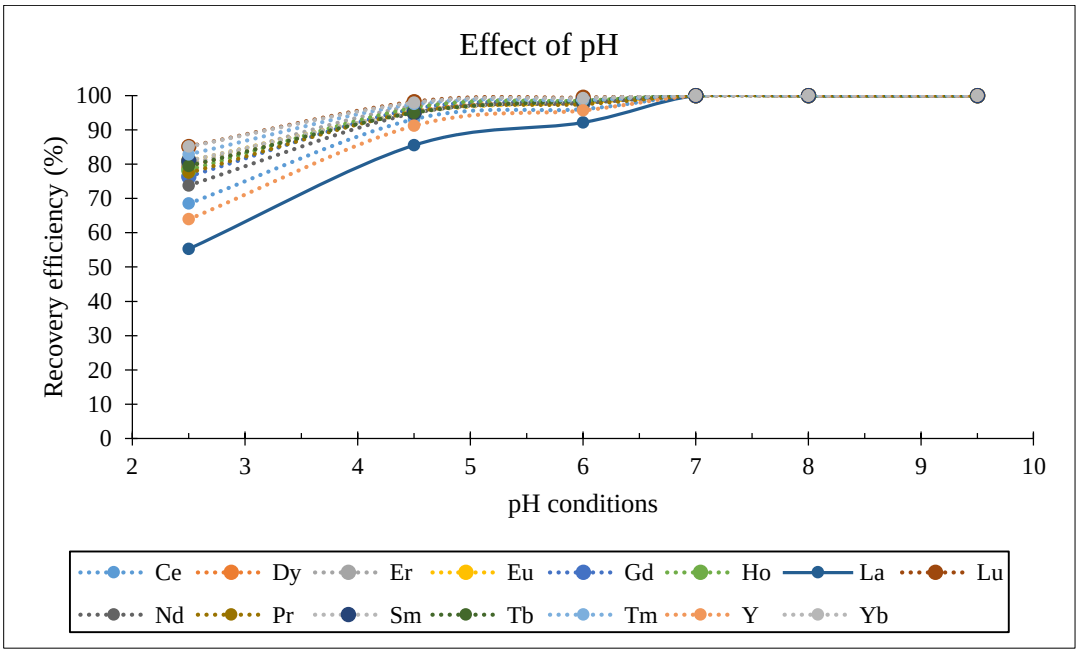


Figure 5.19: REEs recovery efficiency obtained from varying pH of 1 mg L^{-1} REEs adsorptive carrying solutions and 150 mg Mgt (RSD < 5%)

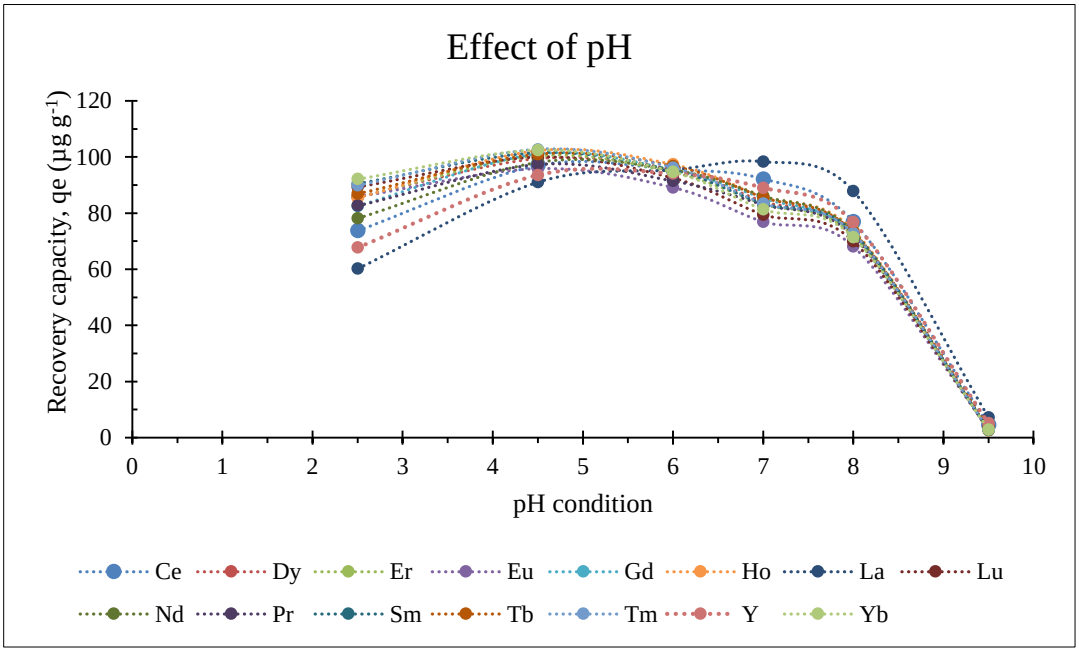


Figure 5.20: REEs recovery capacity obtained from varying pH of 1 mg L^{-1} REEs adsorptive carrying solutions and 150 mg Mgt (RSD < 5%)

5.5.3 The effect of agitation time

The recovery efficiency and capacity obtained from the agitation (150 rpm) of REEs adsorptive carrying solution (1 ppm, 15 mL, pH 4.5), for different agitation periods (30, 60, 90, 135, 180 and 240 minutes), with natural magnetite (Mgt) adsorbent mass of 150 mg in 50 mL centrifuge tubes are presented in Figure 5.21 and 5.22 below. It was obvious that longer agitation periods brought little and diminishing increases on the recovery efficiency of REEs. This could be attributed to the fact that more REEs were rapidly adsorbed within shortest agitation period where the virgin adsorbent, with more adsorption sites available, allowed for more up taking of REEs. The adsorbent was then, progressively, getting saturated and could not accommodate excess REEs rendering insignificant the effect of longer agitation time. Average percentage recoveries for REEs were 76.5, 83.0, 83.8, 84.5, 89.0 and 89.1% for 30, 60, 90, 135, 180 and 240 minutes of continuous agitations. Average adsorption capacities were 81.5, 88.4, 89.2, 89.9, 94.8 and 95.0 µg g^{-1}, but factoring time ratios into the recovery (efficiency) equation gave a different perspective of the removal efficiencies, i.e. when recoveries were brought down to the same agitation time (here, 30 minutes), 81.5, 44.2, 29.7, 19.9, 15.8 and 11.8 µg g^{-1}

were assigned to 30, 60, 90, 135, 180 and 240 minutes of continuous agitations (Figure 5.23).

A separate sequential (relay) batch recovery experiment of REEs was performed to assess the effect of agitation period on the recovery efficiency. The adsorptive carrying solution from the first 30 minutes' agitation was transferred into a second tube containing the same mass of unused (virgin) adsorbent, and agitation of the new mixture continued for another 30 minutes' period. Results showed that the remaining REEs from the first 30 minutes' agitation were all taken up by magnetite during the second 30 minutes' agitation. The recovery efficiency of REEs was 99.8% at 60 minutes, distributed as 76.5% in the first 30 minutes and 23.3% in the second 30 minutes (Figure 5.24). This could not be achieved by 240 minutes of continuous agitation (89.1%). This method is commonly used in metal floatation recovery (Figure 2.5, flow chart on Cu processing operations) and was evaluated by Santos Yabe and de Oliveira (2003) for the removal of toxic metals from industrial effluents by sequential adsorbent treatment.

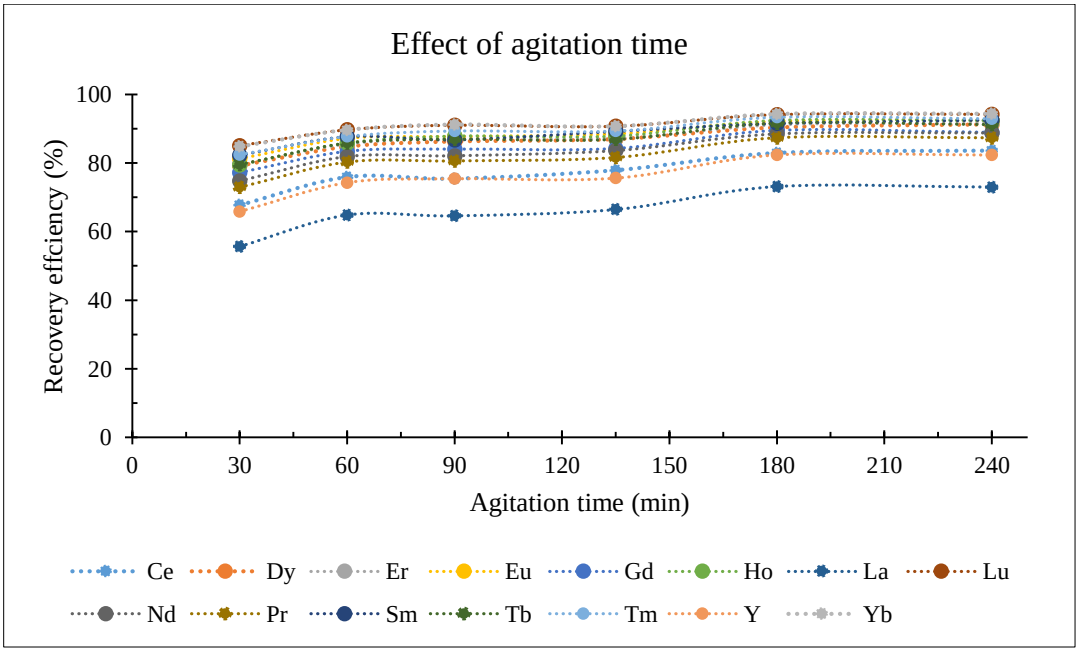


Figure 5.21: REEs recovery efficiency obtained for different agitation times of the adsorptive – adsorbent mixtures at pH 4.5, 150 mg adsorbent and 1.0 mg L^{-1} solution (RSD < 5%)

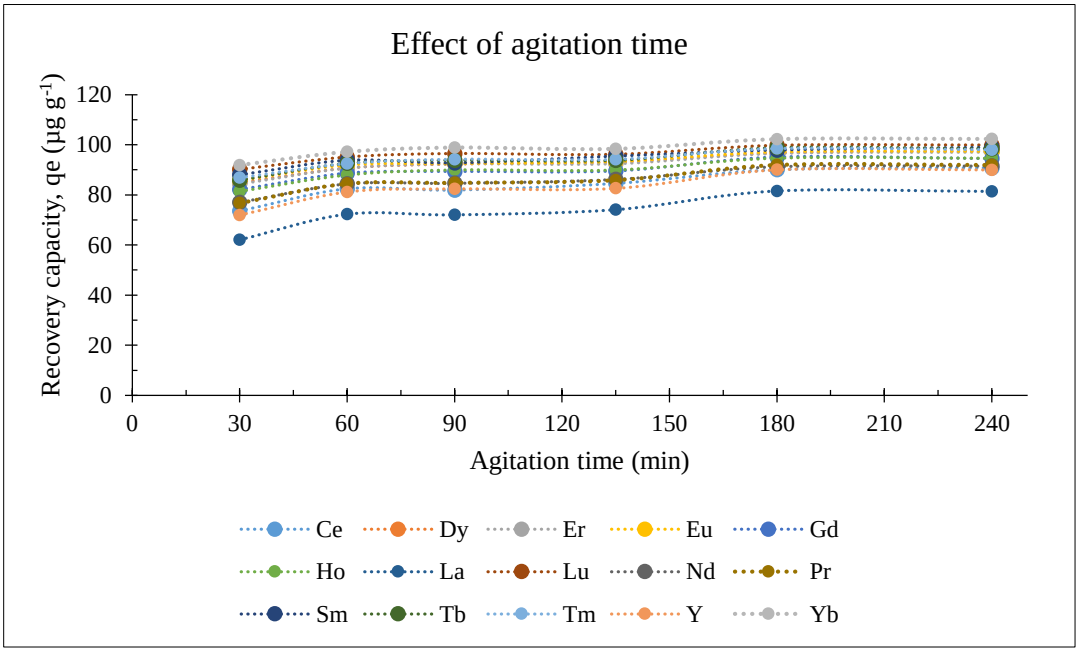


Figure 5.22: REEs recovery capacity obtained for different agitation times of adsorptive – adsorbent mixtures at pH 4.5, 150 mg adsorbent and 1.0 mg L^{-1} solution (RSD < 5%)

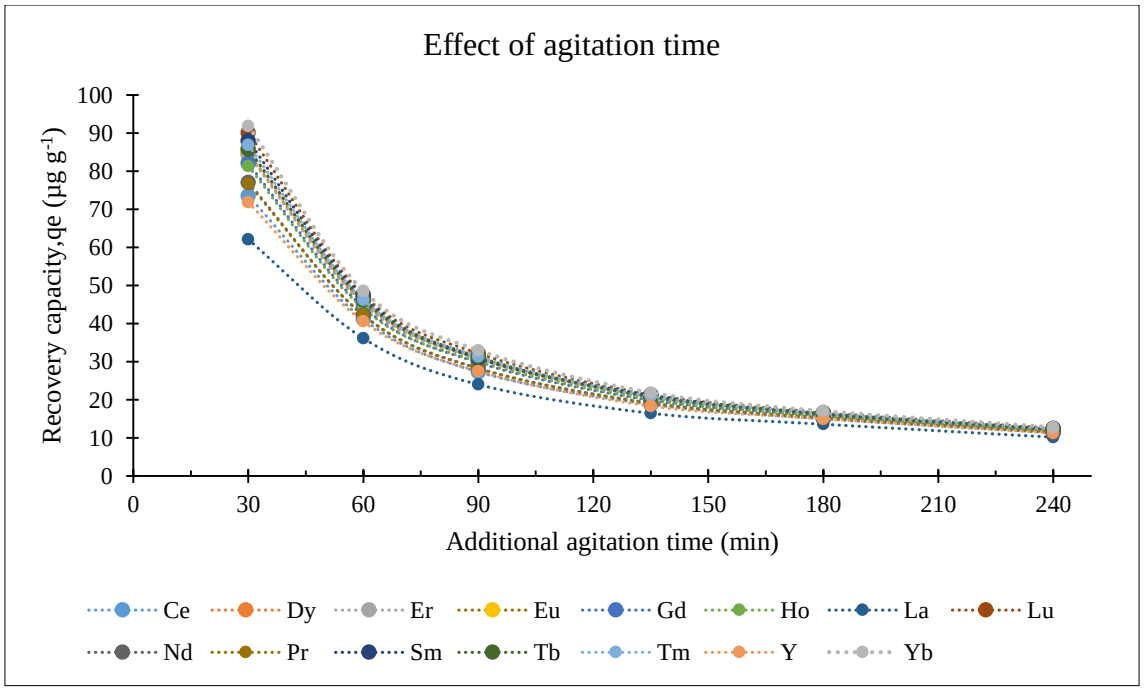


Figure 5.23: Diminishing REEs recovery capacity for different additional agitation times.

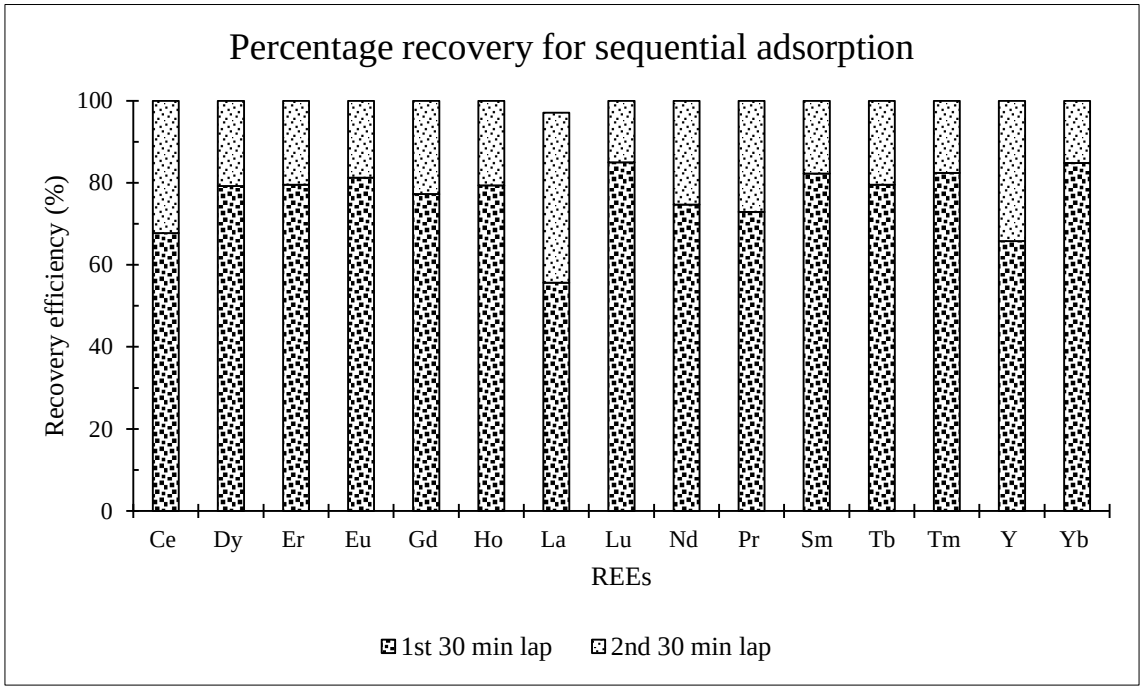


Figure 5.24: REEs recovery efficiency obtained from sequential adsorption experiment

5.5.4 The effect of adsorbate initial concentration

The recovery efficiency and capacity obtained from the agitation (150 rpm, 180 minutes) of REEs adsorptive carrying solution (15 mL, pH 4.5) of different initial concentrations (0.1, 0.5, 1.0, 1.5, 2.0 and 2.5 mg L^{-1}), with natural magnetite (Mgt) adsorbent (150 mg) in 50 mL centrifuge tubes are presented in Figures 5.25 and 5.26 below. The recovery efficiency increased from 59.7% for 0.08 mg L^{-1} adsorptive carrying solution to 99.8% (its peak) for 0.55 mg L^{-1} adsorptive carrying solution, and then it started decreasing with increasing concentrations (Figure 5.25). Despite the increase in adsorptive concentration (the number of target ions in solution), the number of adsorption sites (on mineral solid) remained constant; the imbalance between the two led to the decline of the recovery efficiency because more REEs remained in the adsorptive carrying solution as excess cations. In this experiment, recovery was efficient for adsorbate with initial concentration 0.55 mg L^{-1} where maximum REEs were adsorbed and minimum REEs were left in solution (Table 5.22). Even though the recovery capacity (113 mg g^{-1}) was obtained, for

most REEs (average) for adsorptive carrying solution with initial concentration 1.7 mg L^{-1}, a large amount of adsorptive (REEs) was left in solution.

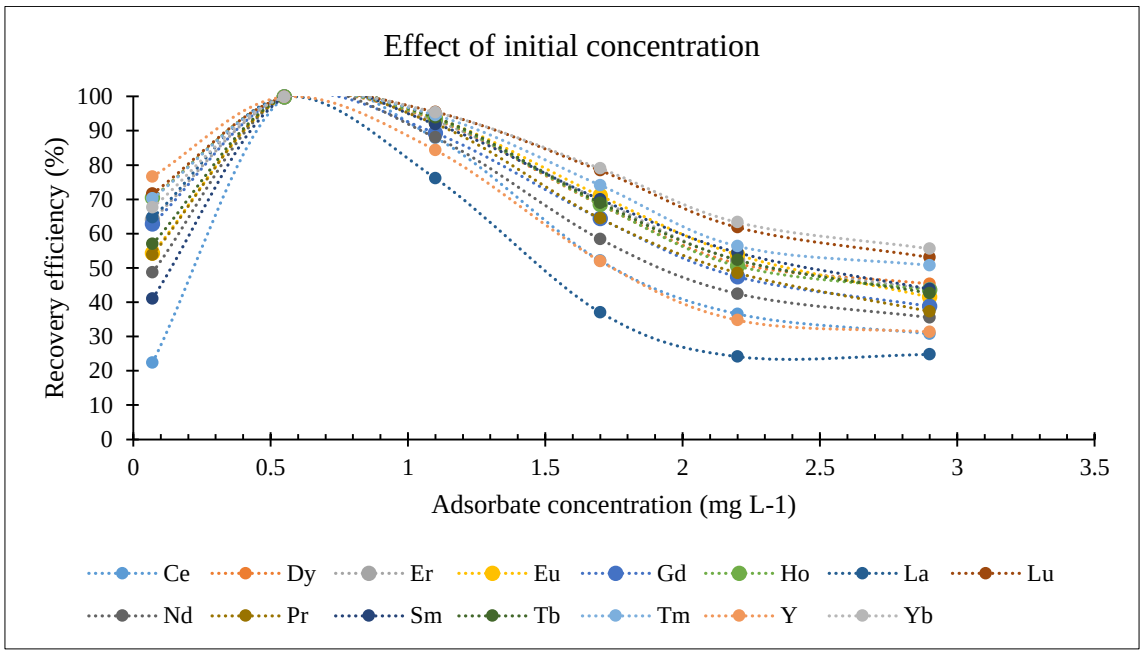


Figure 5.25: REEs recovery efficiency obtained from sequential adsorption experiment at pH 4.5, 150 mg adsorbent and at 150 rpm (RSD < 5%)

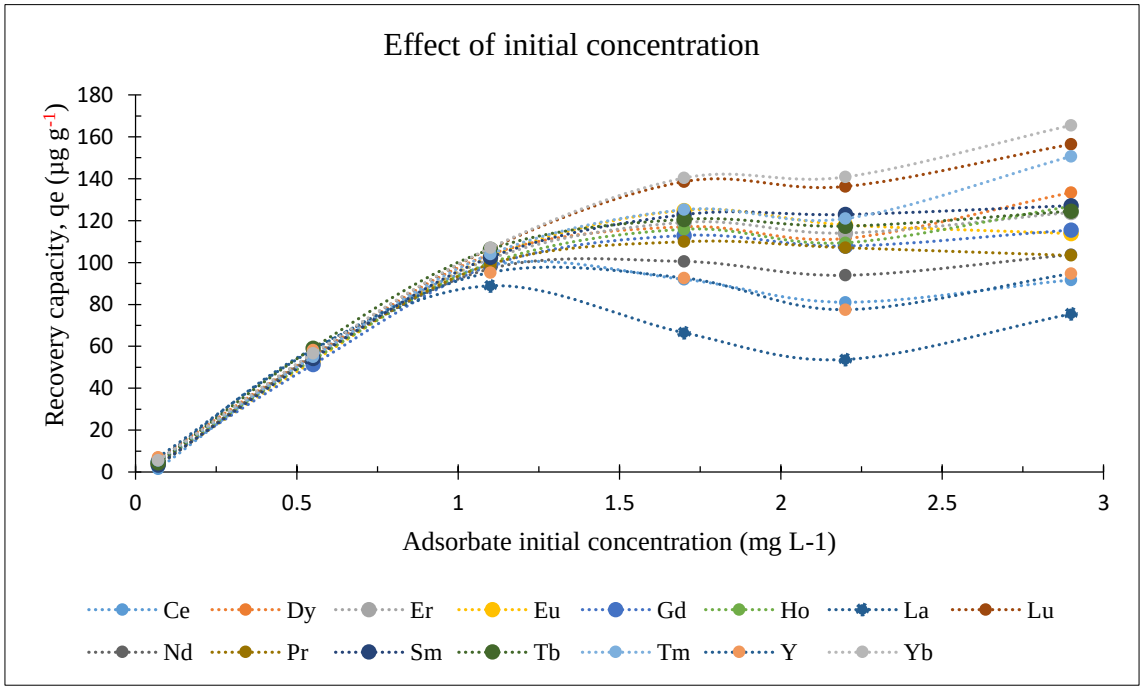


Figure 5.26: REEs recovery efficiency obtained from sequential adsorption experiment at pH 4.5, 150 mg adsorbent and at 150 rpm (RSD < 5%)

Table 5.22: Recovery efficiency and capacity under the effect of initial concentration

Sample	Ci (mg L^{-1})	Cf (mg L^{-1})	Recovered (%)	Not recovered (%)	qe (µg g^{-1})	Ratio (R:nR)
Agitation flask 1	0.08	0.03	59.7	40.3	4.7	1.5
Agitation flask 2	0.55	nd	**99.8**	**0.2**	**55.4**	**499**
Agitation flask 3	1.1	0.1	90.7	9.3	100.8	9.8
Agitation flask 4	1.7	**0.59**	65.1	34.9	**113.3**	**1.9**
Agitation flask 5	2.2	1.11	48.7	51.3	107.5	0.9
Agitation flask 6	2.9	1.69	41.2	58.8	120.5	0.7

5.5.5 The effect of competing ions

The recovery efficiency and recovery capacity obtained from the agitation (150 rpm, 180 minutes) of the first mixture (15 mL, pH 4.5) of fixed REEs concentration (~0.5 mg L^{-1}) and competing ions concentration (~0.5 mg L^{-1}), and of the second mixture (15 mL, pH 4.5) of mixed REEs concentration (~0.5 mg L^{-1}) and competing ions concentrations (1.0 – 2.5 mg L^{-1}), with natural magnetite (Mgt) adsorbent (150 mg) in 50 mL centrifuge tubes are presented in Figure 5.27 and 5.28 below. REEs average recovery efficiency was 99.0% in the fixed concentration mixture with competing ions, but it dropped to 95.0% in the mixed concentration mixture. This raised some speculative predictions as to what the influence of higher concentrations of competing ions on the recovery of REEs would be in the natural environment (e.g. water retain dam) where the gap in concentrations between REEs and most competing ions is normally huge. Elsaidi *et al.* (2018) pointed out that REEs were hard Lewis acids which, in the natural environment, enjoyed competitive advantage in their interactions with hard Lewis bases (e.g. oxy-hydroxides at mineral surfaces) than soft Lewis acid such as trace element cations (Ugwu and Igbokwe, 2018).

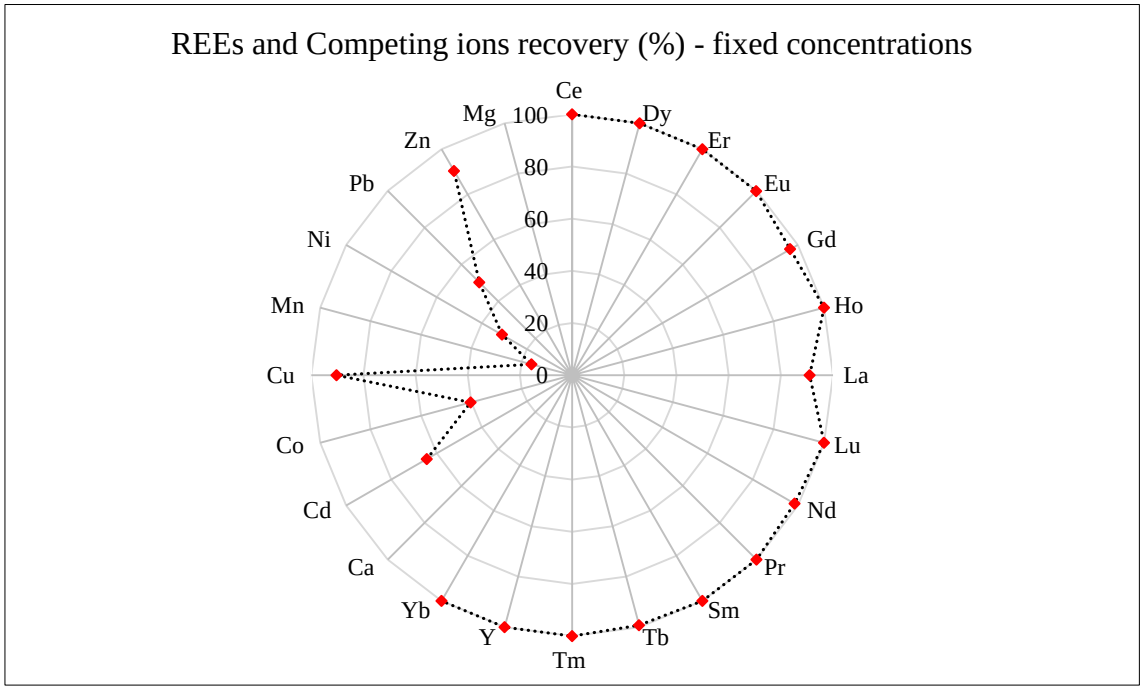


Figure 5.27: REEs and competing ions recovery efficiency obtained from a mixed concentration of target elements solution.

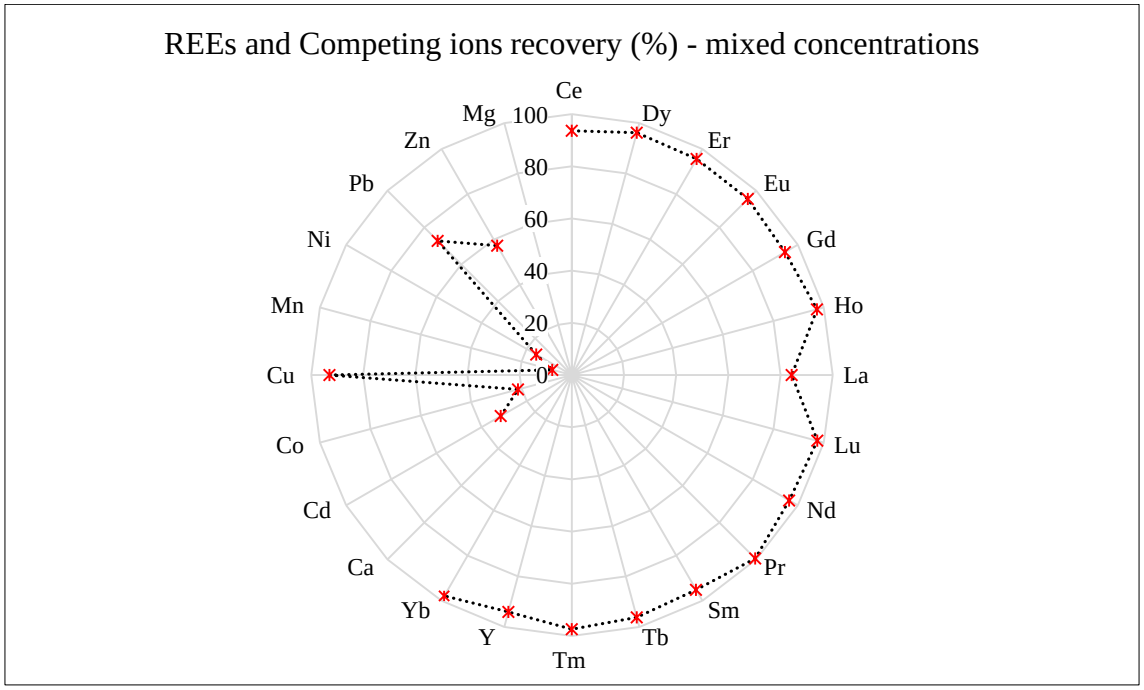


Figure 5.28: REEs and competing ions recovery efficiency obtained from a mixed concentration of target elements solution.

5.5.6 Adsorption Isotherm studies

5.5.6.1 Langmuir Isotherm Model

The experimental data from the effect of varying initial concentration was employed to plot REEs concentration (C_{ads}) in the solid phase (µg g^{-1}) as a function of REEs concentration (C_{eq}) in the liquid phase (mg L^{-1}) at equilibrium. Curvilinear lines (Langmuir isotherms) were obtained, but only Cerium (Ce) plot is shown in Figure 5.29 below. The same data were used in the linear expression of the Langmuir equation to plot the ratio of REEs liquid to solid concentrations (C_{eq}/C_{ads}), in L mg^{-1}, as a function of REEs concentration (C_{eq}) in the liquid phase (mg L^{-1}) at equilibrium. Figure 5.30 below was obtained for Cerium.

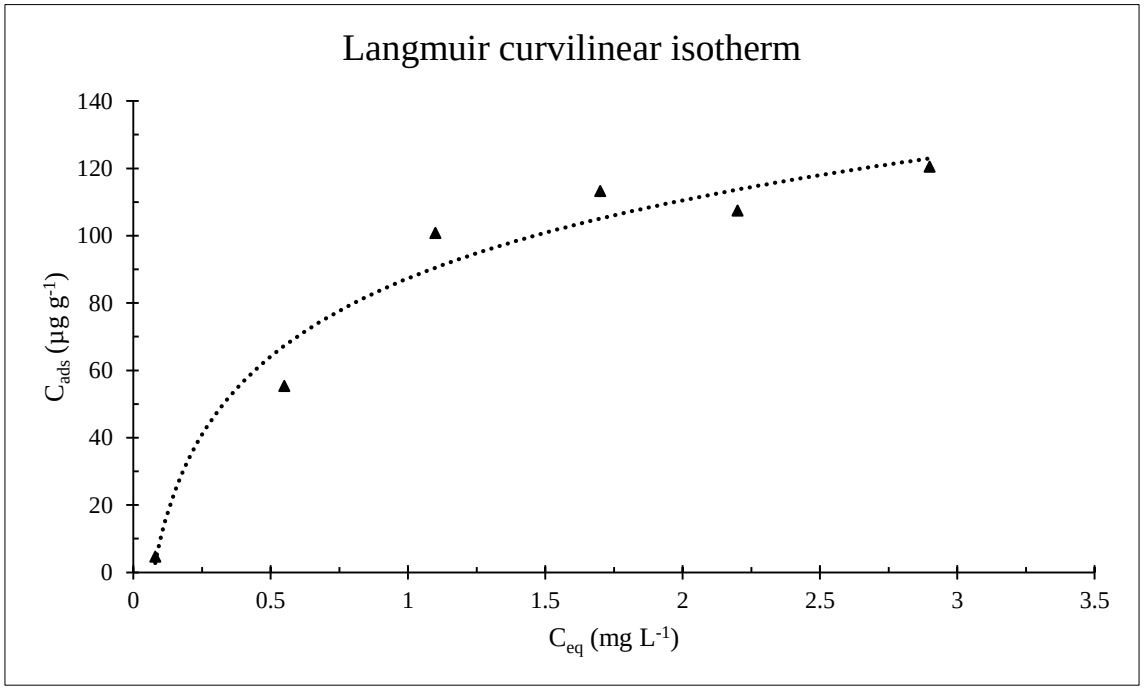


Figure 5.29: Langmuir adsorption isotherm for interactions of Ce with Mgt

The maximum concentration of adsorbate (mg g^{-1}) on the adsorbent ($q_{(max)}$) and its corresponding concentration (mg L^{-1}) in the adsorptive carrying solution (K_L) calculated from the linear equations are presented in Table 5.23 below. The two parameters do meet, in principle, at the equilibrium adsorption point in the Langmuir adsorption isotherm. Highly curved isotherms corresponded to higher K_L and small $q_{(max)}$ (less favourable

adsorption, e.g. Ca, La, Y), and less curved isotherms corresponded to lower K_L and larger $q_{(max)}$ (more favourable adsorption, e.g. Lu, Tm, Yb). It was observed that higher K_L gave a good correlation between the experimental (q_{exp}) and the calculated (q_{max}) values of adsorbate on the mineral adsorbent. The separation factor ($R_L < 1$) indicated that adsorption was favourable for all REEs. The correlation coefficient (0.97) was very good and indicated that experimental data fitted strongly in the Langmuir adsorption model. Additionally, experimental data fitted well in the curvilinear expression of the Langmuir isotherm.

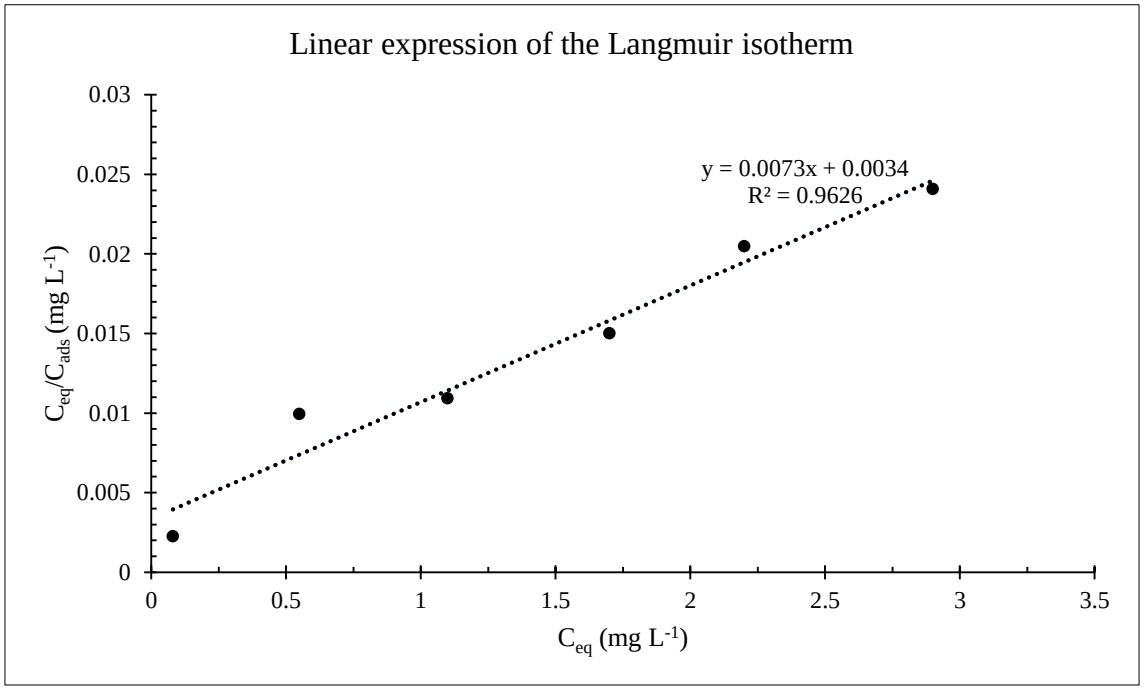


Figure 5.30: Langmuir adsorption isotherm for Ce adsorptive on Mgt adsorbent

5.5.6.2 Freundlich Isotherm Model

The experimental data from the effect of varying initial concentration was employed to plot the natural logarithm of REEs concentrations (C_{ads}) in the solid phase (µg g^{-1}) as a function of the natural logarithm of REEs concentrations (C_{eq}) in the liquid phase (mg L^{-1}) at equilibrium. Linear plots were obtained, from which the Freundlich isotherm constant (K_F) and the adsorption intensity (n) were calculated. The plot for Ce is shown

in Figure 5.31 below. The values for K_F ((mg g^{-1})/(mg L^{-1})$^{1/n}$) and n are presented in Table 5.24 below.

The affinity of Mgt for metal species, expressed as K_F, was higher for Lu, Tm and Yb. The adsorption intensity was greater than 1 (n > 1 or 1/n < 1) implying stronger interaction between adsorbate and adsorbent and favourable adsorption for all REEs except Ce (Lyubchik *et al.*, 2011). This meant that their adsorption isotherms departed a little from linearity and tended toward an S-shaped adsorption isotherm within the experimental concentration range. This was also evidenced by the values of the slopes (~1) in Freundlich line equations. The plotted experimental parameters produced a good linear relationship (R^2 = 0.95), an indication that the Freundlich equation was applicable to REEs adsorption onto Mgt.

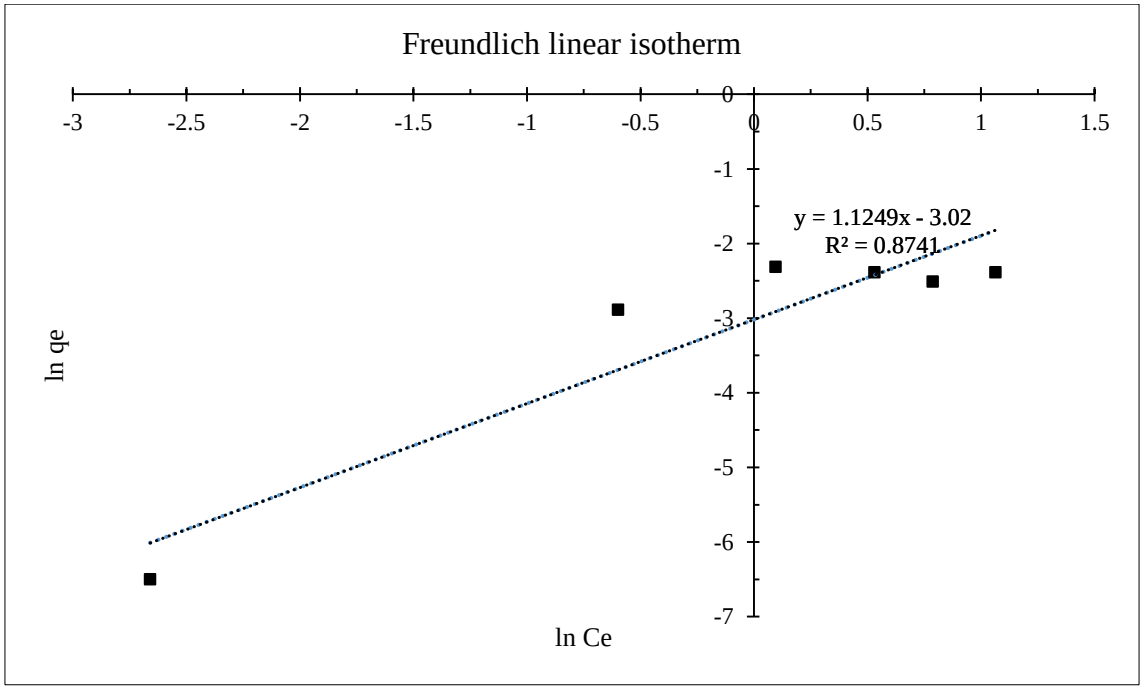


Figure 5.31: Freundlich adsorption isotherm for Ce adsorptive on Mgt adsorbent

5.5.6.3 Dubinin-Radushkevich Isotherm Model

The experimental data from the effect of varying initial concentration was employed to plot the natural logarithm of REEs concentrations (C_{ads}) in the solid phase (µg g^{-1}) as a function of the Polanyi constant the calculation of which required REEs concentrations

(C_{eq}) in the liquid phase (mg L^{-1}) at equilibrium (Bleam, 2017b). Linear plots were obtained, from which the Dubinin-Radushkevich (D-R) isotherm constant (K_{ad}, mol^2 (kJ $mol)^{-1}$) and the D-R adsorption capacity (X_m, mg g^{-1}) were calculated. The adsorption energy, E_s (J mol^{-1}), was also calculated using K_{ad}. Table 5.25 presents all calculated results. The adsorption capacity (calculated), X_m, was much similar to the experimental adsorption capacity (qe) and the goodness of fit, the coefficient correlation (R^2), indicating the fitting of experimental data in the D-R isotherm model, was consistently higher (~0.95). The energy of adsorption pointed out that the process of REEs adsorption onto Mgt followed an ion exchange mechanism because its values fell within the limits set in literature for this mechanism, i.e. between 8 and 16 kJ mol^{-1} (Inglezakis and Zorpas, 2012).

5.5.7 Adsorption Kinetics studies

In order to understand the kinetics of REEs adsorption by natural magnetite, the experimental data from the effect of varying agitation times was fitted into the linear expression of the pseudo first-order (PFO) rate and the pseudo second-order (PSO) adsorption Kinetics rate equations. Plots were obtained for all REEs and PSO values presented in Table 5.26 were calculated from individual REE's linear equations.

5.5.7.1 Pseudo-First Order adsorption kinetics (PFO)

Plots generated from PFO linear expressions did not give the best R^2 as shown by the example of PFO plot for Ce in Figure 5.32 below. Therefore, PFO was not a good candidate for the adsorption kinetics for REEs adsorption by Mgt.

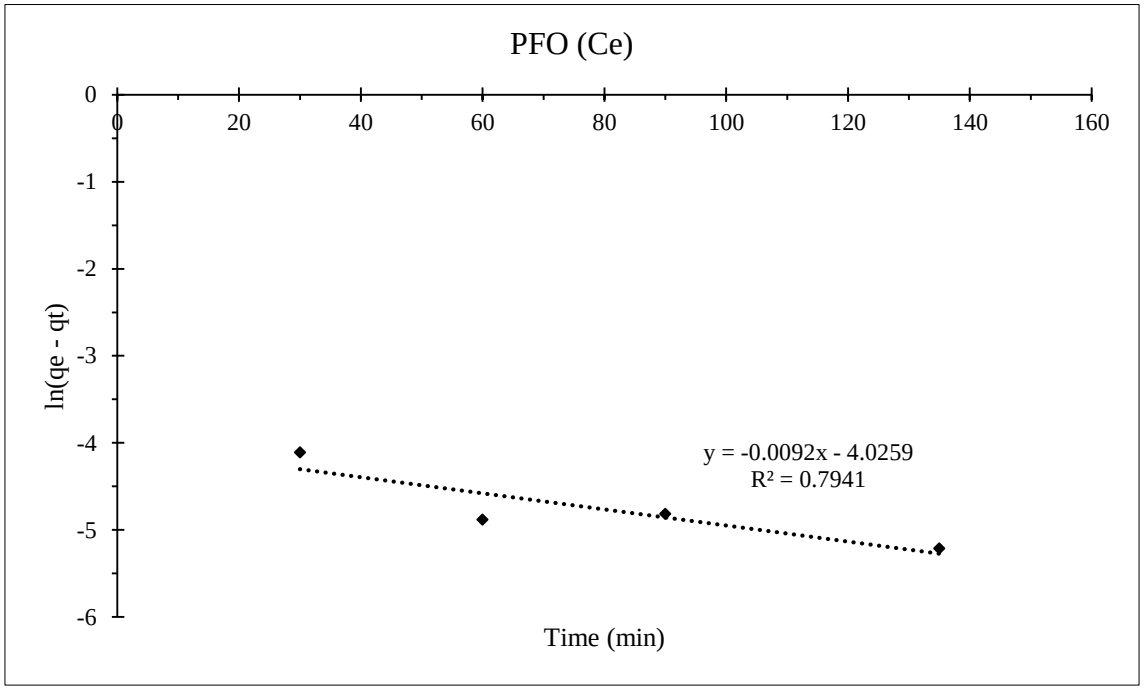


Figure 5.32: Pseudo-first order kinetic isotherm for Ce adsorptive on Mgt adsorbent

5.5.7.2 Pseudo-Second Order adsorption kinetics (PSO)

Plots generated from PSO linear expressions yielded the best R^2 as shown by the example of PSO plot for Ce in Figure 5.33 below. Therefore, PSO was the best candidate for the adsorption kinetics for REEs adsorption by Mgt. The calculated adsorption capacity for PSO was slightly on the lower side, but within close range, when compared with the experimental adsorption capacity of Mgt. Adsorption kinetics rate constant k_2 for PSO together with the calculated amount of metal ions adsorbed onto the adsorbent (qe), given in Table 5.26 below, were all in support of this conclusion.

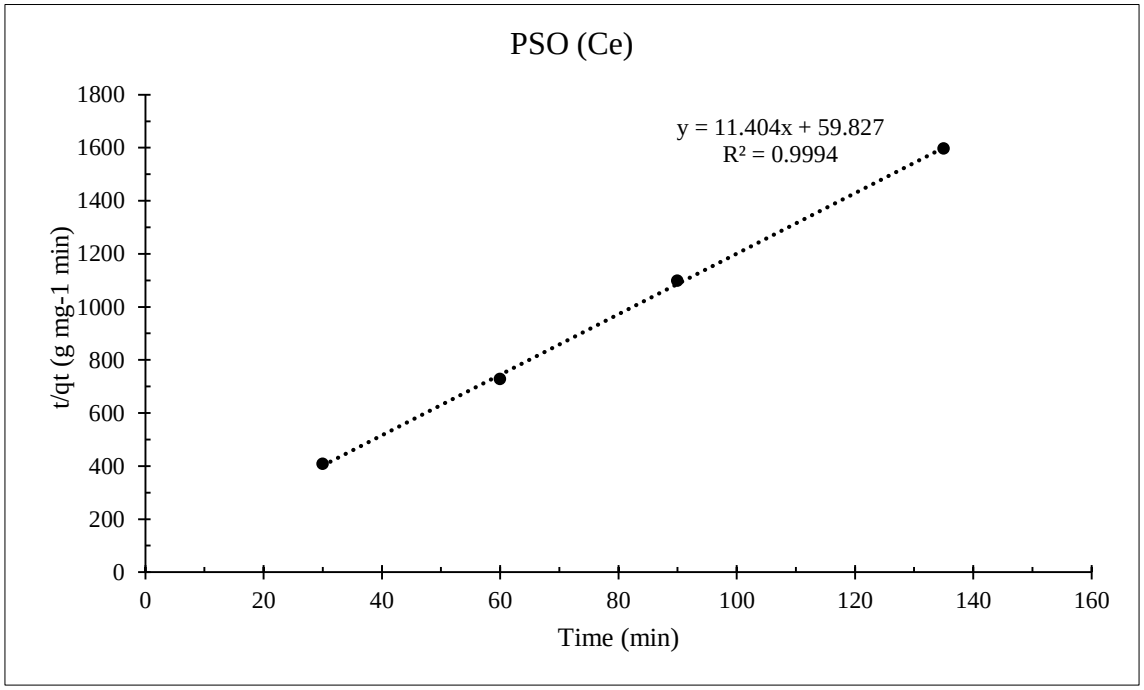


Figure 5.33: Pseudo-second order kinetic isotherm for Ce adsorptive on Mgt adsorbent

Natural magnetite (150 mg) was used to adsorb a complete spectrum of REEs from a 1.0 mg L^{-1} adsorptive carrying fluid for 180 min agitation time at an agitation speed of 150 rpm, at room temperature. The correlation coefficient (R^2) of the equilibrium data was acceptable for all three isotherm models considered in this study. However, the adsorption was best described by the Langmuir model with higher adsorbed amount (q_{max}) and higher adsorbent affinity (K_L) for most REEs cations. The percentage recovery was 94.8%. In addition, the adsorption fitted the PSO kinetic model. These assessments of results echoed the observation by Ugwu and Igbokwe (2018) that the PSO kinetic model and Langmuir, Freundlich and Rubinin-Radushkevich isotherm models provide the best description for most of the adsorption of ions on clays and oxides. Thermodynamic studies could give some clear indications regarding the nature of adsorption mechanisms, even though better understanding of sorption mechanisms is done by using technologies and spectroscopic studies (Ugwu and Igbokwe, 2018).

5.5.8 Cost analysis

To determine the economic viability of REEs recovery using natural magnetite, the following calculations were made based on estimated REEs global market of 149.500

tons at USD 4.5 billion for the current year (Jollicoe, 2019). The recovery did not target one particular REE but all REEs in adsorptive carrying solution. Their desorption (separation) was not factored in cost analysis either.

149.500 tons (REEs) at 4.5 billion (USD)

149 000 kg (REEs) at 4 500 000 000 (USD)

1 kg (REEs) at 4 500 000 000/149 000 = 30 100.33 (USD)

The average REEs recovery capacity obtained from the Langmuir isotherm model was 0.161 mg (REEs) g^{-1} (Mgt) or (161 g (REEs) kg^{-1} (Mgt)).

1 kg $\equiv 1000\ g$ (REEs) at 30 100.33 (USD)

161 g (REEs) at 30 100 x 161/1000 = 4 996.66 USD

The market share of the two main groups of REEs do differ (e.g. LREEs = 62.5% and HREEs = 37.5%) just as the market values for independent REEs do differ as well (e.g. Dy is the most valuble) (Jellicoe, 2019). This value (USD/ounce), encompassing all REEs, compared with precious metals in the following decreasing order: Rh (5400) > Pd (1838), Au (1477.30) > REEs (936.24) > Pt (908) > Ag (17.14).

Table 5.23: Calculated values from Langmuir adsorption isotherm equation

Isotherm	Parameter (unit)	Ce	Dy	Er	Eu	Gd	Ho	La	Lu	Nd	Pr	Sm	Tb	Tm	Y	Yb
Langmuir	qmax (mg g^{-1})	0.098	0.178	0.165	0.151	0.150	0.170	0.068	**0.249**	0.121	0.127	0.178	0.159	**0.224**	0.099	**0.277**
	K_L (L mol^{-1})	**4.245**	0.972	1.129	1.437	1.221	1.011	**33.000**	0.610	2.084	2.078	1.012	0.285	0.662	**3.965**	0.520
	R_L	0.178	0.490	0.455	0.398	0.435	0.491	0.026	0.607	0.318	0.314	0.480	0.765	0.589	0.187	0.640
	R^2	0.955	0.945	0.954	0.912	0.948	0.950	0.873	0.943	0.966	0.949	0.949	0.967	0.929	0.939	0.946
	qexp (mg g^{-1})	0.092	0.117	0.119	0.125	0.113	0.116	0.066	**0.139**	0.101	0.110	0.123	0.121	**0.125**	0.093	**0.140**

Table 5.24: Calculated values from Freundlich adsorption isotherm equation

Isotherm	Parameter (unit)	Ce	Dy	Er	Eu	Gd	Ho	La	Lu	Nd	Pr	Sm	Tb	Tm	Y	Yb
Freundlich	K_F (mg g^{-1})/(mol L^{-1})$^{1/n}$	0.048	0.071	0.067	0.024	0.064	0.066	0.049	0.104	0.057	0.060	0.066	0.066	0.072	**0.060**	0.079
	n	0.889	1.222	1.121	1.038	1.130	1.125	**1.469**	**3.438**	1.033	1.050	0.995	1.076	1.111	**1.420**	1.084
	R^2	**0.874**	0.957	0.947	0.934	0.944	0.950	**0.804**	**0.759**	0.910	0.953	0.943	0.929	0.965	**0.892**	0.974
	qexp (mg g^{-1})	0.092	0.117	0.119	0.125	0.113	0.116	0.066	**0.139**	0.101	0.110	0.123	0.121	**0.125**	0.093	**0.140**

Table 5.25: Calculated values from Dubinin - Radushkevich adsorption isotherm equations

Isotherm	Parameter	Ce	Dy	Er	Eu	Gd	Ho	La	Lu	Nd	Pr	Sm	Tb	Tm	Y	Yb
D-R	Xm	**0.088**	0.105	0.104	0.104	0.098	0.102	**0.070**	0.118	0.093	0.097	0.107	0.108	0.111	**0.086**	0.121
	Kads	**2.00E-09**	3.00E-09	3.00E-09	3.00E-09	3.00E-09	3.00E-09	**2.00E-09**	3.00E-09	3.00E-09	3.00E-09	3.00E-09	3.00E-09	3.00E-09	2.00E-09	3.00E-09
	Es	**1.58E+04**	1.29E+04	1.29E+04	1.29E+04	1.29E+04	1.29E+04	**1.58E+04**	1.29E+04	1.29E+04	1.29E+04	1.29E+04	1.29E+04	1.29E+04	**1.58E+04**	1.29E+04
	R2	0.989	0.940	0.952	0.956	0.952	0.951	0.972	0.930	0.978	0.970	0.959	0.970	0.936	0.973	0.925
	qexp	0.092	0.117	0.119	0.125	0.113	0.116	0.066	**0.139**	0.101	0.110	0.123	0.121	**0.125**	0.093	**0.140**

X_m and q_e (mg g^{-1}). K_{ads} (mol^2 (kJ^2)$^{-1}$) and E_s (J mol^{-1})

Table 5.26: Calculated values from PSO adsorption kinetic model equation

Kinetics	Parameter (unit)	Ce	Dy	Er	Eu	Gd	Ho	La	Lu	Nd	Pr	Sm	Tb	Tm	Y	Yb
PSO	$q_{e(calc)}$ (g mg^{-1})	0.088	0.096	0.095	0.096	0.092	0.093	0.078	0.098	0.089	0.089	0.100	0.096	0.096	0.086	0.100
	k_2 (mg g^{-1} min^{-1})	2.174	2.960	3.229	3.513	3.887	2.981	1.994	4.758	2.754	2.896	3.255	3.560	3.634	2.474	4.458
	R^2	0.9994	1.0000	0.9998	0.9999	0.9998	0.9998	0.9991	0.9998	0.9998	0.9997	0.9993	0.9997	0.9998	0.9993	0.9998
	q_{exp} (g mg^{-1})	0.092	0.117	0.119	0.125	0.113	0.116	0.066	**0.139**	0.101	0.110	0.123	0.121	**0.125**	0.093	**0.140**

5.5.9 Adsorption thermodynamics studies

5.5.9.1 Activation energy

Rate constants, k_1 and k_2, from experimental measurements, were determined at two different temperatures (273.15 K and 308.15 K). Plots of the natural logarithm of rate constants (ln k) as a function of the inverse of absolute temperatures (1/T) were obtained. Figure 5.34 shows one (activation energy of Ce) of such many REEs plots obtained. The rate constant values together with values of E_a calculated from the line equation are presented in Table 5.27 below.

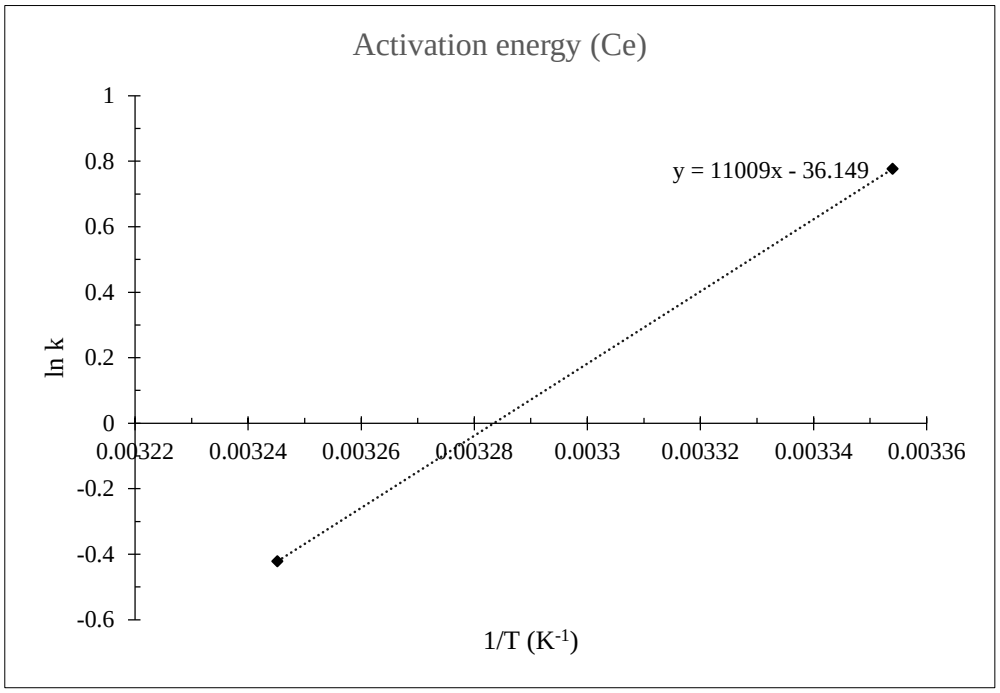


Figure 5.34: The Arrhenius equation plot used to find the activation energy for the adsorption of Ce onto Mgt

Rate of adsorption decreased with increases in temperature, in conformity to the Arrhenius equation. REEs had positive E_a, i.e. they required energy to cross the energy barrier for adsorption to occur. The average activation energy was 50.8 kJ mol^{-1}, the lowest and highest activation energy were 15.93 kJ mol^{-1} (Tb) and 102.32 kJ mol^{-1} (Sm) respectively. Comparing the E_a obtained with demarcation limits set in literature (Inglezakis and Zorpas, 2012) it could be said that adsorption of some REEs (Dy, Er, Eu, Ho, Lu, Tb and Yb) onto Mgt was of the physisorption type of

mechanism (Ea < 40 kJ mol^{-1}) whereas other REEs (Ce, Gd, La, Nd, Pr, Sm and Y) onto Mgt was of the Chemisorption type of mechanism (E_a > 40 kJ mol^{-1}). Most of those classified as undergoing physisorption could be further clustered as undergoing ion exchange (40 kJ mol^{-1} > E_a > 24 kJ mol^{-1}). Saha and Chowdhury (2011) pointed out that the activation energy for physisorption is usually no more than 4.2 kJ mol^{-1}. They classified chemisorption into reactions requiring between 8.4 and 83.7 kJ mol^{-1} as activated chemisorption and reactions with Ea nearing zero as non-activated chemisorption. A compilation of E_a for adsorption of trace elements ions and dye molecules onto various low cost adsorbents (mostly of biological nature) had 102.78 and -15.65 kJ mol^{-1} as the highest and the lowest E_a respectively, with the rest ranging heavily between 24 and 7 kJ mol^{-1}.

5.5.9.2 Heat of activation parameters

Plots of the natural logarithm of rate constants over temperatures ((ln k)/T) as a function of the inverse of temperatures (1/T) were obtained. Figure 5.35 shows one (Ce) of such many REEs plots obtained. Calculated heats of activation are tabulated below (Table 5.28).

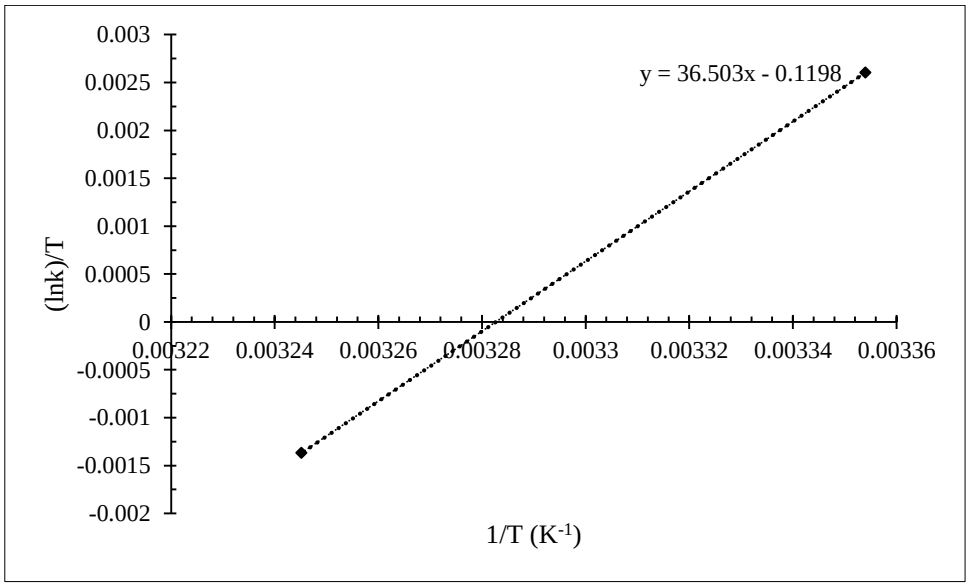


Figure 5.35: The Erying equation plot used to find the activation enthalpy and activation entropy for the adsorption of Ce onto Mgt

Adsorption of REEs onto Mgt required external energy to occur; this is shown by the positive free energy change of activation (ΔG^*). Positive but close to zero

enthalpy change of activation (ΔH^*) suggested that adsorption of REEs onto Mgt was an endothermic process requiring not too much external energy. Entropy changes of activation (ΔS^*) were negative and implied that adsorption followed the path of an activated complex leading to an orderly rearrangement of attracting forces between reacting components and that the adsorbent (Mgt) was favourably receptive to REEs adsorptive ions (Saha and Chowdhury, 2011).

5.5.9.3 Heats of complete and partial adsorption

In order to determine the spontaneity of the adsorption process, calculations of the standard free energy changes, using the Van't Hoff equation, were made possible by using the distribution constants (K_D) obtained from isotherm studies. These ΔG^o were then plotted as a function of temperature to produce a line, the equation of which gave ΔS^o and ΔH^o through calculations. Figure 5.36 shows one (Ce) of such many REEs plots obtained. The distribution constant values together with values of calculated energy changes are given in Table 5.29 below.

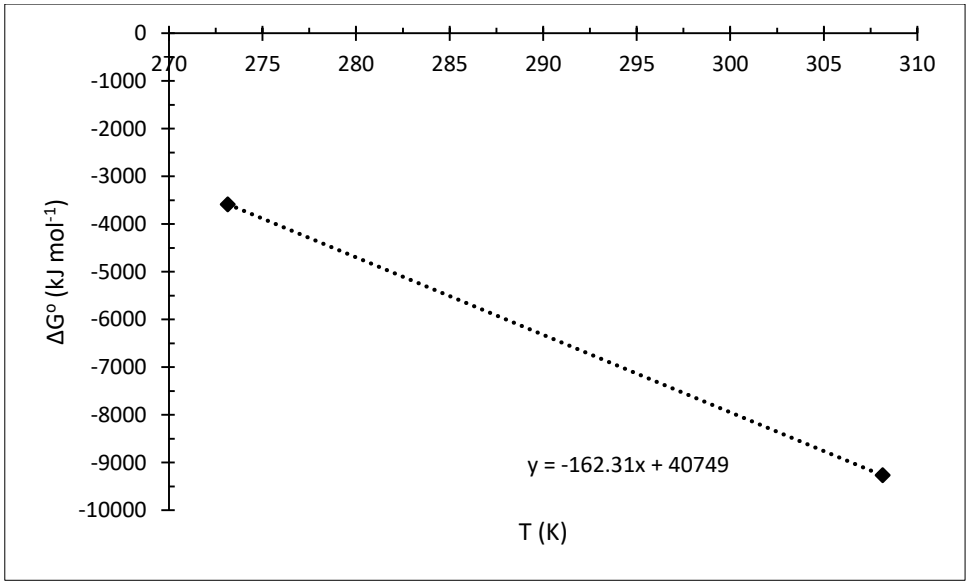


Figure 5.36: The Gibbs free energy equation plot used to find the standard enthalpy and the standard entropy for the adsorption of Ce onto Mgt

The distribution coefficient increased with increase in temperature thereby indicating that the affinity between adsorptive and adsorbent was in direct proportion relation with temperature (Table 5.29). The free energy changes of adsorption were all negative at both temperatures and, as such, they indicated the

feasibility and spontaneity of the adsorption of REEs onto Mgt at these two temperatures. In fact, ΔG^o decreased with increase in temperature, making the reaction more favourable at higher temperature by increasing the mobility of adsorptive in solution and allowing more contacts between adsorptive and adsorbent. Positive standard entropy changes reflected the willingness of Mgt to take up REEs and, by so doing, compromise some surficial structural changes. By ΔH^o and ΔS^o being both positive, the spontaneity of the adsorption process ($-\Delta G^o$) was more dependent on ΔH^o than ΔS^o, i.e. the difference between the energy expended in 'bond braking' and the energy released in 'bond making' at the activated complex could be decisive in making adsorption spontaneous or non-spontaneous.

The magnitude of ΔH^o gave a hint about the type of mechanism that was followed by REEs adsorption onto Mgt. None of the REEs had ΔH^o between 80 – 200 kJ mol^{-1}. Therefore, chemisorption was out of the possible mechanisms. Most REEs had ΔH^o within or slightly above the physosorption bracket of 2.1 – 20.9 kJ mol^{-1} (Saha and Chowdhury, 2011). For most REEs the mechanism predicted on the basis of E_a coincided with the one based on ΔH^o.

Plots for differential (isosteric) enthalpy (ΔH_x), by fitting the adsorptive equilibrium concentration in the solution (C_e) into the integrated Clausius-Clapeyron equation, were obtained (Figure 5.37). Calculations from the line equation gave positive values of ΔH_x (Table 5.30) similar in magnitude to the ones obtained for ΔH^o. Therefore, conclusions derived for ΔH^o in terms of adsorption mechanism remain valid for ΔH_x, i.e. the adsorption of REEs onto Mgt obeyed the physisorption mechanism. According to limits found in Saha and Chowdhury (2011), for $\Delta H_x < 80$ kJ mol^{-1} the process is classified as physisorption and for $80 < \Delta H_x < 400$ kJ mol^{-1} the process classified as chemisorption.

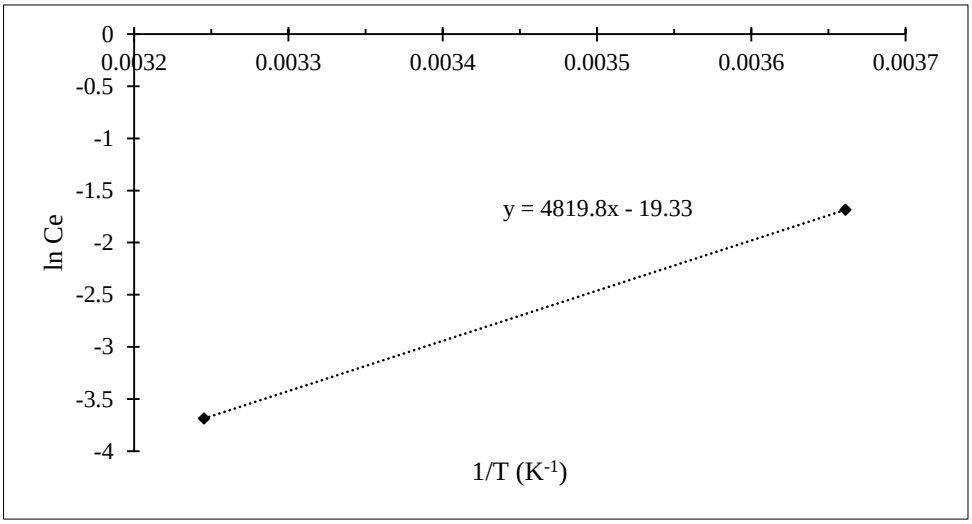


Figure 5.37: The Clausius-Clapeyron equation plot used to find the isosteric heat of adsorption for the adsorption of Ce onto Mgt

Thermodynamics adsorption studies were unanimous in determining the mechanism of REEs adsorption onto Mgt. The heats of adsorption (ΔH^o, ΔH_x), the adsorption energy obtained from D-R isotherm (E_s) and the activation energy (E_a) obtained in this study fell, generally, into the category of chemisorption mechanism. It could be prudent to attribute REEs adsorption onto Mgt to a physico-ion exchange mechanism rather than a purely physical mechanism, for inclusiveness of all REEs. The process showed to be spontaneous, endothermic and entropy dissipative.

Table 5.27: Activation energy for the adsorption of REEs onto natural magnetite calculated by fitting experimental data into the Arrhenius equation

	Ce	Dy	Er	Eu	Gd	Ho	La	Lu	Nd	Pr	Sm	Tb	Tm	Y	Yb
k_1	2.17	2.96	3.23	3.51	3.67	2.98	1.99	4.76	2.75	2.96	3.25	3.56	3.63	2.47	4.46
k_2	0.66	2.18	2.07	2.20	1.58	2.03	0.71	2.83	1.46	1.46	0.85	2.89		1.05	3.10
Ea (kJ mol^{-1})	91.53	23.29	34.12	35.73	64.43	29.38	79.20	39.60	48.40	53.90	102.32	15.93		65.69	27.85

Table 5.28: Activation parameters for the adsorption of REEs onto natural magnetite calculated by fitting experimental data into the Eyring equation

	Ce	Dy	Er	Eu	Gd	Ho	La	Lu	Nd	Pr	Sm	Tb	Tm	Y	Yb
ΔS^* (J mol^{-1})	-198.54	-197.79	-197.91	-197.93	-198.24	-197.86	-198.40	-197.97	-198.07	-198.13	-198.65	-197.71		-196.83	-197.84
ΔH^* (kJ mol^{-1})	0.30	0.08	0.12	0.13	0.22	0.10	0.26	0.14	0.17	0.18	0.34	0.06		0.22	0.10
ΔG^*_1(kJ mol^{-1})	59.50	59.06	59.13	59.14	59.33	59.10	59.42	59.17	59.22	59.26	59.57	59.01		58.90	59.09
ΔG^*_2 (kJ mol^{-1})	61.48	61.03	61.11	61.12	61.31	61.08	61.40	61.15	61.20	61.24	61.56	60.99		60.87	61.15

Table 5.29: Thermodynamic parameters for the adsorption of REEs onto natural magnetite calculated using the classical Van't Hoff equation and the Gibbs free energy equation

	Ce	Dy	Er	Eu	Gd	Ho	La	Lu	Nd	Pr	Sm	Tb	Tm	Y	Yb
K_{D1}	4.85	9.34	10.33	11.78	8.49	12.14	2.72	15.97	7.70	6.89	10.82	10.92	14.06	4.66	16.62
K_{D2}	37.24	28.93	33.96	28.87	19.61	33.48	6.74	39.48	19.67	31.81	26.70			12.95	55.50
$\Delta S°$ (J mol^{-1})	162.31	101.35	106.52	86.14	79.05	95.01	74.80	89.30	85.64	128.05	85.92			87.59	111.64
$\Delta H°$ (kJ mol^{-1})	40.75	22.61	23.79	17.93	16.73	20.28	18.16	18.10	18.76	30.60	18.06			20.43	24.11
$\Delta G°_1$ (kJ mol^{-1})	-3.59	-5.07	-5.30	-5.60	-4.86	-5.67	-2.27	-6.29	-4.64	-4.38	-5.41			-3.50	-6.38
$\Delta G°_2$ (kJ mol^{-1})	-9.27	-8.62	-9.03	-8.62	-7.62	-8.99	-4.89	-9.42	-7.63	-8.86	-8.41			-6.56	-10.29

Table 5.30: Isosteric heat of adsorption for the adsorption of REEs onto natural magnetite calculated using the Clausius-Clapeyron equation

	Ce	Dy	Er	Eu	Gd	Ho	La	Lu	Nd	Pr	Sm	Tb	Tm	Y	Yb
ΔH_x (kJ mol^{-1})	40.07	24.76	26.37	20.23	17.79	22.75	18.32	18.32	20.27	31.96	20.17			22.07	26.92

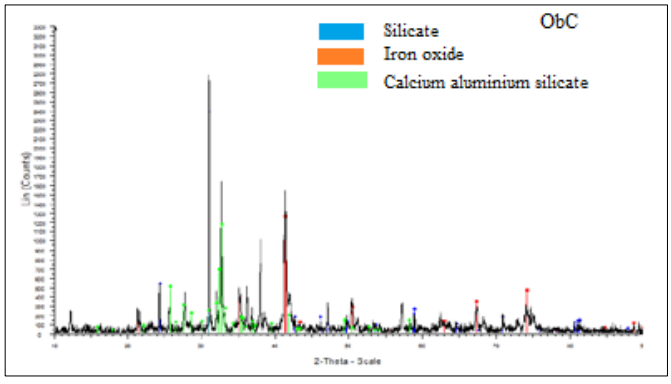
5.6 Characteristics of surface water floor sediments from Phalaborwa

In this section, results obtained from a different set of samples constituted of sediments collected from the floor of the Olifants and the Selati Rivers as well as the WRD within and around the mine area are presented and discussed below.

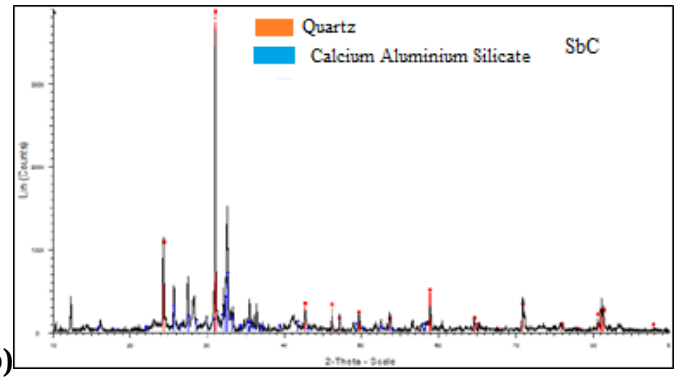
5.6.1 Mineral identification and semi-quantification

5.6.1.1 X-ray diffraction

Sediments characterised for mineral identification produced XRD graphs showing a limited variety of primary minerals such as SiO_2, $CaAlSiO_2$ and Fe_3O_4 for ObC; SiO_2, $CaAlSiO_2$ for SFB and SbC, and only Fe_3O_4 for WRD(s) and WRD(b) relative to characteristics of sediments parent geologic materials (Figure 5.38).



a)



b)

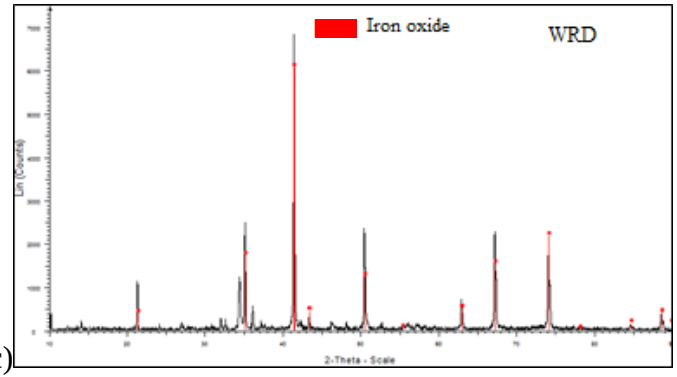
c) 

Figure 5.38: XRD graphs pattern for mineral identification in sediments (a) ObC (b) SbC and (c) WRD

5.6.1.2 X-ray fluorescence

Results from the assessment of major elements, as metal oxides (wt%), and LOI (wt%) from sediment samples using XRF, were converted into quantitative amounts (mg kg^{-1}) of elements. A marked contrast was noted between river sediment, on one side, and WRD sediment on the other. This was evidenced, for instance, by Si (23.71 - 25.53 > 3.84 mg kg^{-1}), Al (6.20 - 7.15 > 0.93 mg kg^{-1}), Fe (4.18 - 7.60 < 24.50 mg kg^{-1}) and Ca (3.03 - 4.52 < 16.57 mg kg^{-1}), i.e. more Si and Al in river sediment and more Fe and Ca in WRD sediments (Table 5.31). These results connected well with XRD data except for calcium measured in WRD(s) which may have, probably, come from secondary minerals.

Other results from XRF analysis, for trace elements assessment, are presented in Table 5.32. WRD(s) sediment was defined by high Cu (3857 mg kg^{-1}) and Ni (1839 mg kg^{-1}) content whilst river sediment contained elevated amounts of Cr, more in the Olifants River (ObC = 17989 mg kg^{-1}, OaC = 29185 mg kg^{-1}) and less in the Selati River (SbC = 2336 mg kg^{-1}). The elevated amounts of copper and Nickel can be associated with land run off and/or trench canalization of mine waste collected as sediments in WRD. The high amounts of chromium in river sediments may be attributed to physical weathering the original precursors.

Table 5.31: Major elements expressed as weight percentage composition in sediment samples after conversion from weight percentage metal oxides assessed by XRF analysis.

Element	ObC	SFB	SbC	OaC	WRD(s)
Si (wt%)	**24.76**	**24.90**	**25.53**	**23.71**	3.84
Al (wt%)	**6.63**	**6.20**	**7.00**	**7.15**	0.93
Fe_{Total} (wt%)	**7.60**	**4.18**	**5.69**	**5.89**	**24.50**
Mn (wt%)	0.12	0.15	0.10	0.12	0.19
Mg (wt%)	**2.75**	**1.87**	**2.45**	**2.84**	**3.67**
Ca (wt%)	**3.67**	**4.52**	**3.03**	**3.69**	**16.57**
Na (wt%)	1.05	1.52	1.15	0.84	0.12
K (wt%)	0.85	1.64	1.07	1.01	0.27
Ti (wt%)	1.32	0.55	0.80	0.56	0.64
P (wt%)	0.74	0.36	0.09	0.07	0.86
Cr (wt%)	0.56	0.03	0.18	0.19	0.03
Ni (wt%)	0.02	0.01	0.02	0.02	0.14
C (wt%)	2.20	3.64	3.03	3.77	**5.53**

Table 5.32: Trace elements composition (mg kg^{-1}) in sediments samples measured by XRF analysis

Element	Cr (mg kg^{-1})	Co (mg kg^{-1})	Cu (mg kg^{-1})	Ni (mg kg^{-1})	Pb (mg kg^{-1})	Zn (mg kg^{-1})	U (mg kg^{-1})
ObC	**17,989**	69.6	145.3	251.6	59.3	265.1	nd
SFB	271.1	22.5	210.1	110.1	19.2	61.78	nd
SbC	**2,336**	38.3	175.9	154.7	93.4	165.2	nd
OaC	**2,9185**	76.7	128.5	274.5	45.2	322	nd
WRD(s)	220.5	151.6	**3,857**	**1,839**	55.1	261.7	2.8

5.6.1.3 Elemental analysis: total carbon to sulphur ratio (C/S)

Figure 5.39 shows relative (vertical axis) and absolute (data label) elemental distribution of C, H, N and S as weight percentage. It brings into perspective the correlation between relative and actual content of an element in a given sample. Most important was the carbon to sulphur ratio and their presumed link to acid

generating and buffering capacities of materials containing them. Both, the absolute and relative contents of carbon and sulphur in sediments point at the fact that precursor rocks contain more carbonate than sulphide minerals. Therefore, as the rock dissolves, carbonates have a greater potential to consume the acidity generated by sulphides.

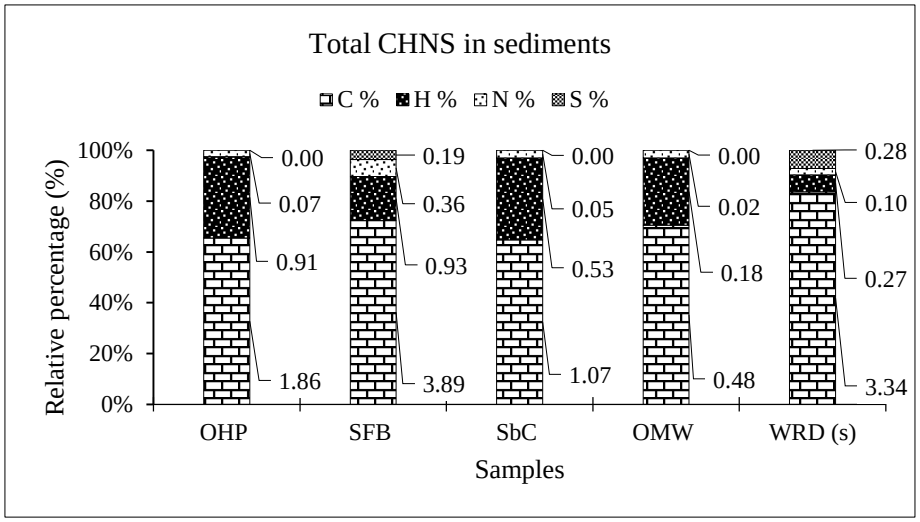


Figure 5.39: Elemental composition expressed as C, H, N, S wt% (data label) and as relative percentage (vertical axis) in sediment samples

5.6.1.4 Sediment grain size distribution and texture

Fractionation analysis of sediment particles, using Malvern 3000, produced results which are shown in Table 5.33 below. Silt constituted the dominant fraction with 50 to 60% in river sediment and over 85% in WRD(s) sediment. In addition to silt, there was more clay and less sand in WRD sediment, but less clay and more sand in river sediment. The increased particles surface area of WRD sediment is associated with the improvement of their adsorptive characteristics, i.e. it gives to sediments a texture favourable for the scavenging of trace elements (Zhao *et al.*, 2017). However, when conditions deteriorate, these particles with increased surface area can leach out more trace elements (Reichelt-Brushett, Clark and Birch, 2017).

Table 5.33: Sediment grain sizes and texture

Particle fraction	SFB (%)	SbC (%)	OMW (%)	WRD(s) (%)	WRD(b) (%)
Clay (<2 µm)	8.62	9.93	5.33	**9.81**	**12.09**
Silt (2 – 50 µm)	61.54	54.04	51.80	**87.20**	**86.67**
Very fine sand (50-100 µm)	19.14	21.93	29.94	**2.99**	**1.25**
Fine sand (100-250 µm)	10.71	14.1	12.93	0.00	0.00
Medium sand (250-500 µm)	0.00	0.00	0.00	0.00	0.00
Coarse sand (500-1000 µm)	0.00	0.00	0.00	0.00	0.00
Very coarse sand (1000-2000 µm)	0.00	0.00	0.00	0.00	0.00
Total sand (50-2000 µm)	29.85	36.03	42.87	2.99	1.25
Sediment texture	**Silty loam**	**Silty loam**	**Silty loam**	**Silt**	**Silt**

5.6.2 Characteristics of sediment leachates

Leachate chemistry of two selected sediment samples SbC and WRD(s) was conducted to assess their characteristics. Both sediments produced solutions of alkaline paste pH of 8.8 and 9.5 and leachates EC of 1700 and 5300 µS cm^{-1} for SbC and WRD(s) respectively. Leachates chemical composition indicated amounts of trace elements (mg kg^{-1}) as follows: Cd (0.04 and 0.8), Co (4.0 and 7.4), Cu (1.7 and 66.7), Fe (40.6 and 5.6), Mn (250.9 and 312.2) Ni (5.0, 128.8) and Zn (8.18 and 12.6) for SbC and WRD(s) respectively. The release of more trace metals from WRD(s) was attributed to the high amount and scavenging ability of sediment dominant particles (clay and silt) and to the amorphous nature of secondary Fe minerals. Leached out amounts of Mn were elevated both in river and dam sediments whilst Cr and Pb were not detected in both. Elements in leachates, arranged in decreasing order of their amounts, were Mn > Fe > Zn > Ni > Co > Cu > Cd in SbC and Mn > Ni > Cu > Zn > Co > Fe > Cd in WRD(s).

5.7 Sequential extraction

Metal concentration expressed in relative percentage of selected elements (Cd, Co, Cr, Cu, Fe, Mn, Ni, Pb, Zn) that dissociated from sediments geochemical phases, as suggested by the BCR extraction protocol, are presented in Figure 5.40. A set of four paired and parallel graphs were drawn to show, for each sample, an expanded version of the three bioavailable phases on the left and a contracted version of the three bioavailable phases caped with their respective residual phases in order to bring out the contrast between the reactive (mobile) phase and the inert (residual) phase. A glance observation shows that nearly all metals, and more so Cr, Fe, Ni, Pb and Zn, shared a preferential association with the residual phase whereas Mn demonstrated a consistently high affinity for the mobile phase. As noted by Massolo et al., (2012) and Kumar et al., (2014), the partitioning behaviour observed in this study, particularly, for Fe and Mn in sediments was common to most sediments samples. Negligible dissolution of Fe was noted in all sediment samples (< 5% of total Fe) which could be attributed to its association with primary minerals in sediment samples. The solubility of Mn was important in the mobile fraction (55.8–83.8% of total Mn) probably due to Mn oxides sensitivity to reaction condition changes.

Samples SFB and SbC from the Selati River produced a similar fractionation pattern for Cr, Fe, Ni and Pb (residual phase > 95%), Cd and Co (mobile phase ~ 34%) and Mn (mobile phase > 65%). Unpacking these mobile phases into their constituent fractions revealed the dominance of Cd (20%) in the oxidizable fraction for both SFB and SbC, the codominance of Co (~14%) in the reducible and oxidizable fractions in SFB and its dominance (23%) in the oxidizable fraction in SbC. The exchangeable and reducible fractions of Mn accounted for 36 and 25% in SFB and 56 and 20% in SbC. The high mobility of manganese could be attributed to its affinity with easily soluble carbonate compounds and its spontaneous participation in ion exchange reactions facilitated by weak surficial attachments to sediments (Nordstrom and Alpers, 1999). Copper was, almost entirely, found in the oxidizable fraction in SFB (10%) and SbC (48%) suggesting its association with OM and possibly with sulphide precipitates.

Mobile fractions in ObC showed a pattern similar to SFB and SbC even though characterised by a general increase in bioavailable content for Co, Cr, Cu, Ni and Zn, with remarkably high exchangeable, reducible and oxidizable fractions for copper (37, 24 and 25%). The presence of most metals in the reducible and oxidizable phases gave an indication that variations in redox conditions, besides changes in pH, could turn on their latent pollution potential.

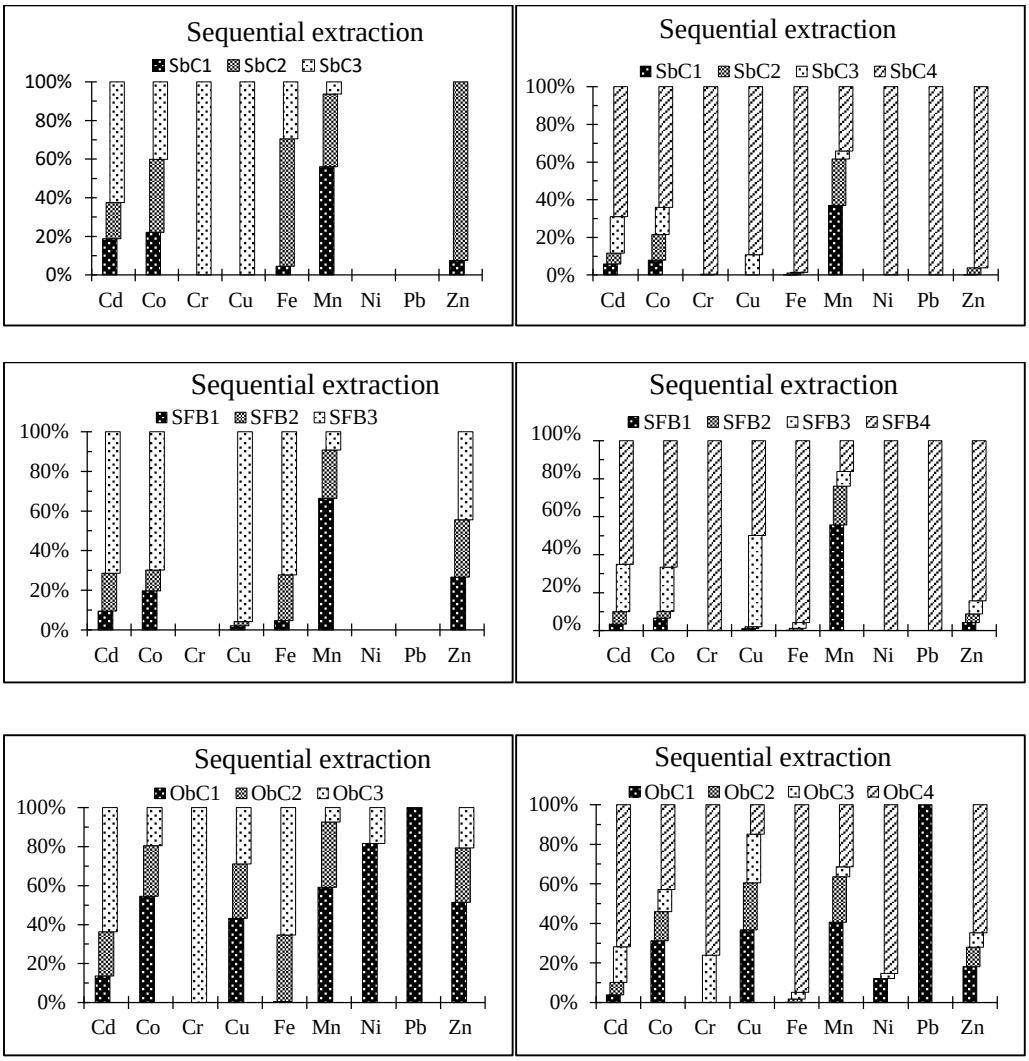


Figure 5.40: (a) Relative distribution of trace metals in various BCR (mobile) fractions of the Selati and Olifants Rivers sediment within a copper mine area. (b) Mobile fractions (left) caped with residual fractions.

Equal relative percentage fractionations for any two given metals do not equate to their corresponding extracted amounts (Nemati *et al.*, 2011; Rosado, Usero and

Morillo, 2016; Vidmar *et al.*, 2017). As a result, relative (%) and absolute (mg kg^{-1}) amounts of metals in mobile fractions carry two different connotations as far as the mobility and bioavailability of metals are concerned. For the case in point, the amounts of Fe determined using XRF analysis were also reflected in the amounts of Fe obtained from summed up concentrations of SE steps which were, by far, higher than corresponding SE amounts of other metals. The explanation to this could be that Fe is a major component of the earth crust (sediment) mineralogy and as such much of Fe forms part of its crystalline structure. Hence, due to the occlusion and high stability of Fe in sediments' residual crystalline structure, only a small relative percentage was extracted in the mobile phase. Conversely, this small relative percentage of Fe released into mobile phase translated into larger amounts, in quantitative terms, when compared with other metals. Table 5.34 compares metals content in mobile fractions expressed as relative (%) with actual (mg kg^{-1}) amounts arranged in decreasing order. Cumulative amounts of Cr, Cu, Cd, Ni, Pb and Zn from sediments exchangeable, reducible and oxidizable phases constituted, relative to sediments toxicity standards, a potential hazard for aquatic life (Table 5.35).

Table 5.34: Decreasing order of relative (%) and actual (mg kg^{-1}) bioavailable amounts of metals in extracted mobile fractions

Order	ObC		SFB		SbC	
	(%)	(mg kg^{-1})	(%)	(mg kg^{-1})	(%)	(mg kg^{-1})
1	Pb (100)	Fe (9566)	Mn (65.8)	Fe (4146)	Mn (83.8)	Fe (1158)
2	Cu (85.0)	Cu (5081)	Co (35.9)	Mn (2476)	Cu (50.1)	Mn (7310)
3	Mn (68.6)	Mn (2199)	Cd (31.1)	Co (69.8)	Cd (35.0)	Cu (675)
4	Co (57.1)	Cr (331)	Cu (10.8)	Cu (51.5)	Co (33.5)	Zn (56.3)
5	Zn (35.5)	Pb (181)	Zn (3.9)	Zn (13.3)	Zn (15.7)	Co (47.3)
6	Cd (28.2)	Co (147)	Fe (1.5)	Cd (10.7)	Fe (4.2)	Cd (10.5)
7	Cr (23.9)	Zn (124)	Cr (0.4)	Cr (8.0)		
8	Ni (14.8)	Ni (104)				
9	Fe (5.1)	Cd (11.0)				

5.8 Biological significance of metal concentration in sediments

Bioavailable metal concentrations in sediments were used to predict sediments potential hazard effects on benthic micro invertebrates. The empirical SQGs methodology known as PEC was used to predict the frequent occurrence of hazardous biological effects. Sediment metal concentrations in ObC, SFB and SbC sediments, reported in Table 5.35, were translated into PEQs for toxicity associated with adverse hazardous effects on benthic micro invertebrates attributed to a combination of contaminants.

Table 5.35: Bioavailable concentration of trace elements in sediments

Elements	Cd mg kg^{-1}	Cr mg kg^{-1}	Cu mg kg^{-1}	Ni mg kg^{-1}	Pb mg kg^{-1}	Zn mg kg^{-1}	PEC quotient
PEC or hazard rating	4.98	111	149	48.6	128	459	**0.5**
ObC	**11**	**331**	**5081**	**103.5**	**181**	123.5	**7.1**
SFB	**10.7**	8	51.5	nd	nd	13.3	**0.6**
SbC	**10.5**	nd	**674.5**	nd	nd	56.3	**2.2**

Contaminants potential toxicity hazards were assessed by rudimentary division of individual metal concentrations by their PEC guidelines. Resulting contaminants quotients greater than one (PEQs > 1) were indicative of potential toxicity hazard. All ObC metal concentrations exceeded their PEC guidelines thereby giving PEQs of 2.20 > 1 (Cd), 2.98 > 1 (Cr), 34.0 > 1 (Cu), 2.1 > 1 (Ni), 1.4 > 1 (Pb), except 0.27 < 1 (Zn). Two SbC metal concentrations were greater than their PEC guidelines giving PEQs of 2.1 > 1 (Cd), 4.5 > 1 (Cu) and, only one SFB metal concentration exceeded its PEC guideline with PEQ of 2.1 > 1 (Cd). A quick comparison showed that Cu had a greater potential to contribute towards ObC and SbC sediments hazard effects and that Cd extended a similar but moderate potential to all sediments. However, for an improved assessment of expected sediment hazard effects, i.e. a combination of elements hazard effects, sediments mean PEQs were calculated and compared with threshold PEQ (0.5). All sediments had PEQs > 0.5, *viz*, 7.14 (ObC), 0.64 (SFB) and 2.24 (SbC). Bioavailable concentrations of metallic contaminants in ObC, SFB and SbC

sediments, rather than their total concentrations, were used to assess the frequent occurrence of harmful effects on benthos. Therefore, characterizing ObC, SFB and SbC sediments as polluted rivers may not be an overestimation of their poor quality as it may be by using the conservative approach which attributes observed toxic effects to total metal concentration of a single contaminant (Burton Jr., 2002).

In a similar study by Atibu *et al.*, (2013), sediments from Luilu and Musonoie Rivers, impacted by industrial and fast spreading artisanal mining in Kolwezi town (Congo D R), total metal concentrations were compared directly with TEC guidelines for the protection of aquatic life. Luilu River sediments were more contaminated principally with Cu (47,5 > **35.7** mg kg^{-1}), Co (13,2 > **35.0** mg kg^{-1}), Pb (851.1 > **35.0** mg kg^{-1}) and Cr (69.3 > **37.3** mg kg^{-1}) than in Musonoie River with Cu (371 > **35.7** mg kg^{-1}) and Co (240 > **35.0** mg kg^{-1}). In another study, (Xu and Li, 2015) compared the degree of contamination of metals in sediments from fourteen rivers along the southern Bohai Sea, China, with threshold effect level (TEL) and probable effect level (PEL), and classified sediments in groups based on these SQGs. In this region characterised by high population density, considerable urbanization and industrialisation, most sediments ($\geq$ 80%) fell into the minimal effect range ($\leq TEL$) for Cu, Zn, Pb and Cd, and only a few sediments (< 10%) were classified within probable effect range ($\geq PEL$) for the same metals. Wojtkowska (2011) used the same criteria to determine the safety for organisms in the Utrata River.

5.9 Geochemical speciation modelling of surface water

Dissolved concentration of major ions and trace elements were determined and used as input data for geochemical speciation modelling. Simulations of waters from the stretch of the Olifants River before the confluence (ObC), the stretch of the Selati River before the confluence (SbC), the computation of the mixing of these two waters (OS mix) and the water retain dam (WRD) were run using the input data given in Table 5.36. Electron potentials (pe) were calculated from oxidation-reduction potential (ORP) measured in the field. They were indicative of oxidizing surface water conditions (~ pe= +7) (Muchez and Corbella, 2012).

Table 5.36: PHREEQC input data used for water simulation in the copper mine area

SOLUTION	#SbC	SOLUTION	# ObC	SOLUTION	#OS mix	SOLUTION	#WRD
temp	20.76	temp	19.7	ObC	20	temp	25.5
pH	8.9	pH	8.32	SbC	1	pH	8.6
pe	6.94	pe	7.45			pe	7.08
redox	pe	redox	pe			redox	pe
units	mg/l	units	mg/l			units	mg/l
density	1	density	1			density	1
Ca	66.7	Ca	15.6			Ca	598.5
K	6.53	Cl	39.3			K	80.1
Mg	108.13	Co	0.007			Mg	776.7
Cl	133.3	Cu	0.022			Na	1.26
Co	0.005	F	0.19			Cl	563
Cu	0.027	K	1.009			F	6.14
F	1.83	Mg	33.75			**Fe**	**0.16**
S(6)	421.6	N(5)	0.49			S(6)	4464.7
Mn	0.003	Na	0.397			Ni	0.7
Na	2.23	Pb	0.106			Mn	0.187
Pb	0.27	S(6)	33.6			Cu	0.067
Zn	0.75	Zn	0.192			Pb	1.321
-water	1 # kg	-water	1 # kg			Zn	4.77
						-water	1 # kg

5.9.1 Soluble species distribution in surface water

PHREEQC output indicated a wide variety of soluble species in surface water. Nevertheless, only a few species that contributed up to over 95% molar concentration (> 10^{-7} mol kg^{-1}) of selected individual elements in solution composition (Figure 4.41) were considered significant. Dominant free ion species were Co^{2+}, Mn^{2+}, Zn^{2+}, Ni^{2+} and Fe^{2+} whereas Cu (II), Pb (II) and Fe (III) were associated with hydroxides ($Cu(OH)^{+}$, $Cu(OH)_2$, $PbOH^{+}$, $Fe(OH)_3$, $Fe(OH)_4^{-}$ and $Fe(OH)^{2+}$). Metal sulphate species were common in WRD ($CoSO_4$, $MnSO_4$, $NiSO_4$, $PbSO_4$, $ZnSO_4$ and $FeSO_4$) with sizable contribution of molar concentration except for Cu(II) and Fe(III) which showed weaker affinity for sulphate ions. At near-neutral pH, most divalent metal hydroxides were assumed to exhibit minimum solubility which could be enhanced as pH departs from either sides of it (Nordstrom

and Alpers, 1999). The order of abundance of bioavailable species for each element could be deduced from Figure 5.42 and Figure 5.43 further below (e.g. $Fe(OH)_3$ > $Fe(OH)_4^-$ > $Fe(OH)_2^+$ in WRD).

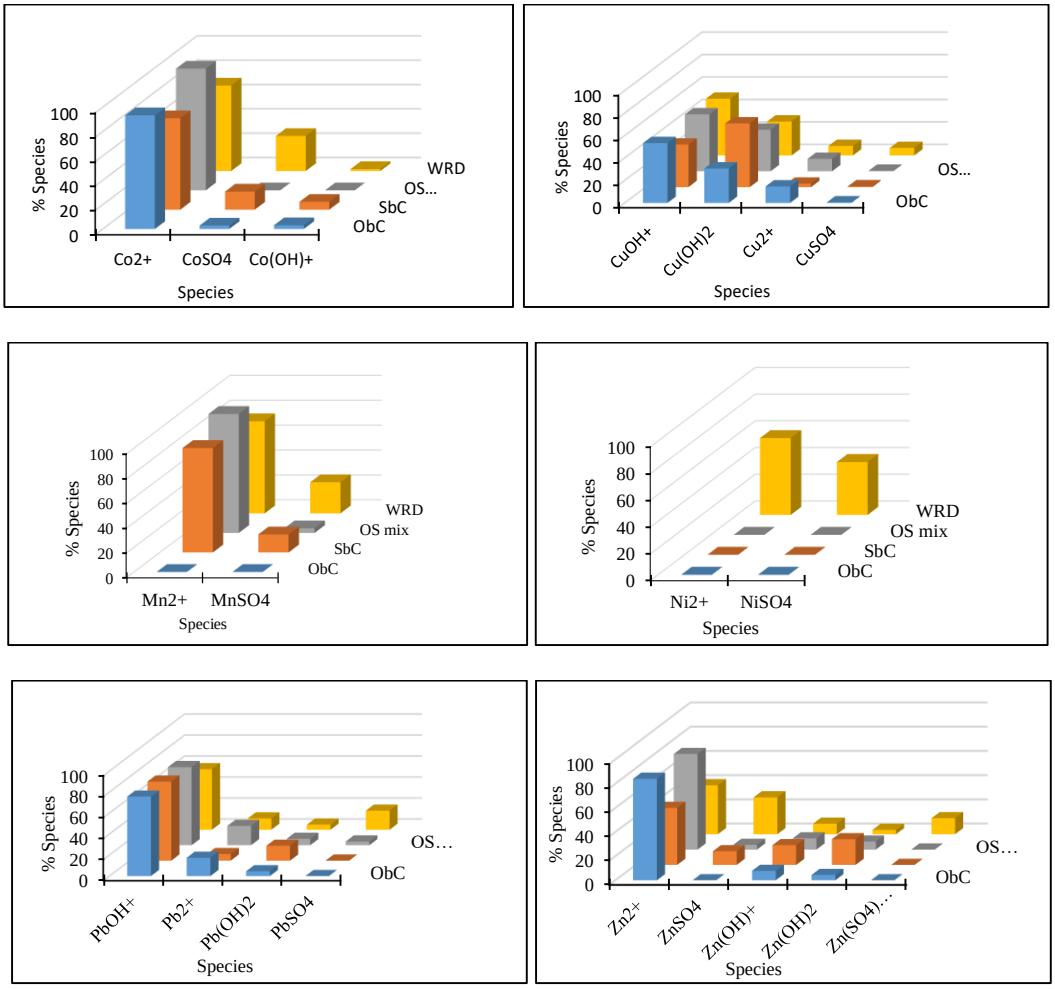


Figure 5.41: Predominant soluble metal species which contributed over 95% of the total concentration for a given metal in surface water.

5.9.2 Mineral precipitates

Only compounds with positive saturation index (SI > 0), presented in Figure 5.42, were taken from mineral saturation indices output obtained from PHREEQC calculations. A general observation showed that precipitates were oxides, hydroxides, oxy- and oxyhydroxy- sulphates and chlorides of various trace metals. The chemical composition of these precipitates was suggestive of a reaction medium favourable for the removal of Cu, Co, Pb and Zn ions from water via binding to sinking compounds formed under oxic conditions. There were more

precipitates variety with comparatively higher SI in WRD compared to the ones obtained in river stretches. Mineral precipitates accumulated in this manner do limit the mobility of potentially toxic aqueous metal species through adsorption and constitute a reservoir of trace metals susceptible to remobilization when reaction conditions favour the dissolution of precipitates (Jamieson, 2011; Majzlan *et al.*, 2018; Pedersen *et al.*, 2019). The survival of sediments dwelling benthos is dependent on the quality of sediments as is the wellbeing of fish to the quality of surface water (Besser, Brumbaugh and Ingersoll, 2015). Calcite precipitation could be attributed to high Ca^{2+} and SO_4^{2-} in WRD.

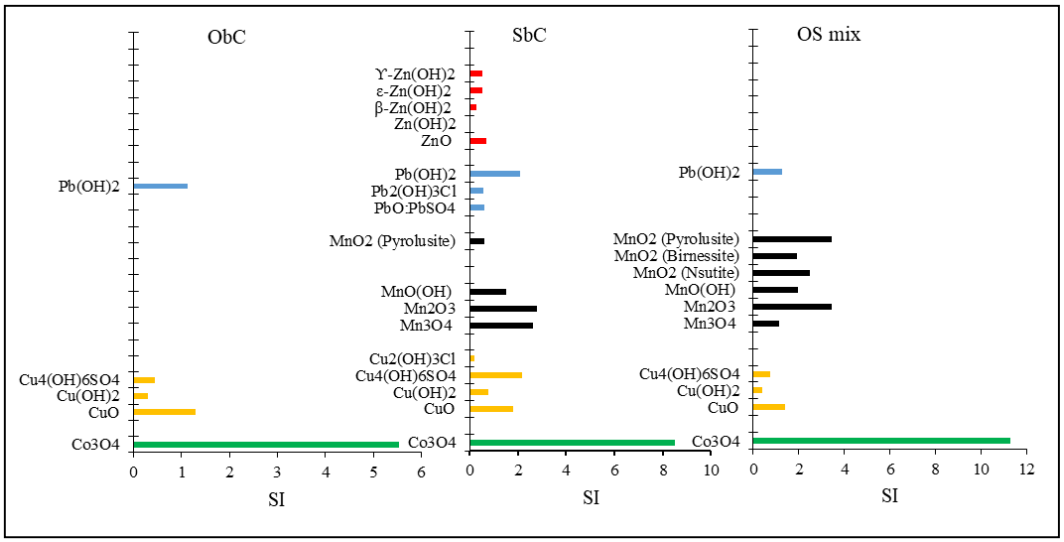


Figure 5.42: Surface water simulation precipitates obtained from PHREEQC output data

Keeping Fe in WRD input data for predictive speciation revealed the potency of Fe to form oxide and hydroxide precipitates with higher SI (Figure 5.43). A suite of iron oxide compounds in copious amounts namely, cuprous ($CuFeO_2$) and cupric ($CuFe_2O_4$) ferrihydrites, cobalt ferrihydrite ($CoFe_2O_4$), maghemite (γ-Fe_2O_3), magnetite ($FeO.Fe_2O_3$), magnesioferrite (Fe_2MgO_4), goethite (α-FeOOH), lepidocrite (γ-FeOOH) and hematite (α-Fe_2O_3) were identified. A large number of these precipitates coupled with their high SI may have been determinant to their scavenging potential for toxic metals from water and indicative of super saturation assumption of surface water with respect to these deposits. Goethite (coarse particles) and hematite (fine particles) are common and stable precipitates

(Nordstrom and Alpers, 1999). Ferrihydrites ($Fe(OH)_3$) dissolve and convert to hematite (α-Fe_2O_3) at pH 5 - 9 and to goethite (α-FeO(OH)) outside these pH brackets. The presence of tenorite (CuO) in surface water was indicative of an oxic reaction media.

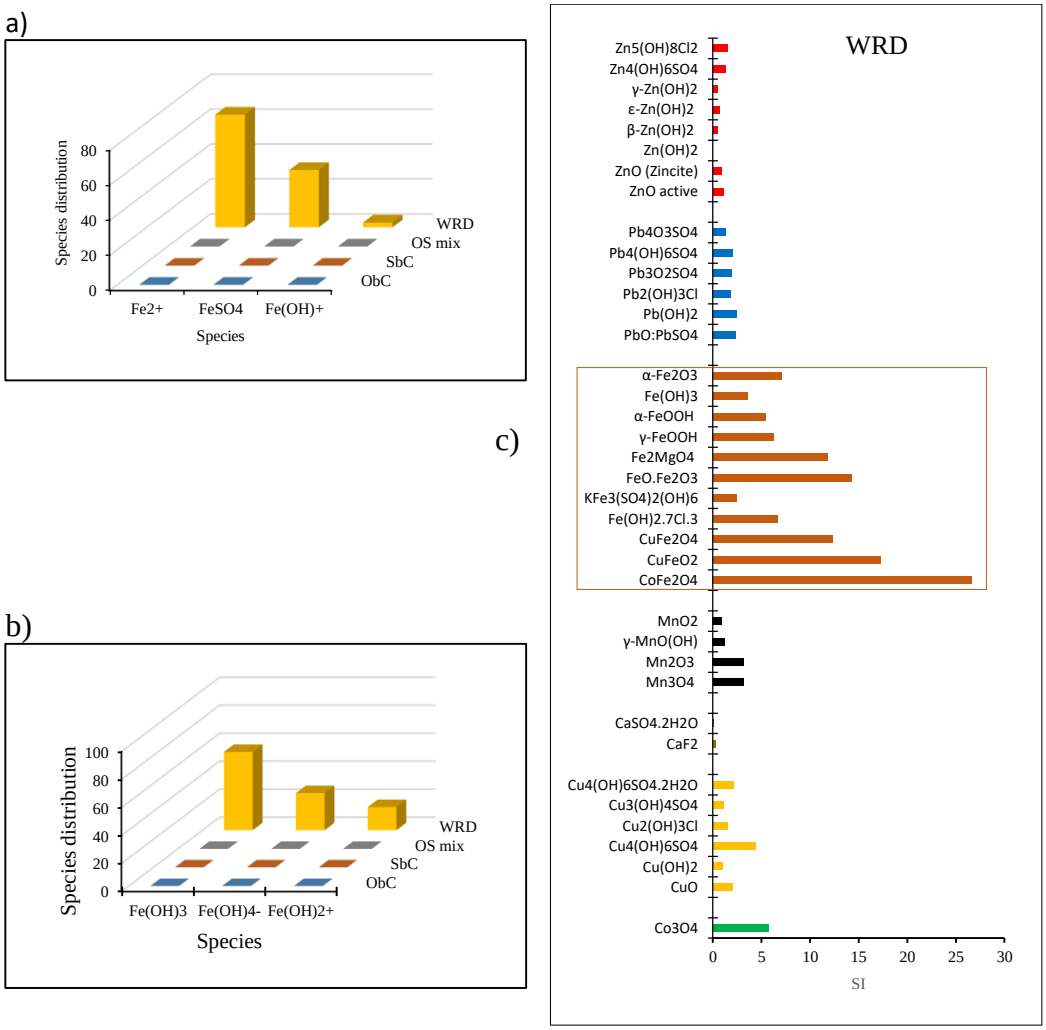


Figure 5.43: a) and b) Iron soluble species in surface water and c) iron precipitates in WRD

5.10 Characteristics of stream water from Kitwe

5.10.1 Physicochemical parameters

Table 5.37 presents physico-chemical results obtained from stream water samples measurements. All samples were categorised as near neutral and slightly alkaline with pH values ranging from 7.09 to 8.42. Their EC extended from 0.25 to 3.74

mS cm^{-1}. Sracek and co-reseachers (2012) reported that pH in the tributaries of the Kafue Rivers (*viz.* Mwambashi, Mindolo, Uchi and Lwanshimba streams) was always close to neutral, but the EC ranged between 0.5 and 1.7 mS cm^{-1} as opposed to EC between 2.15 and 3.74 mS cm^{-1} measured for the same streams in this study. A lower pH (0.12) and a higher EC (> 20 mS cm^{-1}), registered for sample W7, made an exception. The segregation of EC values into intervals of [4-3], [3-2], [2-1] and [< 1] mS cm^{-1} largely reflected the influence of Ca^{2+}, Mg^{2+} and SO_4^{2-} concentration (mg L^{1-}) variations in stream water samples at various sampling spots. Dominant soluble ions emanated more likely from the oxidative dissolution of sulphide minerals and counteracting carbonate minerals dissolution processes which maintained the pH at near neutral environment but released elevated amounts of soluble ions expressed by high values of EC. Furthermore, secondary minerals such as evaporites (e.g. soluble sulphate salts) may have contributed additional soluble ions to stream water.

5.10.2 Chemical composition

Water samples collected downstream near tailings dumps had elevated concentrations of SO_4^{2-} (850 - 2200 mg L^{-1}), Ca^{2+} (115 - 285 mg L^{-1}) and Mg^{2+} (150 - 260 mg L^{-1}). Conversely, lower concentrations of SO_4^{2-} (4 – 186 mg L^{-1}), Ca^{2+} (14 - 62 mg L^{-1}) and Mg^{2+} (19 – 28 mg L^{-1}) were determined in W1, W11, W22 and W23 samples located away from tailings dumps. Concentrations of SO_4^{2-} (500 – 1000 mg L^{-1}), Ca^{2+} (100 – 250 mg L^{-1}), Mg^{2+} (50 – 100 mg L^{-1}) reported by Sracek (2012) in Mwambashi, Mindolo, Uchi and Lwanshimba streams were lower than the concentrations measured in respective and corresponding streams W16, W21, W31 and W35 in this study (see Table 5.38). A marked increase in the amounts of SO_4^{2-}, Ca^{2+}, Mg^{2+} released by tailings dumps into water was noted in the current findings.

Lower pH and elevated concentrations of NO_3^- at W7 signaled the possibility of a fortuitous anthropogenic input from the community around that particular site. High concentrations (µg L^{-1}) of Cu, Fe, Mn, Zn and Al determined as 0.45, 590, 360, 280 and 21 respectively at W7 were associated with possible dissolution of oxides of Fe, Mn and Al and the subsequent remobilization of Cu and Zn triggered by high acidity. By contrast, elevated concentrations (µg L^{-1}) of Co, Cu and Mn were

determined as 1.59, 0.11 and 460 respectively for W18, located a few meters downhill from the slag mountain. These concentrations were attributed to leachates from the proximal residual slag discarded from less efficient metal extraction processes used in earlier years (Beale, 1985a). Much higher concentrations of Co (2000 µg L^{-1}) and Mn (9000 µg L^{-1}) reported in Uchi stream were attributed to process water from treatment plant (Sracek *et al.*, 2012). Aluminum and silicon had low concentration in water because of slow or no release attributed to their association with inert and slow weathering minerals such as feldspar.

Table 5.37: Dissolved concentrations of major ions and selected trace elements in stream water samples from a mine area in Kitwe

Sample	GPS	pH	EC mS cm^{-1}	Ca mg L^{-1}	K mg L^{-1}	Mg mg L^{-1}	Na mg L^{-1}	Co µg L^{-1}	Cu µg L^{-1}	Fe mg L^{-1}	Mn mg L^{-1}	Ni mg L^{-1}	Zn mg L^{-1}	S mg L^{-1}	Si mg L^{-1}	Al mg L^{-1}	F^{-} mg L^{-1}	Cl^{-} mg L^{-1}	NO_3^{-} mg L^{-1}	SO_4^{2-} mg L^{-1}
Domestic use		6-9	ng	30	50	30	100	ng	1	0.1	0.05	ng	3			0.15	1	100	6	200
Livestock		ng	ng	100	ng	500	2000	1	5.00	10	10	1.00	20			5	2	1500	ng	1000
Irrigation		6.584	ng	ng	ng	ng	70	0	2.00	15	0.02	0.20	1			5.00	2	ng	ng	ng
Drinking water		6-9		200		150	200	0.5	1300	0.3	0.8	0.1	5			0.2	1.5	250	10	400
Aquatic toxicity									13	1		0.47	0.12			0.75				
W1	12˚49′18″ S 28˚13′09″ E	7.09	0.65	62.2	61.75	19.47	0.07	0.00	nd	nd	0.01	**0.62**	0.01	73.50	0.70	**0.22**	0.06	14.97	**11.89**	122.67
W2	12˚48′36″ S 28˚13′46″ E	7.53	3.27	**245**	24.02	**254.00**	0.20	0.01	**0.06**	**0.34**	**0.15**	**1.24**	**0.15**	875.14	1.39	0.09	0.41	20.08	3.20	1535
W4	12˚48′41″ S 28˚13′41″ E	7.87	3.74	**265.6**	49.20	**199.2**	0.21	0.01	**0.06**	0.01	**3.38**	**1.50**	0.01	1001.00	1.68	nd	0.17	8.73	372.68	1728
W5	12˚48′40″ S 28˚13′42″ E	7.78	3.35	**282.6**	43.60	**174.2**	0.19	0.00	0.00	nd	0.00	**1.15**	0.00	2760.00	1.29	0.05	0.32	11.39	**14.87**	**1643**
W6	12˚48′32″ S 28˚13′56″ E	7.38	1.11	46.76	5.02	37.08	0.09	0.02	nd	nd	nd	**0.89**	nd	80.50	0.99	0.04	0.41	57.61	5.77	**268.6**
W7	12˚48′25″ S 28˚13′35″ E	**0.12**	**>20**	61.30	6.90	50.90	0.11	0.01	**0.45**	**0.59**	**0.36**	**0.94**	**0.28**	125.70	1.04	**0.21**	nd	**124.75**	**9744**	**623.2**
W17	12˚48′56″ S 28˚11′26″ E	8.07	1.52	54.40	9.80	45.05	0.18	0.00	0.01	nd	nd	**0.77**	nd	44.25	0.87	nd	0.21	**127.33**	**84.35**	**327.7**
W39	12˚48′50″ S 28˚12′13″ E	7.9	1.58	61.25	6.60	63.50	0.11	nd	0.01	0.01	0.00	**0.83**	0.03	147.50	0.91	nd	0.34	68.03	0.17	**487.1**
W11	12˚48′55″ S 28˚09′00″ E	7.69	0.25	14.98	1.63	12.96	nd	0.00	0.01	nd	0.01	**0.64**	0.00	3.48	0.73	0.03	0.19	8.18	0.08	4.89
W13	12˚47′23″ S 28˚06′19″ E	7.63	3.58	**277.6**	31.66	149.60	0.12	0.00	nd	nd	nd	**0.0**	nd	896.80	0.57	0.07	0.11	25.45	4.37	**2185**
W15	12˚47′36″ S 28˚06′04″ E	8.00	0.85	34.98	0.64	39.45	0.04	0.00	**0.04**	0.02	nd	**0.52**	0.02	87.60	0.59	0.05	**8.80**	10.34	nd	**254.9**

Table 5.37 (continued): Dissolved concentrations of major ions and selected trace elements in stream water samples from a mine area in Kitwe

Samples	GPS	pH	EC mS cm^{-1}	Ca mg L^{-1}	K mg L^{-1}	Mg mg L^{-1}	Na mg L^{-1}	Co µg L^{-1}	Cu µg L^{-1}	Fe mg L^{-1}	Mn mg L^{-1}	Ni mg L^{-1}	Zn mg L^{-1}	S mg L^{-1}	Si mg L^{-1}	Al mg L^{-1}	F^- mg L^{-1}	Cl^- mg L^{-1}	NO_3^- mg L^{-1}	SO_4^{2-} mg L^{-1}
W18	12˚50′27″ S 28˚12′43″ E	7.52	1.30	68.30	5.55	34.00	0.03	**1.59**	**0.11**	nd	**0.46**	**0.82**	0.09	177.25	0.91	0.07	0.29	24.49	1.79	**511.16**
W19	28˚13′08″ E	7.52	1.59	68.85	8.10	64.90	0.15	0.01	**0.05**	0.05	0.03	**0.92**	0.03	127.00	1.05	0.07	0.26	76.27	31.86	467.49
W20	12˚50′38″ S 28˚12′30″ E	7.43	1.38	59.35	5.95	59.00	0.07	0.03	0.10	nd	0.01	**0.77**	0.06	227.72	0.87	0.04	0.23	44.69	0.94	449.88
W16	12˚42′53″ S 28˚07′16″ E	7.89	3.31	186.5	18.00	215.0	0.19	0.01	**0.08**	0.40	**0.02**	**1.22**	**0.22**	710.00	1.37	0.13	0.56	56.89	1.30	**1740**
M21	12˚47′05″ S 28˚11′55″ E	7.49	2.68	191.4	11.50	88.90	0.42	0.00	nd	nd	nd	**1.07**	nd	682.00	1.19	0.03	0.67	17.96	**12.04**	**1081**
W35	12˚53′24″ S 28˚13′41″ E	7.57	2.15	119.5	11.40	65.00	0.11	nd	0.01	0.00	nd	**0.90**	nd	290.00	1.00	0.05	0.13	16.41	nd	**903.56**
W9	12˚47′25″ S 28˚13′35″ E	7.44	0.40	30.44	33.02	13.22	0.02	0.00	0.01	0.09	0.01	**0.71**	0.01	34.26	0.79	0.08	0.26	13.23	nd	9.13
W22	12˚46′56″ S 28˚12′36″ E	7.54	1.16	33.78	6.84	36.81	0.18	0.00	**0.03**	nd	0.00	**0.81**	nd	40.35	0.90	0.02	0.15	54.31	**223.97**	186.88
W23	12˚46′25″ S 28˚14′06″ E	7.45	0.88	27.27	4.74	28.92	0.10	0.01	0.01	0.01	nd	**0.48**	nd	69.90	0.54	0.03	0.16	33.09	**46.11**	161.28
W37	12˚47′29″ S 28˚12′01″ E	8.42	1.60	53.50	11.85	76.85	0.11	nd	nd	0.08	0.01	**1.03**	nd	94.10	1.14	nd	0.29	66.86	0.39	**221.37**
W30	12˚49′53″ S 28˚14′06″ E	7.83	1.53	65.95	8.75	56.65	0.07	6.35	0.01	0.06	**0.36**	**0.65**	0.00	233.25	0.73	0.04	0.29	35.58	3.03	**524.32**
W31	12˚49′42″ S 28˚14′12″ E	7.98	2.01	116.5	8.45	59.30	0.10	0.85	0.01	nd	0.01	**0.92**	0.01	208.00	1.00	nd	0.32	32.04	4.68	**883.05**
W33	12˚49′34″ S 28˚13′42″ E	7.86	2.08	128.0	8.75	63.85	0.10	0.69	**0.03**	0.09	0.01	**0.88**	0.03	244.00	0.99	nd	0.25	35.84	5.77	**895.08**

5.11 Characteristics of tailings and stream bed sediment from Kitwe

5.11.1 Mineral identification and semi-quantification

5.11.1.1 X-ray diffraction

Mineral identification obtained initially in the form of XRD graph patterns were tabulated to present minerals commonalities and differences among samples (Table 5.38). The wide variety of minerals identified in tailings samples demonstrates that tailings is a mixture of crushed rock and fluids discarded at different mineral processing stages, and supports the term " chief waste stream" ascribed to tailings by (Kossoff *et al.*, 2014). Quartz, hematite and zircon, the common and inert constituents of most geologic materials, were identified in tailings as well as in sediments samples. Sulphide minerals identified in sediments collected at WS31, down-stream of waste dump T32, were attributed to tailings weathered particles which were carried downstream by water and settled at the bottom of the stream as they migrated through the stream water. They formed part of milled solid waste (tailings) discarded at concentrator step of copper sulphide ore processing (Beale, 1985a; Langa *et al.*, 2014; Kalichini *et al.*, 2017; Ndoro and Witika, 2017). Sediment sample (WS23), located away from waste mine dumps, contained less mineral types and did not indicate any presence of sulphide minerals. Dolomite was identified in tailings but not in sediments principally because of its high solubility characteristic (Price, 2009). Geologic material (tailings) hosted both sulphide and carbonate minerals. Other minerals identified in tailings and sediments were a mix of primary and secondary minerals (Aluminosilicates, carbonates, sulphates, oxides and hydroxides) from which a variety of dissolved elements could be released and by which significant control could be exerted on soluble trace elements in water.

Table 5.38: Mineral identification converted from XRD graph patterns of tailings (T32 and T45) and sediments (WS31 and WS32) into a tabulated format

no	Mineral	Formula	T32	T45	S31	S23
1	Quartz, Hematite, Zircon	SiO_2, Fe_2O_3, $ZrSiO_4$	id	id	id	id
2	Pyrite, Chalcopyrite	$CuFe_3S_8$, $CuFeS_2$	id	id	id	x
3	Dolomite	$CaMg(CO_3)_2$	id	id	x	x
4	Cuprite, Goethite, Titanium aluminate, Amnesite, Diopside, Periclase, Corundum	Cu_2O, $FeO(OH)$, $TiAl_2O_5$, $Al_2H_4Mg_2SiO_9$, $Ca_{40}FeMg_{40}Al_3Si_{80}$, MgO, Al_2O_3	id	x	x	x
5	Chalcopyrite, Amphibole, Arkemanite, Tremolite, Aluminium sulphate penta-hydrated, magnesium hydroxide silicate, cobalt carbonate di-hydrated	Cu_2S, $TiCa_{30}F_4Fe_{46}H_{35}K_{30}Mg_{30}Na_6Al_{40}Si_{100}O_{400}$, $Ca_2MgSi_2O_7$, $Ca_2F_2Mg_5Si_8O_2$, $Al_2(SO_4)_3.5H_2O$, $Mg_3Si_4O_8(OH)_6$, $Co_3(CO_3)_3.H_2O$	x	id	x	x
6	Malachite	$Cu(OH)_2CuCO_3$	x	x	id	id
7	Dikite, Rutile, Aluminium calcium hydroxide tetra-hydrated	TiO_2, $Al_2H_4Si_2O_9$, $Al_2CaH_{16}O_{12}$	x	x	id	x
8	Kaolinite	$Al_2Si_2O_5(OH)_4$	x	x	x	id

id = identified, x = not identified

5.11.1.2 X-ray fluorescence

Oxides of major elements and Loss on Ignition (LOI) expressed as weight percentage (wt%) of tailings and sediments samples were obtained using XRF. Their elemental concentrations, obtained after calculative conversions, indicated that in both, tailings (T12, T32 and T45) and sediments (WS6, WS19, WS21, WS23, WS31, WS35), average concentrations (wt% tailings, wt% sediment) were in the order Si (22.21, 34.82) > Al (5.16, 4.80) > C (3.78, 1.69) > Fe (1.74, 2.32) > Mn (0.22, 0.06) and Ca (6.99, 1.15) > K (4.42, 1.36) > Mg (4.05, 0.91) > Na (0.56 > 0.13). There were more Ca, K, Mg, Na, Mn, Al and C in tailings than in sediments whereas the levels of Si and Fe were higher in sediments than in tailings. Results for the same elements in sediments at WS35 followed the pattern observed for tailings. This observation suggested an accumulated deposition of weathered particles transported from old tailings upstream of WS35. Chemical

formulae of the detected minerals in this present study revealed that large amounts of base metals found in geologic materials form part of carbonate, sulphide/sulphate and silicate minerals, this is in agreement with notes by Price (2009). With reference to the lithology of the Lower Roan (RL), carbon could be assumed to have come predominantly from inorganic (carbonate) rather than organic sources (Kříbek *et al.*, 2010).

Determination of trace elements in tailings (T32) and in proximal downstream sediments (WS31) showed distinctly elevated concentration (in mg kg^{-1}) of Cu (1075, 697.98) and Co (385.30, 196.73) as compared to Cr (34.27, 59.61), Zn (9.70, 27.78) and Pb (3.23, 19.33). This finding demonstrates that the levels of Cu and Co were higher in tailings than in sediments whilst the detected concentrations of Cr, Zn and Pb were higher in sediments than in tailings samples. The difference was attributed to the nature of tailings parent material (Figure 5.44).

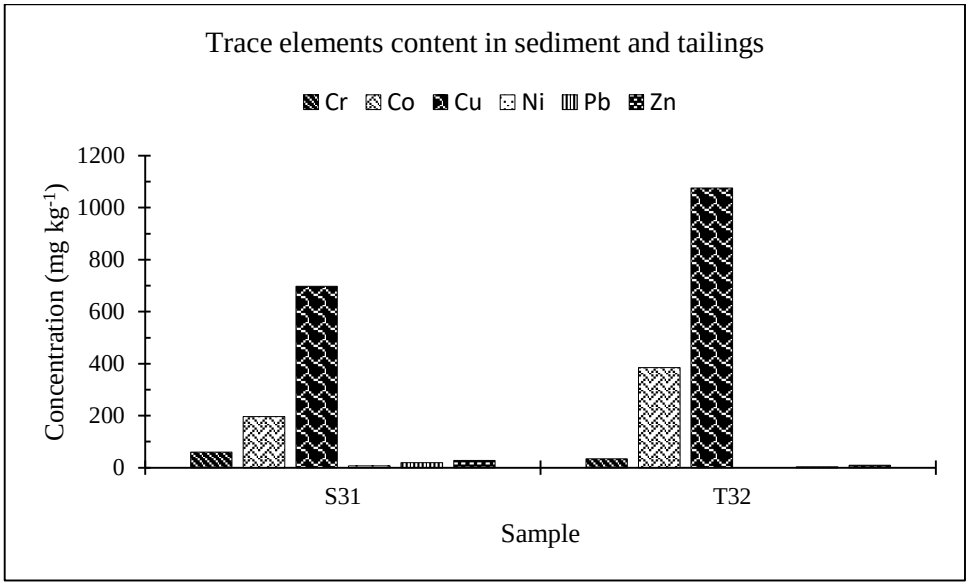


Figure 5.44: Trace elements content in sediment and tailings (converted from weight percentage element oxides)

5.11.2 Elemental analysis: carbon to sulphur ratio (C/S)

Carbon and sulphur total weight percentage analysis in tailings showed minimum, mean and maximum values of 3.03 wt%, 3.72 wt% and 4.84 wt% for carbon and 0.09 wt%,

0.82 wt% and 1.44 wt% for sulphur, giving C/S ratios of 33.67, 4.43 and 3.36 respectively (Figure 5.45). In sediments, carbon and sulphur total weight percentage minimum, mean and maximum values were 0.15 wt%, 1.03 wt% and 3.56 wt% for carbon and 0.01 wt%, 0.14 wt% and 0.46 wt% for sulphur giving C/S ratios of 12.0, 7.7 and 7.8 respectively.

Tailings and sediments C/S ratios suggested an amount of carbonate minerals in large excess compared to sulphide minerals. Previous findings by Sracek (2010) indicated that non-acid water will ensue from chemical interactions between such disproportionate antagonist minerals. The main events in the chemistry of acid producing and acid neutralizing minerals interaction involves the oxidative dissolution of sulphide minerals in contact with oxygen and water producing acidity (H^+ and Fe^{3+}) and sulphate ions (equation 5.10); the hydrolysis of Fe^{3+} to produce more H^+ and ochres deposition with co-precipitation of trace elements (equation 5.11) and the acidic dissolution of buffering minerals (carbonates, silicates, hydroxides) with subsequent flush of base metals and remobilization of sequestered trace elements (equation 5.12) (Nordstrom and Alpers, 1999; Dold, 2014a).

$$FeS_2\,(s) + 3.75\,O_2\,(g) + 0.5\,H_2O\,(l) \rightarrow Fe^{3+}\,(aq) + 2SO_4^{2-}\,(aq) + H^+\,(aq) \quad \text{Equation 5.10}$$

$$Fe^{3+}\,(aq) + 3\,H_2O\,(l) \leftrightarrow Fe(OH)_3\,(s) + 3\,H^+\,(aq) \quad \text{Equation 5.11}$$

$$CaCO_3\,(s) + 2\,H^+\,(aq) + 2SO_4^{2-}\,(aq) \leftrightarrow Ca^{2+}\,(aq) + H_2CO_3\,(l) \quad \text{Equation 5.12}$$

Since carbonate minerals, in equation 5.12, prevent the lowering of pH by moping out H^+ from equations 5.10 and 5.11, they create conditions which induce some $Fe(OH)_3$ to also cover sulphide minerals surface thereby reducing the reaction rate of equation 1 (the rate determining step).

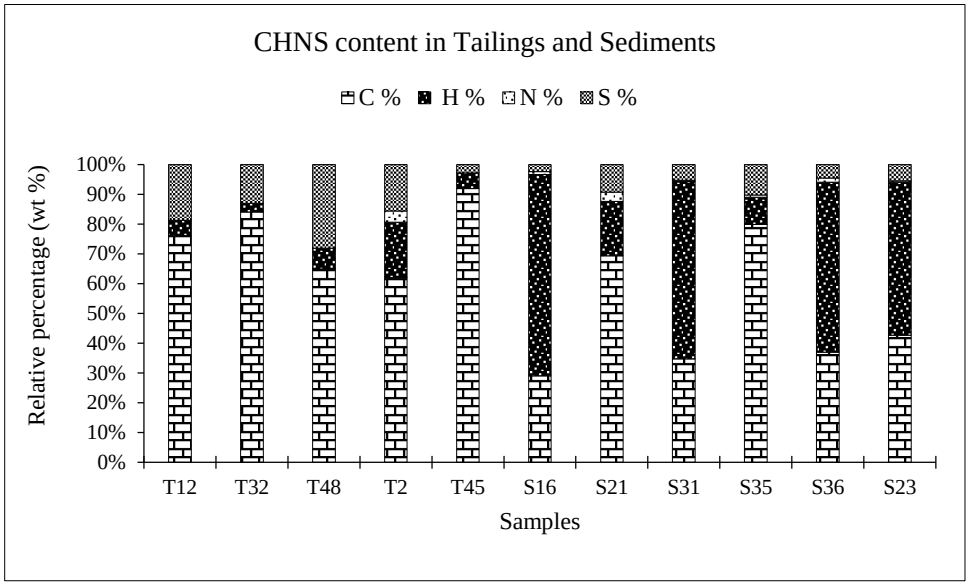


Figure 5.45: Elemental content (wt% C, H, N and S) in sediments and tailings

5.11.3 Leachates chemical of tailings and stream floor sediment

5.11.3.1 Major ions

Figure 5.46 shows major anions concentration in tailings obtained from leachates using Toxicity Characteristic Leaching Procedure (TCLP). Sulphate concentration in tailings, obtained from a similar and parallel leaching run using DI water as extracting fluid, is also shown alongside. Fluoride and sulphate were the dominant anions in acetic acid leachates whereas sulphate was the only dominant anion in DI water leachates. It can be assumed that only readily soluble secondary minerals constituted the main source of sulphate found in tailings leachates, although mineral identification remained silent about sulphate minerals due to limitations of the XRD technique.

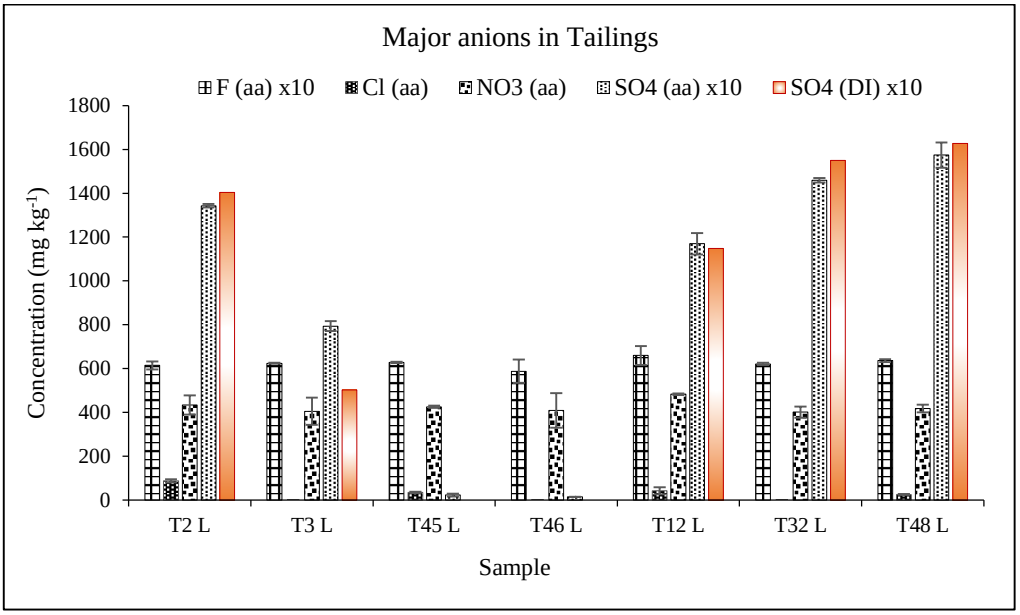


Figure 5.46: Bar chart plot of concentration of major anions in tailings obtained by TCLP (acetic acid = aa) (pattern fill) and sulphate concentration in tailings obtained by DI water leaching (solid fill). Actual concentration for F^- and SO_4^{2-} are ten times higher than the concentrations of Cl^- and NO_3^-.

Figure 5.47 shows major cations concentration in tailings obtained from both acetic acid and DI water leachates. TCLP subjected tailings to low pH conditions which favoured some mineral dissolution to take place and leach out more soluble ions. The rise in pH at the end of leaching process meant that acid buffering minerals took part in the reactions and were a principal source of major cations released into leachates. It was observed that T45 and T46 contained less soluble compounds as their DI water leachates contained much less Ca, Mg as well as SO_4^{2-} as opposed to their acetic acid leachates. This observation suggested that DI water is a milder leaching fluid, as compared to acetic acid leaching fluid, with much less potency to chemically weather most primary minerals identified in tailings, among which a variety of silicates, sulfides and oxides (Table 5.39).

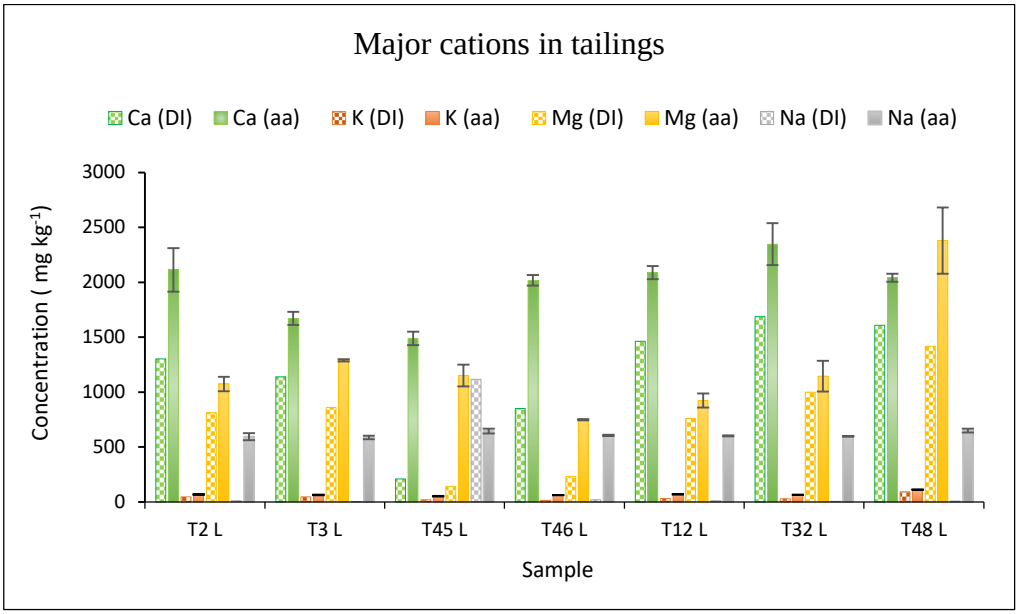


Figure 5.47: Side by side bar chart plot of concentration of major cations in tailings obtained through DI water leaching (DI) and TCLP (acetic acid = aa)

5.11.3.2 Trace elements

The amounts of trace elements in TCLP leachates were much lower for Cd, Cr, Ni, Pb and Zn, moderate for Co and Fe and higher for Cu and Mn (Figures 5.48 and 5.49). Leachates concentration indicated positive correlations of Mn with Cu and Fe with Co suggesting that the extent of oxides/oxi-hydroxides of Mn and Fe dissolution played an important role in Cu and Co liberation from tailings. Other sources of Cu and Co included soluble carbonate minerals and oxides/oxi-hydroxides of Al.

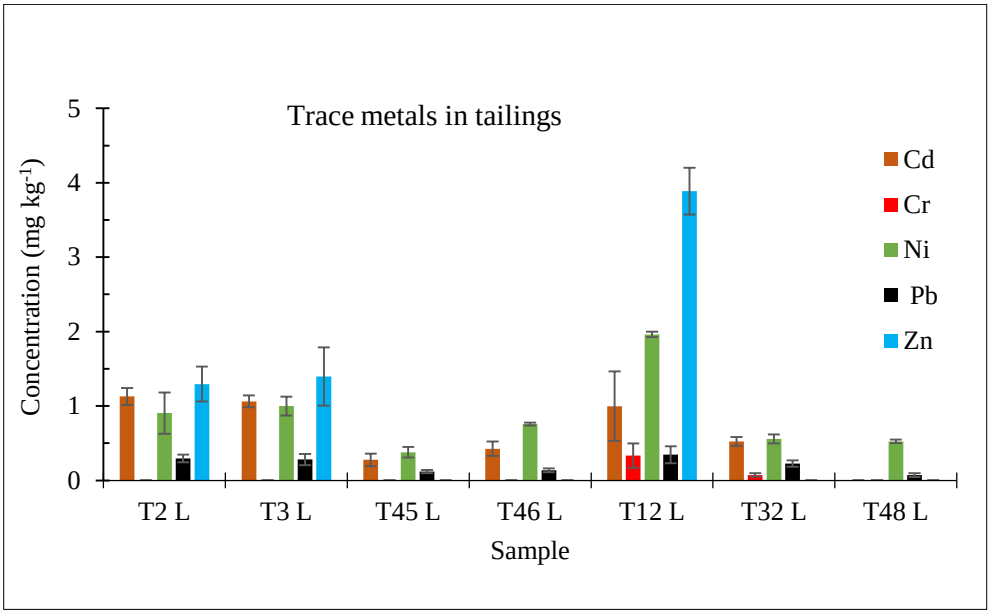


Figure 5.48: Concentration of trace metals in tailings obtained by TCLP.

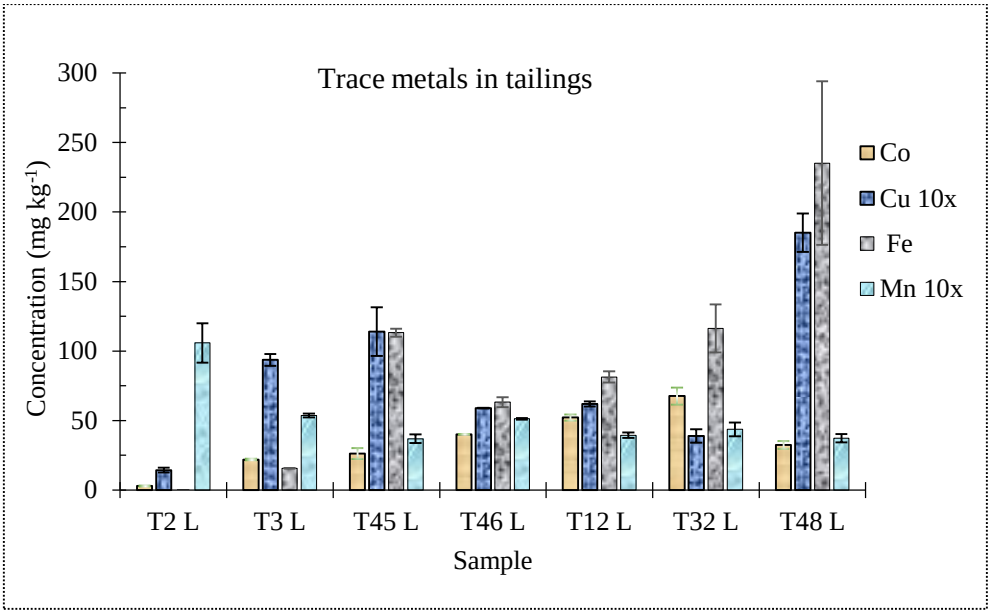


Figure 5.49: Concentration of trace metals in tailings obtained by TCLP. The actual concentrations of Cu and Mn can be obtained by multiplying the concentrations presented in this by ten (10x) than other trace elements investigated in this study.

5.11.3.3 Chemical composition of tailings and stream floor sediment digests

Vigorous microwave aided heating of tailings with *aqua regia* (3HCl:1HNO_3, 12 mL) released large amounts (mg kg^{-1}) of major cations except for Na, which was not detected probably due to its amount being below the detection limit of the instrument used. The amounts (mg kg^{-1}) detected in tailings were Ca (42036), K (13936), Mg (54144); in T12, Ca (85080), K (7008), Mg (40944) and the amounts detected in sediments were WS23, Ca (1323), K (1378), Mg (1113). These amounts were larger than their corresponding amounts from leaching, by far. A similar observation was made for trace and other elements concentrations (mg kg^{-1}) with Al (11292), Co (303.6), Cu (2484), Fe (84234), and Mn (5440) detected in T2; Al (30924), Co (373.9), Cu (2686), Fe (25632) and Mn (1997) detected in T12; and Al (43080), Co (39.0), Cu (948.2), Fe (34800) and Mn (494.2) detected in WS23. A general and common trend in these results, that is that higher amounts of elements released from tailings than sediments, extended to both, leaching and aqua regia digestion, extraction processes. The mean values of major and trace elements concentration (mg kg^{-1}) extracted by digestion from solid samples (Tailings</>Sediments) were: Al (12434<**24774**), Ca (58368>5594), K (6374.>1379), Mg (44622.00>6153), Co (407.0>126.7), Cu (3368>1320), Fe (24754**<27600**), Mn (3790>494.2) and Zn (40.8<150.0).

The correlation between high amounts of Mn and Cu, less amounts of Fe and Co observed in leachates (Figure 5.49) was reversed in digests where the observed correlation was between high amounts of Fe and Cu, and less amounts of Mn and Co. The undissolved portion of oxides/oxi-hydroxides of Fe in TCLP contained more Cu than Co in its corresponding oxides/oxi-hydroxides of Mn. Vigorous attack by *aqua regia* dissolved a greater portion of oxides/oxi-hydroxides of Fe (Al included) and Mn. The amounts of Cu and Co liberated in digests gave indices pointing at Fe and Mn oxide/oxi-hydroxides as principal sources of Cu and Co respectively. Soluble carbonates contributed more Cu, Co and other trace elements.

5.12 Hierarchical clustering multivariate of water sampling points (Kitwe)

5.12.1 Clustering sampling points by spatial similarities relative to Tailings points

The Hierarchical clustering output (complete, Euclidean) of stream water at different sampling points produced, based on the adopted criterion of 90% similarities, a four cluster dendrogram (Figure 5.50). The ranking of clusters showed sampling points, from left to right, in descending order of their levels of contamination. The same order applied also to sub clusters. Cluster 1, a lone member cluster (W7) positioned at the far right, was mainly characterised by a very low pH, a very high EC and an elevated concentration of NO_3^-. No plausible explanation was found for extreme analytical results of W7 sample except for a sporadic unchecked influent of anthropogenic nature. The associative similarities of sampling points in the remaining clusters were primarily influenced, from right to left, by the attenuation of EC, Ca^{2+}, Mg^{2+} and SO_4^{2-} with a few other elements exerting a minor influence. Cluster 2, a five-member cluster (W13 – W2), had elevated amounts of EC, Ca^{2+}, Mg^{2+} and SO_4^{2-} attributed to their proximal location within and around tailings environments (TD25, TD15A) except for W16 located on Mwambashi River which is connected to TD15A and receive the bulk of its water from tailings dumps in Chambishi. Cluster 3 was comprised of sampling points positioned on streams linked to a similar source of contamination *viz*, tailings dam (W21 = Mindolo stream), tailings dumps (W31 and W33 = Uchi stream, W35 = Lwanshimba stream) and had moderately elevated amounts of EC, Ca^{2+}, Mg^{2+} and SO_4^{2-}. Cluster 4, on the far left, was indicative of sampling points which had in common attenuated concentration of influential parameters mentioned above.

The lower the percentage similarities, the less significant the association details. At 70% similarities, clustering of sampling points was less rigorous and yielded only two clusters: cluster A (a single member cluster) and cluster B (a less discriminate group of the remaining members) in which further associative and distributive details of sub clusters were refined at higher percentage similarities. In spite of W23 and W9 being spatially far from sources of contamination, they were grouped within the same sub cluster as W1 and W11 which were spatially located in the vicinity of sources of contamination. W1 and W11 were not affected by drainage from tailings because they were situated on the

upstream side of tailings. The attenuated concentration at W6 could be due to the fact that it received mixed waters in varying proportions, *viz.* more water from Kitwe stream and less water from TD25. Other members of the sub cluster (W17, W22, W37) had no link with mine waste.

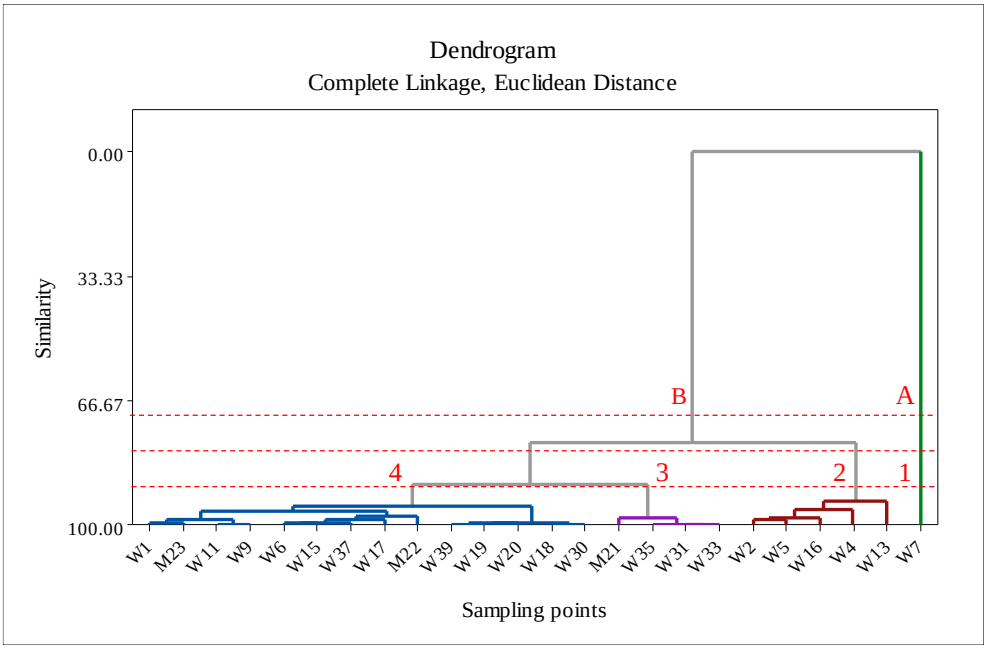


Figure 5.50: Grouping of stream water sampling points according to their spatial similarities in chemical composition. Colours and numbers indicate different clusters at 90% similarities.

5.12.2 Clustering experimental parameters by behavioural similarities in samples

In Figure 5.51 below, four main clusters (A, B, C and D) were identified at 50% similarities, *viz.* a nine elements cluster (EC – Mn), a six elements cluster (Cu – Cl), a two elements cluster (pH, F), and a single element cluster (Co). At 90% similarities, clusters were refined further to twelve clusters among which eight single member clusters, three two-member clusters and one four-member cluster were identified. Similarities for elements in cluster 7 (Ni and Si) approached 100% and were linked to primary mineral sources. Similarities in cluster 9 involved more parameters (EC, SO_4^{2-}, Ca^{2+}, Mg^{2+}) which were associated with secondary mineral sources. Figure 5.51 showed that, at adopted 90%

similarities, clusters 7 and 9 played a determinant role in segregating sampling points by spatial similarities (Figure 5.51) as opposed to single element clusters.

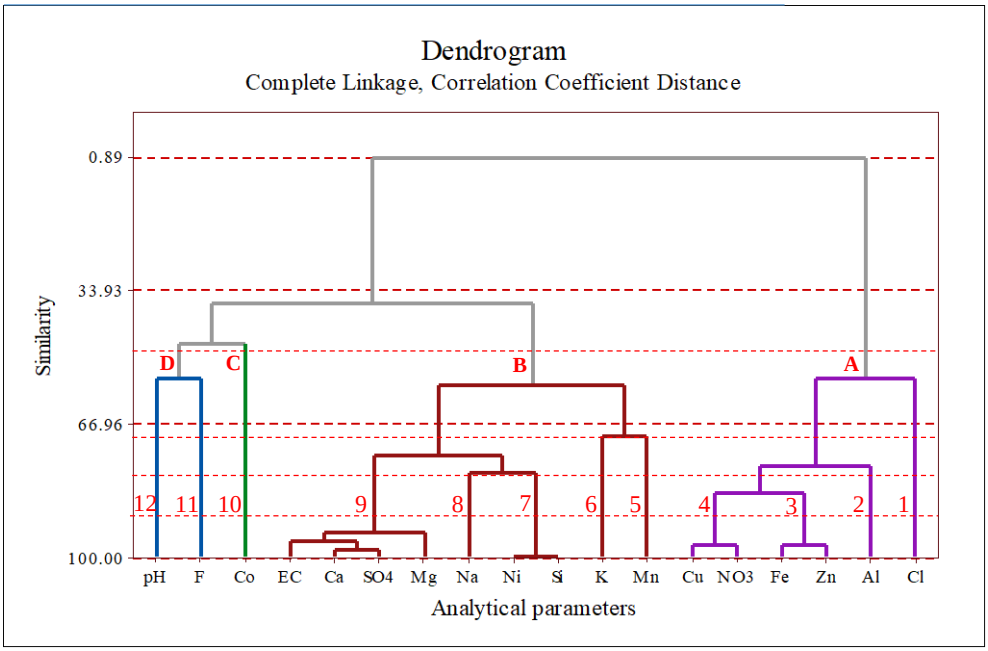


Figure 5.51: Grouping of stream water analytical parameters according to their behavioural similarities in different stream water samples. Clustering at 50% and 90% similarities are indicated.

CHAPTER 6 CONCLUSION AND RECOMMENDATIONS

This chapter gives a short résumé of the findings of the study. It also gives some recommendations derived from these findings.

6.1 Conclusion

Leaching was used to replicate the effects of changes in environmental conditions on geologic materials in order to determine the amount of pollutants leached out in liquid phase and/or leachable amount of pollutants in solid phase. Sequential extraction was used to mimic the effects of incremental changes in the severity of environmental conditions on the distribution of bioavailable pollutants in solid phases. Geochemical modelling was used for assessing actual separate and mixed water simulations, and predictive evaporated water simulations. The adsorption potential of Mgt was put to test with recovery of REEs. Surface water remained, as always, the theatre of geochemical changes.

A variety of mine waste, surface water and its floor sediments from a copper mine area defined by sulphide chalcolithic rock mineralogy particularly rich in carbonate, were subjected to qualitative, semi-quantitative and quantitative techniques for geochemical characterisation, analytical determination and speciation modelling.

Based on the results obtained in this study, the following conclusions were drawn:

- Surface water, in both study areas, was slightly alkaline. For Phalaborwa water, the EC was generally lower in flowing water (rivers) but much higher in contained water (WRD). The mixing of SbC and ObC waters, at a ratio of 1:20, had no effects on pH but greatly influenced the attenuation of EC for SbC water. Surface water in rivers and WRD shared the same water classification, SO_4^{2-}-Mg^{2+}-Cl^{-}-Ca^{2+}, with pronounced concentration in WRD. Trace elements had a wide range and higher concentration in WRD (Co, Cu, Ni, Pb and Zn) than in rivers (Cu, Zn). For Kitwe water, the EC was lower in streams with remote or no connection with tailings dumps but quite high in streams with proximal connections with tailings dumps. The dominance of SO_4^{2-}, Mg^{2+} and Ca^{2+} was commensurable with EC and was seen to

commandeer the clustering of water sampling points by similarity of variables and observations. Relatively high concentrations of Co, Cu, Mn and Ni were spotted at W18 only, located a few meters downhill the slag mountain.

- Rocks and sand leachates content were clearly different from PG leachates content but were all reflective of their respective mineralogical composition. The elevated ions content in PG leachates stemmed from the amorphous, readily soluble nature of its main mineral ($CaSO_4.2H_2O$) which gave PG a higher predisposition to release not only associated contaminants but also REEs. As such, PG posed a greater threat to the environment but could also be a sure source for REEs recovery.

- Assorted solid waste samples displayed varied characteristics. Marked differences in their metal oxides and trace elements content (XRF) as well as differences in their grain size distribution (granulometry) influenced the outcome of their interaction with water. Cu-crust leachates with acidic paste pH and WRD-PG leachates with alkaline paste pH contained high amounts of soluble ions. Copper concentration was exceedingly high in Cu-crust leachates and comparatively low in Mgt leachates. Non-geologic materials leachates (ED, CFC) contained moderately high amount of soluble ions and noticeable Cu concentration (ED).

- Sediments had high C/S ratio and contained, principally, less reactive and/or non-reactive crystalline minerals with more Cr in silty loam river sediments and more Cu and Ni in silty WRD sediments. Fractionation of river sediments revealed a strong association of Cr, Fe, Ni, Pb and Zn with the residual phase and the affinity of Mn and Cu for the bioavailable phase.

- Investigative speciation simulations of surface water (WRD) showed abundant content of Co^{2+}, Zn^{2+}, Mn^{2+} and Fe^{2+} (free) and $CuOH^+$, $Cu(OH)_2$, $Pb(OH)^+$, $Fe(OH)_3$ (complexed) soluble species. The potency of Fe to form deposits (SI > 1, log K_{eq} < 0) was particularly shown in WRD by the dominance of its precipitates and their large SI obtained from geochemical simulations. Deposited minerals were as a result of the oxidized environment. Predictive evaporation simulations, using Cu_crust leachates, revealed that hot and dry seasons could precipitate the deterioration of surface water

with dire consequences on aquatic biota and terrestrial animals because of high concentrations and deposition of salts resulting from excessive loss of water.

- Natural magnetite did not leach out detectable amounts of REEs prior to its use as adsorbent and showed good recovery of REEs under optimised experimental conditions. However, the use of surface water as adsorptive bearing fluid cannot be recommended because of its negligible content of REEs; instead, apatite concentrate and PG could be used as REEs source materials
- Fast weathering acid producers (pyrite and chalcopyrite) and soluble acid neutralizers (dolomite) were identified, among a variety of crystalline minerals, in tailings and stream sediments proximal to tailings dumps in Kitwe study site. The chemistry of stream water reflected the influence of these minerals on the types and amounts of chemicals analysed. Leaching of tailings revealed their predisposition for immediate, parsimonious and partial release of major ions and trace elements whereas digestion of tailings projected their potential for delayed and near total release of major ions and trace elements under rough conditions. The latter potential may remain locked for a long time due to the geologic setting of the area.

6.2 Recommendations

Based on the findings, the following recommendations were made:

- A constructed horizontal adsorption profile in which flow through bags containing natural magnetite could be placed in series to facilitate sequential recovery of REEs from a solution with elevated content of this adsorptive.
- Coupling geochemical modelling with some purposeful software, such as PEST, could enhance the presentation and interpretation of results. It could also relate, in a more meaningful way, modelled results with experimental results.

REFERENCES

Abbassi, R., Khan, F. and Hawboldt, K. (2009) Prediction of minerals producing acid mine drainage using a computer-assisted thermodynamic chemical equilibrium model. *Mine Water and the Environment*, 28(1), pp. 74–78.

Abraham, M.R. and Susan, T.B. (2017) Water contamination with heavy metals and trace elements from Kilembe copper mine and tailing sites in Western Uganda; implications for domestic water quality. *Chemosphere*, 169, pp. 281–287.

Adamu, H., Luter, L., Musa, M.L. and Umar, B.A. (2013) Chemical speciation: a strategic pathway for insightful risk assessment and decision making for remediation of toxic metal contamination. *Environment and Pollution*, 2(3), pp. 92–99.

Addo-Bediako, A., Marr, S.M., Jooste, A. and Luus-Powell, W.J. (2014) Human health risk assessment for silver catfish *Schilbe intermedius* Rüppell, 1832, From two impoundments in the Olifants River, Limpopo, South Africa. *Water SA*, 40(4), pp. 607–614.

Alvarez-Puebla, R.A., Valenzuela-Calahorro, C. and Garrido, J.J. (2004) Retention of Co(II), Ni(II), and Cu(II) on a purified brown humic acid. Modeling and characterization of the sorption process. *Langmuir*, 20(9), pp. 3657–3664.

Apostoli, P., Cornelis, R., Duffus, J., Hoet, P., Lison, D. and Templeton, D. (2006) Elemental speciation in human health risk assessment. *Environmental Health Criteria* (Vol 234). World Health Organization, p. 238.

Ashton, P.J., Love, D., Mahachi, H. and Dirks, P. (2001) An Overview of the Impact of Mining and Mineral Processing Operations on Water Resources and Water Quality in the Zambezi, Limpopo and Olifants Catchments in Southern Africa. *Contract Report to the Mining, Minerals and Sustainable Development (SOUTHERN AFRICA) Project, by CSIR- Environmentek, Pretoria, South Africa and Geology Department, University of Zimbabwe, Harare, Zimbabwe. Report No. ENV-P-C 2001-042.*, p. xvi + 336.

Atibu, E.K., Devarajan, N., Thevenon, F., Mwanamoki, P.M., Tshibanda, J.B., Mpiana, P.T., Prabakar, K., Mubedi, J.I., Wildi, W. and Poté, J. (2013) Concentration of metals in surface water and sediment of Luilu and Musonoie Rivers , Kolwezi-Katanga , Democratic Republic of Congo. *Applied Geochemistry*, 39, pp. 26–32.

Atkinson, C.A., Jolley, D.F. and Simpson, S.L. (2007) Effect of overlying water pH , dissolved oxygen , salinity and sediment disturbances on metal release and sequestration from metal contaminated marine sediments. *Chemosphere*, 69(9), pp. 1428–1437.

Avenant-Oldewage, A. and Marx, H.M. (2000) Bioaccumulation of chromium, copper and iron in the organs and tissues of Clarias gariepinus in the Olifants River, Kruger National Park. *Water SA*, 26(4), pp. 569–582.

Aznar-Sánchez, J.A., Velasco-Muñoz, J.F., Belmonte-Ureña, L.J. and Manzano-Agugliaro, F. (2019) 'Innovation and technology for sustainable mining activity: a worldwide research assessment. *Journal of Cleaner Production*, 221, pp. 38–54.

Banks, D., Younger, P.L., Arnesen, R.T., Iversen, E.R. and Banks, S.B. (1997) Mine-water chemistry: the good, the bad and the ugly. *Environmental Geology*, 32(3), pp. 157–174.

Beale, C.O. (1985) Copper in South Africa-Part I. *Journal of the Southern African Institute of Mining and Metallurgy*, 85(3), pp. 73–80.

Beale, C.O. (1985) Copper in South Africa-Part II. *Journal of the Southern African Institute of Mining and Metallurgy*, 85(4), pp. 109–124.

Benson, N.U., Anake, W.U. and Olanrewaju, I.O. (2013) Analytical relevance of trace metal speciation in environmental and biophysicochemical systems. *American Journal of Analytical Chemsistrystry*, 4, pp. 633–641.

Besser, J.M., Brumbaugh, W.G. and Ingersoll, C.G. (2015) Characterizing toxicity of metal-contaminated sediments from mining areas. *Applied Geochemistry*, 57, pp. 73–84.

Bleam, W. (2017) Clay mineralogy and chemistry. In: *Soil and environmental chemistry*. Academic Press, pp. 88–146.

Bleam, W. (2017) Surface Chemistry and adsorption. In: *Soil and environmental chemistry*. Academic Press, pp. 385–440.

Boocock, C.N. (2002) Environmental impacts of foreign direct investment in the mining sector in Sub-Saharan Africa. *Global Forum on International Investment*, OECD, Paris, p. 35.

Bouchez, J., Gaillardet, J, France-Lanord, C., Maurice, L. and Dutra-Maia, P. (2011) Grain size control of river suspended sediment geochemistry: Clues from Amazon River depth profiles. *Geochemistry, Geophysics, Geosystems*, 12(3), pp. 1–24.

Burton Jr., G.A. (2002) Sediment quality criteria in use around the world', *Lymnology*, 3(2), pp. 65–75.

Cailteux, J., Binda, P.L., Katekesha, W.M., Kampunzu, A.B., Intiomale, M.M., Kapenda, D., Kaunda, C., Ngongo, K., Tshiauka, T. and Wendorff, M. (1994) Lithostratigraphical correlation of the Neoproterozoic Roan Supergroup from Shaba (Zaire) and Zambia, in the central African copper-cobalt metallogenic province. *Journal of African Earth Sciences*, 19(4), pp. 265–278.

Calas, G. (2017) Mineral resources and sustainable development. *Elements*, 13(5), pp. 301–306.

Cappuyns, V. and Swennen, R. (2008) The Use of leaching tests to study the potential mobilization on heavy metals from soils and sediments: a comparison. *Water Air Soil Pollution*, 191(1–4), pp. 95–111.

Carbone, C. *et al.* (2013) 'The role of AMD secondary minerals in controlling environmental pollution : Indications from bulk leaching tests', *Journal of Geochemical Exploration*. Elsevier B.V., 132, pp. 188–200.

Carvalho, F.P. (2017) Mining industry and sustainable development : time for change. *Food and Energy Security*, 6(2), pp. 61–77.

Castillo, M.L.A., Alonso, E.V., Cordero, M.T.S., Pavón, J.M.C. and Torres, A.G.D. (2011). Fractionation of heavy metals in sediment by using microwave assisted sequential

extraction procedure and determination by inductively coupled plasma mass spectrometry. *Microchemical Journal*, 98(2), pp. 234–239.

Chou, I., Seal, R. R. and Wang, A. (2013) 'The stability of sulfate and hydrated sulfate minerals near ambient conditions and their significance in environmental and planetary sciences', *Journal of Asian Earth Sciences*. Elsevier Ltd, 62, pp. 734–758.

Cipullo, S., Prpich, G., Campo, P. and Coulon, F. (2018) Assessing bioavailability of complex chemical mixtures in contaminated soils : progress made and research needs. *Science of the Total Environment*, 615, pp. 708–723.

Currell, G. (2015) *Scientific Data Analysis*. Oxford University Press, USA.

Dold, B. (2010) Basic concepts in environmental geochemistry of sulphide mine-waste management. In: Kumar, E.S. (ed.), *Waste Management*. IntechOpen, pp. 173–198.

Dold, B. (2014) Evolution of acid mine drainage formation in sulphidic mine tailings. *Minerals*, 4(3), pp. 621–641.

Dold, B. (2014) Submarine tailings disposal (STD)—a review. *Minerals*, 4(3), pp. 642–666.

Edwards, K.J., Bond, P.L., Druschel, G.K., Mcguire, M.M., Hamers, R.J. and Banfield, J.F. (2000) Geochemical and biological aspects of sulfide mineral dissolution : lessons from Iron Mountain , California. *Chemical Geology*, 169(3–4), pp. 383–397.

Elsaidi, S.K., Sinnwell, M.A., Devaraj, A., Droubay, T.C., Nie, Z., Murugesan, V., Mcgrail, B.P. and Thallapally, P.K. (2018) Extraction of rare earth elements using magnetite@MOF composites. *Journal of Materials Chemistry A*, 6, pp. 18438–18443.

EMERITE Consortium (2003) *(Environmental Regulation of Mine water in The European Union) Mining Impacts on the Fresh Water Environment: Technical and Managerial Guidelines for Catchment Scale Management - A Research Project of the European Union 5th Framework Programme*. Available at: www.minewater.net/ermite.

Eriksson, S.C. (1984) Age of carbonatite and phoscorite magmatism of the Phalaborwa Complex (South Africa). *Chemical Geology*, 46(4), pp. 291–299.

Ettler, V., Mihaljeviča, M., Kříbekb, B., Kone, L., Ková, L., Mihaljevič, M., Majer, V., Pení, V. and Nyambe, I. (2014) Surprisingly contrasting metal distribution and fractionation patterns in copper smelter-affected tropical soils in forested and grassland areas (Mufulira, Zambian Copperbelt). *Science of the Total Environment*, 474, pp. 117–124.

Ettler, V., Cihlová, M., Jarošíková, A., Mihaljevič, M., Drahota, P., Kříbek, B., Vaněk, A., Penížek, V., Sracek, O., Klementová, M., Engel, Z., Kamona, F. and Mapani, B. (2019) Oral bioaccessibility of metal(loid)s in dust materials from mining areas of northern Namibia. *Environment International*, 124, pp. 205–215.

Foth, D.H. (1990) *Fundamentals of Soil Science*. Willey J. & Sons (Eds.), 8th ed.

Frick, C. (1986) The Phalaborwa syenite intrusions along the west-central boundary of the Kruger National Park. *Koedoe*, 29(1), pp. 45–58.

Gitari, M.W., Akinyemi, S.A., Ramugondo, L., Matidza, M. and Mhlongo, S.E. (2018) Geochemical fractionation of metals and metalloids in tailings and appraisal of environmental pollution in the abandoned Musina Copper Mine, South Africa. *Environmental geochemistry and health*, pp. 1–19.

Gorman, M.R. and Dzombak, D.A. (2018) A review of sustainable mining and resource management : Transitioning from the life cycle of the mine to the life cycle of the mineral. *Resources, Conservation & Recycling*, 137, pp. 281–291.

Grobler, D.G. (1999) Copper poisoning in wild ruminants in the Kruger National Park : Geobotanical and environmental investigation. *Onderstepoort Journal of Veterinary Research*, 66, pp. 81–93.

Guo, Y., Huang, P., Zhang, W., Yuan, X., Fan, F., Wang, H., Liu, J. and Wang, Z. (2013) Leaching of heavy metals from Dexing copper mine tailings pond. *Trans. Nonferrous Met. Soc. China*, 23(10), pp. 3068–3075.

Hageman, P.L., Seal, R.R., Diehl, S.F., Piatak, N.M. and Lowers, H.A. (2015) Evaluation of selected static methods used to estimate element mobility , acid-generating and acid-

neutralizing potentials associated with geologically diverse mining wastes. *Applied Geochemistry*, 57, pp. 125–139.

Hall, S.J. and Silver, W.L. (2013) Iron oxidation stimulates organic matter decomposition in humid tropical forest soils. *Global Change Biology*, 19(9), pp. 2804–2813.

Hasenmueller, E.A., Hasenmueller, E.A., Criss, R.E., Winston, W.E. and Shaughnessy, A.R. (2017) Stream hydrology and geochemistry along a rural to urban land use gradient. *Applied Geochemistry*, 83, pp. 136–149.

Hee, J., Kim, B. and Chon, C. (2018) Characterization of iron and manganese minerals and their associated microbiota in different mine sites to reveal the potential interactions of microbiota with mineral formation. *Chemosphere*, 191, pp. 245–252.

Heinrjch, E.W. (1970) The Palabora carbonatitic complex - A unique copper deposit. *The Canadian Mineralogist*, 10(3), pp. 585–588.

Hem, J.D. (1962) *Chemistry of Iron in Natural Water*. US Geological Survey Water-Supply paper 1459.

Hem, J.D. (1985) *Study and Interpretation the Chemical of Natural Characteristics of Natural Water*. US Geological Survey Water-Supply paper 2254.

Ho, H.H., Swennen, R., Cappuyns, V., Vassilieva, E. and Tran, T.V. (2012) Necessity of normalization to aluminum to assess the contamination by heavy metals and arsenic in sediments near Haiphong Harbor , Vietnam. *Journal of Asian Earth Sciences*, 56, pp. 229–239.

Hoadley, M., Limpitlaw, D. and Weaver, A. (2002) Mining, Minerals and Sustainable Development in Southern Africa. In: *Report of the Regional MMSD Process*, p. 77.

Hodges, C.A. (1995) Mineral resources, environmental issues, and land use. *Science*, 268(5215), pp. 1305–1312.

Hornig-kjarsgaard, I. (1998) Rare Earth Elements in Sovitic Carbonatites and their Mineral Phases. *Journal of Petrology*, 39(11), pp. 2105–2121.

Howie, R.A., Cairncross, B. and Dixon, R. (1996) Minerals of South Africa,

Johannesburg (Geological Society of South Africa), 1995. *Mineralogical Magazine*, 60(402), pp. 854–855.

Hudson-Edwards, K.A., Jamieson, H. E. and Lottermoser, B. G. (2011) Mine Wastes: Past, Present, Future. *Elements*, 7, pp. 375–380.

Hudson, T.L., Fox, F.D. and Plumlee, G.S. (1999) *Metal Mining and the environment: Alexandria. Virginia.* American Geological Institute (AGI) Environmental Awareness Series 3.

Ibragimow, A., Walna, B. and Siepak, M. (2013) Physico-chemical parameters determining the variability of actually and potentially available fractions of heavy metals in fluvial sediments of the middle Odra river. *Archives of Environmental Protection*, 39(2), pp. 3–16.

Inglezakis, V.J. and Zorpas, A.A. (2012) Heat of adsorption , adsorption energy and activation energy in adsorption and ion exchange systems Heat of adsorption , adsorption energy and activation energy in adsorption and ion exchange systems. *Desalination and Water Treatment*, (May 2015), p. 10. doi: 10.1080/19443994.2012.669169.

James, B.R. and Brose, D.A. (2012) Oxidation-Reduction Phenomena. In: Huang, P.M. and Li, Y. and Sumner, M.E. (eds.) *Handbook of Soil Sciences: Properties and Processes*, 2, CRC Press, p. 24.

Jamieson, H.E. (2011) Geochemistry and Mineralogy of Solid Mine Waste : Essential Knowledge for Predicting Environmental Impact. *Elements*, 7, pp. 381–386.

Jamieson, H.E., Walker, S.R. and Parsons, M.B. (2015) Mineralogical characterization of mine waste. *Applied Geochemistry*, 57, pp. 85–105.

Jellicoe, B.C. (2019) The relevance of rare earths to South Africa. In: *National Science & Technology Forum : Advanced manufacturing and Automation*, p. 51.

Jena, V., Gupta, S., Dhundhel, R.S., Matic, N., Devic, N., Raipur, A., Republicki, J., Za, Z. and Istrazivanja, G. (2013) Determination of Total Heavy Metal By Sequential

Extraction in Soil. *International Journal of Research in Environmental Science and Technology*, 3(1), pp. 35–38.

John, D.A. and Leventhal, J.S. (1995) Bioavailability of metals. In: DuBray, E.A. (Ed), Preliminary compilation of geoenvironmental mineral deposit models: U.S Geological Survey. Open-File Report 95-831, pp. 10–18.

Jones, R.T. and Mackey, P.J. (2015) An Overview of Copper Smelting in Southern Africa. In: Southern African Institute of Mining and Metallurgy (ed.), *Copper Cobalt Africa, incorporating the 8th Southern African Base Metals Conference*, Livingstone, Zambia, pp. 499–504.

Kajjumba, G.W., Emik, S., Öngen, A., Özcan, H.K. and Aydın, S. (2018) Modelling of Adsorption Kinetic Processes-Errors, Theory and Application. In: *Advanced sorption process applications*. IntechOpen, p. 19.

Kalichini, M., Corin, K.C., O'Connor, C.T. and Simukanga, S. (2017) The role of pulp potential and the sulphidization technique in the recovery of sulphide and oxide copper minerals from a complex ore. *Journal of the Southern African Institute of Mining and Metallurgy*, 117(8), pp. 803–810.

Karaca, O., Cameselle, C. and Reddy, K.R. (2016) Characterization of Heavy Metals in Mine Tailings and Lake Sediments: Implications on Remediation. In: *Geotechnical Special Publication*, pp. 12–21.

Kirchman, D.L. (2010) Degradation of organic material. In: *Processes in Microbial Ecology*. New York, Oxford University Press Inc., pp. 79-98.

Kollias, K., Mylona, E., Adam, K., Papassiopi, N. and Xenidis, A. (2014) Suppression of Pyrite Oxidation by Surface Silica Coating. *Journal of Geoscience and Environment Protection*, 2, pp. 37–43.

Kossoff, D., Dubbin, W.E., Alfredsson, M., Edwards, S.J., Macklin, M.G., Hudson-Edwards, K.A. (2014) Mine tailings dams : Characteristics , failure , environmental impacts , and remediation. *Applied Geochemistry*, 51, pp. 229–245.

Kot, A. and Namiesnèik, J. (2000) The role of speciation in analytical chemistry. *Trends in Analytical Chemistry*, 19(2–3), pp. 69–79.

Kotze, P., Du Preez, H.H. and Van Vuren, J.H.J. (999) Bioaccumulation of copper and zinc in Oreochromis mossambicus and Clarias gariepinus, from the Olifants River, Mpumalanga, South Africa. *Water SA*, 25(1), pp. 99–110.

Kříbek, B., Majer, V., Veselovský, F. and Nyambe, I. (2010) Discrimination of lithogenic and anthropogenic sources of metals and sulphur in soils of the central-northern part of the Zambian Copperbelt Mining District: A topsoil vs. subsurface soil concept. *Journal of Geochemical Exploration*, 104(3), pp. 69–86.

Kwok, K.W.H., Batley, G.E., Wenning, R.J., Zhu, L., Vangheluwe, M. and Lee, S. (2014) Sediment quality guidelines: Challenges and opportunities for improving sediment management. *Environmental Science and Pollution Research*, 21(1), pp. 17–27.

Landner, L. and Reuther, R. (2004) Metals in Society and in the Environment. A Critical Review of Current Knowledge on Fluxes, Speciation, Bioavailability and Risk for Adverse Effects of Copper, Chromium, Nickel and Zinc. *Environmental Pollution*.

Langa, N.T.N., Adeleke, A.A., Mendonidis, P. and Thubakgale, C.K. (2014) Evaluation of sodium isobutyl xanthate as a collector in the froth flotation of a carbonatitic copper ore. *International Journal of Industrial Chemistry*, 5(3–4), pp. 107–110.

Lark, R.M., Hamilton, E.M., Kaninga, B., Maseka, K K., Mutondo, M., Sakala, G.M. and Watts M.J. (2017) Nested sampling and spatial analysis for reconnaissance investigations of soil : an example from agricultural land near mine tailings in Zambia. *European Journal of Soil Science*, 68, pp. 605–620.

Lin, Z. (1997) Mobilization and retention of heavy metals in mill-tailings from Garpenberg sulfide mines, Sweden. *Science of the Total Environment*, 198(1), pp. 13–31.

Lindahl, J. (2014) *Towards Better Environmental Management and Sustainable Exploitation of Mineral Resources*, SGU-report 2014:22.

Lindsay, M.B.J., Moncur, M.C., Bain, J.G., Jambor, J.L., Ptacek, C.J. and Blowes, D.W. (2015) Geochemical and mineralogical aspects of sulfide mine tailings. *Applied Geochemistry*, 57, pp. 157–177.

Livingstone, D. (2009) *A Practical Guide to Scientific Data Analysis*. (Vol. 341). Chichester: Wiley.

Lottermoser, B.G. (2011) Recycling, Reuse and Rehabilitation of Mine Wastes. *Elements*, 7, pp. 405–410.

Lovley, D.R. (1987) Organic Matter Mineralization with the Reduction of Ferric Iron: A Review. *Geomicrobiology journal*, 5(3–4), pp. 375–399.

Lydall, M.I. and Auchterlonie, A. (2011) The Democratic Republic of Congo and Zambia: a Growing Global "Hotspot" for Copper-Cobalt Mineral Investment and Exploitation. In: *The Southern African Institute of Mining and Metallurgy, 6th Southern Africa Base Metals Conferenc*e, *Phalaborwa*, pp. 25–37.

Lyubchik, S., Lyubchik, A., Lygina, O., Lyubchik, S. and Fonseca, I. (2011) Comparison of the Thermodynamic Parameters Estimation for the Adsorption Process of the Metals from Liquid Phase on Activated Carbons. In: Carlos, J. and PirajÃ¡n, M. (Ed.), *Thermodynamics - Interaction Studies - Solids, Liquids and Gases. IntechOpen*, pp. 95–122.

Majzlan, J., Martin, Š., Chovan, M., Luptáková, J., Milovská, S., Milovský, R., Jele, S., Sýkorová, M., Pollok, K., Göttlicher, J. and Kupka, D. (2018) Mineralogy and geochemistry of the copper-dominated neutral mine drainage at the Cu deposit Ľ ubietová-Podlipa (Slovakia). *Applied Geochemistry*, 92, pp. 59–70.

Marguí, E., Salvadó, V., Queralt, I. and Hidalgo, M. (2004) Comparison of three-stage sequential extraction and toxicity characteristic leaching tests to evaluate metal mobility in mining wastes. *Analytica Chimica Acta*, 524(1–2), pp. 151–159.

Massolo, S., Bignasca, A., Sarkar, Santosh K., Chatterjee, M., Deb Bhattacharya, B. andAlam, A. (2012) Geochemical fractionation of trace elements in sediments of Hugli

River (Ganges) and Sundarban wetland (West Bengal, India). *Environmental Monitoring and Assessment*, 184(12), pp. 7561–7577.

McGowan, R.R., Roberts, S., Foster, R.P., Boyce, A.J. and Coller, D. (2003) Origin of the copper-cobalt deposits of the Zambian Copperbelt: An epigenetic view from Nchanga. *Geology*, 31(6), pp. 497–500.

McGowan, R.R., Roberts, S. and Boyce, A.J. (2005) Origin of the Nchanga copper-cobalt deposits of the Zambian Copperbelt. *Mineralium Deposita*, 40(6–7), pp. 617–638.

Meck, M., Love, D. and Mapani, B. (2006) Zimbabwean mine dumps and their impacts on river water quality – a reconnaissance study. *Physics and Chemistry of the Earth*, 31(31), pp. 797–803.

Mehta, N., Cocerva, T., Cipullo, S., Padoan, E., Dino, G.A., Ajmone-Marsan, F., Cox, S.F., Coulon, F. and Luca, D.A.D. (2019) Linking oral bioaccessibility and solid phase distribution of potentially toxic elements in extractive waste and soil from an abandoned mine site : Case study in Campello Monti , NW Italy. *Science of the Total Environment*, 651, pp. 2799–2810.

Michalke, B. (2003) Element speciation definitions, analytical methodology, and some examples. *Ecotoxicology and Environmental Safety*, 56(1), pp. 122–139.

Mileusni, M., Siyowi, B., Fred, A., Ru, S., Mapaure, I. and Maruwa, P. (2014) Assessment of agricultural soil contamination by potentially toxic metals dispersed from improperly disposed tailings , Kombat mine , Namibia. *Journal of Geochemical Exploration*, 144, pp. 409–420.

Mine Geological and Mineralogical Staff, P.M.C. (1976) The geology and the economic deposits of copper, iron, and vermiculite in the Palabora Igneous Complex: a brief review. *Economic Geology*, 71, pp. 177–192.

Miwa, T., Murakami, M. and Mizuike, A. (1989) Speciation of copper in fresh waters. *Analytica Chimica Acta*, 219, pp. 1–8.

Montoneri, E., Boffa, V., Quagliotto, P., Mendichi, R., Michele, R., Gobetto, R. and Medana, C. (2008) Humic acid-like matter isolated from green urban wastes. part i: structure and surfactant properties. *BioResources*, 3(1), pp. 123–141.

Mossop, K.F. and Davidson, C.M. (2003) Comparison of original and modified BCR sequential extraction procedures for the fractionation of copper , iron , lead , manganese and zinc in soils and sediments. *Analytica Chimica Acta*, 478(1), pp. 111–118.

Muchez, P. and Corbella, M. (2012) Factors controlling the precipitation of copper and cobalt minerals in sediment-hosted ore deposits : Advances and restrictions. *Journal of Geochemical Exploration*, 118, pp. 38–46.

Naderi Peikam, E. and Jalali, M. (2016) Application of inverse geochemical modelling for predicting surface water chemistry in Ekbatan watershed , Hamedan , western Iran. *Hydrological Sciences Journal*, 61(6), pp. 1124–1134.

Ndoro, T.O. and Witika, L.K. (2017) A Review of the Flotation of Copper Minerals. *International Journal of Sciences: Basic and Applied Research*, 34(2), pp. 145–165.

Nejeschlebová, L., Sracek, O., Mihaljevič, M., Ettler, V., Kříbek, B., Knésl, I., Vaněk, A., Penížek, V., Dolníček, Z. and Mapani, B. (2015) Geochemistry and potential environmental impact of the mine tailings at Rosh Pinah , southern Namibia. *Journal of African Earth Sciences*, 105, pp. 17–28.

Nemati, K., Abu Bakar, N.K., Bin Abas, M.R., Sobhanzadeh, E. and Low, K.H. (2011) Comparison of unmodified and modified BCR sequential extraction schemes for the fractionation of heavy metals in shrimp aquaculture sludge from Selangor, Malaysia. *Environmental Monitoring and Assessment*, 176(1–4), pp. 313–320.

Newton, I. (2014) *Minitab Cookbook*. Packt Publishing Ltd.

Nicholson, R.V., Gillham, R.W. and Reardon, E.J. (1989) Pyrite oxidation in carbonate-buffered solution: 2. Rate control by oxide coatings. *Geochimica and Cosmochimica Acta*, 54(2), pp. 395–402.

Nordstrom, D.K. and Alpers, C.N. (1999) Geochemistry of acid mine waters. In: Plumlee,

G.S. and Logsdon, M.J. (eds), *The environmental geochemistry of mineral deposits*. Reviews in Economic Geology V. 6A,. Soc. Econ. Geol. Inc., Littleton, CO, pp. 133–160.

Nyirenda, T.M., Zhou, J., Xie, L., Pan, X. and Li, Y. (2015) Determination of Carbonate Minerals Responsible for Alkaline Mine Drainage at Xikuangshan Antimony Mine, China: Using Thermodynamic Chemical Equilibrium Model. *Journal of Earth Science*, 26(5), pp. 755–762.

NYSDEC (2014) *Screening and Assessment of Contaminated Sediment*. New York State Department of Environmental Conservation. Division of Fish, Wildlife and Marine Resources.

Okoro, H.K. and Fatoki, O.S. (2012) A Review of Sequential Extraction Procedures for Heavy Metals Speciation in Soil and Sediments. *Journal of Environmental & Analytical Toxicology*, 1(3), pp. 1–9.

Owens, C.L., Nash, G.R., Hadler, K., Fitzpatrick, R.S., Anderson, C.G. and Wall, F. (2019) Apatite enrichment by rare earth elements : A review of the effects of surface properties. *Advances in Colloid and Interface Science*, 265, pp. 14–28.

Papyrakis, E., Hess, S. and Van Beukering, P. (2006) *Mining in Zambia: Contemplations of Economic Development.* Poverty Reduction and Environmental Management, Copperbelt Project. (IVM) the Vrije Universiteit, The Netherland, p. 14.

Parkhurst, D.L. and Appelo, C.A.J. (1999) *User's guide to PHREEQC (Version 2) - a computer program for speciation, and inverse geochemical calculations*. U.S. Geological Survey, Water-Resources Investigations Report 99-4259.

Parkhurst, D.L. and Appelo, C.A.J. (2013) Description of Input and Examples for PHREEQC Version 3 — A Computer Program for Speciation , Batch-Reaction , One-Dimensional Transport , and Inverse Geochemical Calculations. In: *U.S. Geological Survey Techniques and Methods, book 6, Chap. A43*, p. 497.

Passos, D.A.E., Alves, J.D.P.H., Garcia, C.A.B. and Costa, A.C.S. (2011) Metal fractionation in sediments of the Sergipe River, Northeast, Brazil. *Journal of the Brazilian Chemical Society*, 22(5), pp. 828–835.

Pedersen, K.B., Jensen, P.E., Ottosen, L.M., Evenset, A., Christensen, G.N. and Frantzen, M. (2019) Metal speciation of historic and new copper mine tailings from Repparfjorden, Northern Norway , before and after acid , base and electrodialytic extraction. *Minerals Engineering*, 107, pp. 100–111.

Perera, N.P. (1981) Mining and Spoiled Land in Zambia: An Example of Conflicting Land Use in the Third World. *GeoJournal*, 2(2), pp. 95–103.

Piatak, N.M., Hammarstrom, J.M., Robert, RS., Briggs, P.H., Meier, A.L., Muzik, T.L. and Jackson, J.C. (2004) *Geochemical Characterization of Mine Waste at the Ely Copper Mine Superfund Site , Orange County , Vermont.* Open-File Report 2004-1248.

Piatak, N.M., Hammarstrom, J.M. and Ii, R.R.S. (2006) *Geochemical Characterization of Mine Waste, Mine Drainage, and Stream Sediments at the Pike Hill Copper Mine Superfund Site, Orange County, Vermont*. U.S. Geological Survey, SIR 2006-5303.

Pietrobelli, C., Marin, A. and Olivari, J. (2018) Innovation in mining value chains : New evidence from Latin America. *Resources Policy*, 58, pp. 1–10.

Pourret, O., Lange, B., Houben, D., Colinet, G., Shutcha, M. and Faucon, M.P. (2015) Modeling of cobalt and copper speciation in metalliferous soils from Katanga (Democratic Republic of Congo). *Journal of Geochemical Exploration*, 149, pp. 87–96.

Price, W.A. (2009) *Prediction manual for drainage chemistry from sulphidic geological materials, MEND (Mine Envirinment Neutral Drainage) Report 1.20.1*, *Natural Resources Canada*.

Rae, J.E. . and Allen, J.R.L. (1993) The Significance of Organic Matter Degradation in the Interpretation of Historical Pollution Trends in Depth Profiles of Estuarine Sediment. *Estuarine Research Federation*, 16(3), pp. 678–682.

Ramirez-llodra, E., Trannum, H.C., Evenset, A., Levin, L.A., Andersson, M., Erik, T., Hilario, A., Flem, B., Christensen, G., Schaanning, M. and Vanreusel, A. (2015) Submarine and deep-sea mine tailing placements : A review of current practices , environmental issues , natural analogs and knowledge gaps in Norway and internationally. *Marine Pollution Bulletin*, 97(1–2), pp. 13–35.

Rauret, G., López-Sánchez, J.F., Sahuquillo, A., Rubio, R., Davidson, C., Ure, A. and Quevauviller, P. (1999) Improvement of the BCR three step sequential extraction procedure prior to the certification of new sediment and soil reference materials. *Journal of Environmental Monitoring*, 1(1), pp. 57–61.

Reichelt-Brushett, A., Clark, M. and Birch, G. (2017) Physical and Chemical Factors to Consider when Studying Historical Contamination and Pollution in Estuaries. In: Weckström, K., Saunders, K.M., Gell, P.A. and Skilbeck, C.G. (eds), *Applications of Paleoenvironmental Techniques in Estuarine Studies*. Springer, pp. 239–276.

Roberts, D., Nactegaal, M. and Sparks, D.L. (2005) Speciation of Metals in Soils. *Chemical processes in soils*, Willey, pp. 619–654.

Rosado, D., Usero, J. and Morillo, J. (2016) Ability of 3 extraction methods (BCR, Tessier and protease K) to estimate bioavailable metals in sediments from Huelva estuary (Southwestern Spain). *Marine Pollution Bulletin*, 102(1), pp. 65–71.

Rouquerol, F., Rouquerol, J. and Sing, K. (1999) *Adsorption by Powders and Porous Solids Principles, Methodology and Applications*. Academic Press. p. 485.

Saha, P. and Chowdhury, S. (2011) Insight Into Adsorption Thermodynamics. In: Tadashi, M. (Ed.), *Thermodynamics*. IntechOpen, pp. 349–364.

Saleem, M., Iqbal, J. and Shah, M.H. (2015) Geochemical speciation, anthropogenic contamination, risk assessment and source identification of selected metals in freshwater sediments - a case study from Mangla Lake, Pakistan. *Environmental Nanotechnology, Monitoring and Management*, 4, pp. 27–36.

Santos Yabe, M.J. and de Oliveira, E. (2003) Heavy metals removal in industrial effluents by sequential adsorbent treatment. *Advances in Environmental Research*, 7(2), pp. 263–

272.

Sarkar, S.K., Favas, J.C.P., Rakshit, D. and Satpathy, K.K. (2014) Geochemical Speciation and Risk Assessment of Heavy Metals in Soils and Sediments, In: *Environmental Risk Assessment of Soil Contamination*. IntechOpen, pp. 723–756.

Seymore, T., Duperez, H.H., Vuren, J.H.J. van, Deacon, A. and Strydom, G. (1994) Variations in selected water quality variables and metal concentrations in the sediment of the lower Olifants and Selati Rivers, South Africa. *Koedoe*, 37(2), pp. 1–18.

Shahid, A. and Qiren, L. (2010) Tailings Dam Failures: A review of the Last one Hundred Years. *Geotechnical News*, 28, pp. 1–4.

Simpson, S.L., Batley, G.E. and Maher, W.A. (2016) Chemistry of sediment contaminants. In: *Sediment Quality Assessment: A Practical Guide*, CSIRO, pp. 46–75.

Soltani, F., Abdollahy, M., Petersen, J., Ram, R. and Javad Koleini, S.M. (2019) Hydrometallurgy Leaching and recovery of phosphate and rare earth elements from an iron- rich fl uorapatite concentrate : Part II : Selective leaching of calcium and phosphate and acid baking of the residue. *Hydrometallurgy*, 184, pp. 29–38.

Soltani, N., Moore, F., Keshavarzi, B. and Sharifi, R. (2014) Geochemistry of Trace Metals and Rare Earth Elements in Stream Water, Stream Sediments and Acid Mine Drainage from Darrehzar Copper Mine, Kerman, Iran. *Water Quality, Exposure and Health*, 6(3), pp. 97–114.

Songolo, M., Moono, W.S. and Mwenya, W.M. (2016) Achieving Sustainable Mine Waste Management Practices through Capacity Building of Stakeholder Engagement the Case of the Zambian Minerals Industry. *American Scientific Research Journal for Engineering, Technology, and Sciences*, 26(1), pp. 39–51.

Sracek, O., Mihaljevič, M., Kříbek, B., Majer, V. and Veselovský, F. (2010) Geochemistry and mineralogy of Cu and Co in mine tailings at the Copperbelt, Zambia. *Journal of African Earth Sciences*, 57(1–2), pp. 14–30.

Sracek, O., Filip, J., Mihaljevič, M., Kříbek, B., Majer, V. and Veselovský, F. (2011) Attenuation of dissolved metals in neutral mine drainage in the Zambian Copperbelt. *Environmental Monitoring and Assessment*, 172(1–4), pp. 287–299.

Sracek, O., Kříbek, B., Mihaljevič, M., Majer, V., Veselovský, F., Vencelides, Z. and Nyambe, I. (2012) Mining-related contamination of surface water and sediments of the Kafue River drainage system in the Copperbelt district, Zambia: An example of a high neutralization capacity system. *Journal of Geochemical Exploration*, 112, pp. 174–188.

Stefansson, A. (2007) Iron (III) Hydrolysis and Solubility at 25 ° C. *Environmental Science and Technology*, 41(17), pp. 6117–6123.

Szögi, A.A., Hunt, P.G., Sadler, E.J. and Evans, D.E. (2004) Characterization of oxidation-reduction processes in constrcted wetlands for swine wastewater treatment. *Applied Engineering in Agriculture*, 20(2), pp. 189–200.

Taraškevičius, R., Zinkutė, R., Stakėnienė, R. and Radavičius, M. (2012) Case Study of the Relationship between Aqua Regia and Real Total Contents of Harmful Trace Elements in Some European Soils. *Journal of Chemistry*, 2013, p. 15.

Tardif, S., Cipullo, S., Sø, H.U., Wragg, J., Holm, P.E., Coulon, F., Brandt, K.K. and Cave, M. (2019) Scirning the solid phase distribution of Cr, Cu and As in contaminated soil after 40 years of ageing. *Science of the Total Environment*, 652, pp. 744–754.

Tessier, A., Campbell, P.G.C. and Bisson, M. (1979) Sequential Extraction Procedure for the Speciation of Particulate Trace Metals. *Analytical Chemistry*, 51(7), pp. 844–851.

Torremans, K., Gauquie, J., Boyce, A.J., Barrie, C.D., Dewaele, S., Sikazwe, O. and Muchez, P. (2013) Remobilisation features and structural control on ore grade distribution at the Konkola stratiform Cu-Co ore deposit, Zambia. *Journal of African Earth Sciences*, 79, pp. 10–23.

Ugwu, I.M. and Igbokwe, O.A. (2018) Sorption of Heavy Metals on Clay Minerals and Oxides : A Review. In: *Advanced Sorption Process Applications.* IntechOpen, p. 23.

Ure, A.M., Quevauviller, P., Muntau, H. and Griepink, B. (1993) Speciation of Heavy Metals in Soils and Sediments. An Account of the Improvement and Harmonization of Extraction Techniques Undertaken Under the Auspices of the BCR of the Commission of the European Communities. *International Journal of Environmental Analytical Chemistry*, 51(1–4), pp. 135–151.

Vidal, O., Rostom, F., François, C. and Giraud, G. (2017) Global Trends in Metal Consumption and Supply : The Raw Material – Energy Nexus. *Elements: An International Magazine of Mineralogy, Geochemistry, and Petrology*, 13, pp. 319–324.

Vidmar, J., Zuliani, T., Novak, P., Drinčić, A., Ščančar, J. and Milačič, R. (2017) Elements in water, suspended particulate matter and sediments of the Sava River. *Journal of Soils and Sediments*, 17, pp. 1917–1927.

de Villiers, S. and Mkwelo, S.T. (2009) Has monitoring failed the Olifants River, Mpumalanga? *Water SA*, 35(5), pp. 671–676.

W&EMBC (2006) *Acid mine drainage: mining & water pollution issues in BC*. Environmental Mining Council of British Columbia.

Wali, A., Colinet, G. and Ksibi, M. (2015) Speciation of Heavy Metals by Modified BCR Sequential Extraction in Soils Contaminated by Phosphogypsum in Sfax, Tunisia. *Environmental Research, Engineering and Management*, 70(4), pp. 14–26.

Wentworth, C.K. (1922) A Scale of Grade and Class Terms for Clastic Sediments. *The Journal of Geology*, 30(5), pp. 377–392.

Wepener, V., Van Huren, J.H.J. and Du Preez, H.H. (1999) The implementation of an aquatic toxcity index as a water quality monitoring tool in the Olifants River (Kruger National Park). *Koedoe*, 42(1), pp. 85–96.

Wojtkowska, M. (2011) Content of Selected Heavy Metals in Water. *Environment Protection Engineering*, 37(3), pp. 55–62.

Xu, C., Wang, L., Song, W. and Wu, M. (2010) Carbonatites in China : A review for genesis and mineralization. *Geoscience Frontiers*, 2010(1), pp. 105–114.

Xu, L. and Li, J. (2015) Speciation and degrees of contamination of metals in sediments from upstream and downstream reaches along the catchment of the southern Bohai Sea, China. *International Journal of Environmental Research and Public Health*, 12(7), pp. 7959–7973.

Yang, X., Tapani Makkonen, H. and Pakkanen, L. (2019) Rare Earth Occurrences in Streams of Processing a Phosphate Ore. *Minerals*, 9(5), p. 262.

Yuan, C.G., Shi, J.B., He, B., Liu, J.F., Liang, L.N. and Jiang, G.B. (2000) Speciation of heavy metals in marine sediments from the East China Sea by ICP-MS with sequential extraction. *Environment International*, 30(6), pp. 769–783.

Zhang, C., Yu, Z., Zeng, G., Jiang, M., Yang, Z., Cui, F., Zhu, M., Shen, L. and Hu, L. (2014) Effects of sediment geochemical properties on heavy metal bioavailability. *Environment International*, 73, pp. 270–281.

Zhao, G., Ye, S., Yuan, H., Ding, X. and Wang, J. (2017) Surface sediment properties and heavy metal pollution assessment in the Pearl River Estuary, China. *Environmental Science and Pollution Research*, 24(3), pp. 2966–2979.

APPENDIX

Table A 1: Percentage of metal oxides obtained from XRF analysis

Sample	SiO_2	Al_2O_3	Fe_2O_3	FeO	**Fe_3O_4**	MnO	MgO	CaO	Na_2O	K_2O	TiO2	P2O5	Cr2O3	NiO	LOI	TOTAL
ObC	52.96	12.53	1.16	9.35	**10.51**	0.16	4.56	5.14	1.42	1.02	2.20	0.17	0.82	0.02	8.06	99.56
SbC	54.62	13.23	0.86	7.01	**7.87**	0.13	4.06	4.24	1.55	1.29	1.34	0.21	0.26	0.02	11.10	99.93
WRDs	8.22	1.75	3.73	30.22	33.95	0.25	6.09	23.19	0.16	0.32	1.07	1.96	0.04	0.18	20.27	97.45
TexCon	8.87	1.75	3.39	27.45	30.84	0.17	7.57	25.62	0.18	0.27	0.84	3.44	0.02	0.02	17.93	97.51
Cbt	12.26	2.03	0.32	2.63	2.95	0.04	3.41	42.20	0.18	0.82	0.43	2.28	0.02	0.01	33.99	100.62
Cu_crust	11.45	0.69	5.08	-	5.08	0.08	5.44	37.46	0.00	0.06	0.31	4.11	0.01	0.16	24.33	89.19
Mgt	4.78	0.95	88.05	-	88.05	0.25	3.09	1.26	0.00	0.17	1.76	0.23	0.10	0.06	-0.57	100.13

Table A 2: Percentage of metal converted from percentage of metal oxides. It can be converted further to mg (metal) kg^{-1} (sample).

Sample	Si	Al	Fe^{2+}	Fe^{3+}	Fe_{total}	Mn	Mg	Ca	Na	K	Ti	P	Cr	Ni	C
ObC	24.76	6.63	-	-	7.60	0.12	2.75	3.67	1.05	0.85	1.32	0.07	0.56	0.02	2.20
SbC	25.53	7.00	-	-	5.69	0.10	2.45	3.03	1.15	1.07	0.80	0.09	0.18	0.02	3.03
WRD(s)	3.84	0.93	-	-	24.57	0.19	3.67	16.57	0.12	0.27	0.64	0.86	0.03	0.14	5.53
TexCon	4.15	0.93	-	-	22.32	0.13	4.57	18.31	0.13	0.22	0.50	1.50	0.01	0.02	4.89
Cbt	5.73	1.07	-	-	2.13	0.03	2.06	30.16	0.13	0.68	0.26	1.00	0.01	0.01	9.27
Cu_crust	5.35	0.37	-	-	3.68	0.06	3.28	26.77	0.00	0.05	0.19	1.79	0.01	0.13	6.64
Mgt	2.23	0.50	-	-	63.71	0.19	1.86	0.90	0.00	0.14	1.05	0.10	0.07	0.05	-0.16

Fe^{3+} allocated as 10% Fe total. Weight percentage of element in element oxide: (M wt%) = M_xO_x wt% x Mr M / Mr M_yO_x

Table A 3: Elements (wt%) in tailings and sediments samples obtained using EDS analysis

Sample	wt	C	O	Al	Si	Fe	Mn	Ca	Mg	K	Na	Cu	Co	Ti	Cl	Br	P	S	Cr	Ni	Totals
T12	%	18.6	**47.1**	3.9	**15.6**	3.1	nd	**4.0**	**2.9**	**3.3**	nd	0.9	0.1	0.3	nd	nd	nd	0.3	nd	nd	100.0
T45	%	14.9	**48.0**	4.8	**16.7**	2.0	0.2	**4.1**	**3.1**	**4.2**	0.4	1.2	nd	0.3	nd	nd	nd	nd	nd	nd	100.0
T32	%	11.6	**56.5**	3.9	**16.5**	1.8	0.3	**6.9**	**3.9**	**3.0**	0.5	0.4	nd	0.3	nd	nd	nd	0.5	nd	nd	105.5
S16	%	20.9	**49.9**	5.2	**17.9**	3.0	nd	0.9	0.4	1.1	nd	0.4	nd	0.3	nd	nd	nd	nd	nd	nd	100.0
S21	%	9.0	**53.5**	8.6	**23.9**	2.9	nd	0.2	0.4	0.8	nd	0.3	nd	0.4	nd	nd	nd	nd	nd	nd	100.0
S6	%	20.6	**49.2**	4.4	**20.3**	2.6	nd	0.8	0.5	1.2	0.3	0.4	nd	0.2	nd	nd	nd	nd	nd	nd	100.1
S31	%	14.4	**51.8**	9.6	**15.8**	5.8	0.3	0.3	0.3	1.2	nd	0.3	nd	0.4	nd	nd	nd	nd	nd	nd	100.2
S35	%	18.0	**47.9**	5.1	**14.7**	3.0	nd	3.4	3.3	3.5	nd	0.7	nd	0.3	nd	nd	nd	nd	nd	nd	100.0
S18	%	7.1	**48.9**	5.8	**23.9**	7.8	nd	0.7	0.7	1.6	nd	3.0	nd	0.3	nd	nd	nd	nd	nd	nd	99.9
S23	%	31.8	**46.5**	5.5	**12.8**	2.5	nd	nd	0.2	0.4	nd	0.2	nd	0.2	nd	nd	nd	nd	nd	nd	100.1

Table A 4: Elements (wt%) in sand, rocks and PG samples obtained using EDS analysis

Sample	wt	C	O	Al	Si	Fe	Mn	Ca	Mg	K	Na	Cu	Co	Ti	Cl	Br	P	S	Cr	F	Totals
Sd	%	nd	**53**	3.7	**14**	**5.7**	nd	5.5	**11.3**	**4.1**	0.3	0.1	nd	0.4	nd	nd	**1.3**	nd	nd	nd	100
Rk1	%	nd	**53**	3.9	**13**	**7**	nd	5.3	**9.8**	**5.4**	0.4	0.1	0.06	0.6	nd	nd	**2.1**	nd	nd	nd	100.1
Rk2	%	nd	**55**	1.5	**15**	**4.4**	nd	**11.9**	**8.3**	1.8	0.4	nd	nd	0.1	0.1	nd	**1.7**	nd	nd	nd	99.98
PG	%	nd	**65**	nd	0.3	0.01	nd	**20.4**	0.1	nd	nd	0.2	nd	nd	nd	nd	0.3	**13.1**	nd	1	99.81

Table A 5: Elements (wt%) in assorted solid mine waste and sediments obtained using EDS analysis

Sample	wt	C	O	Al	Si	Fe	Mn	Ca	Mg	K	Na	Cu	Co	Ni	Ti	Cl	Br	P	S	Cr	Totals
CuCrt	%	**27.3**	**43.0**	0.3	1.0	3.1	nd	1.4	**4.1**	nd	nd	11.0	nd	nd	nd	nd	nd	nd	**8.8**	nd	100.0
Mgt	%	6.6	26.1	0.7	1.4	**59.8**	nd	1.0	2.4	nd	nd	0.7	nd	nd	0.8	0.5	0.7	nd	nd	nd	100.7
WRD PG	%	**33.5**	**41.9**	nd	0.4	5.5	nd	0.9	**6.3**	0.6	0.9	0.4	nd	nd	nd	**1.5**	nd	nd	**8.1**	nd	100.0
TexCon	%	8.1	**45.0**	1.0	3.8	**18.6**	nd	**17.7**	**4.6**	0.4	nd	nd	nd	nd	0.4	nd	nd	0.5	nd	nd	100.0
Cbt	%	**16.5**	**49.8**	0.9	4.2	1.8	nd	**24.8**	1.5	0.5	nd	nd	nd	nd	0.3	nd	nd	nd	nd	nd	100.1
WRD(s)	%	**24.3**	**39.3**	0.6	2.8	**18.9**	0.2	9.9	2.7	0.3	nd	0.6	nd	0.2	0.5	nd	nd	nd	nd	nd	100.2
ObC	%	**17.8**	**41.3**	3.5	**13.4**	**15.6**	nd	1.6	2.3	0.4	0.6	nd	nd	nd	3.1	nd	nd	nd	nd	1.3	100.8
SbC	%	**20.3**	**48.5**	5.2	**15.2**	5.6	nd	1.8	1.7	0.8	0.5	nd	nd	nd	0.5	nd	nd	nd	nd	nd	100.0

Table A 6: Other trace elements (mg kg^{-1}) in sediments and assorted solid mine waste obtained using XRF analysis

	Sc	V	Ga	Rb	Sr	Y	Zr	Nb	Mo	Ba	Th	U
Cbt	**43.5**	38.0	1.0	54.4	530.5	**24.2**	141.7	3.9	0.5	386.6	**21.7**	**0.01**
Cu_crust	**15.0**	40.3	nd	16.5	455.1	**44.6**	671.9	6.4	3.0	340.5	**46.1**	**43.6**
Mgt	49.8	720.9	22.1	d.l.	178.6	**10.8**	127.8	3.46	12.1	117.4	**nd**	**15.1**
TexCon	**56.3**	291.8	6.9	15.5	2946	**55.6**	1505	18.3	3.6	564.1	**474.9**	**121.3**
WRD_PG	**11.3**	168.7	4.3	8.4	389.1	**6.6**	179.1	4.8	27.8	67.6	**38.8**	**12.9**
ObC	**27.7**	1111	24.8	30.0	116.7	**16.5**	259.7	20.2	2.1	306.4	**nd.**	**nd**
OaC	**24.6**	1410	24.9	40.3	107.7	**22.3**	474.4	35.0	2.9	428.3	**15.3**	**nd**
SFB	**21.7**	89.0	17.6	88.2	391.9	**20.5**	269.9	7.2	0.1	513.5	**14.2**	**2.8**
SbC	**18.8**	157.4	13.9	49.3	205.2	**21.9**	650.0	13.2	1.6	375.9	**9.9**	**nd**
WRD(s)	**46.6**	395.9	11.1	19.4	2207	**37.0**	367.8	11.8	5.0	596.6	**85.1**	**21.9**

Table A 7: Total concentration, distribution and abundance (%) of redox (Cr and U) species relative to changes of pH and change in magnitude of total concentration of redox species with respect to pe.

Species/Concentration	pH 2, pe (4 →7.5)	pH 4.5, pe (4 →7.5)	pH 7, pe (4 →7.5)	pH 9.5, (4 →7.5)	pH 11, pe(4 →7.5)
Cr(II)	Cr^{2+} (100%)	Cr^{2+} (100%)	Cr^{2+} (100%)	Cr^{2+} (99%)	
Concentration mol kg^{-1}	**$[10^{-21}] \rightarrow [10^{-30}]$**	**$[10^{-21}] \rightarrow [10^{-27}]$**	**$[10^{-23}] \rightarrow [10^{-26}]$**	**$[10^{-33}] \rightarrow [0]$**	**$[0]$**
Cr(III)	Cr^{3+} (100%)	Cr^{3+} (99%)	$Cr(OH)^{2+}$ (59%, 57%)	CrO_2^- (49%, 51%)	CrO_2^- (55%)
			Cr^{3+} (31%)	$Cr(OH)_4^-$ (40%, 42%)	$Cr(OH)_4^-$ (45%)
			$Cr(OH)_2^+$ (10%)	$Cr(OH)_3$ (8%)	
Concentration mol kg^{-1}	**$[10^{-7}]$**	**$[10^{-7}]$**	**$[10^{-7}]$**	**$[10^{-12}] \rightarrow [10^{-18}]$**	**$[10^{-18}] \rightarrow [10^{-24}]$**
Cr(VI)	$HCrO_4^-$ (0%, 99%)	$HCrO_4^-$ (100%)	CrO_4^{2-} (53%)	CrO_4^{2-} (91%)	CrO_4^{2-} (94%)
	$CrO_3SO_4^-$ (0%, 9%)		$HCrO_4^-$ (31%, 41%)	$NaCrO_4^-$ (6%)	$NaCrO_4^-$ (5%)
Concentration mol kg^{-1}	**$[0] \rightarrow [10^{-30}]$**	**$[10^{-39}] \rightarrow [10^{-21}]$**	**$[10^{-16}] \rightarrow [10^{-9}]$**	**$[10^{-7}]$**	**$[10^{-7}]$**
Uranium(III)	U^{3+} (100%, 0%)	U^{3+} (100%, 0%)	U^{3+} (100%, 0%)		
Concentration mol kg^{-1}	**$[10^{-24}]$**	**$[10^{-32}]$**	**$[10^{-18}]$**		
Uranium(IV)	U^{4+} (86%)	U^{4+} (86%)	$U(OH)_5^-$ (99%)	$U(OH)_5^-$ (100%)	$U(OH)_5^-$ (100%)
	UF^{3+} (14%)	UF^{3+} (14%)			
Concentration mol kg^{-1}	**$[10^{-7}] \rightarrow [10^{-22}]$**	**$[10^{-14}] \rightarrow [10^{-26}]$**	**$[10^{-18}] \rightarrow [10^{-22}]$**	**$[10^{-14}] \rightarrow [10^{-26}]$**	**$[10^{-20}] \rightarrow [10^{-23}]$**
Uranium(V)	UO_2^+ (100%)	UO_2^+ (100%)	UO_2^+ (100%)	UO_2^+ (100%)	UO_2^+ (100%)
Concentration mol kg^{-1}	**$[10^{-10}] \rightarrow [10^{-17}]$**	**$[10^{-8}] \rightarrow [10^{-14}]$**	**$[10^{-12}] \rightarrow [10^{-14}]$**	**$[10^{-16}] \rightarrow 10^{-18}]$**	**$[10^{-18}] \rightarrow 10^{-20}]$**
Uranium(VI)	UO_2^{2+} (37%)	UO_2^{2+} (32%)	$(UO_2)_3(OH)_5^+$ (20%)	$(UO_2)_3(OH)_5^+$ (33%)	$(UO_2)_3(OH)_5^+$ (33%)
	$UO_2(SO_4)_2^{2-}$ (27%)	$UO_2(SO_4)_2^{2-}$ (24%)	$(UO_2)_2(OH)_2^{2+}$ (14%)		
	UO_2F^+ (20%)	UO_2F^+ (22%)	UO_2OH^+ (10%)		
	$UO_2(SO)_4$ (15%)	$UO_2(SO)_4$ (14%)			
Concentration mol kg^{-1}	**$[10^{-9}] \rightarrow 10^{-7}]$**	**$[10^{-7}]$**	**$[10^{-7}]$**	**$[10^{-7}]$**	**$[10^{-7}]$**

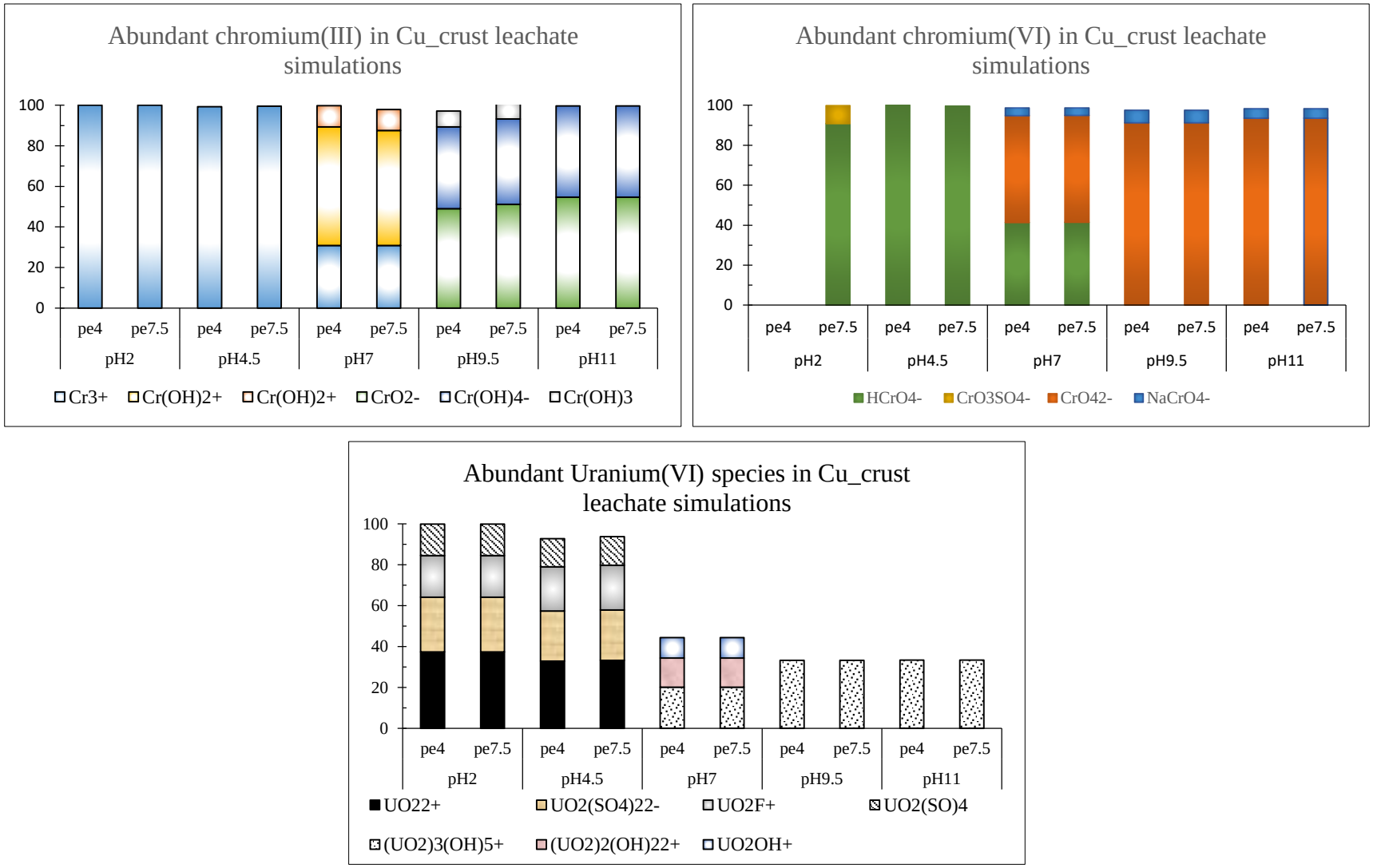


Figure A 1: Evolution of redox (Cr and U) species with respect to incremental changes of pH and pe